Symmetry in copper and silver cryptates

Thesis

SYMMETRY IN COPPER AND SILVER CRYPTATES

A thesis presented to the Faculty of Science at the Open University, Milton Keynes

by
David John Speed
BSc MSc (hons)

A candidate for the degree of
DOCTOR OF PHILOSOPHY
September 2002

NO CD ATTACHED

PLEASE APPLY TO THE UNIVERSITY

CONTAINS

PULLOUTS

Declaration

This document reports investigations carried out during the period of October 1998 to September 2001 by David Speed. Laboratory work was carried out in the chemistry laboratories of Queen's University of Belfast (QUB), David Keir Building, except where noted. The work has been performed in accordance with QUB COSHH guidelines.

Abstract

The cryptand ligands imBT (1,4,7,10,13,16,21,24-Octaaza-bicyclo[8.8.8]hexacosa-4,6,13,15,21,23-hexaene) and amBT (1,4,7,10,13,16,21,24-Octaaza-bicyclo[8.8.8]hexacosane) form interesting disilver(I) and trisilver(I) cryptates, as well as a dicopper(I) and a well studied average valence dicopper(1.5) cryptate. Detailed structural and spectroscopic studies of the silver cryptates show that complex equilibria exist in solution, and the trisilver form appears to be thermodynamically favoured, the additional stabilisation apparently being due to argentophilic interactions.

An optically pure form of the dicopper(I) imBT cryptate was successfully obtained, and is undergoing X-ray diffraction studies aimed at determining whether a copper-copper interaction exists, by direct examination of the electron density.

Synthetic studies aimed at introducing substitution to the imBT and amBT ligands were complicated by competing reactions. A strategy to modify cryptand cavity size by incorporating asymmetric tetraamine caps succeeded, yielding dicopper(I) and disilver(I) cryptates with properties intermediate between cryptates incorporating the related symmetric caps.

Manganese(II) cryptates of imBT and amBT were investigated as potential MRI contrast agents, the iminocryptate showing surprisingly high relaxivity, despite the fact that no water molecules were located in the crystal structure.

The observation of high mass peaks in the FAB mass spectra of imBT and amBT cryptates suggests the presence of 6+4 Schiff base condensation products, as well as the more abundant 3+2 products. It has not proved possible to isolate these molecules as yet, however initial studies aimed at a rational synthesis of the 6+4 condensation products were made, as these ligands could be of great interest for modelling the recently reported Cu_Z site.

Acknowledgements

To Professor Jane Nelson, for a warm welcome to Belfast (and Donegal), her guidance and instruction, enthusiasm and patience, and the endless edits! Also, for the opportunity to attend international conferences, training events, and for trips to the synchrotron. Particular thanks to Professor Vickie McKee for her help with crystal structures, to Dr Charlie Harding for making MK a nice place to visit and the help with magnetochemistry, and Dr Raewyn Town for talking electrochemistry with a proper accent.

Thanks to Dr Mark Nieuwenhuyzen for help with and access to the diffractometer, and Dr Annie Bligh for the MRI trials. Thanks also for useful discussions to Dr Sally Brooker and Dr Nick Fletcher.

To Drs Rob Davies-Colley, Andrea Donnison, and Cathy Bebelman, my NZ mentors, thanks for the opportunity to participate in your projects, and for the encouragement to continue with my own studies.

The staff of CSS Belfast have provided a tremendous environment during my writing up, particular thanks to Drs Scott Wharry and Tom Moody, for helping me see things from an organic perspective, to all of Lab 1 for the laughs, and to the management for their consideration of the demands on a PhD student.

Student life at QUB has been tremendously enjoyable, and for this I thank my fellow PhD students (especially Beatrice, Hamish, Gaia, Gerhard and Raquel), other workers in 1073, the crews of QUB Boat Club, members of the Photographic Societies (especially Gerald, Peter and the mad Greek), and the many others I've encountered who've made a Kiwi welcome in Northern Ireland.

I am grateful to the EPSRC Mass Spectrometry and MAS NMR services, the ASEP microanalysis and MS services, the technical staff at QUB for keeping everything in good working order, and the staff of the Belfast OU office for a pleasant working environment.

I am grateful to the Open University Higher Degrees Committee for the award of a postgraduate studentship.

Finally, to my parents, Roi and John, for constant support over the last 28 years, and to Ann, for putting up with a grouchy student for so long.

Contents

1. Introduction

Symmetry has been a recurring theme in the course of the studies reported in this thesis, the results of which can be seen in the spectroscopic, crystallographic, and electrochemical properties of the systems investigated. It is under the broad umbrella of this attribute that we bring together this diverse collection of studies.

Studies were conducted to better understand some previously reported structures, incorporating the imBT and amBT ligands (6A and 6B in Scheme 1-6). The average valence dicopper(1.5) cryptate of imBT has been studied in great detail, and the dicopper(I) cryptate has an internuclear separation only slightly longer. This system may therefore contain a d^{10}-d^{10} interaction, and studies were carried out in order to determine

whether such an effect exists. We were also interested to observe the effect of slight changes of internuclear separation on the properties of the average valence cryptate, and conducted synthetic studies using asymmetric tetraamine caps to introduce slight changes in strand length, and therefore cryptand cavity size.

The disilver(I) cryptates of imBT and amBT contain a different conformation of the ligand, with close internuclear separations, and a surprising *tris*ilver(I) cryptate had also been prepared on one occasion. Synthetic, structural and spectroscopic studies were performed on these molecules with an aim to elucidating whether d^{10}-d^{10} interactions are involved in stabilising their unusual structures, and also whether a mixed or even average valence state could be attained. NMR studies revealed that a complex equilibrium exists in solution, greatly complicating interpretation of spectroscopic and electrochemical measurements, and so synthetic studies were conducted with the aim of stabilising the dinuclear cryptates, and thereby simplifying their spectra.

Cryptates have found application in medicinal chemistry, where encapsulation of a harmful guest ion or molecule may prevent manifestation of the toxicity. Magnetic Resonance Imaging (MRI) is a field where paramagnetic (and sometimes toxic) ions have potential as contrast enhancing agents, and we investigated some cryptand and podand ligands as hosts for the paramagnetic ion manganese(II).

Modelling of active sites in biomolecules is another area where cryptates are of use. The report of a tetracopper site with nitrogen ligation (Cu_Z) during the course of our studies encouraged us to investigate the heavy peaks observed in the mass spectra of some imBT and amBT cryptates. These are consistent with ligands of double the expected size, with correspondingly larger coordination capacity, and if isolated could be of use in modelling the Cu_Z site.

A detailed review of cryptand chemistry has recently been published (1), and several PhD theses also give useful background information (2-4). The present chapter concentrates on those areas relevant to the studies reported in this thesis, namely: synthetic methods; the d^{10} species copper(I) and silver(I), and their multinuclear chemistry; the modelling of active sites in molecules of biological significance; recent developments in the field of bioinorganic chemistry, with emphasis on multi-copper sites with nitrogen ligation; and MRI, a technique where cryptate chemistry has found application.

The aims of our studies represent only a subset of the wide range of fields where cryptands have found application. This field of chemistry has developed particularly rapidly in the last thirty years, so that examples of the host-guest relationship can now be found not only in traditional cation coordination chemistry, but also in the complexation of neutral, anionic, or even metal-ligand complex guests.

Some of the earliest studies on coordination compounds incorporating synthetic macrocycles were reported by Curtis (5), and Thompson and Busch (6) (*e.g.* Figure 1-1 A and B).

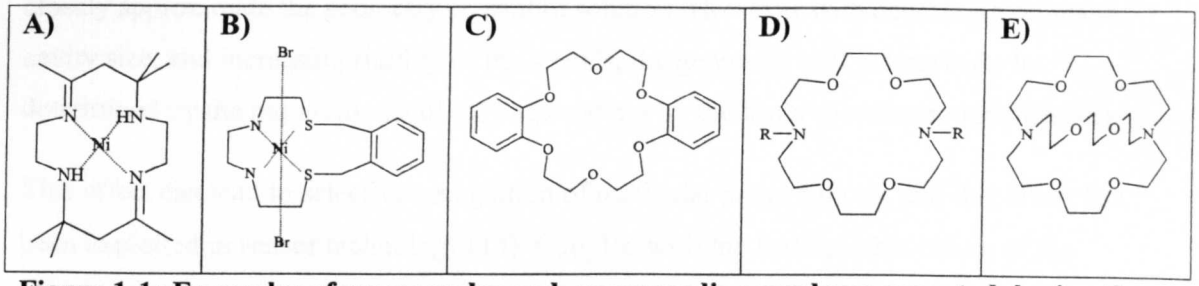

Figure 1-1: Examples of macrocycles and macrocyclic complexes reported during the evolution of cryptate chemistry. Materials reported by A) Curtis, B) Thompson and Busch, C) Pedersen, D) and E) Dietrich, Lehn and Sauvage.

Pedersen (7) introduced a series of novel cyclic polyethers in 1967 (*e.g.* Figure 1-1 C). These molecules constituted a new class of macrocycle, deemed *crown ethers*. Many crown macrocycles incorporating other heteroatom types besides ether oxygenes have been synthesised (8) (*e.g.* Figure 1-1 D). Whilst the capacity of crown ethers to form stable complexes with transition metals was limited (9), a high affinity was observed for Group 1 and Group 2 metal ions (of which isolable crystalline complexes were prepared). Additionally an ability to encapsulate small non-metallic molecules or ions was noted (10-12).

By addition of one, two or three strands across a macrocycle the corresponding macrobi-, tri-, or tetra- cycles may be created, with the consequence that different geometries are attained. The ellipsoidal or spherical cavity thus created can completely encapsulate a suitable guest, resulting in an increase in the thermodynamic and kinetic stability of the complex against dissociation, compared to crown ethers. High selectivity can be attained on the basis of charge and size, governed by the nature and number of the donor atoms present in the ligand.

The name cryptate was proposed by Dietrich, Lehn and Sauvage to describe the manner in which a macrobicyclic host with sufficient flexibility can collapse around a guest ion (or

molecule), effectively 'hiding' it from the external environment and replacing its first solvation sphere (8, 13) (*e.g.* Figure 1-1 E).

In normal solution the distribution of solvent molecules around an ion has a degree of symmetry dictated by such factors as the coordination preference of the ion, the coordinating ability of the solvent, the size of the ion and solvent molecules, and the presence of H-bonds. This symmetry may be preserved to a greater or lesser extent in a cryptated ion. In the larger and more flexible cryptands, the distribution of donors will be strongly influenced by the coordination preference of the encapsulated ion, and may closely approximate the geometry present in solution. However with decreasing cryptand cavity size, and increasing rigidity of the strands, the geometry will increasingly be determined by the requirements of the cage and not by the ion's coordination preferences.

This effect can lead to selective recognition of particular metal cations, and this effect has been exploited in sensor technology (14). Coupled with the hydrophobic nature of the exterior of the cryptate, within which the polar guest lies concealed, cryptates can facilitate guest transport through membranes. This enhanced ability to solubilise polar salts in nonpolar media leads to applications in phase-transfer catalysis and anion activation as well as in transport and selectivity (15-18).

Polyether cryptands are able to bind Group 1 cations, main group cationic guests such as Pb^{2+}, Cd^{2+} and some lanthanides (10-12), although in general, the complexation of transition ion and heavy main group cations is not achieved most effectively with neutral ether-O-donor ligands. Conversely N donors, whether sp^2 N or sp^3 N, are much better equipped to coordinate transition ions and many main Group 3- 14 cations. Several valuable and/or toxic target cations such as Cu^+, Ag^+ , Tl^+, and Hg^{2+} are expected to be efficiently sequestered by N-donor cryptands (azacryptands), leading to potential applications, for example, in hydrometallurgy or detoxification (19).

Azacryptands can be readily protonated, which enables them to encapsulate certain anions, an objective not readily achieved with the analogous O-donor hosts. This is now a rapidly developing area, partly due to the concern about the possible adverse environmental effects of accumulation of common soluble oxoanions such as NO_3^- and PO_4^{3-} in surface waters, and toxic anions present as a result of industrial activity or mining (*e.g.* oxoanions of chromium, selenium, and arsenic). The aim in complexing these anions is not activation, but sequestration to assist in construction of monitoring, purification, or detoxification devices.

Cryptands can be large, in some cases having very many donor atoms, and thus may coordinate more than one ion. A huge variety of multinuclear cryptates are known. In a large cavity, the ions may be effectively isolated from one another, or there may even be room to accommodate a bridging anion in "cascade" fashion (20), thus opening a route to anion recognition. With decreasing cavity size and change in donor distribution, ions may be brought into close proximity. Thus, not only can the chemical environment of an ion be altered by sequestering it within a cryptand, but also the symmetry of its environment can be altered.

Cryptands provide a mechanism for studying ions in strained configurations ("entactic states") which would not otherwise be stable. They are a valuable tool for understanding the catalytics effects observed in many biomolecules, where metal ions are often found in such entactic states.

Characteristic properties of macrocycles include slow rates of formation and dissociation of the complex (21), high ligand field strengths (22) and large stability constants for macrocyclic complexes when compared with the corresponding open chain ligands (23). The term "macrocyclic effect" was coined to describe these properties, which encompass both kinetic and thermodynamic factors. An extension of the macrocyclic effect – the cryptate effect (24) is used to describe the analogously enhanced stability of macrobicyclic systems (cryptates) over macrocyclic systems. In these systems, the stability constants, K, can be as much as 10^5 times larger than analogous macrocyclic complexes

1.1. Synthetic Strategies

Several different synthetic strategies have been developed in recent years to produce cryptands. These can be divided into two main groups, (i) direct synthesis, where cyclisation is effected by conventional organic reactions, and (ii) template methods, which employ a templating agent (which may or may not be desired in the target molecule) to bring about ring closure. In both cases, reaction conditions should be such that cyclisation is favoured over polymerisation.

1.1.1. Direct Synthesis

The different approaches to cryptand assembly by direct synthesis are outlined schematically in Scheme 1-1. Yields are generally improved by use of high dilution conditions to minimise unwanted polymerisation. The high dilution technique is based on the theory that whilst the rate of intramolecular ring closure is first order with respect to the

substrate concentration, intermolecular polycondensation is second order. Therefore the desirable unimolecular reaction is kinetically more favourable under these conditions.

The stepwise process (Scheme 1-1 A) requires two cyclisation reactions (each forming two bonds) but generates an intermediate macrocycle, which may also present interesting properties and allows the introduction of different bridges.

The tripod coupling process (Scheme 1-1 B) is a "one pot" procedure but can suffer from extensive side reactions since it requires formation of three bonds in a single condensation step. These compounds conserve a three-fold symmetry axis through the bridgehead atoms. However, this method can also result in "left-right"- dissymmetric macrocycles when two different tripodal subunits A and B are employed.

Lehn (25) reported the synthesis of macrobicyclic polyamines by direct macrobicyclisation *via* tripode-tripode coupling. This involves simultaneous formation of three C-N bonds *via* C-X and tosylamine condensation reactions, without reverting to high dilution conditions.

The method of tripod capping, figure 1.2 (E), involves the assembly, in a single operation, of five bi- or trifunctional fragments (the number of reactive centres is 12) (26).

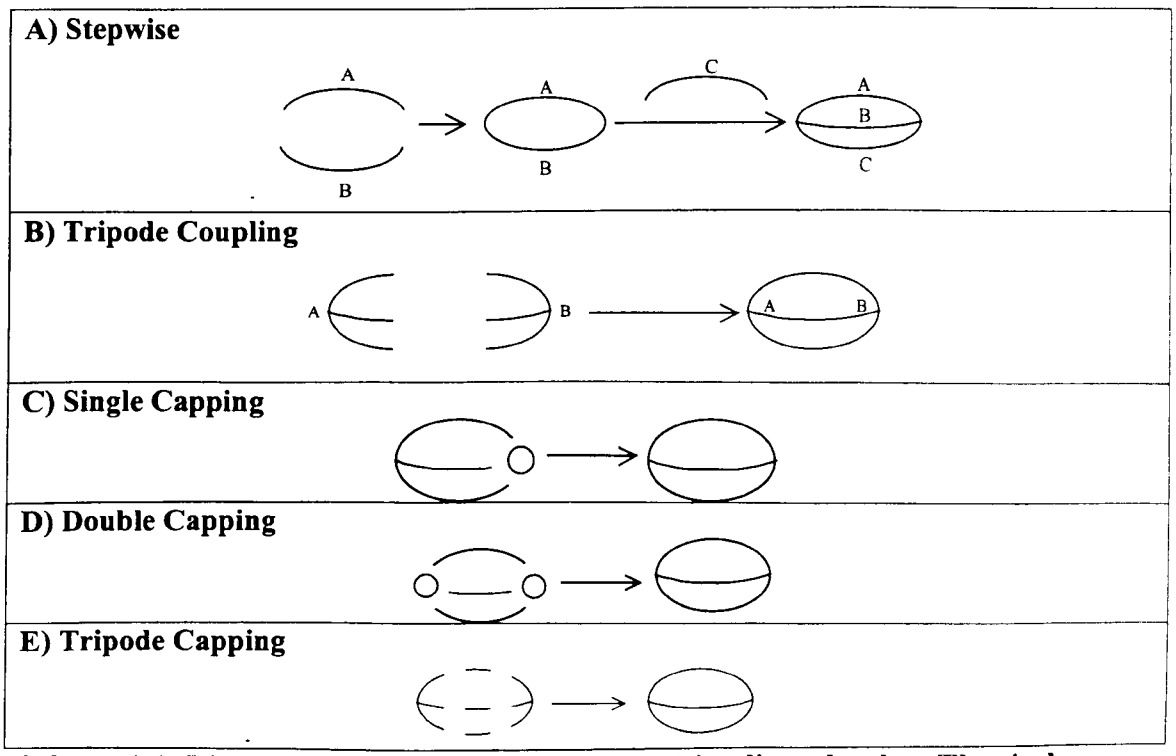

Scheme 1-1: Direct synthesis approaches to macrobicyclic molecules. The circles represent groups retained in the final product.

1.1.2. Template Methods.

1.1.2.1. Exo-template cations

Much of the pioneering work utilising the exo-template effect to construct cryptands was carried out in the period of 1960-1965 by Curtis (5).

Most frequently a metal ion is employed to act as a template for the cyclisation reactions due to the ability of the metal ion to organise the open chain reagents into a conformation conducive to ring closure. Inert cations such as the alkali, alkaline earth and lanthanide ions which form labile complexes are generally employed due to the ease of subsequent removal and substitution with another metal ion *i.e.* transmetallation. One advantage is the increased yield, as a result of partial or total inhibition of the competing reactions, that is, polymerisation and formation of noncyclic compounds. One of the drawbacks is that the macrocycle is generally strongly coordinated to the metal ion and it is sometimes difficult to dissociate the complex for substitution of a different cation (27). A schematic representation of different methods for the exo-template preparation of cryptands and cryptates is given in Scheme 1-2.

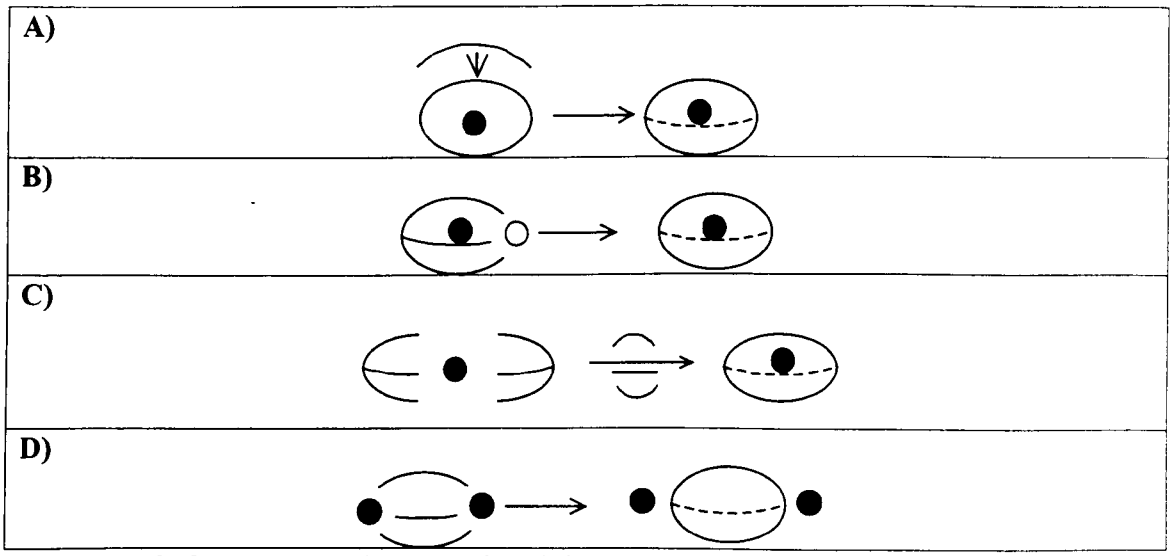

Scheme 1-2: Some synthetic strategies giving access to macrobicyclic molecules. Open circles represent groups retained in the final product; the black dots represent external templates temporarily used for construction purposes.

1.1.2.2. Endo-template

Endo template assembly effects ring enlargement of an existing ring, or adds a further strand to a pre-existing ring; all the pre-existing parts of the molecule are retained (*e.g.* Scheme 1-3).

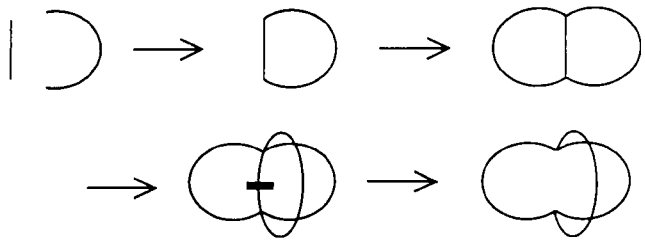

Scheme 1-3: Endo-template synthesis approaches to macrobicyclic molecules.

1.1.3. Podands

Podands are open chain ligands which usually do not have a pre-formed intramolecular cavity inside which a cation can nest. However, they are able to assume a cup shaped structure with an appropriate cavity during complexation causing the whole ligand skeleton to be held in a podate conformation only by the cation – donor interactions. Because the cavity is not preformed, the entropic contribution to complexation is unfavourable and is reflected by a decrease in complex stability (28, 29).

1.1.4. Schiff-base condensation

The ease of formation of an imine bond by a condensation reaction involving a carbonyl group and a primary amine functionality has been widely exploited in the synthesis of nitrogen donor cryptands, macrocycles and podands. The reaction gives good yields, sometimes without the need for templating ions, and the products are easily reduced (*e.g.* with sodium borohydride) to give the corresponding amino ligands.

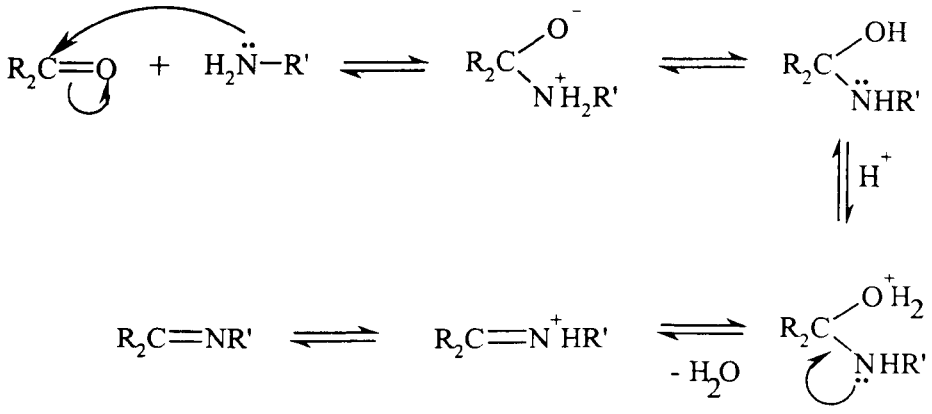

Scheme 1-4: Schiff-base condensation mechanism.

The reaction proceeds via nucleophilic attack by the lone pair of electrons of the amine group on the α carbon of the carbonyl functionality. Rapid deprotonation at nitrogen and reprotonation at oxygen lead to a neutral species. Protonation on oxygen, the intermediate being present in a protic medium, sets the stage for loss of water and formation of a C=N

bond using the nitrogen's lone pair. The loss of a proton forms the neutral imine as illustrated in Scheme 1-4 (30).

This reaction is however reversible, and hydrolysis of the C=N bond can occur with hard acidic metals such as lanthanides. The saturated analogues are not subject to this problem, and they have an associated increased in cavity size and flexibility, often resulting in a wider range and number of metal cations which may be coordinated. Often they show a greater tendency to act as di-nucleating ligands than their imine parent macrocycles (31).

The synthesis of macrocycles from the Schiff base condensation of a number of dicarbonyl precursors and a wide range of aliphatic and aromatic diamines has resulted in a series of mono-, di- and polynucleating ligands of the type [1+1] and [2+2], shown schematically in Scheme 1-5.

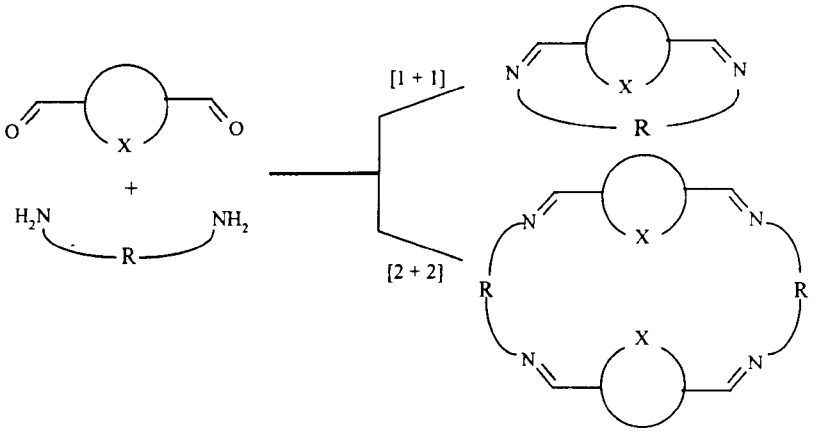

Scheme 1-5: [1+1] and [2+2] macrocycles.
The macrocycles formed consist of one/two head units derived from the dicarbonyl precursor and one/two aliphatic or aromatic lateral units derived from the diamine substituent of the reaction, resulting in the corresponding [1+1] and [2+2] macrocycles respectively (29, 32).

The more recent [2+3] Schiff base condensation has permitted more convenient routes to form metal-free cryptands, through condensation reaction between triamines and dialdehydes in the ratio two:three (Scheme 1-6).

Nelson and co-workers have demonstrated that this effective, high yield tripod-coupling-capping route to azacryptands proceeds in high yield under mild conditions, without the need for high dilution techniques (33). By using a one-pot procedure several symmetric hexa-Schiff base cryptands have been obtained, despite the need for six condensations steps. Yields can, in most cases, be improved by the use of a templating agent, although

this may be due to cryptate insolubility assisting isolation of the product. Once the three dimensional skeleton has been assembled, the Schiff-base cryptands can be readily reduced, with sodium borohydride or lithium aluminium hydride, to generate the analogous octaaminocryptands, which being more chemically robust than their hexaimino-Schiff base precursors, have many advantages as ligands for both cations and anions. These fully saturated ligands have an associated increase in flexibility, water solubility and stability against hydrolysis, the latter two being prerequisite features for biomedical applications.

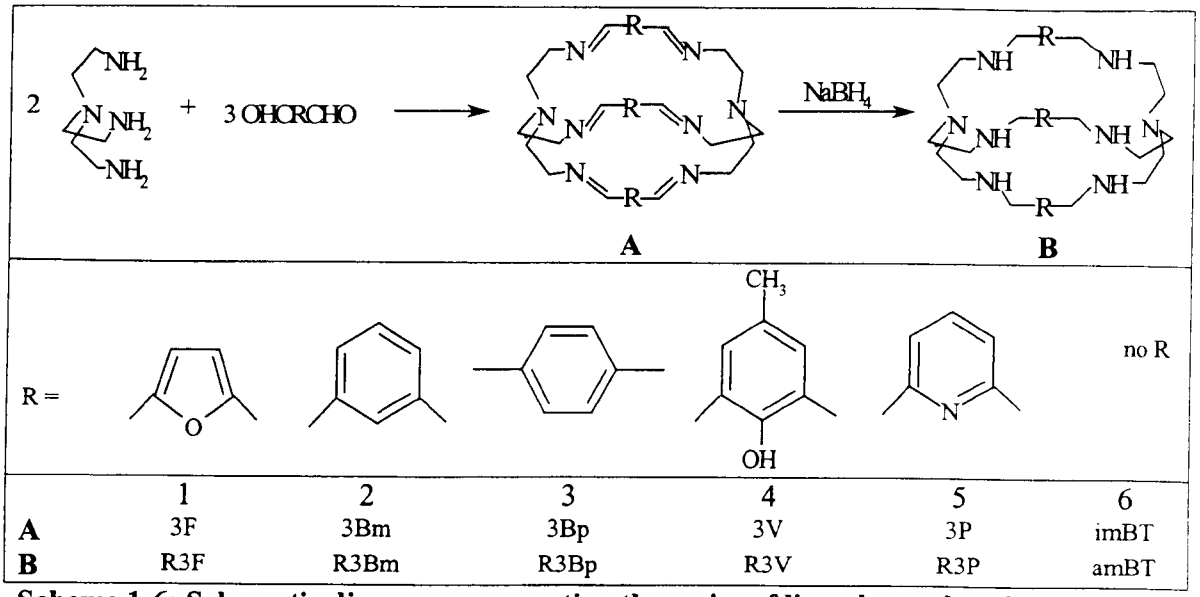

	1	2	3	4	5	6
A	3F	3Bm	3Bp	3V	3P	imBT
B	R3F	R3Bm	R3Bp	R3V	R3P	amBT

Scheme 1-6: Schematic diagram representing the series of ligands employed by the Nelson group.

1.2. Copper and Silver chemistry

1.2.1. Cu (II)

The copper (II) ion has a d^9 configuration, and consequently contains one unpaired electron. It is capable of forming complexes with coordination numbers of 2 - 8 with 4, 5, and 6 being the most common. In octahedral d^9 complexes, the odd electron can occupy either the d_{x2-y2} orbital or the d_{z2} orbital, which normally generate Jahn Teller distortions with strongly tetragonal distortion. 5 co-ordinate complexes may be either trigonal bipyramidal, square pyramidal or quite often something in between (34).

According to the Hard-Soft Acid-Base concept, Cu(II) is classified as a reasonably "hard" metal i.e. small and not easily polarisable, which preferentially coordinates to hard bases e.g. nitrogen and oxygen containing ligands (35). Complexes with soft donors, such as phosphorus, sulfur and bromine containing ligands, can be prepared but are more difficult

to handle due to the possibility of redox reactions. These ligands stabilise the softer Cu(I) cation (35).

In the absence of X-ray crystallography, information on the geometries of a transition metal cation in its complexes, can be revealed by electronic spectroscopy. This arises due to the nature of the splitting of the d orbital with respect to the ligand field.

Copper(II) complexes give rise to two main types of electronic transitions: pure d-d transitions, and charge transfer transitions. The differences in the intensities of the bands observed for the transition metal complexes reflect the nature of the electronic transitions and their compliance with the selection rules which govern these transitions, the Spin and the Laporte selection rules: Spin selection rules states that $\Delta S=0$ for allowed transitions, and the Laporte selection rules states that "In a centrosymmetric molecule or ion the only allowed transitions are those accompanied by a change in parity" (36). Thus, d-d transitions are very weak if at all present for the free ion.

The situation changes upon complexation:

Case 1. The ligand field may enforce a metal environment which lacks a centre of symmetry (*e.g.* tetrahedral) and in this case, the mixing of the d and p orbitals may result in partially allowed, and thus weak, transitions.

Case 2. If the transition metal ion lies in a centre of symmetry, the d and p orbitals cannot mix and these transitions may only become partially allowed by a much less efficient mechanism involving molecular vibrations called "vibronic".

As a result of these rules the intensity of the d-d transitions in tetrahedral complexes should be substantially larger than those observed for a metal ion in an octahedral geometry since the metal is not at a centre of symmetry.

While a d-d transition involves redistribution of electrons which are mainly localised on the metal atom, there are transitions in which an electron moves from an essentially ligand based orbital to a metal based orbital or vice versa. This results in charge being transferred from one part of the co-ordination sphere to another, generating so called charge transfer bands in the electronic spectra.

For the Cu(II) complexes, if the electron passes from the negatively charged ligand based orbital to a metal based orbital it is referred to as a ligand-to-metal charge transfer, LMCT.

As the electron is not localised on the d orbital these transitions are "allowed" electronic transitions in every respect. No selection rule is violated and therefore the absorption intensity is about one thousand times greater than the typical d-d transitions (36).

This results in typical extinction coefficients as follows (36):

Band Type	**ε max ($M^{-1}cm^{-1}$)**
Spin forbidden	<1
Laporte forbidden d-d	20 – 100
Laporte allowed d-d	250
Symmetry allowed	1000 - 50000

Unlike typical transition metal ions, the Cu(II) ion is reluctant to take up a regular. octahedral or tetrahedral stereochemistry. This is because the $3d^9$ outer electronic configuration lacks cubic symmetry and hence yields distorted forms of the stereochemistry. The reason for this is that the Cu^{2+} (d^9); $(t_{2g})^6$ $(e_g)^3$ configuration is doubly degenerate. If Case 1 (see below) were to exist then the single electron in the d_{x2-y2} orbital would provide less efficient shielding, and this would result in the ligands in the xy plane being more strongly attracted towards the nucleus than the ligands in the z axis and therefore the more screened the electrostatic interaction of the Cu(II) ion. In consequence the complex would undergo axial elongation. In some examples the ligand field is so strong that the axial ligands in the z axis move out to infinity and the four co-ordinate square planar geometry is observed.

Conversely axial contraction holds for Case 2 when the unpaired electron is placed in the d_{z2} orbital.

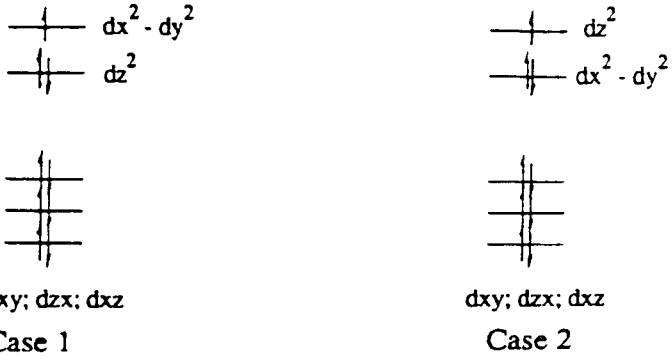

Consequently d_{z2} and d_{x2-y2} become differentiated in energy. This is an example of the operation of the Jahn Teller effect which states that "for a non linear molecule that is in an electronic degenerate state, distortions must occur so as to lower symmetry, remove degeneracy and lower the energy" (36).

Which case arises in practice is a matter of energetics rather than symmetry however. Since the axial elongation affects only two bonds and the planar elongation would weaken four bonds, axial elongation is more common than axial compression. This is also more favoured sterically (37, 38).

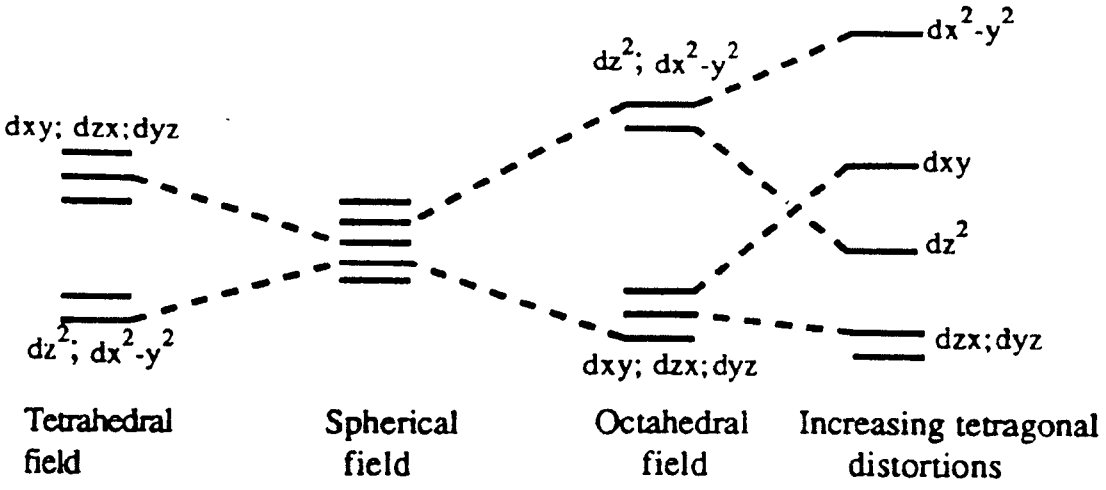

Figure 1-2: An energy level diagram showing the splittings of the d orbitals according to the ligand field applied.

Some Cu(II) complexes may seem to be undistorted from the octahedral geometry, however, low temperature ESR studies indicate that in fact both aforementioned distortions are occurring simultaneously. This hopping from one conformation to another is called the dynamic Jahn Teller effect (35).

a_1'	d_{z2}
e'	d_{x2-y2}; d_{xy}
e''	d_{xz}, d_{yz}

D_{3h} Trigonal pyramidal

In trigonal bipyramidal geometry, the d orbital splitting is calculated for D_{3h} symmetry giving rise to three levels: $A_1 = z^2$; E" = xz, yz, and E' = xy, x^2-y^2. Therefore only two transitions are predicted i.e. xz, yz → z^2 and xz, yz → z^2. However due to Franck Condon vibrational effects these transitions are 'enveloped' into one broad band with a poorly resolved high frequency shoulder.

b_1	d_{x2-y2}
b_2	d_{xy}
a_1	d_{z2}
e	d_{xy}, d_{yz}

C_{4v} square pyramidal

The square pyramidal geometry has a C_{4v} point group with a d_{x2-y2} ground state. Therefore three transitions may occur but again the spectrum observed is broad typically with a low frequency shoulder (39).

In the absence of magnetic fields, the unpaired electron of the Cu(II) has two usually degenerate spin states $M_S = ½$ and $-½$. On application of the magnetic field the degeneracy is removed because the magnetic poles of the unpaired electrons are aligned with the field. The energy difference is field dependent and when the energy gap $g\beta H$ equals the frequency of the microwave radiation applied, a net absorption occurs. This results in a absorption peak being recorded which is usually presented in the first derivative mode to assist resolution as ESR lines are broad for experimental reasons. However a number of factors namely anisotropy, nuclear Zeeman, and zero field effects tend to lead to a much more complicated spectrum.

The $g_{//}$ signal is obtained when the magnetic field is oriented along the molecules axial direction (z axis) and $g_{\perp}$ is obtained when the field is in the equatorial (xy) plane.

The $g_{\perp}$ axes are doubly degenerate and consequently the probability of those transitions are twice as likely as for the $g_{//}$, therefore $g_{\perp}$ typically exhibits greater intensity than observed in the $g_{//}$ spectrum.

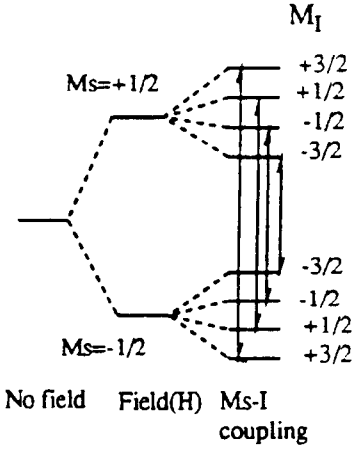

Figure 1-3: The Nuclear Zeeman effect.

If the unpaired electron is associated with a nucleus possessing spin then the energy of the electron will depend on which of the possible nuclear spin states it is coupled to. This gives rise to hyperfine structure consisting of 2I+1 lines of equal intensity (I = nuclear spin state). The copper nucleus has a spin I = 3/2 and thus a hyperfine pattern of four equally intense lines is produced with hyperfine splitting constant, A, ranging between 120-200 G. The hyperfine structure is often observed in the $g_{//}$ and rarely in the $g_{\perp}$, but this depends on the geometry. With irregular geometry hyperfine coupling can be seen in both the $g_{//}$ and $g_{\perp}$.

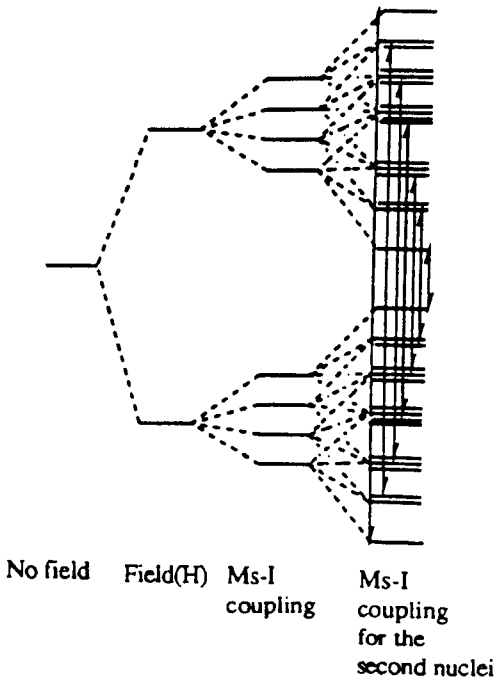

Figure 1-4: Zero Field Splitting.

For dinuclear complexes, in which the magnetic interactions may be mediated via a bridging unit, there may also be further splitting observed resulting from zero field splitting

of the triplet state, (Figure 1-4). As a result of the triplet state splitting, in addition to the $\Delta m = 1$ transitions, the selection rule forbidden transition $\Delta m = 2$ may also arise as a weak half band. The half band, being isotropic, usually exhibits a simple seven line pattern ($2nI+1 = 7$, where n = number of nuclei interacting), arising from the transitions shown in Figure 1-4, with a simple 1:2:3:4:3:2:1 ratio of intensities. The hyperfine splitting constant, A, is typically half that observed for the mononuclear Cu(II) spectrum, because the unpaired spin is distributed over both nuclei (40, 41).

1.2.2. Cu(I)

Cu(I) has a filled $3d^{10}$ shell and therefore lacks ligand field stabilisation. The large number of Cu(I) complexes exist in a variety of stereochemistries with coordination numbers ranging from 2-5 with 4 predominating. The most common stereochemistries are linear two coordinate (42), trigonal planar three coordinate (43), and tetrahedral four-co-ordinate (44) with possible distortions of these geometries arising in the presence of chelating type ligands.

Cu(I) is regarded as being "softer" than Cu(II) and therefore binds to ligands which contain soft basic donors, i.e. phosphorus, sulfur and unsaturated nitrogen containing ligands, increasing the redox potential of Cu(II)/Cu(I) and so favouring Cu(I) (45, 46). Aqueous solutions of Cu(I) are unstable due to disproportionation of Cu(I) to Cu(II) and metallic Cu(0), however the nature of the solvent can strongly influence the stability of Cu(I) relative to Cu(II). In acetonitrile it is apparent that the Cu(I) state is relatively stable (47). Reduction potentials for the Cu(II)/Cu(I) couple tend to be more positive in acetonitrile than in, for example, water or dimethyl sulphoxide.

Copper is remarkable for the small separation between the redox potentials for the Cu(II)/Cu(I) and Cu(I)/Cu(0), and this characteristic is an important factor in its role in electron transfer and catalysis.

$Cu^{+} + e^{-} \rightarrow Cu \qquad E^{\circ} = +0.52\ V$

$Cu^{2+} + e^{-} \rightarrow Cu^{+} \qquad E^{\circ} = +0.15\ V$

So that

$2Cu^{+} \rightarrow Cu^{0} + Cu^{2+} \qquad E^{\circ} = +0.37\ V$ (48)

although, as with other cations with variable valence, the formal potential of the Cu(II)/Cu(I) redox couple is dependent on the co-ordination geometry of the metal ion, the nature of the bulk environment, the types of donor atoms and the proximity of electrostatic influences.

1.2.3. Mixed and Average Valence Copper

Mixed valence complexes are abundant in chemistry and biochemistry. Such systems are of interest because their properties are rarely just the sum of the two independent ions. As with resonating organic molecules, there is frequently an "interaction" between the metal ions, which can result in dramatic changes to the properties of the system. The study of electron transfer in mixed valence transition metal complexes can provide insight into electron transfer in oxidation-reduction, electrochemical and biological processes.

Mixed valence complexes have been classified into 3 categories by Robin and Day (49):

1. Class I: The ions of differing valences are in sites of very different symmetry and ligand field strength, and the properties of the individual ions are clearly recognisable.

2. Class II: There is a sizeable interaction between the individual ions but the individual ions are still clearly recognisable. Delocalisation takes place but the two types of site are still distinguishable and so a delocalised electron does not spend equal time on them.

3. Class III: MV complexes in which the valences are completely shared and the individual ions are indistinguishable.

Mixed valence copper compounds have been known for a long time but only a few detailed studies have been reported. Many of the complexes belong to Class 1 or 2 including those prepared both chemically and electrochemically by Hendrickson et al (50), Gatteschi et al (51) and Gagne et al (52) as well as the half met forms of type 3 centres in hemocyanins reported by Westmoreland et al (53). Dunaj-Jurco and coworkers provided a comprehensive survey and classification of the structures for mixed-valence copper complexes in 1988 (54).

The discovery of mixed valence complexes of copper among other redox-active cations, has lead to a large amount of theoretical work (55, 56). As well as having the ability to act as semi and sometimes even superconductors, class 1 and 2 mixed valence systems are ideally suited to the study of inner sphere electron transfer. Hush (57) was able to show the

close connection to electron transfer reactions and the relation between optical and thermal electron transfer.

1.2.3.1. Spectroscopic Properties of Mixed Valence Copper Centres

The most obvious and striking feature of any mixed valence copper compounds is the presence of intense absorption in the visible region of the spectrum, not present in compounds containing either valence state alone.

$Cu^{I}Cu^{II}$ mixed valence copper dimers have an odd number of electrons and exist in the S=½ state. They are readily classified by the hyperfine structure displayed in their ESR spectra.

In Class I complexes the probability of finding the unpaired electron at the Cu(I) site is effectively zero and the ESR spectrum resembles that of a mononuclear copper (II) complex: 4 lines.

In Class II there is a non-zero but unequal probability of finding the odd electron on either site. This leads to two different sets of hyperfine couplings and many lines can be observed depending on a given molecular orientation.

In Class III complexes the probability of finding the odd electron on either site is identical. Thus the electron interacts equally strong with both copper nuclei resulting in a 7-line hyperfine pattern.

The localisation/delocalisation pattern depends on the measurement temperature and the "time scale" of the method used to probe it. In intermediate Class II/III situations complicated patterns can arise (50).

1.2.4. Ag (I)

In common with copper, the first oxidation state of silver also has a filled $4d^{10}$ shell, and lacks ligand field stabilisation, and is ESR silent. The ion is likewise observed in a variety of stereochemistries, with coordination numbers ranging from 2-6 with 4 predominating. The most common stereochemistries are linear two coordinate and tetrahedral four-co-ordinate (58).

Ag(I) has a similar preference for soft ligands, forming only weak complexes with O-donor ligands. Both the Ag(I) and Ag(II) oxidation states are attainable, and can be stabilised by N-donor macrocycles, however under aqueous conditions they are kinetically and

thermally unstable. Ag(I) is a useful oxidising agent, and the photoreduction process, usually resulting in the precipitation of black Ag(0) is well known.

$Ag^+ + e^- \rightarrow Ag$ $E^\circ = +0.80$ V

$Ag^{2+} + e^- \rightarrow Ag^+$ $E^\circ = +1.98$ V (48)

Ag(I) is also known for its aggregation behaviour, clusters of 2 to 6 are known, and even polymeric structures containing Ag-Ag contacts. Some examples of multinuclear silver complexes are: Steel and coworkers (59, 60) report a structure containing two trigonal planar Ag(I) ions, with a 3.08 Å separation, which may be supported by the bridging N-donor ligands, and a different molecule with pyrazole and pyridine donors, which contains a linear trisilver(I) array with 2.899 Å Ag-Ag separations (similar to the Ag-Ag distance in metallic silver, 2.89 Å) stability in this case is assisted by π-π interactions.

Support of silver-silver interactions by ligand, H-bonding, or packing effects is not necessary however, as several systems containing unsupported silver-silver contacts are known (61-64). The Ag_6 cluster in bis(imidazole) silver(I) reported by Eastland actually incorporates six Ag(I) ions, arranged in three radiating pairs, the three closest ions being only 3.49 Å apart. ESR of the singly oxidised cluster (by exposure to gamma rays) showed no evidence for delocalisation.

Mixed valence silver complexes are known, and reduction of silver(I) clusters to form Ag_2^+ and Ag_4^{3+} occurs reasonably easily (64). A 1:1 Ag(I) complex of a phenanthroline capped porphyrin (65) is spontaneously oxidised to Ag(II), and can then complex a second Ag(I) ion, resulting in a Ag(I)Ag(II) mixed valent complex. Recent work by Bielmann et al (66) on silver oxide (AgO) suggests that the inequivalent silver ions observed in the crystal structure correspond to Ag(I) and Ag(II), with oxygen also present in –1 and –2 valencies.

1.2.5. Cuprophilicity and argentophilicity

The observation of silver's liking for forming clusters, often with internuclear separations similar to, or shorter than observed in elemental silver (2.89 Å) raises the question of a silver-silver interaction, or bond. Similarly for copper(I), where dinuclear structures with remarkably short Cu(I)-Cu(I) separations are known, although there is as yet no evidence for unsupported Cu(I)-Cu(I) interaction.

The "aurophilic effect", referring to a stabilising interaction between d^{10} gold ions is well accepted, and explained in terms of a relativistic contraction of the s orbitals, which allows them to mix more easily with the outer d orbitals.

The silver and copper nuclei are too light to accelerate electrons to relativistic speeds however, and the postulation of analogous "argentophilic" and "cuprophilic" effects to explain the high nuclearity and close inter-ion approaches has been debated in the literature over several decades.

The weight of evidence in favour of the argentophilic effect is now overwhelming. A variety of synthetic/structural studies (*e.g.* (60-64, 67-70)), modelling studies (71, 72) as well as observations reported in this work (see Chapters 2 and 5) support the hypothesis that close approach of silver(I) ions can stabilise a complex, in a manner consistent with the formation of a metal-metal bond of sorts, or at least a strong Van der Waals interaction. Amongst these are reports of silver clusters unsupported by other ligation, bonding interactions or packing effects (61-64).

Cuprophilicity is less well supported in the literature, spectroscopic studies of di-copper(I) systems with short Cu-Cu tend to be complicated by ligand absorptions, and magnetic techniques are of no use for the d^{10} ions. As long ago as 1958, Orgel (73) suggested a hybrid s-d orbital model for bonding between Cu(I) and Ag(I), and in 1987 a review by Jansen (74) concluded that d^{10}-d^{10} interactions do occur, but only when other effects, such as ligand bridging, or an excess of cations, exist to force the d^{10} ions into proximity. He also noted that the nature of the interaction in each of the cases Cu(I), Ag(I), and Au(I) must be different.

The $[Cu_2imBT]^{3+}$ cryptate prepared by Nelson's group contains the first synthetic example of average valence $Cu_2^{1.5}$, with a copper-copper bond. The isostructural cryptate $[Cu_2imBT]^{2+}$ has also been obtained, and contains a copper-copper separation only 0.07 Å larger, which could be indicative of Cu-Cu interaction, although this is sterically demanding of this ligand system for two ions of this size. Studies by Cotton and Poblet (75, 76) refute the existence of a copper-copper interaction, whilst other studies (77) go as far as giving a stretching frequency for $\nu(Cu_2)$ in a dinuclear diphosphane complex with 2.64-2.94 Å internuclear separations. The RR determined value of 104 cm^{-1} is compared to that for $\nu(Au_2)$, 88 cm^{-1}, showing that, on the basis of a force/mass calculation, the interaction in Cu_2 is much weaker.

1.3. Copper Biosites

Copper containing biosites (see summary in Table 1-1) are known to carry out a wide variety of important biological functions, including: electron transfer, dioxygen binding, transport and activation, copper transport and storage, hydroxylation, dismutation and oxidation (78).

In an aqueous medium, copper is remarkable among biologically relevant cations for the fact that redox potentials for the transitions Cu(II)↔Cu(I) and Cu(I) ↔Cu(0) are close together (79). Comparing the Cu(II)↔Cu(I) redox potentials of copper proteins with those of other biologically relevant couples, in particular the Fe(III) ↔Fe(II) redox pairs in functionally analogous iron proteins, reveals mostly higher, more positive, potentials for the copper systems (80).

Biologically active copper centres from proteins have for many years been classified into types 1, 2 and 3 (81). This classification was originally sufficient to correlate function with spectroscopic properties. However these correlations have now been refined and extended due to increasing available structural information, and in recent years several additional biological copper centres have been found that do not fit the conventional type 1-3 classification. These are the trinuclear centres (82), the Cu_A site (83) and the Cu_Z site (84).

Type 1 copper sites function as electron transfer centres in blue copper proteins (85). They are characterised by a strong absorption band ($\varepsilon \sim 2000\text{-}5000\ M^{-1}cm^{-1}$) around 600 nm, a very positive redox potential and an unusually small ($< 65 \times 10^{4} cm^{-1}$) value for the hyperfine coupling constant $A_{//}$ in the ESR spectra (86).

Type 2 copper sites have less intense electronic spectral absorptions ($\varepsilon \sim 500\ M^{-1}cm^{-1}$) than type 1 copper proteins. Copper proteins of this type exhibit normal Cu(II) ESR spectra ($g_{//} > g_{\perp} > 2.00$, $A_{//} > 140 \times 10^{-4}\ cm^{-1}$) (87). Type 2 copper is usually involved in oxidative catalysis during which the substrate reaction intermediate and/or products are co-ordinated to the copper centre.

Type 3 copper centres are characterised by the occurrence of pairs of copper (II) ions which are strongly antiferromagnetically coupled, leading to the absence of any ESR signal.

Proteins containing type 3 copper are involved in the binding and activation of dioxygen, e.g. haemocyanin and tyrosinase (88).

A trinuclear cluster, formed from a type 3 and a type 2 copper site is present in the active sites of groups of related blue copper oxidases, for example ascorbate oxidase, laccase and ceruloplasmin.

Cu_A is a recently discovered dinuclear copper site which is involved in electron transfer. It has also been found in Nitrous oxide reductase (N_2OR) and Cytochrome c oxidase (COX) (89).

N_2OR also contains the only known example of the Cu_Z site, which is the site of N_2O binding in the enzyme, and contains a tetrahedral arrangement of four copper ions with bridging sulfide (84).

Much of the work described in this thesis has been aimed at understanding the processes occurring in the average valence Cu_A site, and at developing techniques applicable to modelling this site, and the newly discovered Cu_Z site.

	Type1	Type2	Type (2+3) trimer	Type3	Cu_A	Cu_Z
Nuclearity	Mononuclear	Mononuclear	Trinuclear	Dinuclear	Dinuclear	Tetranuclear
Function	Electron transfer	Catalysis and redox reactivity	O_2 activation: oxidase function	O_2 activation: transport and oxygenation	Electron transfer	N_2O activation, redox reactivity
Where	Blue copper proteins, *e.g.* plastocyanin	amine oxidases, SOD	ascorbate oxidase, laccase	hemocyanin, tyrosinase	N_2OR, COX	N_2OR

Table 1-1: Properties of unoxidised copper centres in various biomolecules.

1.3.1. The Cu_A centre

The so-called Cu_A site is found in cytochrome c oxidase (COX) and nitrous oxide reductase (N_2OR), and has long been recognised as being unusual. This is largely because of its unique ESR spectrum, with small and unresolved Cu hyperfine splitting in the $g_{//}$ region, and an absorption band at 830 nm associated with a characteristic MCD signal. However, the presence of intense overlapping bands from heme centres always complicates the interpretation of spectral data (90). While formulated for some time as a mononuclear site, it was first recognised as a binuclear copper centre from ^{63}Cu ESR hyperfine splittings, which were backed up by Cu EXAFS, and finally fully demonstrated by protein crystallography (91).

Cytochrome c oxidase resides in the inner mitochondrial membrane and is responsible (as the terminal enzyme of the respiratory chain) for catalysing the reduction of molecular oxygen to water:

$$O_2 + 4Cyt\ c_{red} + 8H^+ \rightarrow 2H_2O + 4Cyt\ c^{3+}{}_{ox} + 4H^+$$

N_2OR is the terminal reductase in a respiratory chain converting N_2O to N_2 in denitrifying bacteria.

$$N_2O + 2e- + 2H^+ \rightarrow N_2 + H_2O$$

Accumulation of N_2O in the atmosphere by the action of denitrifying bacteria has important environmental effects due to its action as a greenhouse gas and its role in the destruction of the ozone layer. The chemistry involved in the binding and activation of N_2O is therefore of considerable interest (92).

1.3.2. Structure and spectroscopic characteristics

1.3.2.1. Crystal structure

Two crystal structures of cytochrome c oxidases, one from Paraccocus denitrificans (4 subunits) and another from beef heart (13 subunits) (93), both at 280 pm resolution, were published with a one-week interval in summer 1995. A few months later M. Wilmanns and coworkers (94) obtained what was described by Holm et al (91) as "the most accurate structure of Cu_A" from a soluble fragment of a quinol oxidase into which the binuclear site had been engineered. The structure of this site consists of two distorted tetrahedral co-ordination units bridged by two Cys-S ligands. Terminal co-ordination is completed by one His-N ligand at each copper atom trans to each other, a Met-S ligand at one copper atom and (in the quinol structure) a backbone Glu-O ligand at the other (a Trp-O is observed in the N_2OR structure instead, see Figure 1-5 below). The Cu–Cu distance was found to be 2.5 A which is suggestive of a metal-metal bond. The oxidised site is a purple Cu(II)Cu(I) chromophore, and is described as class III mixed valent. The Cu_A site was later discovered in N_2OR (95) by comparison of MCD spectra to those of COX, and the crystal structure in this dimeric enzyme was recently reported (see Figure 1-5, (84)).

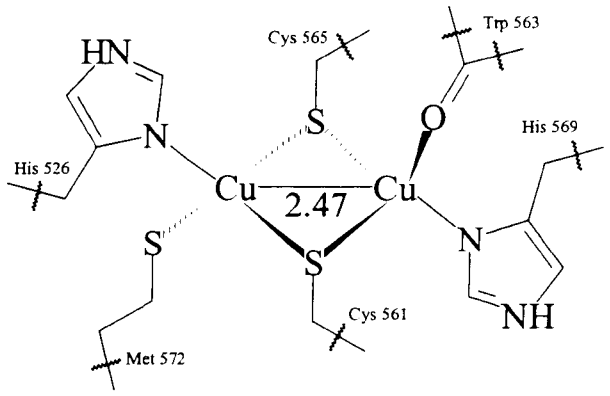

Figure 1-5: Schematic representation of the crystallographically determined Cu_A structure (from N_2OR).

The X-ray crystallographic results helped resolve many long standing controversies relating to the unusual spectroscopic observations. The combined data support a novel dithiolate-bridged delocalised mixed valence ($Cu^{1.5}$-$Cu^{1.5}$) resting-state formulation with 4 co-ordinate distorted tetrahedral copper ions in close proximity. The electronic structure of this novel mixed valence copper thiolate centre is of considerable interest, and has been the subject of many synthetic and theoretical studies.

The unusual ESR characteristics of the oxidised Cu_A centres had previously been attributed to the co-ordination of 2 cysteine residues at one Cu(II) centre (40). The possibility of Cu_A being a dinuclear copper centre was raised when Kroneck and coworkers demonstrated that N_2OR contains, in the resting state, a Cu_A-like centre, having an ESR spectrum similar to that of COX but with some resolved copper hyperfine coupling at $g_{//}$.

The seven-line hyperfine pattern has been analysed in detail at several microwave frequencies and has been shown to be characteristic of a single unpaired electron interacting with 2 equivalent copper nuclei (96). This indicated that Cu_A is a mixed valence class IIIA dimer in which both copper ions must be equivalent. Thus the Cu_A centre is best described by the term *average valence*.

Investigation of the optical properties of Cu_A in COX was complicated by the intense and overlapping transitions from the two cytochromes, a and a_3. Initially, the only absorption band which could be assigned to Cu_A was a peak at ~830 nm. Investigations by Thomson et al (97) revealed the presence of optical transitions of Cu_A at 480 nm and 520 nm. By comparison of Cu_A and Cu_A* (A Cu_A site engineered into the soluble domain of subunit II from the quinol oxidase of *Escherichia coli*), they showed that the electronic structures of the Cu_A and Cu_A* sites are different, and identified the likely structural variation that cause these differences.

The observed short Cu-Cu distance raised a lot of interest regarding the possibility of a Cu-Cu bond. Woodruff et al (98), and Sanders-Loehr et al (99, 100), conducted Resonance Raman studies to address this question, by using the electronic transition of Cu_A near 830 nm to excite specific RR observations of the vibrations of this chromophore. RR experiments were performed on Cu isotopically substituted, genetically modified forms of Cu_A from *Bacillus subtilis* and *Paracoccus denitrificans*. The Cu_A site of native beef heart was probed for comparison.

Peaks below 200 cm^{-1} were not significantly enhanced and no attempt was made to assign them to specific modes. However, excitation of the band at ~830 nm enhances the peak below 200 cm^{-1} indicating that vibrations below 200 cm^{-1}, which are selectively enhanced with far-red excitation, may be associated with vibrations of a Cu-Cu bond.

$^{63/65}Cu$ isotope labelling experiments indicated that peaks at 125 and 139 cm^{-1} contained most Cu-Cu stretching vibrational character. The RR excitation profiles are consistent with this assignment. While this evidence is indicative of a Cu-Cu bonded structure, neither of these observations constitute conclusive evidence as to whether Cu atoms are bonded or non-bonded. This is because Cu-S-Cu modes could be expected in similar regions with similar isotopic shifts to Cu-Cu modes. However, the frequency location of this peak compared to Cu-Cu stretching frequency assigned in model complexes, is not incompatible with a direct Cu-Cu bond in addition to the thiolate bridges.

1.3.3. The Cu_Z centre

In March 2000 the structure of the copper-containing enzyme, nitrous oxide reductase, was announced by Brown *et al* (84). A key area of the determined structure differed substantially from earlier predictions: although it was known to be a dimer, the total number of copper atoms had previously been put at 8 per dimer, rather than 12 as has now been shown. There are two metal clusters within each monomer, a dicopper centre, similar to the Cu_A centre found in cytochrome c oxidase, as well as a *tetra*copper centre, denoted Cu_Z (Figure 1-6). Within the site, Cu(III) and Cu(IV) are bridged, and do not make a direct contact, and the four metals take the form of a distorted tetrahedron. The original assignment of the bridging group as hydroxide (or water) was in contradiction of previous spectroscopic studies (101) which had shown that all copper centres contributing to the electronic spectra should be coordinated to sulfur. Subsequent analytical studies (102) determined that sulfur was indeed present in the site, and the presence of bridging sulfide was later confirmed in a crystal structure with improved resolution (103).

A combination of MCD, XAS, ESR and DFT techniques was used by Chen et al (104) to determine the oxidation states of the copper atoms in the reduced form of the enzyme. The total spin of the site was determined to be ½, and the majority of this resides on Cu_I (predominantly in the II oxidation state), which together with Cu_{IV} (predominantly in the I oxidation state) forms the substrate binding edge (84). Simultaneous 2 electron reduction of the substrate is achieved by Cu_{IV} providing one electron, and Cu_{II} providing a second electron via the bridging sulfide (in the reduced form Cu_{II} and Cu_{III} are both in the I oxidation state). The dimeric structure brings Cu_Z and Cu_A sites into proximity, so that rereduction of the Cu_Z site can be performed by Cu_A.

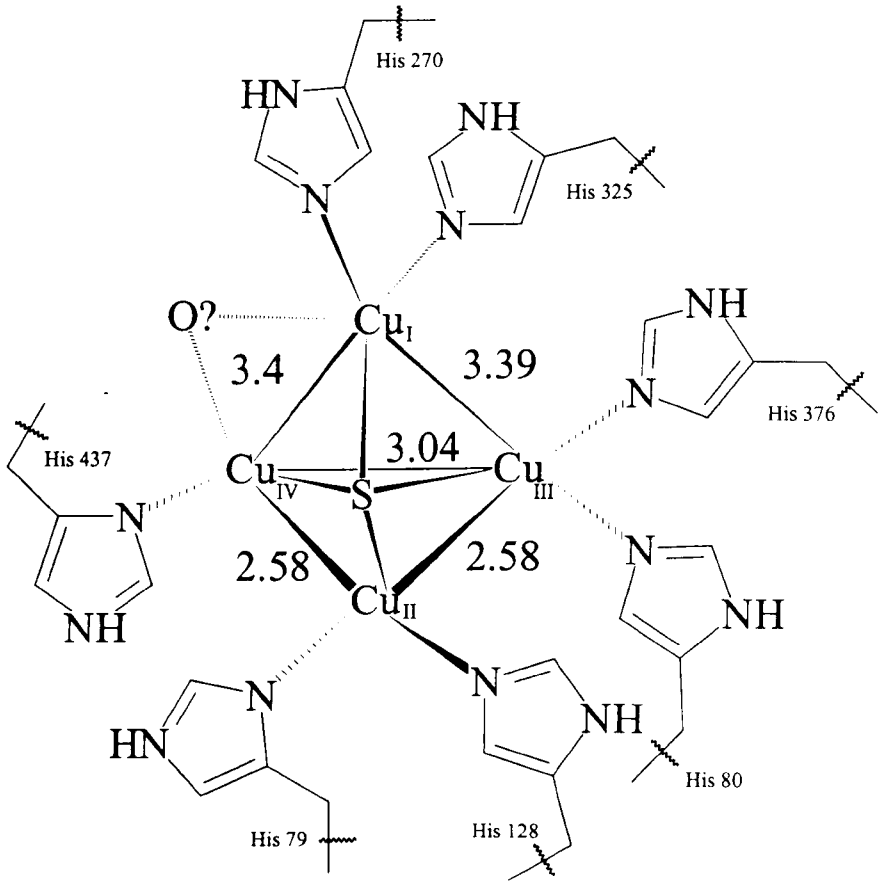

Figure 1-6: Diagram of the CuZ site in N2OR.

1.3.4. Cryptates as models for copper biomolecules

Limited types of modification can be effected on proteins without disruption of protein structure and/or function. This coupled with their large size and complex structures often make detailed studies of proteins difficult (e.g. X-ray crystallography). It is therefore apparent that model complexes must be used to obtain information on structures and reaction mechanisms which is unavailable directly from studies on the proteins themselves (105).

The aim of synthetic model studies is to duplicate the spectroscopic features and ultimately the function of the active site in a low molecular weight complex of known structure. This is generally a cyclic process, and as understanding of a particular metalloprotein develops, older models quickly become obsolete (106, 107). In modelling metalloproteins, the aim is to mimic the ligation, geometry and possible environment of the active site in question. If this is achieved it should be possible to reproduce the spectroscopic and other properties of the metalloprotein. The relative importance of each of the above factors varies from case to case, as does the relative importance of matching particular properties.

1.3.5. Average valence dicopper complexes - potential Cu_A site models

Even prior to the X-ray crystallographic characterisation of Cu_A, models for the site were being postulated (90, 108-111). Since then, several classes of synthetic molecules have been prepared, which succeed in reproducing the delocalised $Cu^{1.5}$-$Cu^{1.5}$ state.

1.3.5.1. Tolmans model

Although several complexes with bis(μ-thiolato) dicopper(I,I) cores are known (112), fully delocalised 'Class III' mixed-valence dicopper (I, II) complexes are extremely rare, and no example of such a species bridged by thiolates appeared in the literature until Tolman et al (113) reported their preparation of a molecule with a $[Cu_2(\mu\text{-}RS)_2]$ core (see Figure 1-7). This molecule closely mimics the resting-state Cu_A geometry, oxidation state and high degree of electron delocalisation (as shown by ESR studies).

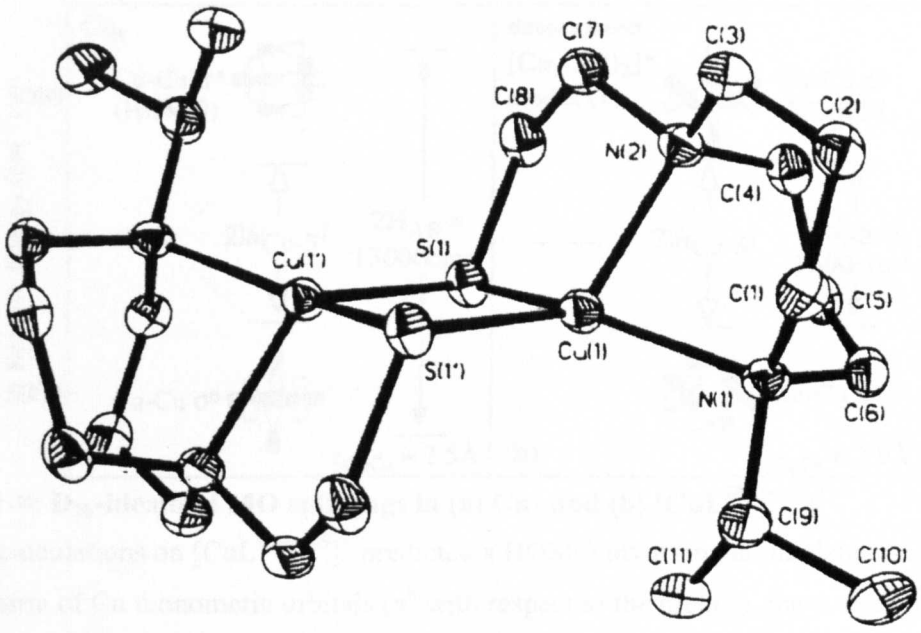

Figure 1-7: X-ray crystal structure of the average valence dicopper complex prepared by Tolman et al, $[CuL^{iPrdacoS}]^+$.

The Cu_2S_2 unit is planar with an average Cu-Cu distance of 2.92 Å, significantly longer than that reported for Cu_A. Each metal ion is in a distorted trigonal pyramidal site, with N1 and the bridging thiolate sulfur atoms defining the trigonal plane. The co-ordination geometry for each Cu is analogous to those of the trigonal type 1 copper protein sites and model complexes except that a NS_2 rather than an N_2S donor is incorporated. Also similar to type 1 centres, the ligand arrangement in this thiolate model can be construed to be intermediate between geometries favourable for Cu(I) or Cu(II) oxidation levels, presumably in order to accommodate redox reactions and to stabilize a Cu(1.5)Cu(1.5) form.

Investigation of the absorption, MCD and S K-edge of $[CuL^{iPrdacoS}]^+$ enabled an MO splitting diagram to be prepared, and compared to that of Cu_A (Figure 1-8).

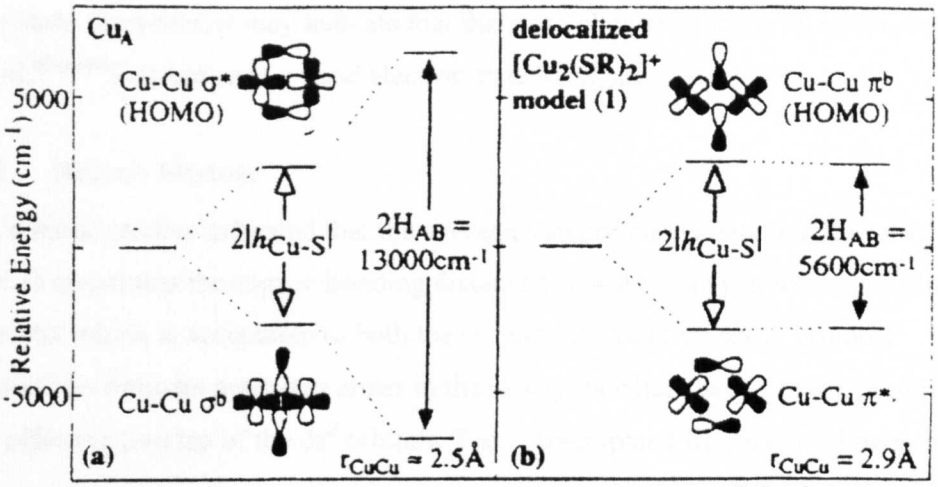

Figure 1-8: D_{2h}-idealised MO splittings in (a) Cu_A and (b) $[CuL^{iPrdacoS}]^+$

Xα-SW calculations on $[CuL^{iPrdacoS}]^+$ predicted a HOMO involving an in plane π-bonding combination of Cu monomeric orbitals (π^b with respect to the metals), the π-antibonding combination (π*) being filled and at lower energy. Significantly, the greater energy of the π^b combination than its π* counterpart indicates that the splitting in $[CuL^{iPrdacoS}]^+$ is dominated by Cu-S interactions and demonstrates that the valence delocalisation in this case is mediated by the bridging ligation rather than by direct Cu-Cu overlap. On the basis of the large Cu-Cu separation (2.9 Å) it has been assumed that only ligand contributions are significant. Similar Cu-S HOMO covalencies were measured for $[CuL^{iPrdacoS}]^+$ and Cu_A, and this increase of $2H_{AB}$ in Cu_A to 13000 cm^{-1} is assigned to a direct Cu-Cu bonding interaction resulting from the significantly shorter Cu-Cu separation in Cu_A (~2.5 Å).

In contrast with delocalisation in $[CuL^{iPrdacoS}]^+$, which is mediated exclusively by the sulfur bridges, the pathway for delocalisation in Cu_A is seen to contain comparable contributions from both Cu-Cu and Cu-S interactions. These results provided the basis for understanding the origin of valence delocalisation in Cu_A and $[CuL^{iPrdacoS}]^+$. The delocalisation observed in $[CuL^{iPrdacoS}]^+$ indicates that the value of $2H_{AB}$ = 5600 cm^{-1} is large relative to the vibronic trapping energetics of this dimer. Electronic coupling in $[CuL^{iPrdacoS}]^+$ was found to be large indicating that bridging superexchange contribution can be an efficient mediator of valence delocalisation. Direct 2.5 Å Cu-Cu bonding interaction in Cu_A is more than double the magnitude of $2H_{AB}$ relative to the already large value found in $[CuL^{iPrdacoS}]^+$, thus stabilising the delocalisation of Cu_A despite its lower-symmetry protein environment.

The electrochemical behaviour of $[CuL^{iPrdacoS}]^+$ revealed that the reduction is completely irreversible, and the oxidation is chemically reversible only at high scan rates (> 1.0 Vs^{-1}). The authors have interpreted this as indicating significant stabilisation of the mixed

valence state. However, it may indicate that there is a change of shape on redox, suggesting that $[CuL^{iPrdacoS}]^+$ is not such a good electron transfer agent.

1.3.5.2. Nelson Models

Nelson's initial studies indicated that the average-valence copper site is achievable within a host which constrains the copper-bonding distance (~2.4 Å) in a symmetric co-ordinate environment which is acceptable to both the +1 and +2 oxidation state. Trigonal bipyramidal co-ordinate geometry arises in the azacryptate host due to redox preferences and the effective overlap of the dz^2 orbitals. The 3 azacryptand ligands are shown in Figure 1-9.

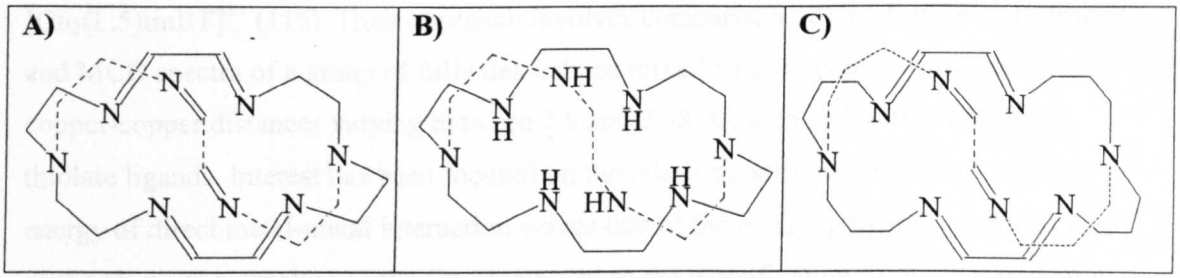

Figure 1-9: Three ligands prepared by Nelson, which have been used to prepare average valence dicopper cryptates. A) imBT, B) amBT, C) imBistrpn.

The similarity of the structures obtained allowed the comparative interpretation of the observed electronic spectra. Each average valence dicopper cryptate shows an intense UV absorption around 300 nm which probably consists of a charge transfer transition. There are also longer wavelength absorptions at 600-650 nm (ε = 1500-3500 $M^{-1}cm^{-1}$) and a more intense band in the region 750-850 nm ($\varepsilon \sim 5000\ M^{-1}cm^{-1}$).

All MCD bands exhibited temperature dependence indicating that they arise from a paramagnetic ground state. In the 600-1100 nm region, differently signed MCD bands are observed for each of the complexes. Those between 600 and 950 nm correspond to the variously allowed electronic absorption bands. The similarity of the MCD and optical spectra irrespective of ligand unsaturation, suggests that neither metal-to-ligand charge transfer nor the opposite is involved in this region. The spectrum can be assigned to transitions within the d-orbitals delocalised over the Cu_2^{3+} assembly. It was proposed that the unpaired electron of the mixed-valence complex is in the antibonding dz^2 based molecular orbitals (110).

The similarity of the ESR parameters for 3 systems which contain different co-ordination sites (amine versus imine) supports the hypothesis that these signals arise from delocalisation between the 2 copper nuclei (114). The SOMO is largely composed of the

two equivalent dz^2 orbitals on copper. The temperature independence of the ESR parameters show that this is a relatively strong bond, and since the unpaired electron is anti-bonding, the σ-bond must be even stronger.

An understanding of the electronic structures of average valence dicopper systems may help elucidate the pathways of electron delocalisation within the dicopper unit, and to understand the role that such centres play in long distance electron transfer between redox centres in proteins.

Thomson and coworkers have presented an interpretation of the electronic transitions observed in the low-temperature magnetic circular dichroism and absorption spectra of $[Cu_2(1.5)imBT]^{3+}$ (115). Their approach involves comparison of the electronic absorption and MCD spectra of a group of fully delocalised mixed valence copper compounds with copper-copper distances varying between 2.9 and 2.38 Å., with and without bridging thiolate ligands. Interest has been focused on the relative contribution to the delocalisation energy of direct metal-metal interaction versus that of the bridging ligands. A description of the electronic structure of the Cu_A centre led to the identification of the MV transition between the highly covalent bonding and antibonding copper-thiolate molecular orbitals, Ψ and Ψ*, responsible for the electron exchange. In the case of a mixed valence copper (I,II) dimer the energy separation of the two Cu-Cu bonding and antibonding states is a direct measure of the delocalisation energy.

The magnetic properties and optical spectra of the dicopper cryptates can be interpreted by considering a $[Cu_2]^{3+}$ unit which is perturbed by a trigonal ligand field around each copper ion. When only the first co-ordination sphere is considered the unit can be considered to have D_{3d} symmetry.

As the molecule is axially symmetric, orbital angular momentum of the copper 3d orbitals is maintained about the unique axis with $M_L = 0, \pm1, \pm2$ to give the molecular orbitals shown in Figure 1-10.

The dimer possesses one unpaired electron and therefore all the electronic states will be doubly degenerate, with $S = ½$.

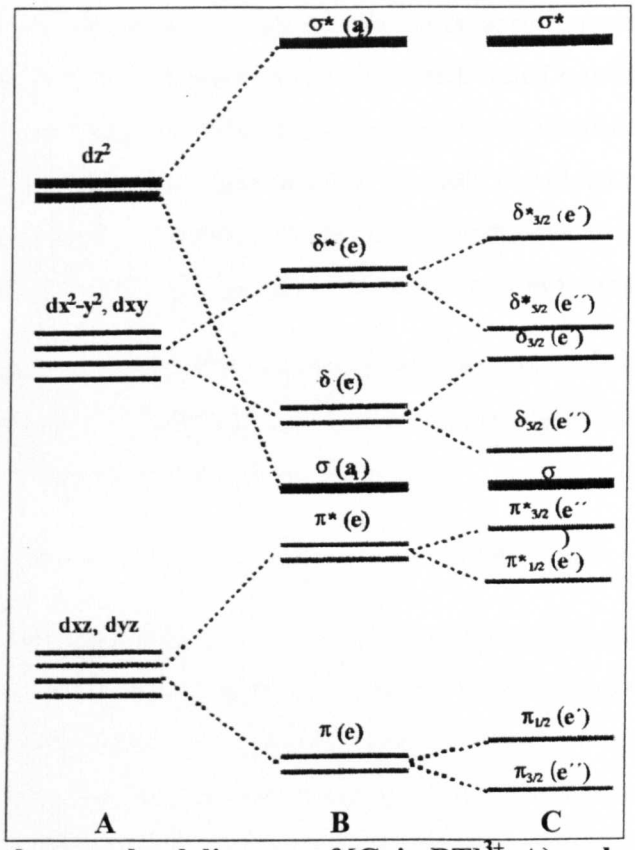

Figure 1-10: Proposed energy level diagram of $[CuimBT]^{3+}$, A) under C_{3v}, B) under D_{3d}, and C) after taking into account the effect of first order spin orbit coupling.

The low temperature ESR spectrum of $[Cu_2imBT]^{3+}$, described by Harding et al, exhibits an axial set of g values of $g_{\perp} = 2.148$ and $g_{//} = 2.004$ (114). The ground state has been assigned to $^2A_{2u}$ ($^2\Sigma^*$), on the basis of the g value ordering $g_{\perp} > g_{//}$. Spin-orbit coupling would be expected to mix a $^2A_{2u}$ ground state with $2E_u$ (Π^*) excited states giving rise to an orbital contribution to the magnetic moment along the X and Y axes.

The 4.2 K absorption and MCD spectra between 25 000 and 7500 cm^1 were determined, and interpreted with regard to the view that the visible and near IR spectra of these compounds are dominated by the Cu-Cu entity, the effect of the ligands being limited to the splitting of the Cu 3d atomic orbitals.

For the MCD spectrum (summary in Table 1-2), all the observed transitions below 22 000 cm^{-1} are formally d-d transitions arising from the d-orbital manifold. It can be shown that nine transitions are possible within the total d-orbital manifold to the single hole of a $[Cu_2]^{3+}$ dimer. According to the selection rules of D_{3d} only five of these transitions are electric dipole allowed although out of state spin-orbit coupling relaxes these selection rules.

A Gaussian analysis was carried out on both the absorption spectrum and the MCD spectrum to determine the position and intensity of the individual transitions. The data and results are summarised in Table 1-2. Nine transitions have been identified in both the absorption and MCD spectrum. The observation of formally forbidden transitions under D_{3d} suggests that the centre of inversion is absent, that the effective symmetry around the copper ions is lowered from D_{3d} to D_3 and that inter-state spin-orbit coupling is operative.

The absorption spectrum is dominated by an intense transition at 13 800 cm^{-1} (band 5). The transition moment integral for transitions from the ground state (gs) to a given excited state (es) within the copper dimer is expected to be of the form:

$$(\Psi_{es} \mid r \mid \Psi_{gs}) \sim (1-\alpha^2)(L_{es} \mid r \mid L_{gs}) + \alpha^2(R_A - R_B)$$

where α is the coefficient of mixing and $R_A - R_B$ is the copper-copper internuclear distance. The first term represents the ligand contribution to a given transition and the second term the contribution of the two coppers A and B. Since Cu-N covalency is small (114), ligand contributions to the molecular orbitals are limited and the term $(1-\alpha^2)$ in the transition moment is correspondingly small. Thus the transition moment will be dominated by the second term.

Since this will be zero for transitions which do not involve bonding and anti-bonding molecular orbital combinations of the same orbital, the most intense band in the absorption spectrum should be assigned to the $^2A_2 \rightarrow {}^2A_1$ ($\Sigma^* \rightarrow \Sigma$) transition.

The MCD spectrum is dominated by the C-term temperature-dependent behaviour. An important general result of such analysis is that it predicts that the MCD associated with all excited states except Σ will consist of pairs of C terms opposite in sign but equal in intensity. Therefore $\Sigma^* \rightarrow \Sigma$ transitions should be recognisable as the 'odd-man out' in the MCD spectrum.

The observed MCD transitions between the Σ^* ground state and the Σ, Π, Π^*, Δ, and Δ^* excited states are assigned according to the energy level scheme in Figure 1-10 and are summarised in Table 1-2.

The MV transition energy has been used to elucidate the valence delocalisation energy which is compared with the delocalisation energies in thiolate bridged MV copper dimers. The delocalisation energy of 7100 cm^{-1} is almost entirely due to copper-copper σ overlap at a distance of 2.36 A and represents a metal-metal bond $(\sigma)^2(\sigma^*)^1$ with bond order of 0.5.

Table 1-2: Summary of Gaussian analysis, identifying nine transitions.

Band	MCD position cm^{-1}	Absorption position cm^{-1}	Splitting cm^{-1}	f_{osc}	C_o/D_o	Excited state	Transition
1	9349	9349	1623	0.0001	7.595	$^2\Delta_{*1/2}$	$\delta^* \rightarrow \sigma^*$
2	10972	10972		0.0001	-12.822	$^2\Delta_{*1/2}$	
3	10877	10877	2232	0.0019	0.588	$^2\Delta_{1/2}$	$\delta \rightarrow \sigma^*$
4	13109	13109		0.0042	-0.217	$^2\Delta_{1/2}$	
5	14230	13778		0.060	-0.026	$^2\Sigma$	$\sigma \rightarrow \sigma^*$
6	15718	15978	625	0.020	-0.03	$^2\Pi_{*1/2}$	$\pi^* \rightarrow \sigma^*$
7	16347	16597		0.022	0.03	$^2\Pi_{*1/2}$	
8	18290	18290	924	0.016	0.006	$^2\Pi_{1/2}$	$\pi \rightarrow \sigma^*$
9	19214	19614		0.008	0.016	$^2\Pi_{1/2}$	

1.3.5.3. Lippard models

Two different classes of ligands prepared by Lippard and coworkers (116-119) have yielded a range of dicopper(I) complexes, as well as average valence dicopper(1.5) complexes. The ligands XDK and PXDK contains two carboxylate O-donors, which each bridge a pair of Cu(I) ions, and leave the copper ions able to coordinate to auxiliary ligands as shown in Figure 1-11 (A), where an acetonitrile molecule is present. One electron oxidation with Ag(I) resulted in the formation of the corresponding average valence complexes, with Cu-Cu separations of 2.399-2.425 Å, the shortest yet known. These complexes exhibit the characteristic 7-line ESR spectrum, and molecular orbital studies showed that the mode of electron delocalisation was purely through the copper ions.

In more recent work, dicopper(I) complexes of an N-donor ligand, BBAN, were prepared, however attempts to oxidise these to the average valence failed, unless an anionic bridging ligand (see Figure 1-11 B) was present. The anionic ligand appears to be necessary to the stabilisation of this group of complexes.

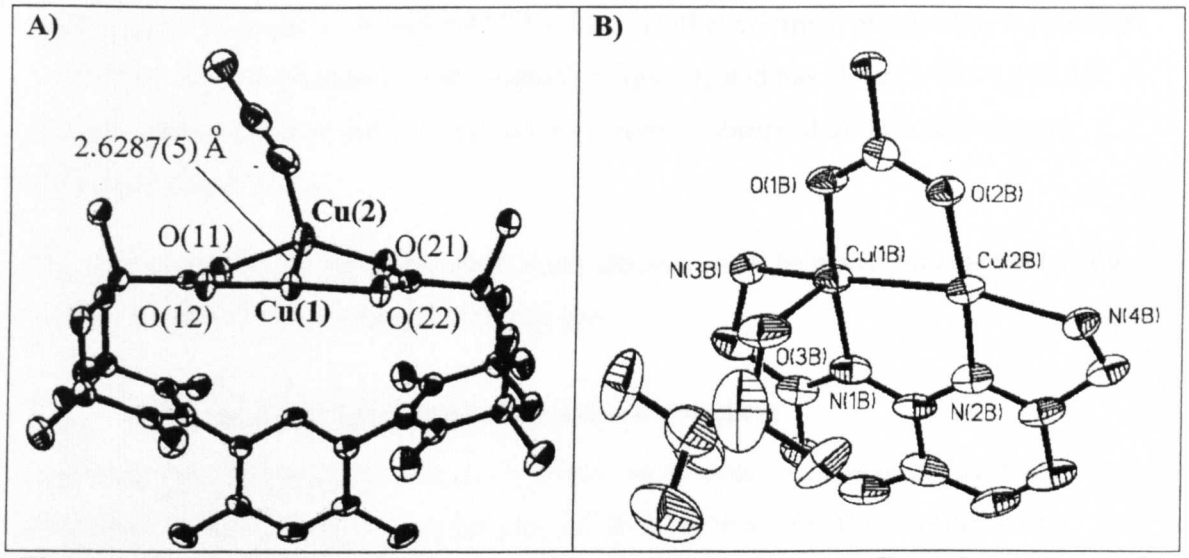

Figure 1-11: Model compounds prepared by the Lippard group. Crystal structures of A) Cu_2(XDK)MeCN, and B) the core of Cu_2(BBAN)(μ-O_2CCPh_3) triflate$_2$.

Whilst the need for anionic ligation is a limitation of these models, and the donor set is significantly different than observed in Cu_A, these models have the advantage of being able to coordinate auxiliary ligands, in the manner that an actual biosite coordinates a substrate molecule.

On the basis of the donor set, Tolman's model is the closet available model, the complex mimics the electron-delocalisation mixed valence redox state and provides the bis-thiolate bridging geometry characteristic of the Cu_A core. However the Cu-Cu distance in the model (2.93 A) is far from that in the protein (~2.6 A) with significantly less acute Cu-S-Cu bridging angles. Nelson's azacryptate series all exhibit shorter Cu-Cu interactions. The lack of any co-ordinate bridging ligands implicates Cu-Cu bonding as the origin of the strong Cu-Cu interaction.

These complexes thus model different elements of the Cu_A site.

1.3.6. Tetracopper Complexes - Potential Cu_Z Site Models

Since the structural determination of the Cu_Z site in 2000 (84), interest has increased regarding the preparation of higher nuclearity N-donor complexes of copper as potential models for this site. Trinuclear clusters were already under investigation as models for the trinuclear sites such as found in laccase and ascorbate oxidase, and tetranuclear copper(I) complexes were known in a variety of different situations: a pendant arm pyridine based macrocycle (120) (planar array of ions with > 7 Å internuclear separation); a more closely bound, hydroxo bridged N-donor macrocycle (121), also with a planar array of ions separated by 3.26-3.45 Å; a planar array of ions with N-donation from bridging thiadiazole

ligands, and Cu-Cu of 3.096 and 3.412 Å (122). Another complex prepared by Rasmussen *et al* (123) combines N-donors with bridging S ligation, and has close (2.766-2.955 Å) internuclear separations, and is luminescent - a feature observed in dinuclear average valence complexes.

We expect that over the next few years, many advances will be made towards models for this newly determined, and highly unusual site.

1.4. Introduction to Magnetic Resonance Imaging

Since its initial development in the early 1980s, the diagnostic technique Magnetic Resonance Imaging (MRI) has become one of the most powerful tools available to medicine today, being able to detect soft tissue in a harmless and non-invasive way, and giving an insight into the human body with an image quality previously undreamt of.

1.4.1. Magnetic Resonance Theory

The principles behind the MRI technique used in diagnostic medicine are similar to those of Nuclear Magnetic Resonance (NMR) as used in investigative chemistry. Unlike NMR, practical medical imaging is restricted at present to water protons. Firstly because H^+ are the most sensitive of all nuclei and secondly because water forms on average 60% by mass of the human body and therefore is one of the most abundant nuclei present in the body (124).

The proton has a spin I= 1/2 which generates in a magnetic field (2I+1) two energy states which are characterised by the nuclear spin quantum number $M_I = +1/2$ and $M_I = -1/2$ and are separated by an amount which is field dependent.

In the absence of a magnetic field these states are degenerate and therefore equally populated, but on application of a magnetic field they become non degenerate, with the lower energy level in NMR parallel to the applied field (corresponding to $M_I = +1/2$) and the upper state ($M_I = -1/2$) antiparallel to the field.

These states are unequally populated, with the relative populations described by a Boltzmann distribution. The NMR phenomenon occurs when nuclei aligned with the applied field are induced to absorb energy and change their spin orientation with respect to their applied field. Irradiation at an appropriate radio frequency (which is applied perpendicular to the magnetic field) causes displacement or perturbation of the induced magnetization from the applied field, which in turn causes a torque force to be generated,

resulting in precession of the spin (Larmour precession). After perturbation the system will behave like any other physical system and return to equilibrium. The return to equilibrium is not instantaneous but usually occurs with a first order rate constant via spin - lattice and spin - spin relaxation.

1.4.1.1. Spin - lattice relaxation (T_1)

Spin-lattice relaxation occurs via interactions between the spin nuclei and the random magnetic fields of the surroundings or lattice (which originate in the rotations and the translations (but not vibrations which are too high in frequency) of the surroundings. This only applies to the component of the magnetic moment which lies in the same dimension as the applied field (usually defined as the z axis), and can occur via a number of mechanisms, such as dipole-dipole interactions with other nuclei. The rate of this relaxation is usually described by T_1, which is in effect the half life time required for a perturbed system of a nucleus to reach equilibrium conditions.

For the ^1H or ^{13}C nuclei in diamagnetic molecules in solution T_1 is of the order of a few seconds.

1.4.1.2. Spin-spin relaxation (T_2)

The components of magnetic moment perpendicular to the applied field (*i.e.* in the x and y dimensions) will also relax to equilibrium, however these can also be affected by an additional contribution to relaxation which involves the upper state transferring its energy to neighbouring identical nuclei by mutual exchange of spin. The relaxation rate constant in the xy plane is characterised by T_2 – small T_2 results in a broad line in the spectrum, and large T_2 a sharp line.

The rate of absorption (resonance) is consequently governed by the rate of relaxation of the protons to the ground state, which in turn relates to the intensity of signal (124, 125). Water protons have a naturally fast relaxation rate and this can be enhanced or catalysed by the close proximity of a paramagnetic ion such as Mn(II), Fe(III), Cr(III), Cu(II) or Gd(III) (126).

Essentially, the theory behind MRI is the same as that of NMR, but the presence of gradient coils creates a different field at each of thousands of points in a volume of tissue, causing the water protons to resonate at slightly different frequencies, producing at each

point a spatially encoded signal which a computer can then decode to produce a digital image (127).

1.4.2. Contrast Agents

One of the earliest observations in NMR spectroscopy was that addition of a paramagnetic species caused significant broadening of the signal. The degree of broadening reflects the extent of the interaction between the unpaired electron and the nucleus in question. Fast relaxing unpaired electrons provide efficient pathways for the nucleus to relax. The nuclear relaxation rate enhancement involves the two mechanisms introduced above (and described by T_1 and T_2).

These parameters govern the signal intensity in an image: decreasing T_1 results in increased signal intensity, decreasing T_2 causes a decrease in intensity of the signal (via line broadening). The conditions under which the experiment is performed influence the relative importance of T_1 and T_2, and are usually chosen so that T_1 dominates.

The relaxation times of water protons are decreased typically by a factor of 10^6 when the oxygen atom of a water molecule becomes coordinated to a highly paramagnetic metal ion such as Gd^{+3}. Relaxation catalysis is governed by a second order rate constant called *relaxivity* which describes the ability of a paramagnetic compound to catalyse relaxation of bulk water protons. This process is affected by the magnitude of the dipole- dipole interactions between the electron spin on the metal and the proton spin of the water molecule coordinated to the metal. Since the efficiency of the relaxation by the local magnetic field produced by the paramagnetic ion falls off with distance, it is important to consider the effects of random translational diffusion of the solvent molecules which bring the nuclei in contact with the paramagnetic ion, as well as the chemical interaction. The contributions to water proton relaxation can be classified as:

Case A of relaxation is often termed as innersphere relaxation and arises when the water molecule is reversibly bound to the ion through its oxygen donor atom, but is still in contact with bulk solvent molecules.

Case B and C of relaxation are often classed as outersphere contributions, and arise through hydrogen bonded water protons (class B) and translational diffusion (class C). These are much more complex effects, and have been less investigated than the inner sphere mechanism. The need for in vivo stability has led to the design of multidentate ligands which tightly complex the paramagnetic ion, thus reducing the number of water

molecules coordinated directly on to the metal, and therefore the innersphere contribution to relaxation. Studies of these new agents have shown that outersphere contributions to relaxation play a more significant role than previously accredited (126).

Transition metal complexes as contrast agents may also offer advantages in terms of tissue specificity (e.g. a porphyrin complex of Mn(II) is being investigated for its potential as an avid tumour agent (128). The bulk of investigations into paramagnetic contrast agents have concentrated on complexes of Gd(III) due to its seven unpaired electrons which combine to give a large magnetic moment with a large relaxivity. In more recent times, attention has turned to the less paramagnetic Mn(II), due to its lower cost, and intrinsically lower toxicity.

Desirable characteristics for a complex to be used as a contrast agent are:

1. Long shelf life.

2. Water solubility; as the complex must be administered intravenously and distributed via the blood plasma into the body's extracellular space, a diagnostic dosage of between 0.1-0.2 mmol/Kg is usual, water solubility is an essential feature of a complex.

3. High thermodynamic stability constants for the complexes and a selectivity towards the coordinated ion, in order to minimise replacement by such ions as Mg(II), Ca(II) or Zn(II) which are present in high concentrations in the human plasma. Kinetic inertness towards dissociation is also a desirable feature, as the free ligand itself can act as a scavenger for those metals which are essential for the biochemistry of the body, and the liberated ions may lead to toxic effects.

4. It is advantageous that the complex is of neutral charge in order to minimise problems of osmolality, although this is not an essential factor.

5. Fast excretion from the body, in order to minimise the potential for toxic side effects.

6. Reversible binding of water molecules in the inner co-ordination sphere with rapid exchange between this region and bulk water (such complexes have been observed to have the most effective enhancement of water proton relaxation).

7. Theoretical calculations show that increasing the number of solvent molecules reversibly bound to the paramagnetic species, and decreasing the binding distance, increases the enhancement of relaxation (2).

1.5. References

1. Nelson, J., V. McKee, and G. Morgan, Progress in Inorganic Chemistry, 1998. **47**: p. 167-316.

2. Martin, N., *Azacryptand hosts for transition, main group, and lanthanide cations* PhD Thesis. 1996: Queen's University Belfast.

3. Coyle, J.L., *Trigonal Based Copper Sites - A Natural Situation* PhD Thesis. 1999: The Open University.

4. Maubert, B., *Cryptand Receptors for Anions and Cations* PhD Thesis. 2000: The Open University.

5. Curtis, N.F., Journal of the Chemical Society, 1960: p. 4409.

6. Thompson, M.C. and D.H. Busch, Journal of the American Chemical Society, 1964. **86**: p. 3651.

7. Pedersen, C.J., Journal of the American Chemical Society, 1967. **89**: p. 7017.

8. Dietrich, B., J.-M. Lehn, and J.-P. Sauvage, Tetrahedron Letters, 1969. **34**: p. 2885-2888.

9. Su, A.C.L. and J.F. Weiher, Inorganic Chemistry, 1968. **7**: p. 176.

10. Arnaud-Neu, F., B. Speiss, and M.J. Schwing-Weill, Helvetica Chimica Acta, 1977. **60**: p. 2633.

11. Anderegg, G., Helvetica Chimica Acta, 1981. **64**: p. 1790.

12. Almassio, M.C., F. Arnaud-Neu, and M.J. Schwing-Weill, Helvetica Chimica Acta, 1983. **66**: p. 1293.

13. Dietrich, B., J.-M. Lehn, and J.-P. Sauvage, Tetrahedron Letters, 1969. **34**: p. 2889-2892.

14. deSilva, A.P., H.Q.N. Gunaratne, T. Gunnlaugsson, A.J.M. Huxley, C.P. McCoy, J.T. Rademacher, and T.E. Rice, Chemical Reviews, 1997. **97**: p. 1515-1566.

15. Lehn, J.M., Science, 1985. **227**: p. 849-856.

16. Lehn, J.M., Pure and Applied Chemistry, 1979. **51**: p. 979.

17. Montanari, F., D. Landini, and F. Rolla, Topics in Current Chemistry, 1982. **101**: p. 147.

18. Quinci, S., P.L. Anelli, H. Molinari, and T. Beringhelli, Pure and Applied Chemistry, 1986. **58**: p. 1503.

19. Lehn, J.M. and F. Montavon, Helvetica Chimica Acta, 1978. **61**: p. 67.

20. Lehn, J.M., Pure and Applied Chemistry, 1980. **50**: p. 2441.

21. Cabbiness, D.K. and D.W. Margerum, Journal of the American Chemical Society, 1970. **92**: p. 2151.

22. Busch, D.H., K. Farmery, V. Goedken, V. Katovic, A.C. Melnyk, C.R. Seperati, and N. Tokel, *Bioinorganic Chemistry*. Advanced Chemistry Series. 1971.

23. Cabbiness, D.K. and D.W. Margerum, Journal of the American Chemical Society, 1969. **91**: p. 6540.

24. Lehn, J.M. and J.P. Sauvage, Journal of the American Chemical Society, 1975. **97**: p. 6700.

25. Dietrich, B., M.W. Hosseini, J.M. Lehn, and R.B. Sessions, Helvetica Chimica Acta, 1985. **68**(2): p. 289-299.

26. Newkome, G.R., V.R. Majestic, and F.R. Fronczek, Tetrahedron Letters, 1981. **22**(32): p. 3035-3038.

27. Fenton, D.E., Pure and Applied Chemistry, 1986. **58**(11): p. 1437-1444.

28. Lindoy, L., *The Chemistry of Macrocyclic Ligand Complexes*. 1989, Cambridge: Cambridge University Press.

29. Dietrich, B., P. Viouand, and J.M. Lehn, *Cambridge V.C. 11*. 1993.

30. Patai, S., *The Chemistry of the Carbon-Nitrogen Double Bond*. 1970, New York: Interscience.

31. McKee, V., M.R.J. Dorrity, J.F. Malone, D. Marrs, and J. Nelson, Journal of the Chemical Society: Chemical Communications, 1992(4): p. 383-386.

32. Nelson, S.M., Pure and Applied Chemistry, 1980. **52**: p. 2461.

33. MacDowell, D. and J. Nelson, Tetrahedron Letters, 1988. **29**(3): p. 385-386.

34. McKillop, K., PhD Thesis. 1987: The Queen's University of Belfast.

35. Shriver, D.F., A. P.W., and C.H. Langford, *Inorganic Chemistry*. 1990, Oxford, Melbourne, Tokyo: Oxford University Press.

36. Cotton, F.A. and G. Wilkinson, *Advanced Inorganic Chemistry*. 2nd ed. 1966, London: Interscience Publishers.

37. Cotton, F.A., G. Wilkinson, and P.L. Gaus, *Basic Inorganic Chemistry*. 2nd ed. 1987, Chichester: John Wiley and Sons.

38. Orgel, L.E., *An Introduction to Transition Metal Chemistry*. 1967, London: Metheven and Co Ltd.

39. Smith, T.D. and J.R. Pilbrow, Coordination Chemistry Reviews, 1974. **13**: p. 178.

40. Banwell, C.N., in *Fundamentals of Molecular Spectroscopy*. 1983, McGraw-Hill: Berkshire.

41. Marrs, D., PhD Thesis. 1990: The Open University.

42. Sorrell, T.N. and D.L. Jameson, Journal of the American Chemical Society, 1983. **105**: p. 6013.

43. Eller, P.G., D.C. Bradley, M.D. Hursthouse, and D.W. Meek, Coordination Chemistry Reviews, 1977. **24**: p. 1.

44. Jardine, F.H., Advances in Inorganic Radiochemistry, 1975. **17**: p. 115.

45. Sakaguchi, U. and A.W. Addison, Journal of the Chemical Society: Dalton Transactions, 1978: p. 600.

46. Yokoi, H. and A.W. Addison, Inorganic Chemistry, 1977. **16**: p. 1341.

47. Hemmerich, P., in *Biochemistry of Copper*, J. Peisach, P. Aisen, and W.E. Blumberg, Editors. 1966, Academic Press: New York, London. p. 15-35.

48. Lide, D., ed. *CRC Handbook of Chemistry and Physics*. 77th ed. . Vol. 1. 1996, CRC Press: Boca Raton.

49. Robin, M.B. and P. Day, Advances in Inorganic Radiochemistry, 1967. **10**: p. 247-405.

50. Hendrickson, D.N., R.C. Long, Y.T. Hwang, and H.R. Chang, in *Biological and Inorganic Copper Chemistry*, K.D. Karlin and J. Zubieta, Editors. 1983, Adenine Press: New York. p. 223-237.

51. Gatteschi, D., C. Mealli, and L. Sacconi, Inorganic Chemistry, 1976. **15**: p. 11.

52. Gagne, R.R., C.A. Koval, T.J. Smith, and M. Cimolino, Journal of the American Chemical Society, 1979. **16**: p. 4571-4580.

53. Westmoreland, T.D., D.E. Wilcox, M.J. Baldwin, W.B. Mimms, and E.I. Solomon, Journal of the American Chemical Society, 1989. **111**: p. 6106-6123.

54. Dunaj-Jurco, M., G. Ondrejovic, and M. Melnik, Coordination Chemistry Reviews, 1988. **83**: p. 1-28.

55. Hubberstey, P. and C.E. Russell, Journal of the Chemical Society: Chemical Communications, 1995: p. 959.

56. Blondin, G. and J. Girerd, Chemical Reviews, 1990. **90**: p. 1359-1376.

57. Hush, N.S. and J.R. Reimers, Abstracts Of Papers Of The American Chemical Society, 1990. **200**: p. 87-88.

58. Lancashire, R., *Silver*, in *Comprehensive coordination chemistry*. 1987, Pergamon.

59. O'Keefe, B. and P. Steel, Inorganic Chemistry Communications, 2000. **3**: p. 473-475.

60. Hartshorn, C. and P. Steel, Inorganic Chemistry Communications, 2000. **3**: p. 476-481.

61. Singh, K., J. Long, and P. Stavropoulos, Journal of the American Chemical Society, 1997. **119**: p. 2942-2943.

62. Angaridis, P., P. Baran, R. Raptis, C. Raptopolou, and A. Terzis, Unpublished data, 2000.

63. Burrows, A.D., M.F. Mahon, and M.T. Palmer, Journal of the Chemical Society-Dalton Transactions, 1998(12): p. 1941-1942.

64. Eastland, G., M. Mazid, D. Russell, and M. Symons, Journal of the Chemical Society: Dalton Transactions, 1980: p. 1682-1687.

65. Giraudeau, A., J. Gisselbrecht, M. Gross, and J. Weiss, Journal of the Chemical Society: Chemical Communications, 1993(13): p. 1103-1105.

66. Bielmann, M., P. Schwaller, P. Ruffieux, O. Groning, L. Schlapbach, and P. Groning, Physical Review B, 2002. **65**: p. 235431-1-5.

67. Howarth, O., G. Morgan, V. McKee, and J. Nelson, Journal of the Chemical Society-Dalton Transactions, 1999. **12**(June 21): p. 2097-2102.

68. Takemura, H., N. Kon, K. Tani, K. Takehara, J. Kimoto, T. Shinmyozu, and T. Inazu, Journal of the Chemical Society: Perkin Transactions, 1997: p. 239-246.

69. Baenziger, N. and A. Struss, Inorganic Chemistry, 1976. **15**(8): p. 1807-1809.

70. Amoroso, A.J., J.C. Jeffery, P.L. Jones, J.A. McCleverty, E. Psillakis, and M.D. Ward, Journal of the Chemical Society-Chemical Communications, 1995(11): p. 1175-1176.

71. Drew, M., D. Farrell, G. Morgan, V. McKee, and J. Nelson, Journal of the Chemical Society-Dalton Transactions, 2000. **9**: p. 1513-1519.

72. Pyykko, P., Chemical Reviews, 1997. **97**: p. 597-636.

73. Orgel, L., Journal of the Chemical Society, 1958: p. 4186.

74. Jansen, M., Angewandte Chemie, 1987. **26**: p. 1098-1110.

75. Cotton, F., X. Feng, M. Matusz, and R. Poli, Journal of the American Chemical Society, 1998. **110**: p. 7077-7083.

76. Poblet, J. and M. Benard, Chemical Communications, 1998: p. 179-180.

77. Che, C.-M., Z. Mao, V. Miskowski, M.-C. Tse, C.-K. Chan, K.-K. Cheung, D. Phillips, and K.-H. Leung, Angewandte Chemie, 2000. **39**(22): p. 4084-4088.

78. Solomon, E.I., M.J. Baldwin, and M.D. Lowery, Chemical Reviews, 1992. **92**: p. 521-542.

79. Kaim, W. and J. Rall, Angewandte Chemie, 1996. **35**: p. 43.

80. Lippard, S.J. and J.M. Berg, *Principles of Bioinorganic Chemistry*. 1994, Mill Valley, California: University Science Books.

81. Malkin, R. and B.G. Malmstrom, Advances in Enzymology, 1970. **33**: p. 177-244.

82. Allendorf, M.D., D.J. Spira, and E.I. Solomon, Proceedings of the National Academy of Science, USA, 1985. **82**: p. 3063.

83. Beinert, H.E., in *Biochemistry of Copper*, J. Peisach, P. Aisen, and W.E. Blumberg, Editors. 1966, Academic Press: New York, London. p. 213-234.

84. Brown, K., M. Tegoni, M. Prudencio, A.S. Pereira, S. Besson, J.J. Moura, I. Moura, and C. Cambillau, Nature Structural Biology, 2000. **7**(3): p. 191-195.

85. Sykes, A.G., Advances in Inorganic Chemistry, 1991. **36**: p. 377.

86. McKee, V., Advances in Inorganic Chemistry, 1993. **40**: p. 323.

87. Solomon, E.I., B.L. Hemming, and D.E. Root, in *Bioinorganic Chemistry of Copper*, K.D. Karlin and Z. Tyeklar, Editors. 1993, Chapman and Hall: New York. p. 3-20.

88. Adman, E.T., Advances in Protein Chemistry, 1991. **42**: p. 145-197.

89. Kroneck, P.M.H., W.E. Antholine, H. Koteich, D.H.W. Kastrau, F. Neese, and W.G. Zumft, in *Bioinorganic Chemistry of Copper*, K.D. Karlin and Z. Tyeklar, Editors. 1993, Chapman and Hall: New York. p. 419-426.

90. Blackburn, N.J., M.E. Barr, W.H. Woodruff, J. van der Oost, and S. de Vries, Biochemistry, 1994. **33**: p. 10401.

91. Holm, R.H., P. Kennepohl, and E.I. Solomon, Chemical Reviews, 1996. **96**: p. 2239-2314.

92. Neese, F., PhD Thesis. 1996: Konstanz University, Germany.

93. Tsukihara, T., H. Aoyama, E. Yamashita, T. Tomizaki, H. Yamaguchi, K. Shinzawa-Itoh, R. Nakashima, R. Yaono, and S. Yoshikawa, Science, 1995. **269**: p. 1069-1074,

94. Wilmanns, M., P. Lappalainen, M. Kelly, E. Sauer-Eriksson, and M. Saraste, Proceedings of the National Academy of Science, USA, 1995. **92**: p. 11955-11959.

95. Dooley, D.M., M.A. McGuirl, A.C. Rosenzweig, J.A. Landin, R.A. Scott, W.G. Zumft, F. Devlin, and P.J. Stephens, Inorganic Chemistry, 1991. **30**: p. 3006-3011.

96. Antholine, W.E., D.H.W. Kastrau, G.C.M. Steffens, G. Buse, W.G. Zumft, and P.M.H. Kroneck, European Journal of Biochemistry, 1992. **209**: p. 875.

97. Farrar, J.A., F. Neese, P. Lappalainen, P.M.H. Kroneck, M. Saraste, W.G. Zumft, and A.J. Thomson, Journal of the American Chemical Society, 1996. **118**: p. 11501-11514.

98. Wallace-Williams, S.E., C.A. James, S. de Vries, M. Saraste, P. Lappalainen, J. van der Oost, M. Fabian, G. Palmer, and W.H. Woodruff, Journal of the American Chemical Society, 1996. **118**: p. 3986-3987.

99. Andrew, C.R., J. Han, S. de Vries, J. van der Oost, B.A. Acerill, T.M. Loehr, and J. Sanders-Loehr, Journal of the American Chemical Society, 1995. **116**: p. 10805-10806.

100. Andrew, C.R., L. P., M. Saraste, M.T. Hay, L. Y., C. Dennison, G.W. Canters, J.A. Fee, C.E. Slutter, N. Nakamura, and J. Sanders-Loehr, Journal of the American Chemical Society, 1995. **117**: p. 10759-10760.

101. Farrar, J., W. Zumft, and A. Thomson, Proceedings of the National Academy of Science, U. S. A., 1998. **95**: p. 9891-9896.

102. Rasmussen, T., B. Berks, J. Sanders-Loehr, D. Dooley, W. Zumft, and A. Thomson, Biochemistry, 2000. **39**: p. 12753-12756.

103. Haltia, T., K. Brown, M. Tegoni, C. Cambillau, M. Saraste, and K. Djinovic-Carugo, J. Inorg. Biochem., 2001. **86**: p. 246.

104. Chen, P., S. George, I. Cabrito, W. Antholine, J. Moura, I. Moura, B. Hedman, K. Hodgson, and E. Solomon, Journal of the American Chemical Society, 2002. **124**: p. 744-745.

105. Solomon, E.I., in *Copper Coordination Chemistry: Biochemical and Inorganic Perspectives*, K.D. Karlin and J. Zubieta, Editors. 1983, Adenine Press: New York. p. 1-92.

106. Fenton, D.E., Pure and Applied Chemistry, 1989. **61**(5): p. 903-908.

107. Hill, H.A.O., Chemistry in Britain, 1976. **12**: p. 119.

108. Larsson, S., B. Kallebring, P. Wittung, and B.G. Malmstrom, Proceedings of the National Academy of Science, USA, 1995. **92**: p. 7167.

109. Beinert, H., European Journal of Biochemistry, 1997. **245**: p. 521-532.

110. Farrar, J.A., P. Lappalainen, W.G. Zumft, M. Saraste, and A.J. Thomson, European Journal of Biochemistry, 1995. **232**: p. 294-303.

111. Harding, C., V. McKee, and J. Nelson, Journal of the American Chemical Society, 1991. **113**: p. 9684.

112. Chanda, R.K., R. Kumar, and D.G. Tuck, Canadian Journal of Chemistry, 1987. **665**: p. 1336-1342.

113. Houser, R.P. and W.B. Tolman, Abstracts of papers of the American Chemical Society, 1994. **208**: p. 350.

114. Harding, C., J. Nelson, M.C.R. Symons, and J. Wyatt, Journal of the Chemical Society: Chemical Communications, 1994: p. 2499.

115. Farrar, J.A., R. Grinter, F. Neese, J. Nelson, and A.J. Thomson, Journal of the Chemical Society: Dalton Transactions, 1997: p. 4083-4087.

116. LeCloux, D.D. and S.J. Lippard, Inorganic Chemistry, 1997. **36**(18): p. 4035-4046.

117. LeCloux, D.D., R. Davydov, and S.J. Lippard, Inorganic Chemistry, 1998. **37**(26): p. 6814-6826.

118. LeCloux, D.D., R. Davydov, and S.J. Lippard, Journal of the American Chemical Society, 1998. **120**: p. 6810-6811.

119. He, C. and S. Lippard, Inorganic Chemistry, 2000. **39**: p. 5225-5231.

120. Ziessel, R. and M.-T. Youinou, Angewandte Chemie, 1993. **32**(6): p. 877-880.

121. McKillop, K.P., S.M. Nelson, J. Nelson, and V. McKee, Journal of the Chemical Society: Chemical Communications, 1988: p. 387-389.

122. Maekawa, M., M. Munakata, T. Kuroda-Sowa, Y. Suenaga, and K. Sugimoto, Inorganica Chimica Acta, 1999. **290**: p. 153-158.

123. Rasmussen, J., H. Toftlund, A. Nivorzhkin, J. Bourassa, and P. Ford, Inorganica Chimica Acta, 1996. **251**: p. 291-298.

124. Saunders, J. and B. Hunter, in *Modern NMR Spectroscopy*. 1988, Oxford University Press: Oxford.

125. Drew, M., O. Howarth, C. Harding, H. Wiebster, N. Martin, and J. Nelson, Journal of Inorganic Biochemistry, 1995. **217**.

126. Lauffer, R., Chemical Reviews, 1987. **87**: p. 901-927.

127. Choppin, G.R. and J.-C.G. Bunzli, *Lanthanide Probes in Life, Medicinal and Environmental Sciences*. 1989, Amsterdam: Elsevier.

128. Koenig, S., R. Brown, and M. Spiller, Magnetic Resonance in Medicine, 1987. **4**: p. 252-260.

2. Di- and tri- silver(I) cryptates

The small cryptand imBT (Figure 2-1 A), was first prepared using a template procedure by Hunter (1), although the reduced analogue, amBT (Figure 2-1 B) had been reported earlier from a direct preparation of the free ligand (2). With only a 2 carbon spacer, these are among the smallest macrobicycles, one result of which is a necessarily short internuclear separation of the cations in their dicopper and disilver cryptates.

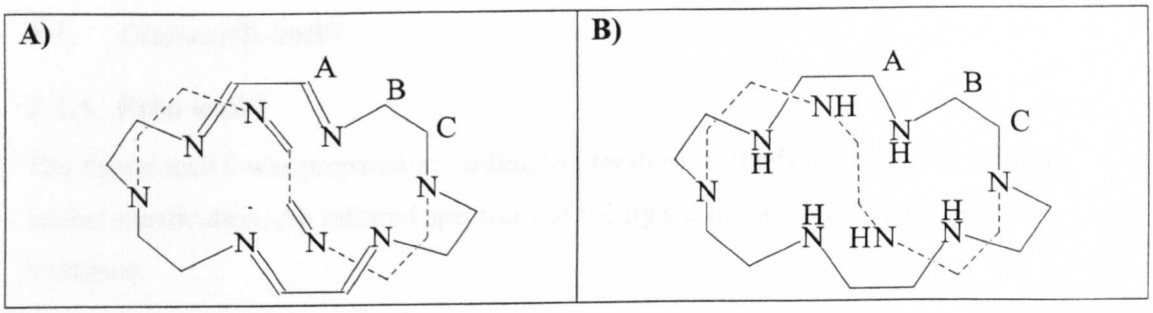

Figure 2-1: The ligands A) imBT and B) amBT which incorporate a two carbon spacer, with a tren-derived cap.

In the case of dicopper(I) imBT (see Chapter 3) the separation is 2.448 Å (Table 2-1), less in fact than is observed in the elemental form. How surprising then to discover that silver(I), with a 0.38 Å larger ionic radius than copper(I), forms not only a di-, but also a trisilver cryptate.

Table 2-1: Comparison of data for metallic, ionic, and cryptated forms of copper(I) and silver(I).

Ion	Ionic radius /Å	M-M - metallic form /Å	M-M for M_2 imBT cryptate /Å	M-M for M_2 amBT cryptate /Å
Cu(I)	0.77	2.56	2.448	Cryptate not known
Ag(I)	1.15	2.89	2.84	2.816

This chapter presents detailed studies of the silver(I) imBT/amBT system, including structural studies (X-ray crystallographic, and computer modelling), as well as spectroscopic (infrared, UV/Vis, solution and solid state NMR) and electrochemical (cyclic voltammetry) investigations.

The aim of this work was to understand the factors controlling the formation and stability of these unforeseen structures, and especially whether argentophilicity contributes to the stabilisation.

In the analogous dicopper cryptates, an average valence dicopper(1.5) form is observed in addition to the dicopper(I) cryptates. We were interested in whether a similar state could be attained in the disilver systems, and carried out electrochemical studies with this aim in mind. Synthetic studies were carried out with the aim of providing additional stability by sterically hindering the cavities, as decomposition was a frequent complicating factor in many of the investigations.

2.1. Disilver(I) imBT

2.1.1. Free imBT

The ligand imBT was prepared according to literature methods (3) and used without further purification. An infrared spectrum of the ligand is shown in Figure 2-2 for reference.

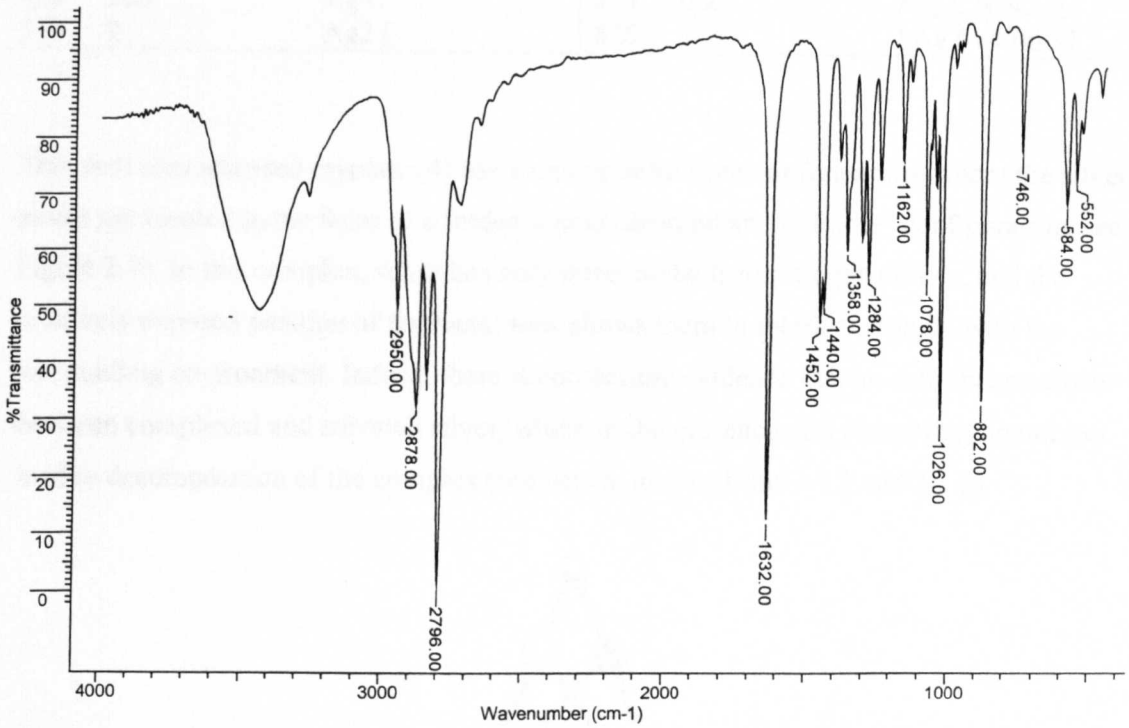

Figure 2-2: Infrared spectrum of free imBT ligand.

2.1.2. Disilver(I) imBT

The disilver cryptate was prepared from the pure ligand and silver(I) perchlorate, according to literature methods ((4), also see section 9.1.1), and its presence confirmed by a range of methods, including FAB mass spectrometry (Table 2-2).

Table 2-2: FAB mass spectrum (EPSRC service) of disilver(I) imBT perchlorate, nitro-benzyl alcohol (NOBA) internal standard, where L = imBT. Peaks of m/z 260 and 618 which have isotope patterns consistent with the presence of silver, were tentatively assigned to Ag:NOBA artefacts. A peak which is proposed to correspond to the 6+4 cryptate (marked *) was also observed (see Chapter 7).

m/z	Abundance /%	Identity	m/z	Abundance /%	Identity
260	7	*Ag NOBA*	618	8	*Ag L NOBA*
359	3	L	673	10	Ag_2 L ClO_4
465	100	Ag L	773	0.2	Ag_2 L $(ClO_4)_2$
573	2	Ag2 L	826	1	*Ag 6+4 imBT

This well characterised cryptate (4) has a unique solid state configuration, where the silver atoms are located in the faces of a folded ligand (denoted an "A-frame" configuration, see Figure 2-3). In this complex, silver has only three contacts to nitrogen donors, and the relatively exposed position of the metal ions allows them to interact strongly with the surrounding environment. Indeed, there is compelling evidence that an equilibrium exists between complexed and solvated silver, which in the presence of a competing ligand can lead to decomposition of the complex (see below, and sections 2.5.2 and 2.1.3).

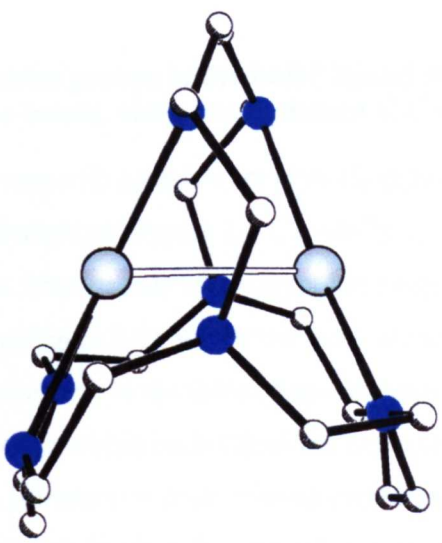

Figure 2-3: X-ray crystal structure of Ag_2 imBT (ClO_4 counterions not shown) showing the "A-frame" conformation (4).

The IR spectrum (Figure 2-5 A) shows the expected CH, perchlorate, and fingerprint region peaks, together a rather more complex imine region (Figure 2-5 B) than is observed for the dicopper complex (Figure 2-5 C, and also in Chapter 3). Infrared reference tables generally list (non-coordinated) imine peaks as occurring between 1690 and 1640 cm^{-1}, and the observed absorbances fall towards the lower end of this range. The low 1599 to

1632 cm^{-1} absorbances for the disilver and dicopper complexes may be a result of conjugation between adjacent imine groups (Figure 2-4), resulting in a weakened imine bond, or could also simply be a result of a weakened bond owing to its involvement in coordination. Alternatively, if neighbouring imine groups have a degree of conjugation, then this implies a degree of double bond character for the C-C bond, and this may be the origin of the peak near 1600 cm^{-1} (C=C stretches are normally observed between 1680 and 1620 cm^{-1}). This is consistent with the experimentally determined crystal structure of the dicopper cryptate, where the C-C bond between the two imines is 1.476 Å long – 0.2 Å shorter than the other C-C bonds in the molecule. The value of 1.476 Å is intermediate between the C-C single bond in ethane (1.54 Å) and the C=C bond in ethene (1.34 Å, (5)), and does suggest a degree of double bond character.

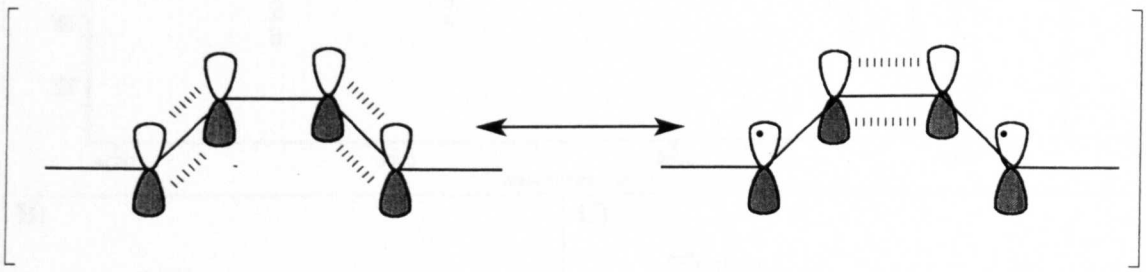

Figure 2-4: Neighbouring imine groups in the imBT ligand may be conjugated, resulting in weakened imine bonds, and a strengthened C-C bond.

All six imine bonds in the dicopper(I) complex are crystallographically equivalent, giving rise to the single 1657 cm^{-1} absorption (Figure 2-5 C), whilst in the disilver imBT complex, this degeneracy is not present. Two strands of the crypt have approximate symmetry (the lower two strands as shown in Figure 2-3), whilst the third strand is different again. The presence of four clear imine stretches in the infrared spectrum of the disilver complex also suggests that the two imine bonds within each strand are not equivalent. This is consistent with solid state NMR studies (6) where at least 5 imine carbon, and nitrogen resonances were present, with the sixth of each likely to be concealed in overlapping peaks. It would thus seem that two pairs of imine bonds (possibly the more intense IR absorptions at high wavenumber, see Figure 2-5 C) have similar stretching frequencies.

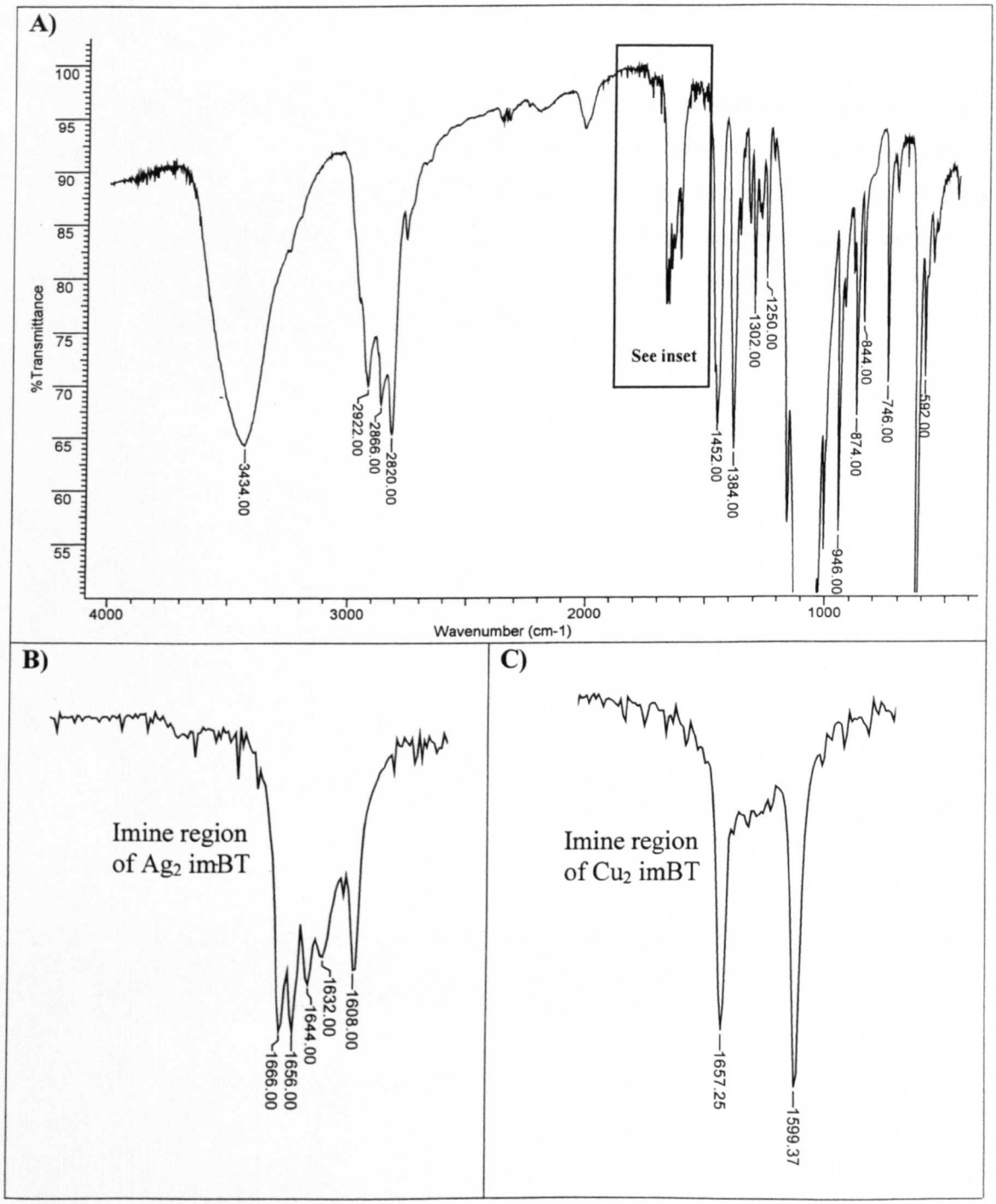

Figure 2-5: Infrared spectrum of Ag_2 imBT $(ClO_4)_2$ (KBr disk). A) The intense perchlorate features at 1094 and 622 cm^{-1} have been allowed to go off scale, other key features include CH stretches between 3000 and 2800 cm^{-1}, and a fingerprint region similar to that of free imBT ligand (Figure 2-2). B) The imine region has been expanded, and is compared to C) the imine region of the dicopper(I) complex.

NMR spectra measured for the disilver complex included samples spiked with free ligand, for comparison with NMR studies of disilver amBT (section 2.4). During preparation of these solutions the colour of the solution was observed to dramatically intensify after

addition of the free ligand, and UV/Vis studies were made in order to confirm this phenomenon (see Figure 2-6).

For two species existing independently in solution, the total absorbance is expected to be equal to the sum of the individual absorbances. In this case however, the experimentally determined spectrum of the mixture absorbs more strongly in the visible and near UV than expected, indicating that imBT and disilver imBT do not exist independently in solution. This observation was also made by Apperley et al (6), who showed clear differences between solid state and solution NMR for this system.

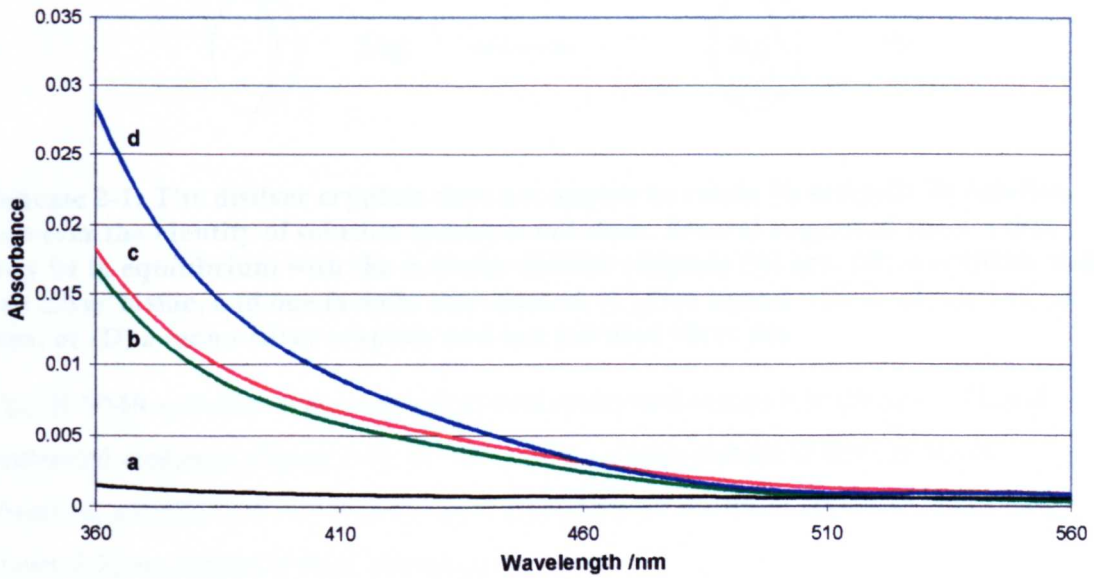

Figure 2-6: UV/Vis spectra (in acetonitrile): comparison of (a) imBT to (b) Ag_2 imBT $(ClO_4)_2$ (each 31 mmol/l). Also shown is (c) the sum of these two spectra (the expected spectrum for a 1:1 mixture of the two), and (d) the actual spectrum of a 1:1 mixture of the two.

Although no mono-silver cryptate has been isolated for this system (treatment of imBT with one equivalent of silver results in formation of the disilver cryptate regardless, (4)), the equilibrium observed would be consistent with the presence of a transient mono-silver species in solution, addition of 1 equivalent of free ligand thereby resulting in an effective doubling of the concentration of mono-silver cryptate (see Scheme 2-1 D). Subsequent electrochemical studies on this complex suggested an alternative explanation, and more discussion is given below, and in section 2.5.2.1.

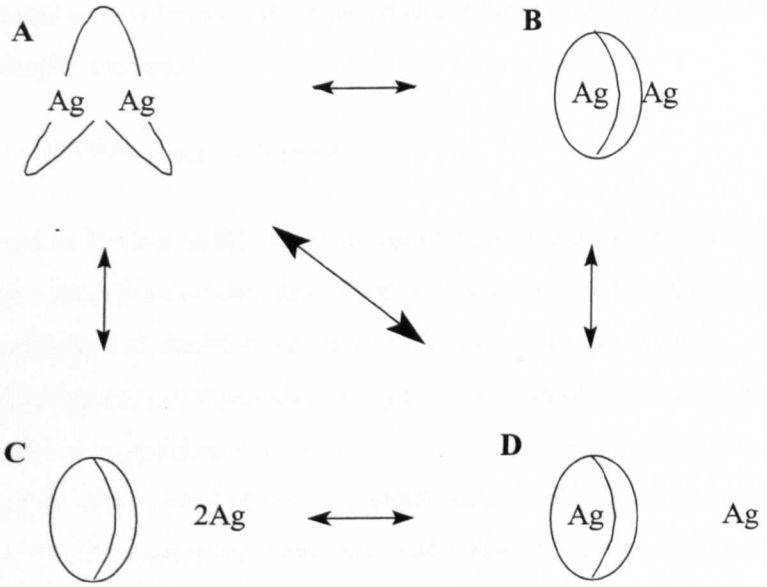

Scheme 2-1: The disilver cryptate does not appear to retain its integrity in solution, however the identity of solution species is not clear. Several suggested species that may be in equilibrium with the A-frame disilver cryptate (A) are: (B) A cryptate with one silver inside, and one facially coordinated, (C) free ligand with 2 solvated silver ions, or (D) a mono-silver cryptate and one solvated silver ion.

The ^{1}H NMR spectrum was measured in both deuterated acetonitrile (Figure 2-7), and deuterated methanol (Figure 2-8). In acetonitrile a simple pattern of three peaks is observed, a singlet and two triplets, showing that proton environments A, B, and C (see Figure 2-1) are subject to time averaging.

Addition of one equivalent of free imBT to a solution of the cryptate in acetonitrile results in a shift in the peak positions (Figure 2-7 B), indicating that the cryptate and free ligand are exchanging, consistent with previous observations and literature reports (above, and (6)).

Interpretation of the deuterated methanol spectrum (Figure 2-8) is less simple: a far more complex spectrum is observed for the cryptate (Figure 2-8 B), and the 1:1 mixture has features similar to those of both free ligand, and the pure complex, as well as some new features. Clearly the behaviour of the cryptate in methanol is different than in acetonitrile.

In order to rationalise this behaviour, let us consider three scenarios, which are not necessarily mutually exclusive:

1) $Ag_2imBT^{2+} \xrightarrow{Dissolving} Ag^+ + AgimBT^+$

Upon dissolution of disilver imBT, there is complete dissociation to form a mono-silver cryptate, and one equivalent of solvated silver (see Scheme 2-1 D). Any measurements made on this solution will therefore relate to a mixture of the two species. Addition of 1 equivalent of free ligand may then result in up to 1 equivalent more of mono-silver cryptate forming. An approximate doubling in UV/Vis absorption would be expected (as is observed), together with a more intense ^1H NMR signal, although with no shift in peak positions – this is not in agreement with observed NMR characteristics in either solvent.

2) $Ag_2imBT^{2+} \Leftrightarrow 2Ag^{2+} + imBT$

Ag_2 $imBT^{2+}$ is in equilibrium with free ligand and solvated silver (see Scheme 2-1 C). Measurements on this solution will reflect the presence of both disilver cryptate and free ligand, and the ^1H NMR may be affected by time averaging. Addition of more free ligand will push the equilibrium towards the Ag_2 $imBT^{2+}$ side, resulting in a somewhat more intense UV/Vis spectrum, and affecting the NMR spectrum either by changing the degree of time-averaging, or by affecting the ratio of disilver cryptate to free ligand signals. This is in agreement with observations in acetonitrile, but it is unclear whether it is consistent with the more complicated behaviour in methanol.

3) $Ag_2imBT^{2+} \Leftrightarrow Ag^+ + AgimBT^+$

Ag_2 $imBT^{2+}$ is in equilibrium with mono-silver cryptate and solvated silver (see Scheme 2-1 D) – thus three species are present in solution at any time, and an NMR spectrum of the solution may be affected by time averaging and therefore be solvent dependent. This is consistent with both acetonitrile (time averaged) and methanol (mono- and di-silver superimposed) spectra. Addition of free ligand will result in complexation of free silver and a concomitant shift in equilibrium, resulting in a more intense UV/Vis spectrum (as observed, see Figure 2-6 (d)). The change in proportions of the dissolved species (note that excess free ligand may also be present now) may affect a time-averaged spectrum by changing peak positions (as observed in the case of acetonitrile). In methanol, where exchange appears to be slower, a decrease in intensity of the di-silver spectrum would be expected, an increase in the mono-silver spectrum intensity, as well as features of the free

ligand. This could account for the reduced intensity of some features upon addition of free ligand and the greater intensity of others. The spectrum in Figure 2-8 (C) could then be explained as: imBT features overlaid predominantly by mono-silver cryptate. The identity of the new feature at 4.55 ppm is not explained by this model however, unless we suggest that a new ligand conformation is present (*e.g.* Scheme 2-1 B), or that it relates to a time averaging effect between the various species present.

Although not a perfect explanation, scenario 3 seems at present to be the best explanation for the observed UV/Vis and NMR characteristics. Two main strategies were attempted in order to simplify the situation (which may also be of use for the analogous amBT complex).

a) Choice of a solvent which less readily solvates silver, thereby making dissociation less favourable

b) "blocking" the vacant coordination sites of the disilver cryptate, in order to hinder interaction with solvent molecules and keep the complex intact in solution

The effect of various solvents on the electrochemical behaviour of Ag_2 imBT is described below in section 2.5.2. Attempts to attach ligands to the exposed silver ions focussed on the (more easily prepared) Ag_2 imBT system (section 2.1.3) although some trials were also made for Ag_2 amBT (section 0). This methodology was expected to be difficult to perfect, as the auxiliary ligand must be strong enough to bind to silver in the A-frame configuration, but not so strong that it strips the silver from the complex, or otherwise mediates decomposition of the complex. Use of ligands with bridging potential (*e.g.* the linear terephthalate or acetylene dicarboxylate moieties) also raises the interesting possibility of forming oligomeric or polymeric structures, and ligands with this potential were included in the investigations.

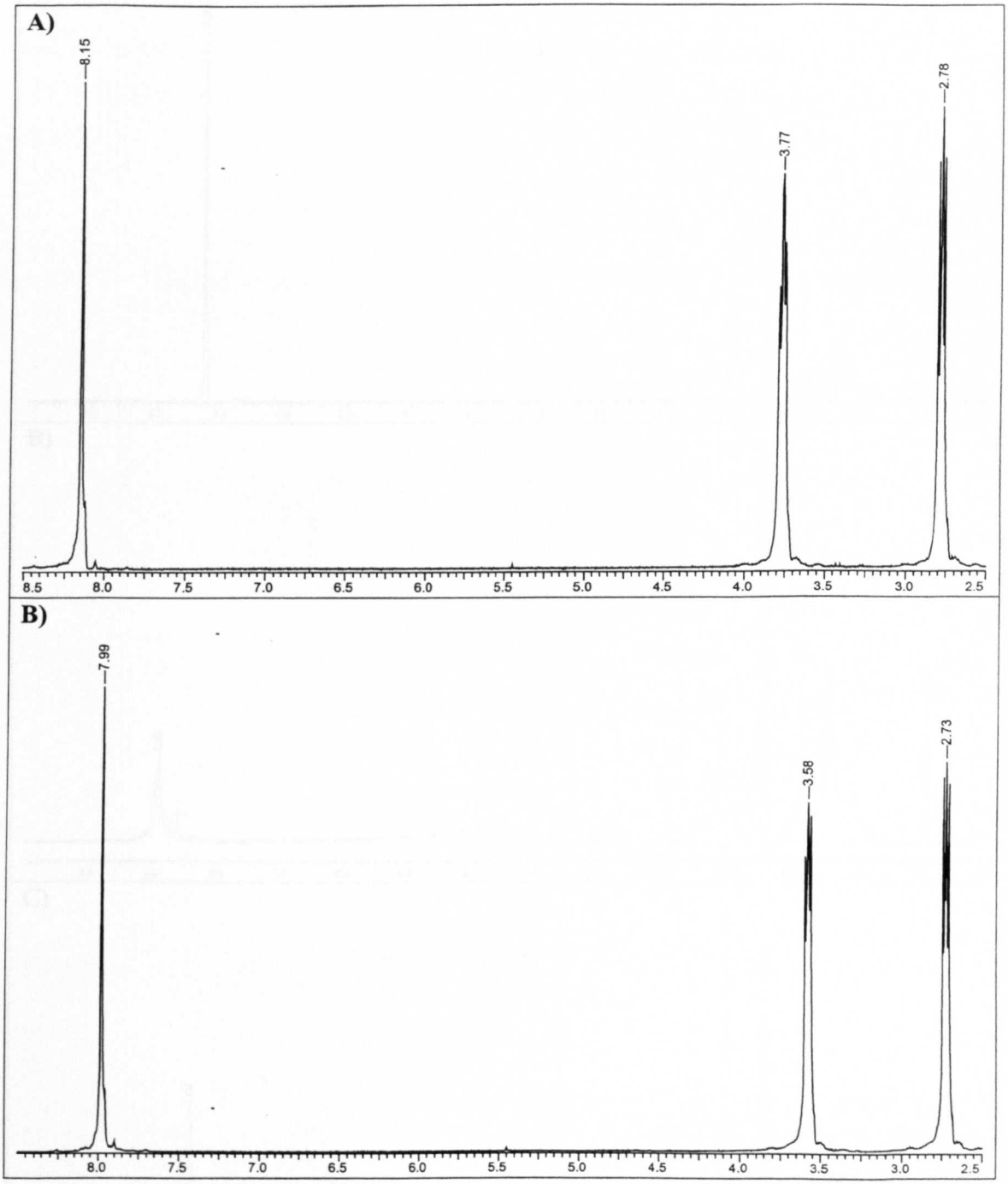

Figure 2-7: ^{1}H NMR of A) Ag_2 imBT and B) 1:1 mixture of imBT and Ag_2 imBT (CD_3CN solvent at room temperature).

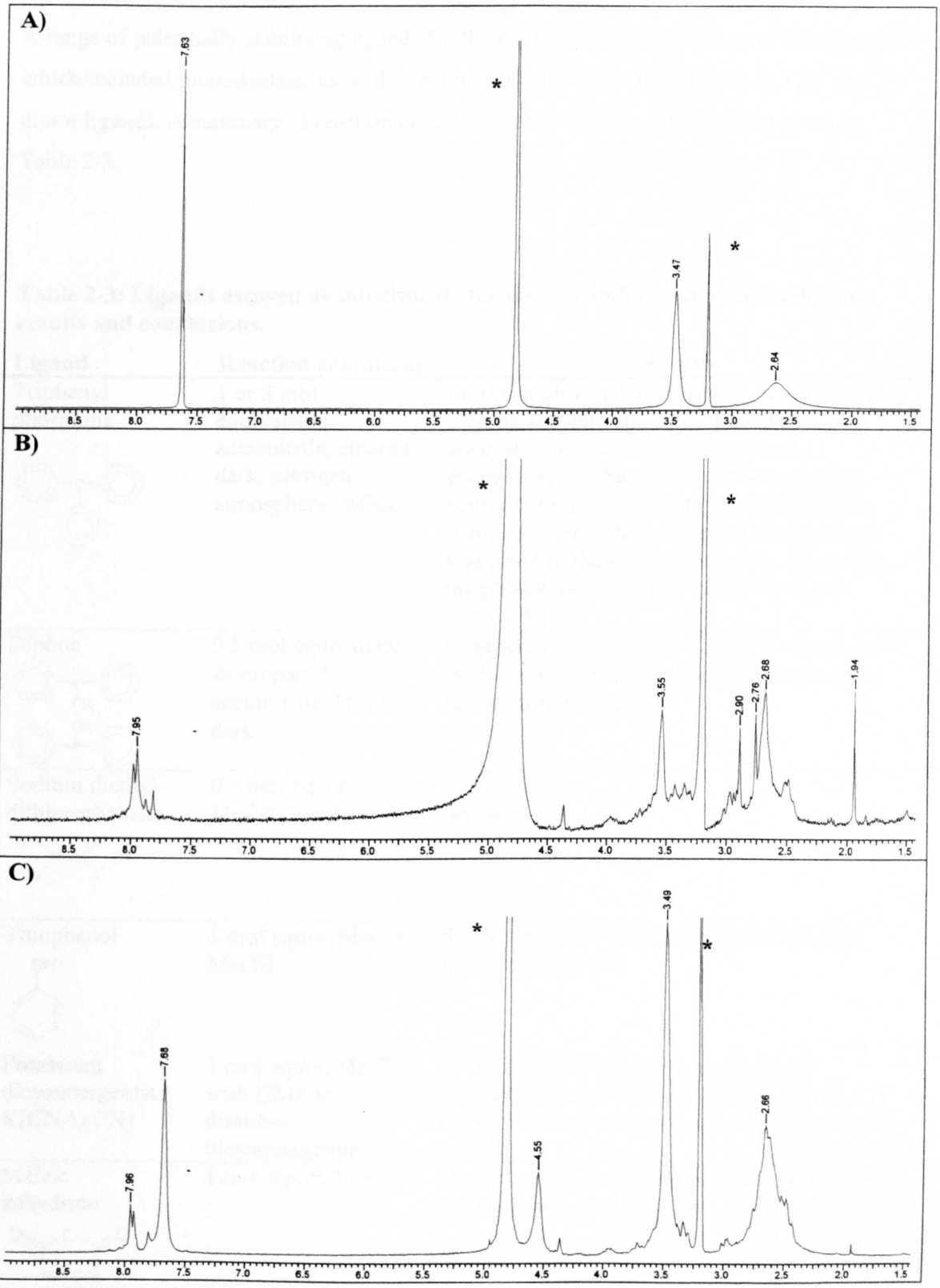

Figure 2-8: ^{1}H NMR of A) imBT, B) Ag_2 imBT, C) 1:1 mixture. CD_3OD solvent at room temperature. * = solvent related peak, TMS = tetramethylsilane internal standard.

2.1.3. Stabilisation ligand for disilver(I) imBT

A range of potentially stabilising ligands for the disilver imBT cryptate were investigated, which included monodentate, as well as potentially chelating and bridging S, P, O and N donor ligands. A summary of reaction conditions, observations and results is given in Table 2-3.

Table 2-3: Ligands essayed as substituents for disilver imBT: reaction conditions, results and conclusions.

Ligand	Reaction conditions	Results
Triphenyl phosphine 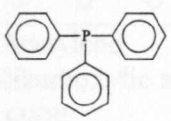	1 or 2 mol equivalents, acetonitrile, ethanol, dark, nitrogen atmosphere, reflux	Products obtained are probably mixtures of starting cryptate and silver phosphines: IR suggests presence of both crypt and phosphine, MS has peaks consistent with starting complex and with silver phosphine complex, elemental analysis of this material was close to the starting complex, suggesting the phosphine is a minor constituent, see section 9.1.2.1.
Diphos 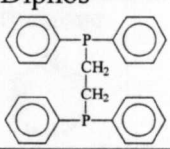	0.5 mol equivalents, isopropanol, acetonitrile, DCM, dark	Regenerates diphos and starting complex, no evidence of cryptate - phosphine interaction, see section 9.1.2.2.
Sodium diethyl-dithiocarbamate 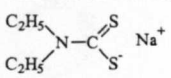	0.5 mol equiv, MeCN, MeOH	See section 9.1.2.3.
Thiophenol 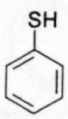	1 mol equiv, MeCN, MeOH	Silver abstracted from crypt by thiophenol, see section 9.1.2.4.
Potassium dicyanoargentate K[CNAgCN]	1 mol equiv, MeCN with DMF to dissolve dicyanoargentate	Silver cryptate with dicyanoargentate counterion formed. Crystallisation resulted in isolation of a breakdown product. See section 2.1.3.1.
Maleic anhydride 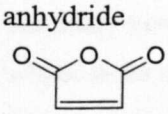	1 mol equiv, MeCN	Identity of the (unstable) product not known. See section 9.1.2.5.
Succinic acid 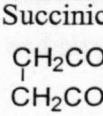	1 mol equiv, MeOH, MeCN	Product appears to break down quickly, identity not known, see section 9.1.2.6.

Ligand	Reaction conditions	Results
Adipic acid 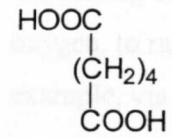	1 mol equiv, MeOH, MeCN	Unstable product, see section 9.1.2.7.
Disodium terephthalate 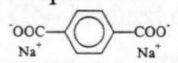	1 mol equiv, H_2O, MeCN	No interaction between carboxylate and cryptate, see section 9.1.2.8.
3-methyl glutaric acid 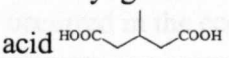	1 mol equiv, MeOH, MeCN	Product appears very unstable, see section 9.1.2.9.
Glutaric anhydride 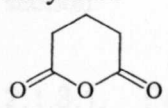	1 mol equiv, MeCN	Product probably a mixture of anhydride and cryptate, see section 9.1.2.10.
Acetylene dicarboxylic acid 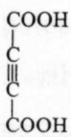	1 mol equiv, H_2O, MeCN	Potassium salt results in decomposition of organic components, leaving crystals of silver perchlorate. Free acid gives an unstable product which appears to quickly decompose in a similar manner to the other carboxylic acids used, see section 9.1.2.11.
Pyridine 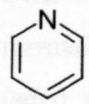	2 mol equiv, Pr^iOH, DMF	No interaction with cryptate, disilver imBT regenerated, see section 9.1.2.12.
Pyridazine 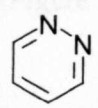	2 mol equiv, Pr^iOH, DMF	No interaction with cryptate, disilver imBT regenerated, see section 9.1.2.12.
Pyrazine 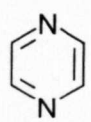	1 or 2 mol equiv, Pr^iOH, DMF	No interaction with cryptate, disilver imBT regenerated, see section 9.1.2.12.
Phenazine 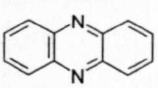	1 or 2 mol equiv, Pr^iOH, DMF	No interaction with cryptate, disilver imBT regenerated, see section 9.1.2.12.

More detail of the experiments performed is given in sections 9.1.2.1 to 9.1.2.12. In summary however, the nitrogen and phosphorous donor ligands failed to bind to silver whilst in its cryptated environment, although they may form simple silver complexes if there is free silver available in solution (*e.g.* as a result of an equilibrium between solvated and cryptated silver).

Conversely, the oxygen and sulphur donor ligands generally interact too strongly, abstracting silver from the crypt to form stable S-donor complexes, or in the case of oxygen, to rapidly decay to inorganic silver with by-products from the organic ligands (for example, via acidic attack at the imine bond).

The only exception is dicyanoargentate, which rather than forming the hoped-for -CN-Ag-CN- bridged dimer or polymer, appears to have resulted in a cryptate with cyanide counterion. The change in colour observed during the reaction suggests that a change has occurred in the coordination sphere of silver, although no X-ray structure is available to support this. Further studies on the silver cyanide cryptate are described in the following section.

2.1.3.1. Potassium dicyanoargentate

The linear dicyanoargentate ion can behave in several different ways (7), and has the potential to form a bridge between two cryptate molecules. Thus, the possibility of forming a –silver cryptate-cyanide-silver-cyanide-silver cryptate--- polymer made this ion of particular interest to us. The insolubility of the potassium salt required it to be dissolved in DMF before addition to the disilver cryptate (use of water to dissolve the anion resulted in formation of a silver mirror). The yellow colour of the solution initially intensified, then faded, and a white precipitate formed, having IR features of both imBT and cyanide (Figure 2-9).

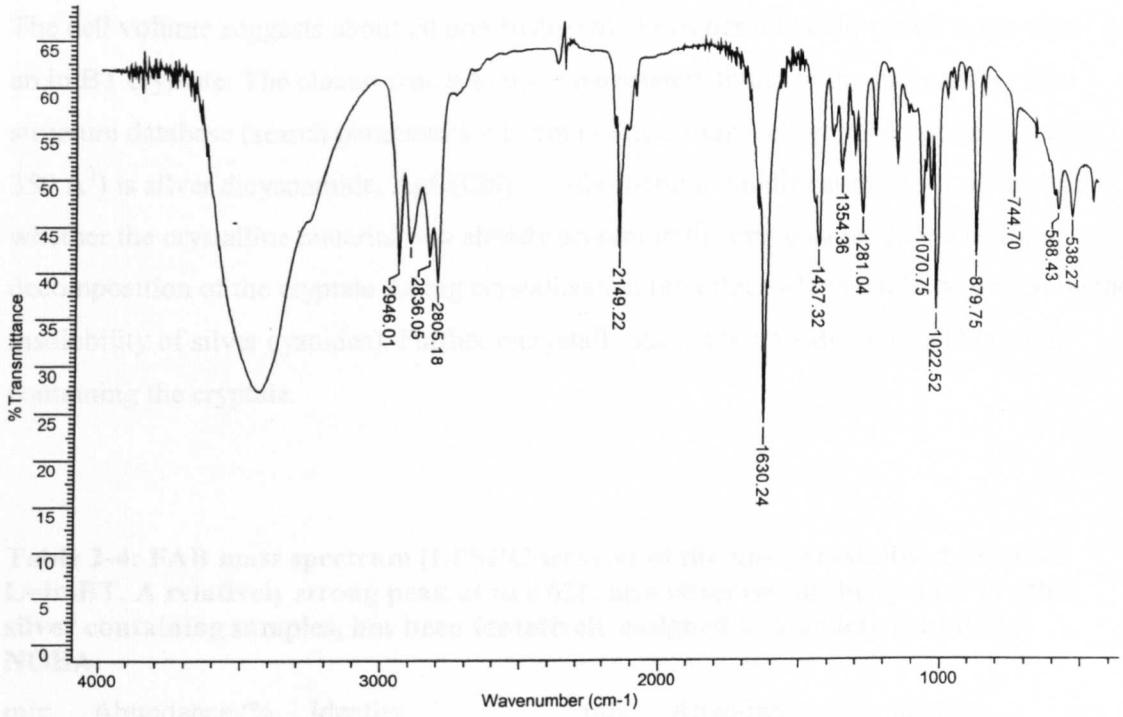

Figure 2-9: Infrared spectrum of a white powder obtained by reaction of dicyanoargentate with Ag_2 imBT. The perchlorate features of the starting cryptate have been lost, and a cyanide stretch at 2149 cm^{-1} is now apparent. Strong CH (2946 — 2805 cm^{-1}) and CN (1630 cm^{-1}) stretches indicate that the cryptand is also present.

The loss of colour (which derives from the Ag → imine charge transfer) initially suggested loss of silver. A FAB mass spectrum (Table 2-4) did in fact confirm the presence of silver – a peak corresponding to Ag imBT was observed – however there was no evidence for the presence of a dimer or larger molecule. No peaks suggestive of CN presence were observed, but neither were the perchlorate peaks normally observed in the starting material. Elemental analysis (Table 2-5) did not conform to predicted values for either a discrete cryptate or a polymer unit, and whilst calculations for a mixture of insoluble silver cyanide or dicyanoargentate with a cryptate did not exactly account for the variation, the solid seems likely to be a mixture of the cryptate with cyanide/cyanoargentate counterion, and inorganic silver or potassium salts.

The loss of colour of the cryptate suggests that some alteration has occurred in the coordination sphere of the silver ions, which could be a result of cyanide coordination, and attempts were made to obtain a crystal to verify the structure. Slow diffusion of ether into a solution in acetonitrile resulted in the formation of tiny colourless crystals. A matrix of X-ray diffraction data was collected, and the cell parameters determined to be: a=5.6186 Å; b=7.1966 Å; c=8.7725 Å; α=90.0320°; β=90.1531°; γ=90.0554°, cell volume=354.709 $Å^3$.

The cell volume suggests about 20 non-hydrogen atoms per unit cell, which is too small for an imBT cryptate. The closest match to these parameters found in the inorganic crystal structure database (search parameters Ag, mmm Laue class, cell volume approximately 350 $Å^3$) is silver dicyanamide, $AgN(CN)_2$ - orthorhombic modification (8). It is unclear whether the crystalline material was already present in the crude sample, or a result of decomposition of the cryptate during crystallisation (an effect which could be driven by the insolubility of silver cyanides). Further recrystallisation attempts did not yield crystals containing the cryptate.

Table 2-4: FAB mass spectrum (EPSRC service) of the un-recrystallised product, L=imBT. A relatively strong peak at m/z 621, also observed in the spectra of other silver containing samples, has been tentatively assigned to a moiety containing NOBA.

m/z	Abundance /%	Identity	m/z	Abundance /%	Identity
360	94	L	466	30	Ag L
392	10	?	621	5	*Ag L NOBA*

Table 2-5: Elemental analysis results of the white precipitate formed from the reaction of the disilver cryptate with potassium dicyanoargentate.

Analysis	%C	%H	%N
Predicted – $Ag_2\ C_{18}H_{30}N_8\ (CN)_2$	38.36	4.83	22.37
Predicted – $[Ag_2\ C_{18}H_{30}N_8\ CN]$ [CN-Ag-CN] monomer unit	33.18	3.98	20.27
Predicted – $[Ag_2\ C_{18}H_{30}N_8]$ $[CN\text{-}Ag\text{-}CN]_2$	29.56	3.38	18.80
Found	21.88	2.31	13.87

2.1.3.1.1. Preparation of related materials for comparison

Thus far the exact identity of the material obtained was not known. Attempts were made to directly prepare a disilver cryptate using silver cyanide, in the hope that comparison of the spectroscopic properties of the two materials may then give an indication of whether dicyanoargentate has been incorporated, or just cyanide. Experimental details are given in section 9.1.1.1.

No cryptate was obtained using silver cyanide alone, however addition of dicyanoargentate to the reaction mixture did yield a pale yellow solid whose infrared spectrum (see section 9.1.1.1) contains the same features as that shown in Figure 2-9. Splitting of the cyanide

stretch is more marked in the present case, and is suggestive of cyanide existing in several different environments.

The FAB mass spectrum (Figure 2-10) contains peaks consistent with a silver cryptate with cyanide and dicyanoargentate counterions. A peak possibly relating to a dimer is also present, although it is barely above the background level, and with the lack of any other evidence for a dimer, this cannot be considered confirmation of dimerisation. The elemental analysis (Table 2-6) did not conform to a simple cryptate with cyanide anion, or to a possible monomer unit incorporating dicyanoargentate bridges. Two possible formulations consistent with the result are suggested however, and others could be envisaged. It is a strong probability that the isolated material is a cryptate incorporating cyanide and/or dicyanoargentate.

Table 2-6: Elemental analysis results for the yellow precipitate, which do not conform exactly to predicted values, but can be explained in terms of a solid containing the ligand, silver, and cyanide ions – possibly in the form of a cryptate.

Analysis	%C	%H	%N
Predicted – $Ag_2\ C_{18}H_{30}N_8\ (CN)_2$	38.36	4.83	22.37
Predicted – $[Ag_2\ C_{18}H_{30}N_8\ CN]\ [CN\text{-}Ag\text{-}CN]$ monomer unit	33.18	3.98	20.27
Predicted – imBT:AgCN mixture (2:5 ratio)	28.12	3.15	18.22
Predicted – $[Ag_2\ C_{18}H_{30}N_8]\ [CN\text{-}Ag\text{-}CN]_2 \cdot 1.5\ H_2O$	28.69	3.61	18.25
Found	28.38	3.14	18.03

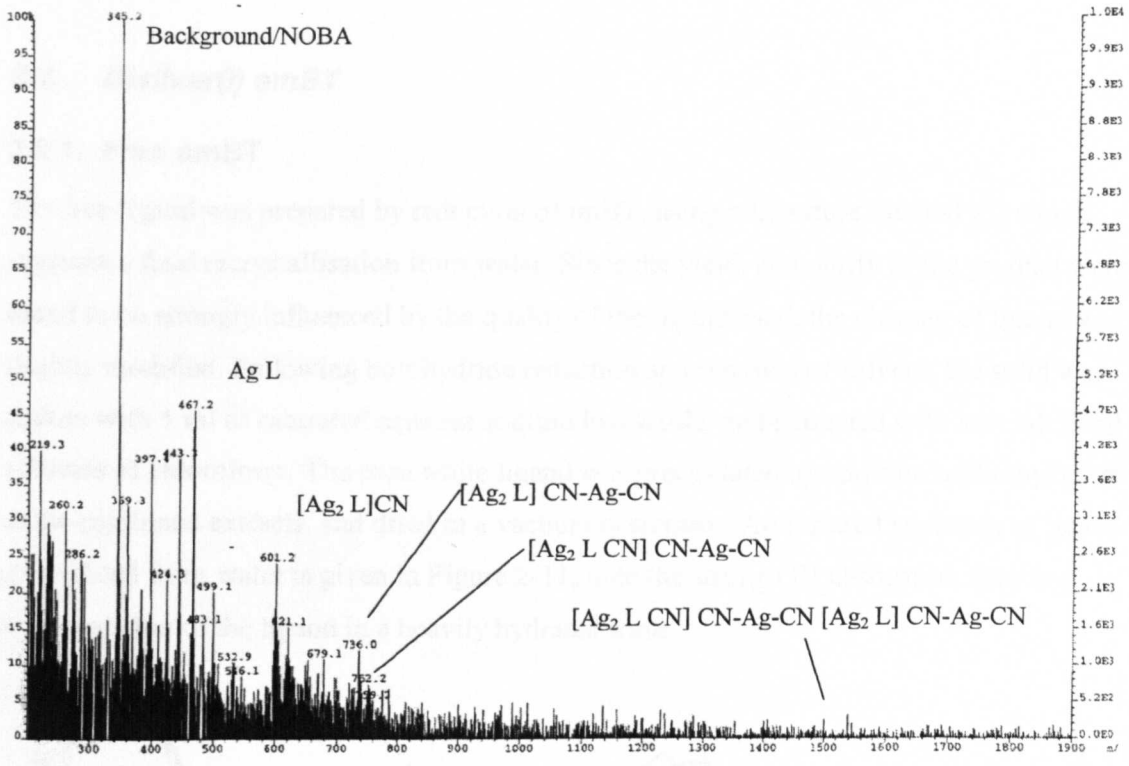

Figure 2-10: FAB mass spectrum of the yellow solid. Note that the high background is owing to poor solubility. A strong peak at m/z 345 is probably a background/NOBA artefact, and has been observed in the spectrum of other unrelated cryptate systems.

2.1.3.1.2. Summary of dicyanoargentate investigation

Direct combination of the dicyanoargentate salt with ligand does not result in a cryptate, suggesting that the anion remains intact, not surprising in view of the high position of cyanide in the spectrochemical series. However, disilver cryptates with a cyanide infrared absorption are formed either by counterion exchange with perchlorate, or via preparation from the free ligand in the presence of silver cyanide. Loss of the yellow colour suggests that the energy of the M→L charge transfer has increased, which may be a result of cyanide coordination.

Although no direct confirmation of these structures was obtained, it is possible that the desired outcome has been achieved – *i.e.* blocking of the exposed silver faces. It is also possible that the poor solubility is in fact a result of dicyanoargentate binding to the exposed silver faces. Unfortunately this sample (together with several others) was lost during lab reorganisation, before NMR or electrochemical studies could be attempted. It is

likely however that the poor solubility, which resulted in a noisy FAB spectrum, would have similarly impacted on the NMR and electrochemistry.

2.2. *Disilver(I) amBT*

2.2.1. Free amBT

The free ligand was prepared by reduction of imBT, using a literature method (3) which suggests a final recrystallisation from water. Since the yield, and purity of the product were found to be strongly influenced by the quality of the ligand used, the cleanup of ligand was slightly modified. Following borohydride reduction and removal of solvent, the solid was shaken with 5 ml of saturated aqueous sodium hydroxide, and extracted with several 50 ml volumes of chloroform. The pure white ligand was precipitated by addition of diethyl ether to the combined extracts, and dried in a vacuum desiccator. An infrared spectrum of ligand crystallised from water is given in Figure 2-11, note the strong OH absorption resulting from isolation of the ligand in a heavily hydrated form.

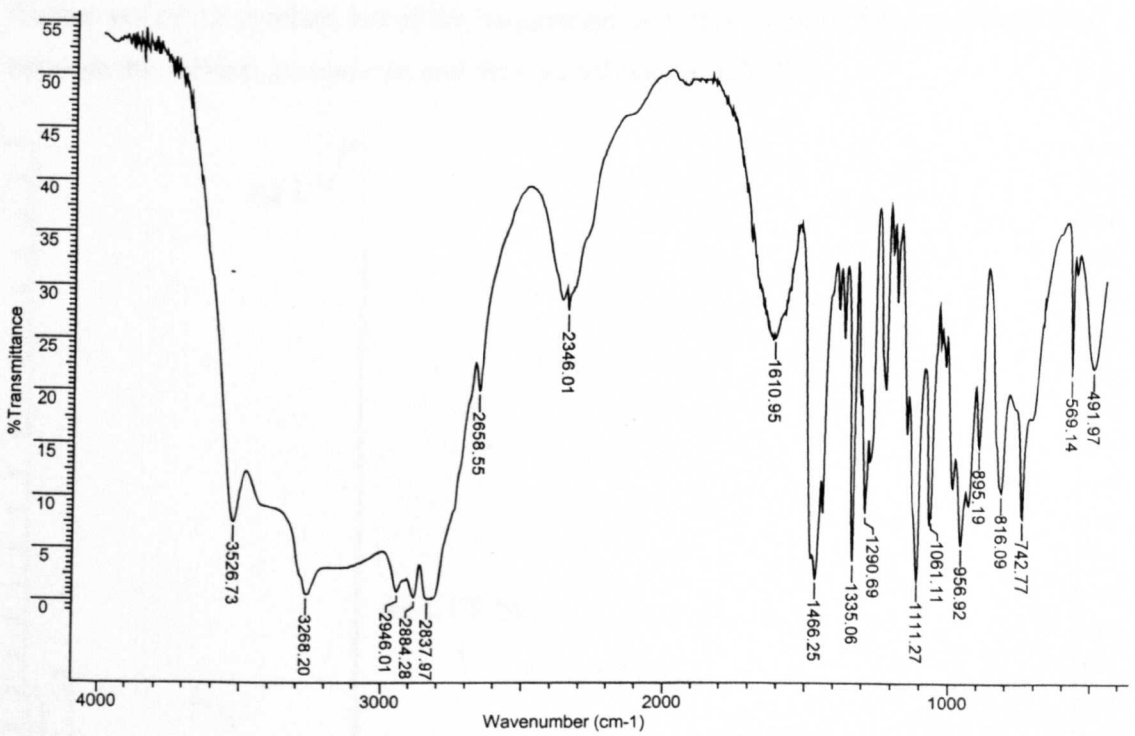

Figure 2-11: Infrared spectrum of free amBT ligand.

2.2.2. Disilver(I) amBT

The disilver(I) complex had previously been prepared and structurally characterised as a BF_4^- salt (9), however variable results from the procedure were obtained, and a reproducible route to the complex was desired.

This cryptate was of particular interest for electrochemical studies in order to investigate the possible stabilisation of higher oxidation states of silver with this amine ligand, as observed in the analogous dicopper series where no dicopper(I) form can be isolated (10).

Initial investigations into the preparation of this compound found that triflate anion readily gave a product, and the optimised procedure for preparation of Ag_2 amBT $(CF_3SO_3)_2$, is given in section 9.1.3.

The FAB mass spectrum contains the expected peaks for this cryptate, although on some occasions a peak with m/z 705 was observed at significant intensity (up to 6% of the base peak). This peak was also observed in other, unrelated, cryptates, and is believed to be a feature, not of the cryptate, but of the background, possibly resulting from an interaction between the solvent, acetonitrile, and the internal standard, NOBA.

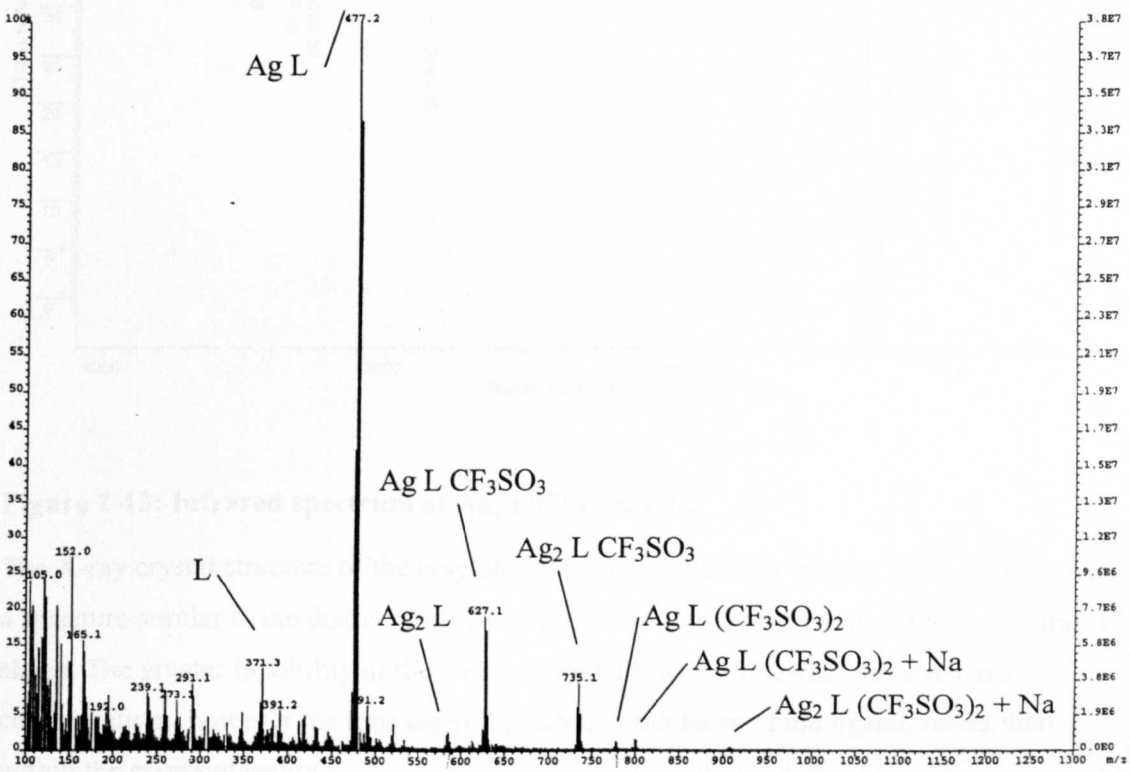

Figure 2-12: FAB mass spectrometric results for Ag2 amBT triflate (EPSRC service).

Analytical results of the crystalline product were generally excellent, as shown in Table 2-7. The infrared spectrum (Figure 2-13) shows NH stretches at 3297 and 3268 cm^{-1}, and the corresponding weak NH bend occurs at 1611 cm^{-1}. CH absorptions are intense between 3000 and 2800 cm^{-1}, and triflate peaks are also strong at 638, 1034, 1159, and 1260 cm^{-1}.

Table 2-7: Summary of elemental analyses for disilver amBT.

Analysis	%C	%H	%N
Predicted – Ag_2 amBT triflate	27.16	4.79	12.67
Found – Mean (standard deviation, N=14)	27.17 (0.22)	4.69 (0.23)	12.49 (0.18)

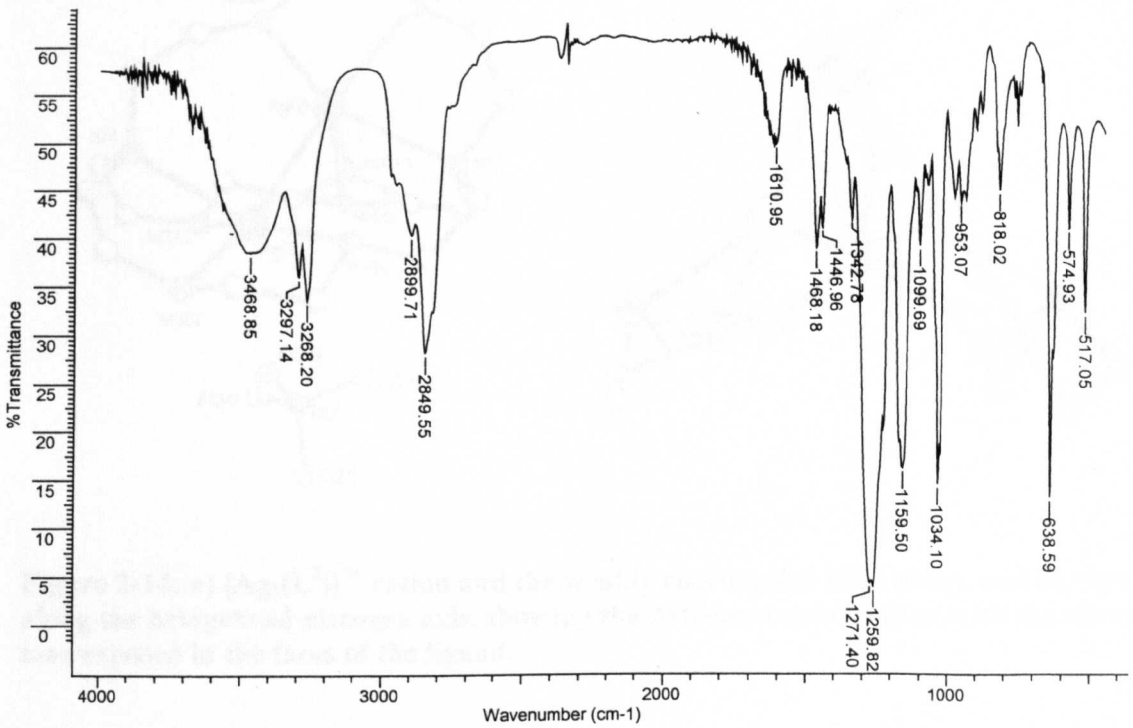

Figure 2-13: Infrared spectrum of Ag_2 amBT triflate.

The X-ray crystal structure of the cryptate with BF_4^- counterion (Figure 2-14, (11)) reveals a structure similar to the disilver imBT complex, with the ligand twisted into an "A-frame" shape. The greater flexibility of the amino ligand allows a somewhat more relaxed conformation, however the ions are still located in the faces of the ligand, rather than within the cryptand cavity.

Disorder in one strand has been modelled as 50% occupancy of N(4A) and N(4A'). Selected bond lengths and angles are given in Table 2-8. The Ag-Ag separation of 2.816 Å

is less than the internuclear distance observed in elemental silver (2.89 Å), indicative of some silver–silver interaction. Evidence exists for such closed shell interactions in other cryptate systems (see Drew et al, and conclusions below (12)).

Each silver(I) ion is coordinated to four nitrogens, the Ag-N_{br} distances are longer (2.490(8)-2.606(7) Å for N(1) and N(2), respectively) but still within bonding distance. One of the BF_4^- counterions interacts weakly with a silver ion (Ag(1)–F(24), 3.19(1) Å).

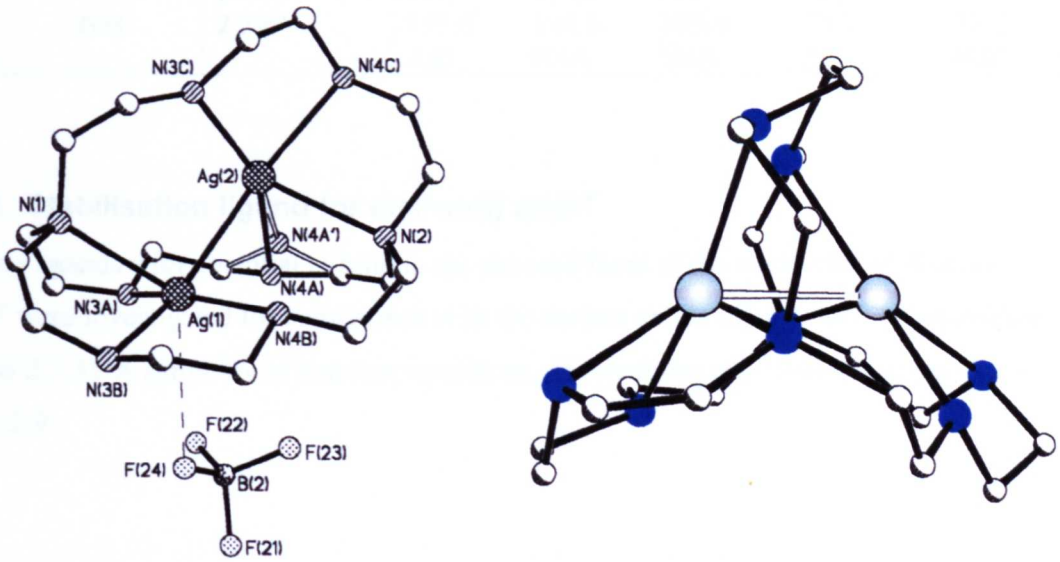

Figure 2-14: a) $[Ag_2(L^2)]^{2+}$ cation and the weakly coordinated BF_4^- anion, and b) view along the bridgehead nitrogen axis, showing the A-frame conformation with the silver ions exposed in the faces of the ligand.

Table 2-8: Selected bond angles and distances for Ag_2 amBT $(BF_4)_2$.

Nucleus 1	Nucleus 2	Bond length (Å)	Bond angle (degrees)				
Ag1	Ag2	2.816					
Ag1	N1	2.469	95.5				
Ag1	N3A	2.359	85.5	76.4			
Ag1	N3B	2.408	150.8	73.9	116.9		
Ag1	N4B	2.353	86.9	125.8	157.2	78.4	
			Ag2	N1	N3A	N3B	
Ag2	Ag1	2.816					
Ag2	N4A	2.342	71.3				
Ag2	N4A'	2.291	91.7	22.1			
Ag2	N2	2.587	93.3	70.4	76.5		
Ag2	N3C	2.314	91.9	155.6	153.1	129.8	
Ag2	N4C	2.399	151.6	125.6	109.9	74.9	77.3
			Ag1	N4A	N4A'	N2	N3C

2.2.3. Stabilisation ligand for disilver(I) amBT

Several ligands with potential to bind to the exposed faces of the silver ions in disilver amBT were investigated for comparison with the studies on the disilver imBT system (see section 2.1.3). A summary of reaction conditions, observations and results is given in Table 2-9.

Table 2-9: Ligands essayed as substituents for disilver(I) imBT: reaction conditions, observations, and results.

Ligand	Structure	Reaction conditions	Results
Triphenyl phosphine	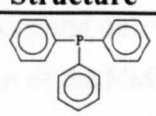	1 mol equiv, MeCN, dark, nitrogen atmosphere	No interaction with cryptate, see section 9.1.4.2.
Diphos	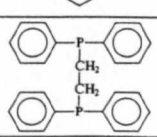	0.5 mol equiv, MeCN, DCM, dark, nitrogen atmosphere	Mixture of silver diphos complex, and silver cryptate. See section 9.1.4.3.
Na diethyl-dithiocarbamate	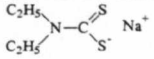	0.5 mol equiv, MeCN, MeOH, dark, nitrogen atmosphere	Abstracts silver to form diethyl-dithiocarbamate complex. See section 9.1.4.4.
Thiophenol	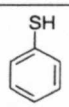	1 mol equiv, MeCN, MeOH, dark, nitrogen atmosphere	Abstracts silver from crypt, forming thiophenol complex, see section 9.1.4.5.
Silver benzoate	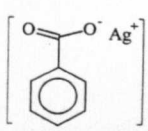	Direct preparation using 1 amBT:2 Ag benzoate	Disilver amBT complex obtained and characterised, see section 2.2.3.1.

The phosphine ligands have proven too weak to coordinate to the cryptated silver ions, however some Ag diphos complex was detected, probably owing to the equilibrium between cryptated and free silver, which would allow direct reaction of silver with the phosphine, without competition from the cryptand ligand.

The S donor ligands however have such a great affinity for silver that they abstract it from the crypt. The benzoate counterion however gave a disilver cryptate using, *mutatis mutandis*, the preparative procedure for the triflate complex. The crystal structure was determined, and is discussed and compared to the triflate complex below. A detailed investigation of the ^{1}H NMR characteristics of this complex is presented in section 2.4.

2.2.3.1. Silver amBT benzoate

The disilver amBT complex was prepared with silver benzoate in place of the triflate salt usually used, full details are given in section 9.1.4.1.

Comparison of the infrared spectrum of the product (Figure 2-15) to that of the triflate complex (Figure 2-13) reveals several strong new peaks, consistent with the presence of benzoate (ring bends and stretches at 718, 1368 and 1558 cm^{-1}, protons at 3058 cm^{-1} and carbonyl at 1596 cm^{-1}), together with strong CH stretches (2800-3000 cm^{-1}) and weaker fingerprint region absorptions resembling those observed for the free amBT ligand.

The cryptate region of the ^{1}H NMR spectrum (discussed in detail in section 2.4.2.1, see Figure 2-20) bears a strong resemblance to that of the triflate variant, the aromatic region being largely unaffected by changes in temperature, whilst the effect of conformational interchange of the cryptand only becomes negligible at –45°C (see section 2.4 for a detailed investigation of the NMR of this system).

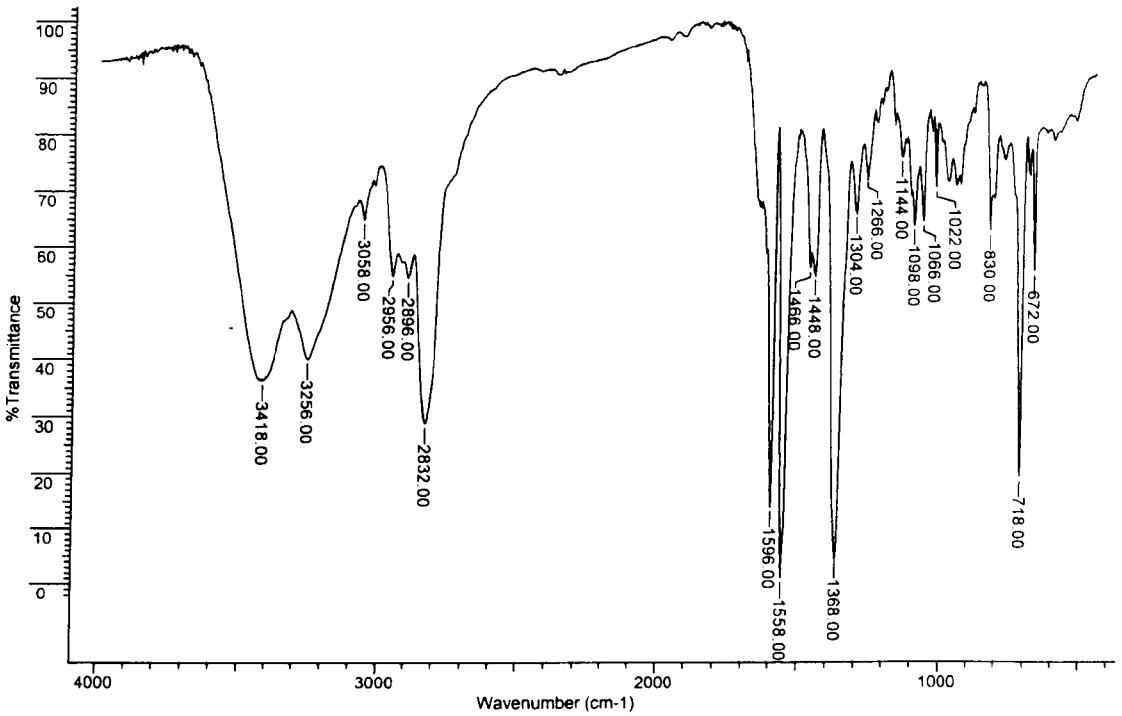

Figure 2-15: Infrared spectrum of disilver amBT benzoate.

The elemental analysis (Table 2-10) is not in exact agreement with the determined structure, which incorporates full occupancy carbonate and water molecules. Given the good R-factor of the structure refinement (0.0485) it seems most likely that the solid isolated contains a mixture of cryptates, one having the X-ray determined composition, and one containing no carbonate or water.

The FAB mass spectrum (Table 2-11) contains peaks of m/z consistent with the presence of the (hard to detect) carbonate ion, albeit at low abundance.

Table 2-10: Elemental analysis of Ag_2 amBT benzoate.

Analysis	%C	%H	%N
Predicted (Ag_2 amBT benzoate$_2$):	46.39	6.33	13.52
Predicted (Ag_2 amBT benzoate$_2$·HCO_3·H_2O):	43.62	6.21	12.33
Prediction for 33% HCO_3 and H_2O content	45.41	6.29	13.10
Found:	45.44	6.30	12.87

Table 2-11: FAB mass spectrum (EPSRC service) of Ag_2 amBT benzoate, L = amBT.

m/z	Abundance /%	Identity	m/z	Abundance /%	Identity
262	6.5	*Ag NOBA ?*	648	1.5	Ag_2 L CO_3
348	15	Ag benzoate$_2$	707	1.7	Ag_2 L benzoate
477	100	Ag L	769	0.7	Ag_2 L benzoate HCO_3
585	7	Ag_2 L			

Graphical representations of the asymmetric unit and packing diagram are shown in Figure 2-16 A and B, full crystallographic details are given in section 9.1.4.1.1. The crystal contains a disilver cryptate molecule of similar conformation to that seen with BF_4^- counterion (Figure 2-14), together with two benzoate ions, a water molecule, and a bicarbonate ion. This unexpected component could result from atmospheric uptake of CO_2, or else from partial breakdown of benzoate, or an impurity in the silver benzoate used for cryptate preparation. Although protons were not located, the alignment of the bicarbonate and neighbouring benzoate strongly suggests that they are bridged by two protons, making their formal identities benzoic acid and bicarbonate. Bond lengths in the tetrafluoroborate and benzoate cryptate molecules are broadly similar, however silver to benzoate oxygen distances are shorter than the silver to fluorine distances, which may suggest some degree of interaction. Whether this results in the desired stabilisation of the cryptate cannot be said, however NMR studies of this compound were performed in order to ascertain this fact (see section 2.4).

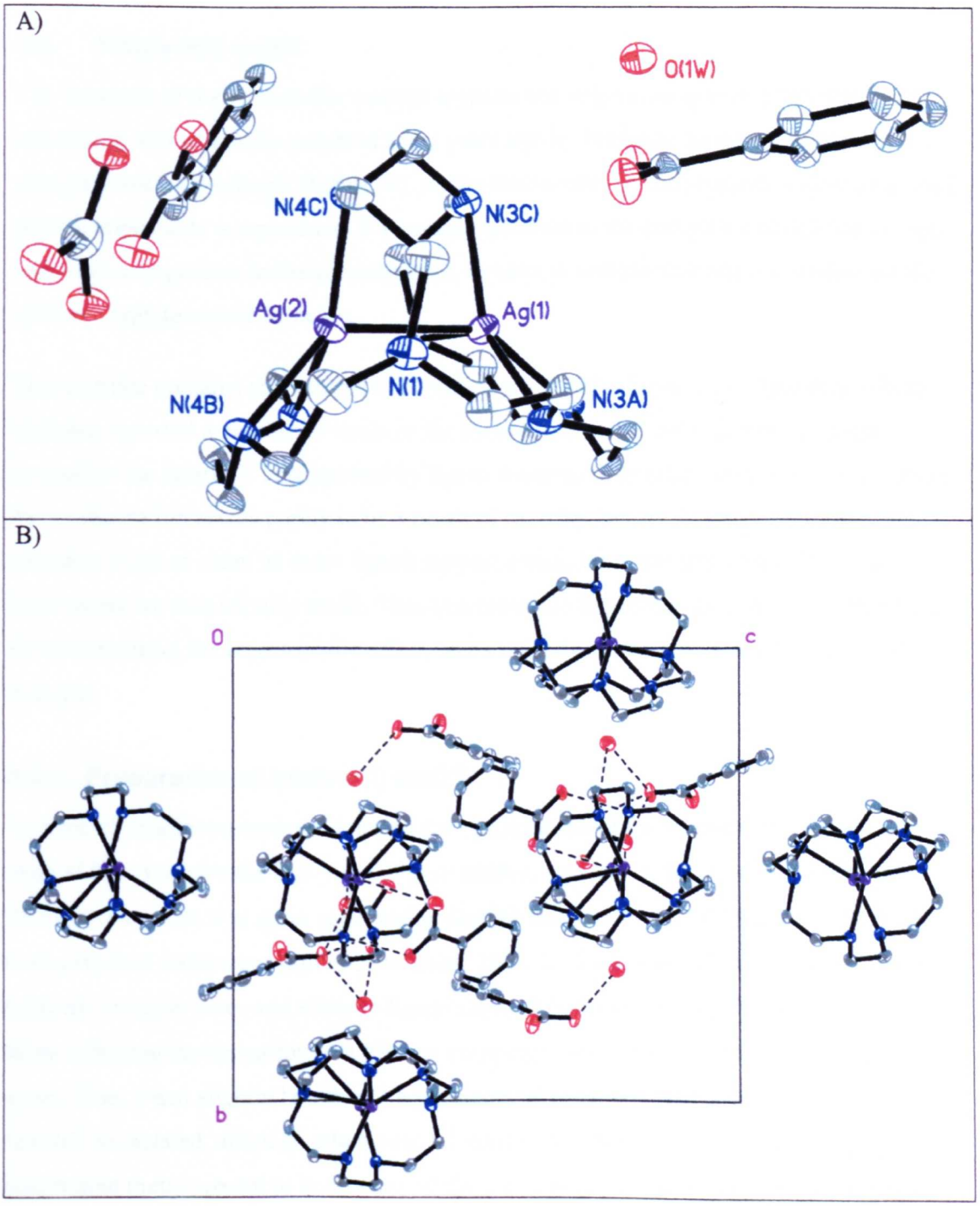

Figure 2-16: A) Crystal structure of disilver amBT benzoate, showing the A-frame configuration, in relation to the benzoate and carbonate moieties, and B) packing diagram showing benzoate and bicarbonate counterions.

2.3. Trisilver(I) amBT

The structure of the remarkable trisilver cryptate has only recently been published (11), although it was originally prepared some years ago by Professor Nelson, and structurally characterised by Professor McKee (9). At the time however, the preparative procedure had proven impossible to reproduce. A reproducible route to the complex was desired in order that a full comparison to the spectroscopic, structural, and electrochemical studies on the disilver cryptates could be made.

This cryptate contains an example of a triangular silver(I) cluster, a configuration which has been reported a number of times in the literature (*e.g.* (13-16)). In some of these molecules the cluster is unsupported by ligand framework or other effects, whilst in others the configuration seems purely to be a result of external factors. In the present case, the situation is not as clear, as some ligand support exists, but at the same time the metal-metal separations are suspiciously small. Thus this molecule represents an interesting opportunity for investigating the argentophilic effect, and some of our attention was directed towards this goal.

2.3.1. Preparation of trisilver(I) amBT

A range of conditions were used during the optimisation of this preparation, and the method found to give the best yield of pure trisilver cryptate is described in section 9.1.5. Triflate counterion was again used, and in fact the two complexes of different nuclearity were prepared under very similar conditions. Table 2-12 summarises the effects of using different reaction times and silver to ligand ratios. It is interesting to note that the key factor affecting the formation of a trisilver complex is the time allowed for reaction to occur. Even when slightly less than 3 equivalents of silver are used, the trisilver complex can still be isolated, although when only 1.2 equivalents were used, there was evidently insufficient metal present to isolate any trisilver complex. Use of greater excesses of silver results only in the formation of a larger amount of black inorganic silver.

Table 2-12: Effect of silver to ligand ratio and reaction time on the identity of the product isolated (determined by elemental analysis and FAB mass spectrometry).

Ag:ligand ratio	Product isolated after 1-10 days	Product isolated after 10-20 days
1.2:1	None	Very small yield of disilver
2.2:1	Disilver	Trisilver
3.5:1	Disilver	Trisilver
4.0:1	Disilver	Trisilver
4.7:1	Disilver with inorganic silver	Trisilver

The FAB mass spectrum (Table 2-13) was consistent with the desired product, as was the elemental analysis (Table 2-14), although the solvent incorporated in the crystal appeared to have been lost prior to analysis. The IR spectrum (Figure 2-17) is very similar to the dinuclear cryptate, some peak broadening possibly resulting from slight dampness of the sample. Nevertheless, some clear differences can be observed in the fingerprint region, a feature at 980–940 cm^{-1} is simpler in the trinuclear cryptate, and there are slight shifts in frequency for other fingerprint region peaks.

Table 2-13: FAB mass spectrum of trisilver amBT triflate (EPSRC service).

m/z	Abundance /%	Identity	m/z	Abundance /%	Identity
477	100	AgL	779	1	AgL $(CF_3SO_3)_2$
627	1	AgL CF_3SO_3	884	1.5	Ag_2L $(CF_3SO_3)_2$
735	37	Ag_2L CF_3SO_3	990	2	Ag_3L $(CF_3SO_3)_2$

Table 2-14: Elemental analysis of trisilver amBT triflate, showing good agreement with predicted values.

Analysis	%C	%H	%N
Predicted – Ag_3L $(CF_3SO_3)_3$	22.10	3.71	9.82
Predicted – Ag_3L $(CF_3SO_3)_3 \cdot H_2O \cdot EtOH \cdot \frac{1}{2}Et_2O$	24.32	4.49	9.08
Found	21.97	3.76	9.69

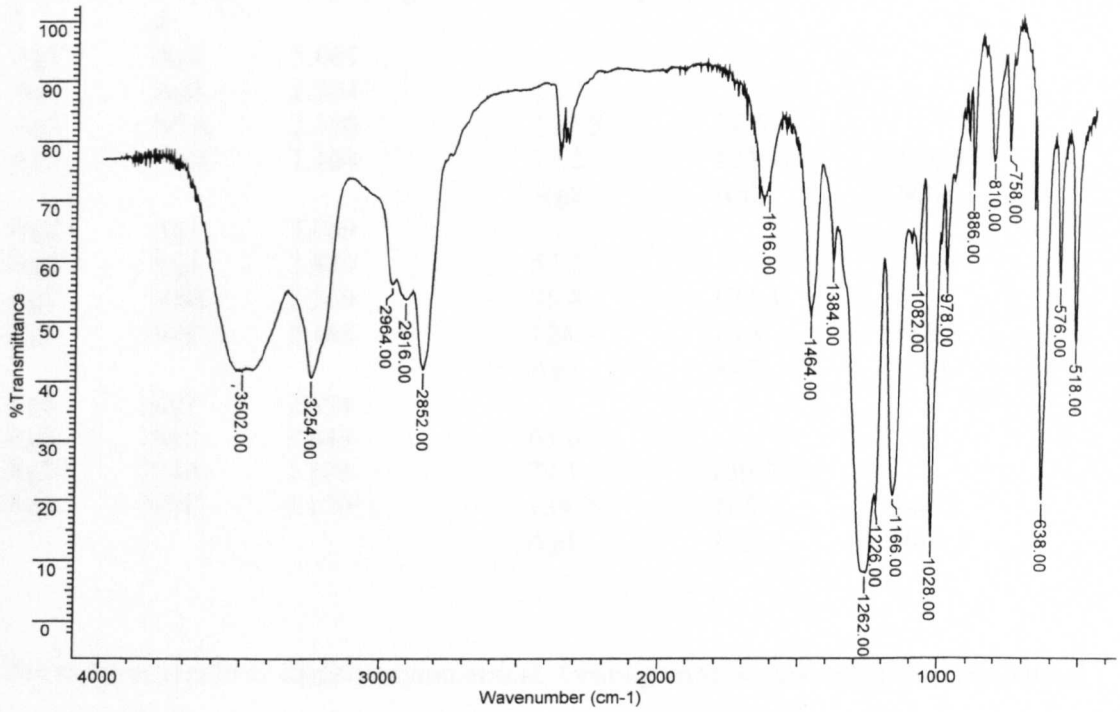

Figure 2-17: Infrared spectrum of Ag_3 amBT triflate (KBr disk).

The X-ray crystal structure of the complex previously prepared revealed a triangular array of silver ions, with the metal nuclei being located in the faces of the ligand, and not held within the crypt. Bond lengths and angles are given in Table 2-15 below.

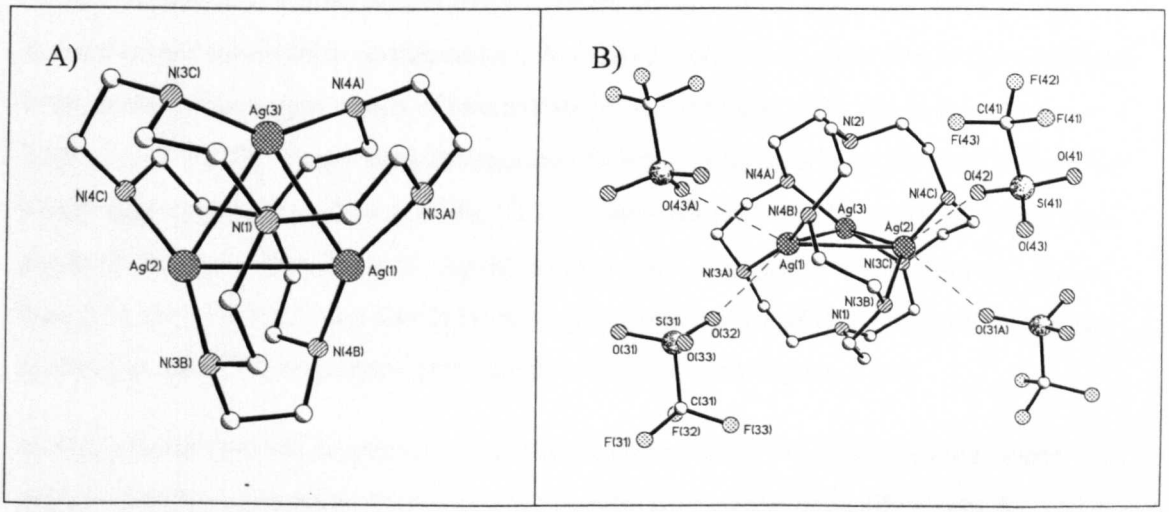

Figure 2-18: A) View down the pseudo 3-fold axis of the $[Ag_3 amBT]^{3+}$ cation, B) weak interactions between Ag(I) ions and triflate anions. O(31A) and O(43A) are symmetry equivalents of O(31) and O(43).

Table 2-15: Selected bond lengths and angles for trisilver amBT triflate.

Nucleus 1	Nucleus 2	Bond length (Å)	Bond angle (degrees)		
Ag1	Ag2	3.089			
Ag1	Ag3	2.854	57.1		
Ag1	N3A	2.180	125.5	77.6	
Ag1	N4B	2.164	75.2	123.1	158.5
			Ag2	Ag3	N3A
Ag2	Ag1	3.089			
Ag2	Ag3	2.849	57.3		
Ag2	N3B	2.169	75.4	122.4	
Ag2	N4C	2.188	124.9	76.8	159.3
			Ag1	Ag3	N3B
Ag3	Ag1	2.854			
Ag3	Ag2	2.849	65.6		
Ag3	N4A	2.178	79.1	130.9	
Ag3	N3C	2.170	134.9	81.9	144.2
			Ag1	Ag2	N4A

The trisilver cluster is slightly asymmetrical, forming an isosceles rather than equilateral triangle, with two of the silver–silver distances near 2.85 Å, and the other being slightly longer at 3.09 Å, two angles of ~57.2°, and one of 65.6°. The two shorter silver–silver distances are less than the internuclear distance in elemental silver (2.89 Å), indicative of some silver–silver interaction, such as that observed in related di-silver(I) systems (12). Each Ag(I) is near-linear 2-coordinate (ignoring close contacts to other silver ions), linking together a pair of 2° amino donors from different strands of the cryptand host (the N_{br} donors are not involved in coordination). Ag(1) and Ag(2) each show two weak additional interactions with oxygen atoms of two triflate ions, Ag-O distances are in the range 2.857(7) – 3.167(7). These weak interactions do not involve Ag(3) or the third triflate ion which may explain the splitting of the ^{19}F resonance observed in the MAS spectrum (see Figure 2-19), the difference in N–Ag–N angle at Ag(3) compared to the other two silver ions (158.5(3), 159.3(3) and 144.2(3)° for Ag(1), Ag(2) and Ag(3), respectively) and the splitting in the ^{109}Ag resonance of the trisilver cryptate (see Figure 2-19).

As the trisilver cryptate is apparently the thermodynamically favoured product, some degree of stabilisation must result from the coordination of the third silver ion. A comparison of the strain inherent in the ligand conformation for disilver and trisilver amBT was made using computational techniques. Table 2-16 lists the results of calculations based on a classical (empirical) model (MM2 theory) and a semi empirical model (mopac PM3 theory, performed using the Chem 3D package) for the ligand in the absence of any guest

or counterions. The steric energy result obtained from the MM2 calculation comprises terms for the energies involved in distorting bonds lengths, angles and torsions from their optimal values, as well as 1,4 Van der Waals interactions. The PM3 method uses approximations to solve the Schrödinger equation for the molecule, and thus gain an estimate of the heat of formation. The most useful application of the results of these calculations is not in their absolute values, which at this level of sophistication are not expected to be in close agreement with real values, but rather in their relative values in different systems.

Table 2-16: Results of computations for the amBT ligand in the conformations present in di- and trisilver cryptates.

	Steric energy (MM2 theory/ kcal/mole)	Heat of formation (PM3 theory/ kcal/mole)
Conformation of Ag_2 amBT	307	290
Conformation of Ag_3 amBT	334	309

Both computational theories suggest that the ligand conformation present in the disilver cryptate is slightly more stable than in the trisilver cryptate, possibly resulting from a general outward stretching of the strands to accommodate the three ions. The apparent thermodynamic preference for trisilver cryptate shows that a significant degree of additional stability must result from the increased nuclearity. Destabilising influences such as the increased strain in the ligand, increased order in the cryptate (*i.e.* decreased entropy), the loss of N_{br} coordination, the closer proximity of positively charged ions, and the overall increase in charge on the molecule, must be outweighed by changes in the silver coordination environment (as evidenced by the shorter Ag-N bonds than in the disilver cryptate, and the close silver-silver contacts), together with changes in solvation and crystallisation energies. In light of the observation of stabilising Ag(I)-Ag(I) interactions in other systems (12), we believe that the close proximity of three silver ions in this molecule must be a significant factor in the stability of the cryptate (see conclusions below).

2.4. Solid state and solution NMR studies

A variety of NMR experiments were performed on the silver amBT system in order to try and understand the processes occurring in solution. Studies on the silver imBT system have suggested that decomplexation occurs in some solvents, possibly resulting in the formation

of a mono-silver cryptate, and initial investigations into the related amBT cryptates suggests that their behaviour is not simple either.

A fresh sample of a previously characterised cryptate, cadmium(II) amBT tetrafluoroborate was prepared for comparison of solid state and solution NMR spectra, as the guest ion in this complex lies in a symmetric environment, and its solution NMR has already been investigated (17) (reproduced in Figure 2-22).

2.4.1. Solid state (CP MAS) NMR studies

2.4.1.1. Disilver amBT

The crystal structure of the disilver cryptate (Figure 2-14 and Figure 2-16) shows that there is at least some (and possibly a lot of) asymmetry within the ligand. Two strands are approximately symmetrical, whilst the third (upper strand as shown in Figure 2-16) whose nitrogens are coordinated to two different silver ions is clearly different.

In the solid state NMR spectra (Figure 2-19) the ^{13}C signals are less well resolved than in the free ligand, or the symmetric monocadmium cryptate, where 3 distinct environments are seen, corresponding to the two cap carbons and one imine carbon. Nevertheless, at least four peaks can be discerned (55.1, 53.6, 49.7 and 47.3 ppm, not counting spinning side bands around 120 ppm) and there are additional shoulders which may relate to more fine structure concealed by broadening and overlapping. This is consistent with at least one non-equivalent strand as observed in the crystal structure.

The ^{15}N spectrum was weak for both the disilver and trisilver cryptates, as well as for the free ligand, although the cadmium complex gave a good spectrum. In this symmetric environment, two signals relating to the secondary amino N (-345 ppm) and the (non-protonated) bridgehead N (-359 ppm) are observed (identity confirmed by dipolar decoupling experiment). There is a suggestion of four signals in the less symmetric disilver cryptate, however these are very weakly separated from the background. The chemical shift (342 to 352 ppm) is similar to those in the cadmium cryptate, as well as to several weak peaks for the free ligand.

No ^{109}Ag spectrum could be obtained for the disilver cryptate, owing to lack of sample in the first instance, and a broken probe when the further sample required had been obtained. A ^{19}F spectrum was observed, and shows a strong overlapping doublet at -76.1 and -77.1 ppm, the two main environments are possibly those fluorines with a relatively close Ag-F

contact, and those without. Additional fine structure may also be obscured by peak broadening. Spinning side bands are present at -19 and -134 ppm.

2.4.1.2. Trisilver amBT

The crystal structure of the trisilver cryptate (Figure 2-18) has approximate threefold symmetry, although the silver-silver contacts are not all the same - the three ions form an isosceles triangle with one longer side. In the solid state NMR (Figure 2-19), this results in a very similar ^{13}C spectrum to the disilver cryptate, suggesting that the metal asymmetry is reflected in a loss of symmetry in the ligand framework. The ^{15}N spectrum is more clearly defined than the dinuclear complex, the two peaks are tentatively assigned to bridgehead nitrogen (-346 ppm) and secondary nitrogen (-353 ppm). There is also a strong similarity in the ^{19}F spectra, the trisilver cryptate also having a doublet at near identical chemical shift to the disilver cryptate.

A ^{109}Ag spectrum was observed in this case, and shows two signals at 460 and 532 ppm (compared to $AgNO_3$ standard). Small changes in the coordination environment of silver are known to result in relatively large changes in the ^{109}Ag MAS NMR chemical shift (18). The two observed resonances may result from a change in environment induced by the relatively close contacts with triflate oxygen made by two of the silver ions at the base of the isosceles triangle of metals. In comparison, the ^{113}Cd spectrum contains a strong 65.3 ppm singlet, consistent with the symmetric environment.

2.4.2. Solution NMR

Although crystals of the trinuclear cryptate can be obtained starting with the disilver analogue, it is difficult to obtain a bulk sample of trinuclear cryptate uncontaminated with the dinuclear material, so solution measurements have in general been restricted to fresh solutions of disilver amBT.

2.4.2.1. Disilver amBT

^1H NMR spectra for disilver amBT triflate and disilver amBT benzoate were compared to the free ligand spectrum, and spectra of samples spiked with one equivalent of free ligand. Spectra were collected at temperatures from –65 to +35°C (see Figure 2-20). Deuterated methanol was used for these experiments, both to allow access to lower temperatures than could be achieved in water or acetonitrile, and with the hope of avoiding the exchange processes which appear to be supported by other solvents.

The known asymmetry of the ligand conformation in crystals of the disilver cryptate, and the observation of more than three carbon signals in the solid state NMR spectrum, both led us to expect that the solution NMR spectra would not be simple. In the solid state, two strands appear approximately equivalent, and if a similar conformation exists in solution we may expect to see two, probably overlapping, sets of signals in a 2:1 intensity ratio. In such a frozen conformation, protons attached to the same carbon would be inequivalent, leading to a very complicated situation indeed.

This prediction is borne out in fact, although conformational freezing in deuterated methanol solvent was not observed until temperature was as low as –45°C (Figure 2-20 1st column). At temperatures above ambient two broad signals are observed, and the larger has a shoulder suggesting that two broad features are overlapping. With benzoate counterion this shoulder is partly resolved, and the trend of sharper resolution in the cryptate with benzoate counterion continues throughout the temperature profile.

The difference in behaviour between the cryptates with triflate and benzoate counterions lends weight to the hypothesis that the observed cryptate spectrum is that of a disilver cryptate, rather than a dissociation product (as has been postulated for the disilver imBT system in acetonitrile, see section 2.1.2), *viz*

- existence of exchange is demonstrated by the effect of adding free ligand to the triflate cryptate solution (Figure 2-20 2nd column, whereupon features intermediate between cryptate and ligand are observed, rather than a superimposition of the two spectra)

- That exchange does not in fact happen when the counterion is benzoate is also shown by the effect of adding free ligand to this solution (Figure 2-20 4th column, where observed features are consistent with free ligand peaks, overlying other peaks similar to those in the cryptate only).

- The lack of exchange in methanol for disilver amBT benzoate suggests that the disilver cryptate moiety is intact,

- and the similarity between the cryptate spectra at –45°C shows that for these counterions, disilver amBT is the dominant species when exchange processes are removed.

Decoupling, NOE, and COSY experiments were performed with the aim of helping to assign specific features in the spectrum, and the results of these experiments are summarised in section 9.1.6. The cadmium amBT cryptate whose solution ^{1}H NMR spectrum was previously assigned (17) was also used for comparison (Figure 2-22).

At temperatures close to ambient the spectrum (with either counterion) takes the form of a single broad coalesced feature, in the region expected for NCH_2. As temperature is lowered however, the ^{1}H NMR spectrum starts to become much more complex showing that the exchange rate is becoming slower than the NMR timescale.

In the X-ray structures of the disilver cryptate (Figure 2-14 and Figure 2-16) one strand of the cryptand appears to be different from the other two, doubling the possible number of resonances with respect to the symmetric host conformation. In comparison to the (conformationally frozen) spectrum of the symmetric cadmium amBT cryptate (Figure 2-22 A), at least eight cap proton resonances and four spacer resonances are possible – assuming the two ends of the cryptate are equivalent and the signals can be resolved (Figure 2-22 B).

In deuterated methanol below –45°C (Figure 2-21) a complex and overlapped set of triplet, doublet and multiplet resonances between 1.8 and 3.6 ppm is observed. Peaks with approximate relative intensity of 1, lying at the extremities of the spectrum may represent the single cryptand strand. There is also a suggestion of an analogous pattern with relative intensity of approximately 2, although these features are more severely overlapping. Some assignments are proposed in section 9.1.6, on the basis of decoupling, NOE, and COSY experiments. These are only tentative however, given the uncertainty about the effects of slight asymmetry in the dinuclear cryptate, and also about the possibility of the existence of more than one conformation in solution, as noted in other related disilver cryptates ((12, 19)).

	Metal	C	N	F
amBT	N/A	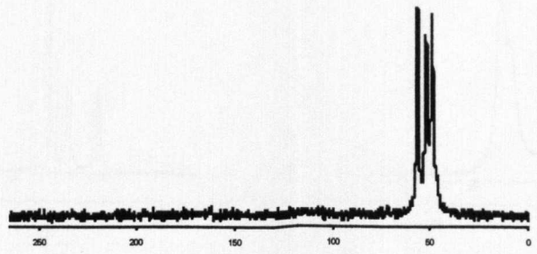	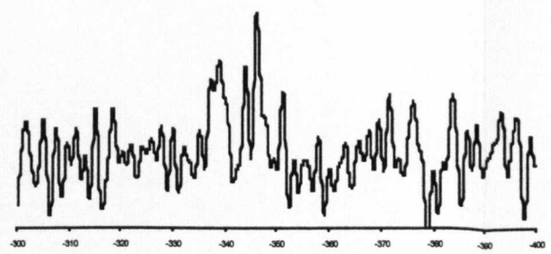	N/A
Ag2 amBT		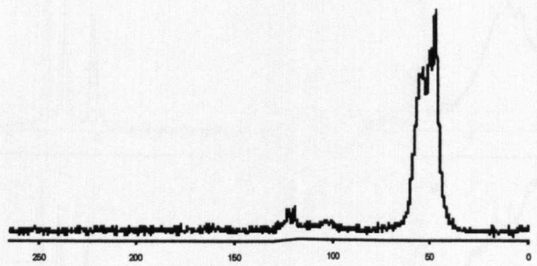	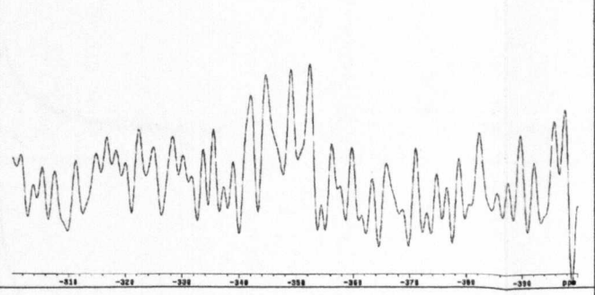	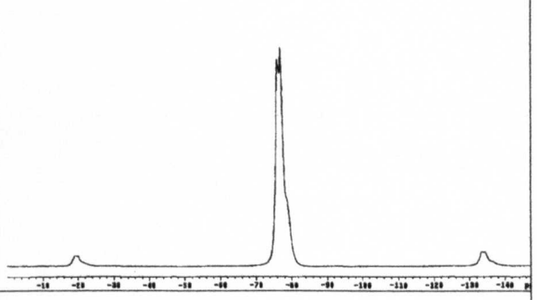
Ag3 amBT	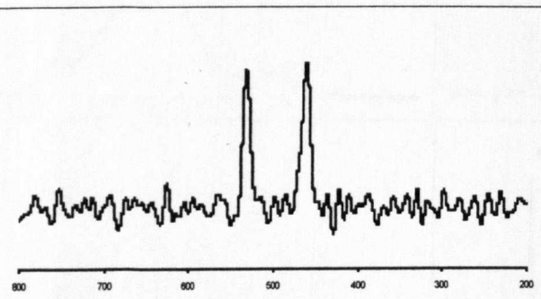	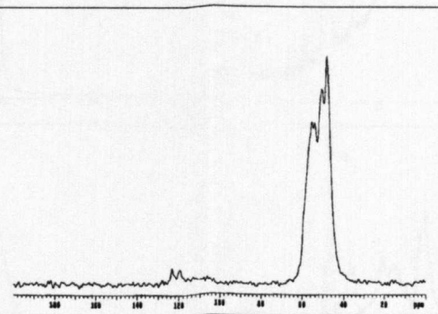	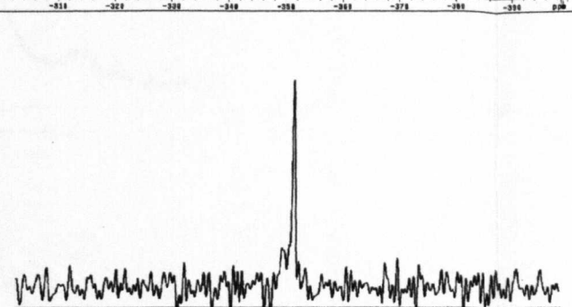	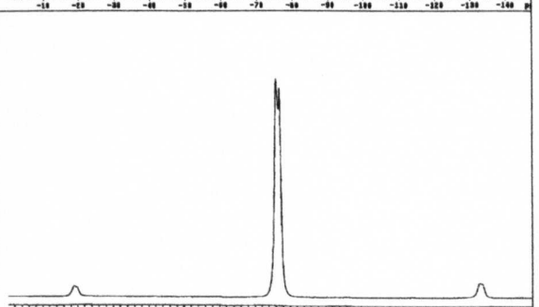
Cd amBT	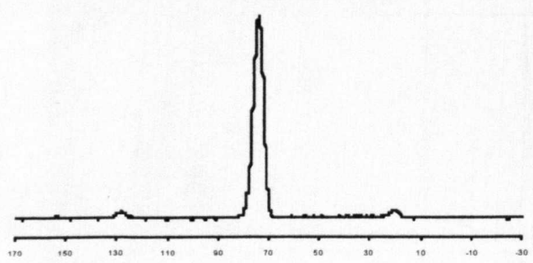	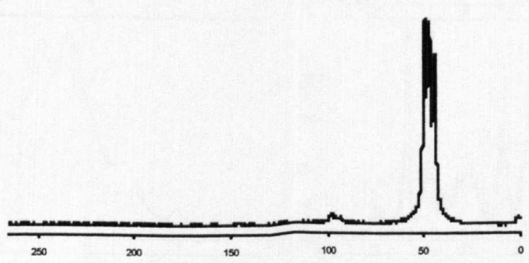	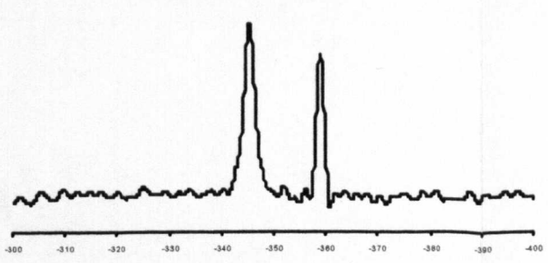	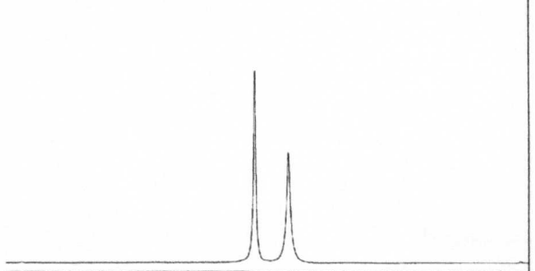

Figure 2-19: Solid state MAS spectra for amBT ligand, disilver amBT triflate, and cadmium amBT tetrafluoroborate, showing signals for the guest metal (where available), carbon, nitrogen, and fluorine.

T	Ag_2 amBT triflate	1 Ag_2 amBT triflate:1 amBT	Ag_2 amBT benzoate	1 Ag_2 amBT benzoate: 1 amBT	amBT
35°	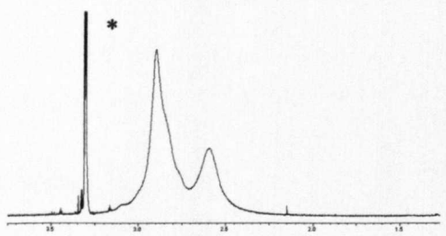	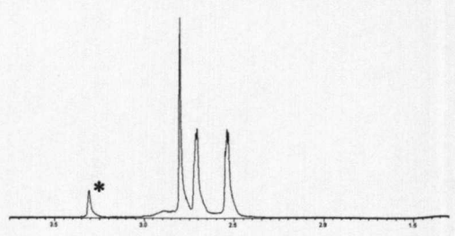	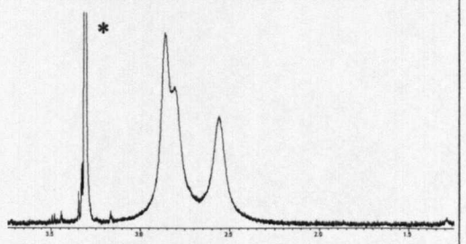	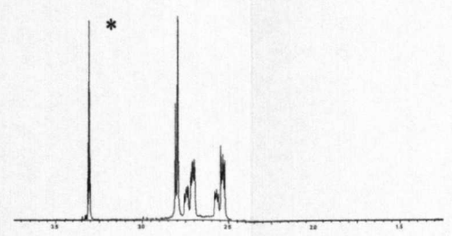	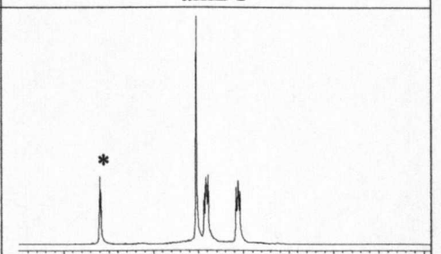
15°	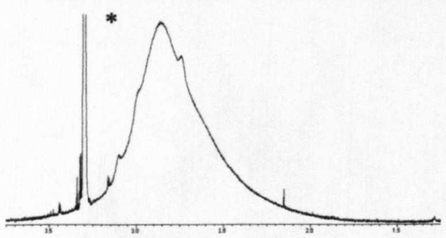	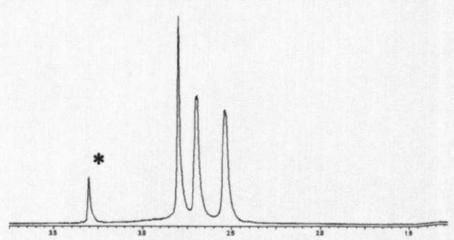	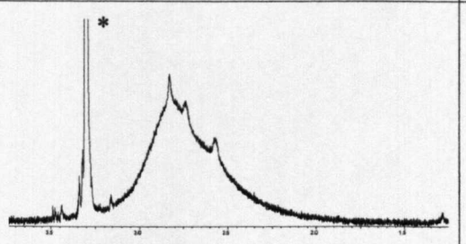	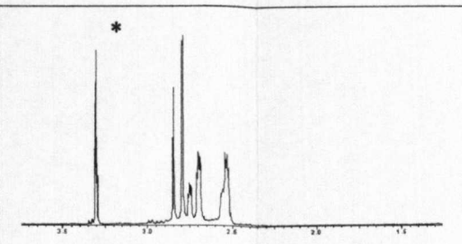	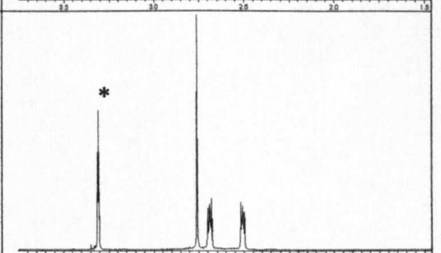
-5°	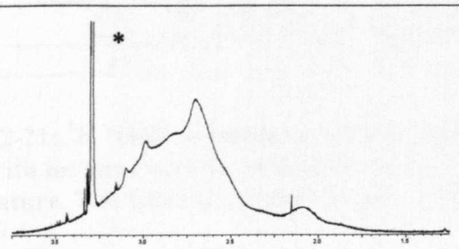	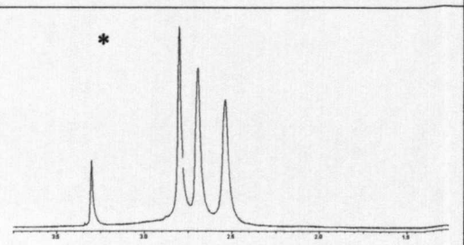	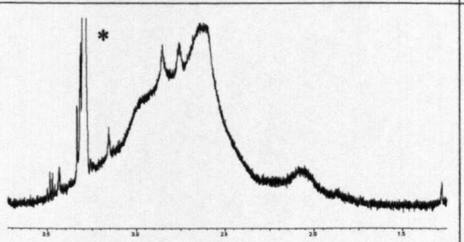	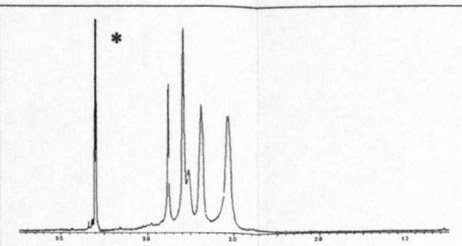	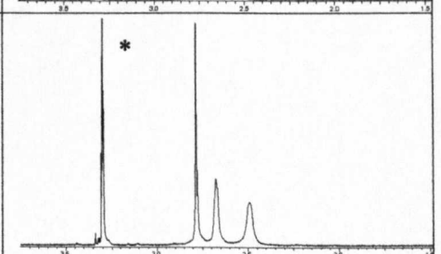
-25°	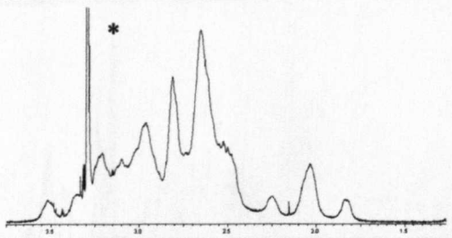	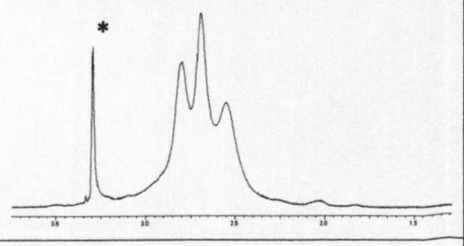	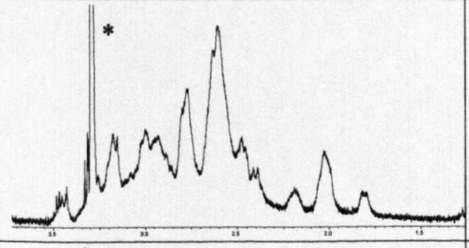	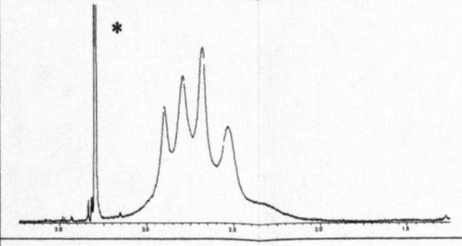	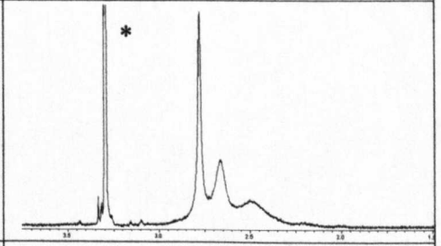
-45°	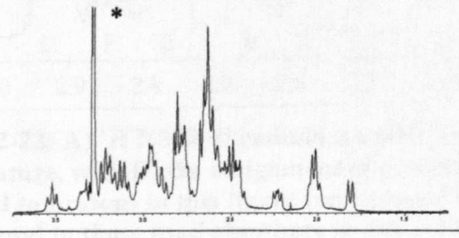	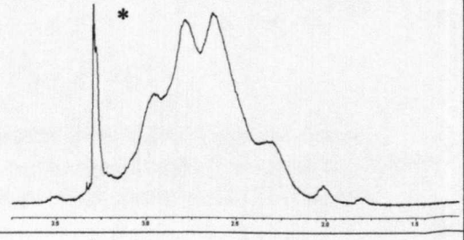	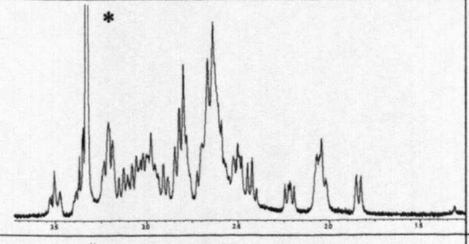	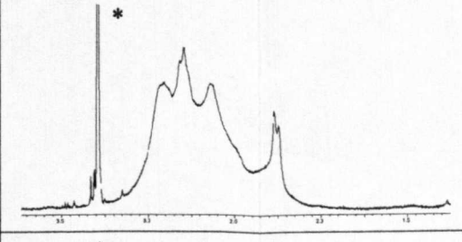	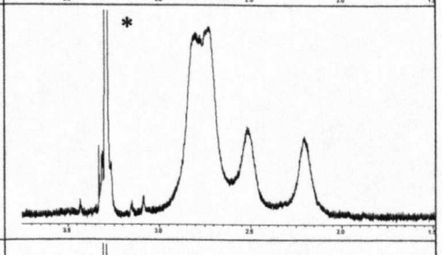
-65°	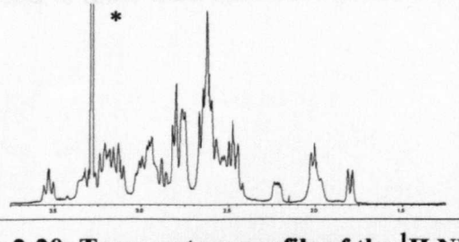	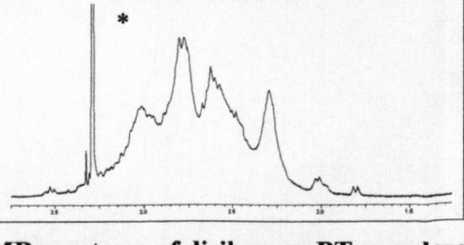	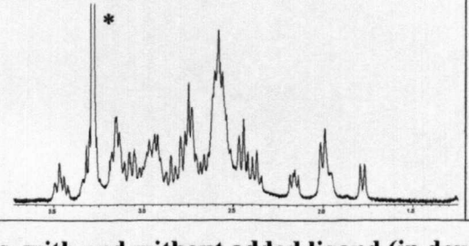	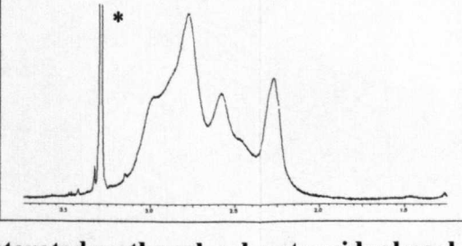	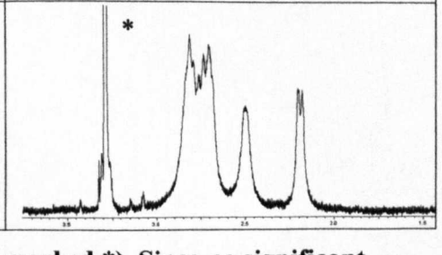

Figure 2-20: Temperature profile of the ^{1}H NMR spectrum of disilver amBT complexes, with and without added ligand (in deuterated methanol, solvent residual peak marked *). Since no significant change was observed in the aromatic region of the benzoate complex spectrum, this area has not been included.

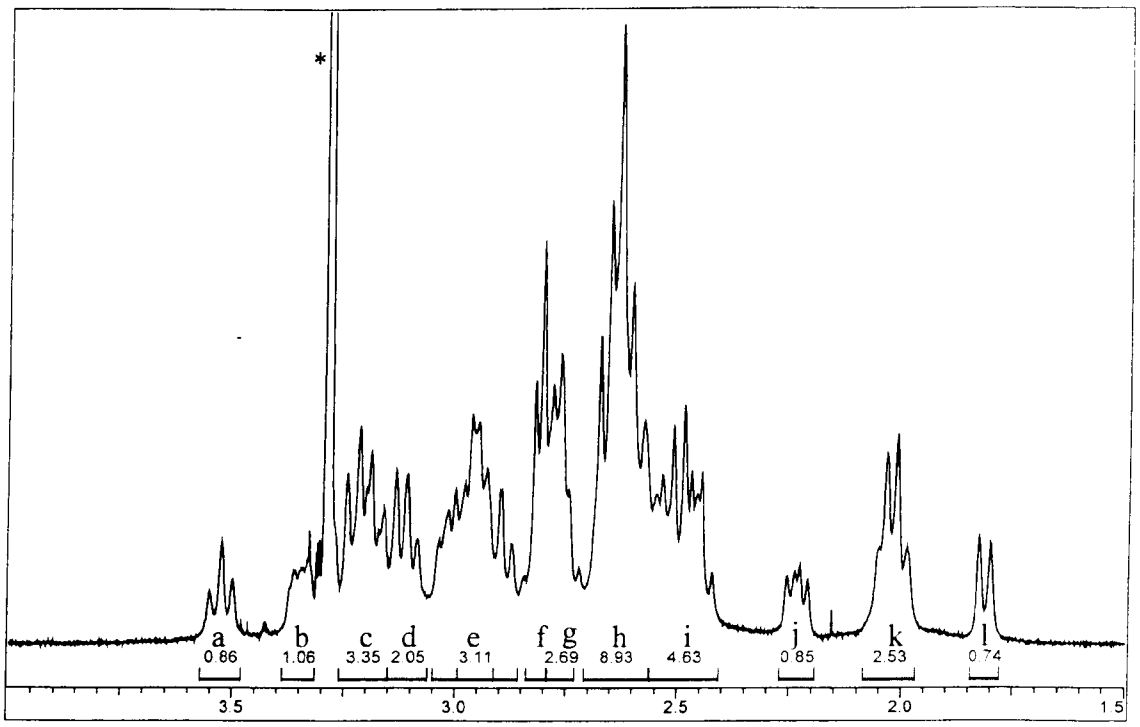

Figure 2-21: ^{1}H NMR spectrum of disilver amBT triflate in deuterated methanol at –45°C, with integral values (normalised to a total of 36 CH protons) indicated below each feature. The letter codes correspond to analysis and assignments given in section 9.1.6.

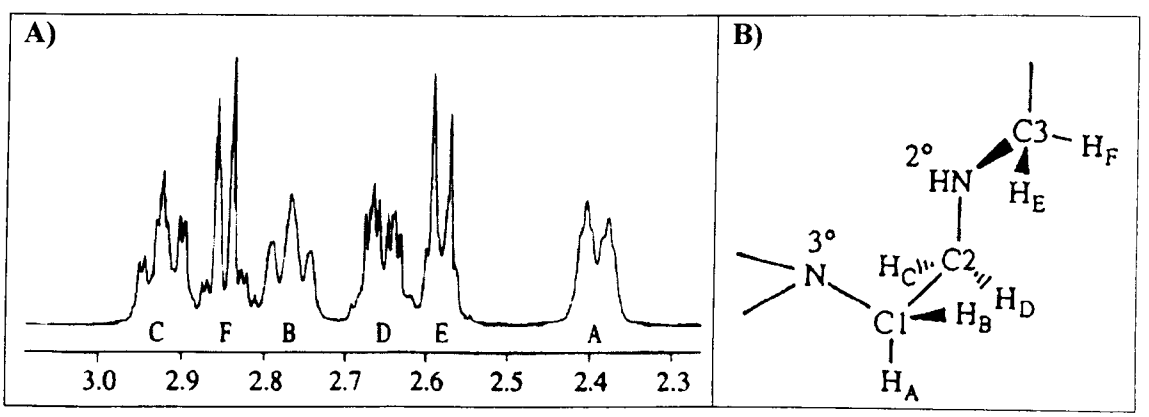

Figure 2-22: A) ^{1}H NMR of cadmium amBT tetrafluoroborate in D_2O at room temperature, with B) the assignment of protons in the spectrum. Note that the letters assigned to protons in this figure (reproduced from Thompson et al (17)) do not correspond to those used elsewhere in this study.

2.5. Electrochemical studies

Experimental conditions used to carry out cyclic voltammetric measurements are given in section 9.1.7, together with comparisons of voltammograms of electrolyte solutions, electrodes, free ligand, and free silver.

2.5.1. Disilver(I) amBT

A complicated and variable set of voltammograms of the disilver amBT cryptate were recorded on several occasions. The marked differences between voltammograms recorded under similar conditions, on different occasions, together with the similarity of many features to those observed for free ligand or silver salts strongly suggests that much of the observed electrochemical activity is due to ligand and free silver, rather than the cryptate. This is not entirely surprising, in view of the dissociative behaviour of this cryptate which was revealed by the NMR studies (section 2.4.2.1).

Several strategies were attempted to prevent this dissociation and to improve the quality of the cryptate voltammogram, and the results of these are discussed in this section.

Initial studies were made using electrolyte solutions in acetonitrile, and other solvents (butyronitrile, propionitrile, propylene carbonate) were investigated later with the aim of a) finding a system which would not support the silver stripping phenomenon, and b) allowing access to temperatures where conformational freezing was observed in the ^{1}H NMR spectra (below the freezing point of acetonitrile). Addition of excess free ligand to the cryptate solution was also attempted, with the aim of coordinating any free silver generated in the course of the experiments.

Previous sections in this chapter (sections 2.1.3 and 0) have dealt with attempts to "block" the exposed silver faces with auxiliary ligands. Unfortunately the cryptate samples incorporating cyanide ions were lost before electrochemical studies could be performed, although we anticipated that their insolubility may have led to difficulty in obtaining useful data.

In acetonitrile at room temperature (Figure 2-23 A) the voltammograms were broad, irreversible and prone to stripping phenomena. In addition to the stripping peak close to 0.2 V an irreversible oxidation wave was observed, peaking at +1.21 V (feature *a* in Table 2-17), which is not present in electrolyte, ligand, or silver salt voltammograms, and whose magnitude was unaffected by rotation rate of the electrode (*i.e.* not diffusion limited, data

not shown). This peak was present in the first scan of each set of three, indicating that it does not result from oxidation of a previously reduced species. Together, these observations suggest that a species formed oxidatively has adsorbed onto the electrode. This adsorption peak was increasingly reduced in magnitude as the minimum voltage was increased to –1.8 V, then –1.4 V, and was completely eliminated when voltage was not allowed to go below –1 V. This suggests that the adsorbed species is reductively removed at voltages below –1 V, and this transformation is apparent as a broad reduction wave in the voltammograms (peaking at –1.09 to –1.28 V depending on the range under investigation). The large separation, and the broadness of these related peaks is consistent with a chemical transformation occurring in addition to the electron transfer, and at least part of the transformation involves adsorption in this case. We speculate that this relates to the ligand, rather than the metal, and that the ligand must be in the form of a cryptate (since this feature was not observed in silver salt or free ligand voltammograms).

A sharp strong reduction just below 0 V represents reduction of Ag(I) to Ag(0) which plates the electrode, and generates the corresponding stripping oxidation. The resulting change from a platinum to silver surface may be responsible for some of the variation in peak position and intensity observed for redox features below the stripping waves.

In the full range voltammogram (black line in Figure 2-23 A) an oxidation is observed at 0.13 V (feature *b* in Table 2-17). Addition of free ligand (Figure 2-23 B) markedly reduced the stripping peak, and this oxidation is more clearly resolved, and a corresponding reduction (-0.22 V) also becomes apparent. The most likely candidate for a redox process in this voltage range is a one-electron reduction of the disilver Ag(I)Ag(I) assembly to Ag(I)Ag(0).

A reduction wave at –0.65 V is present in all of the voltammograms (feature *c* in Table 2-17). We speculate that this may represent reduction of water introduced together with the analyte, although it would have to be a reasonable amount (near one molar equivalent) to result in such a significant reduction current. In the ligand only voltammogram in acetonitrile (see section 9.1.7, Figure 9-10 C) a weak redox wave at more negative potential was proposed as a water reduction. The shift to smaller reduction potential in the present case could indicate reduction of water involved in H-bonding, and therefore more easily reduced.

When voltage is restricted to above –1.4 V more detail in the reduction phase is observed (Figure 2-23 A), a feature at –0.97 V is resolved (feature *d* in Table 2-17), which was presumably obscured by the –1.1 to –1.3 V wave. There is no clear oxidation to correspond to this (clearly irreversible) reduction, and it may be due to decomplexation from the cryptate resulting from reduction of the second Ag(I). Such a transformation would be irreversible, and would also make the Ag(0) thus formed available to participate in the stripping phenomenon. This feature appears to overlap an adjacent wave in the corresponding voltammogram with excess ligand (Figure 2-23 B).

Gosser (20) suggests the use of low temperatures as a method of stabilising reactive species, and improving reversibility. We also hoped that at low temperature, slowing of the exchange processes would simplify the voltammograms – especially by removing the source of solvated silver and thereby preventing the stripping phenomenon.

In fact, use of lower temperatures did help to remove these interferences, but quality of the voltammograms deteriorated as the faradaic current diminished in response to slower diffusion rates, and they were in general unusable by temperatures where the ^{1}H NMR spectra showed conformational freezing.

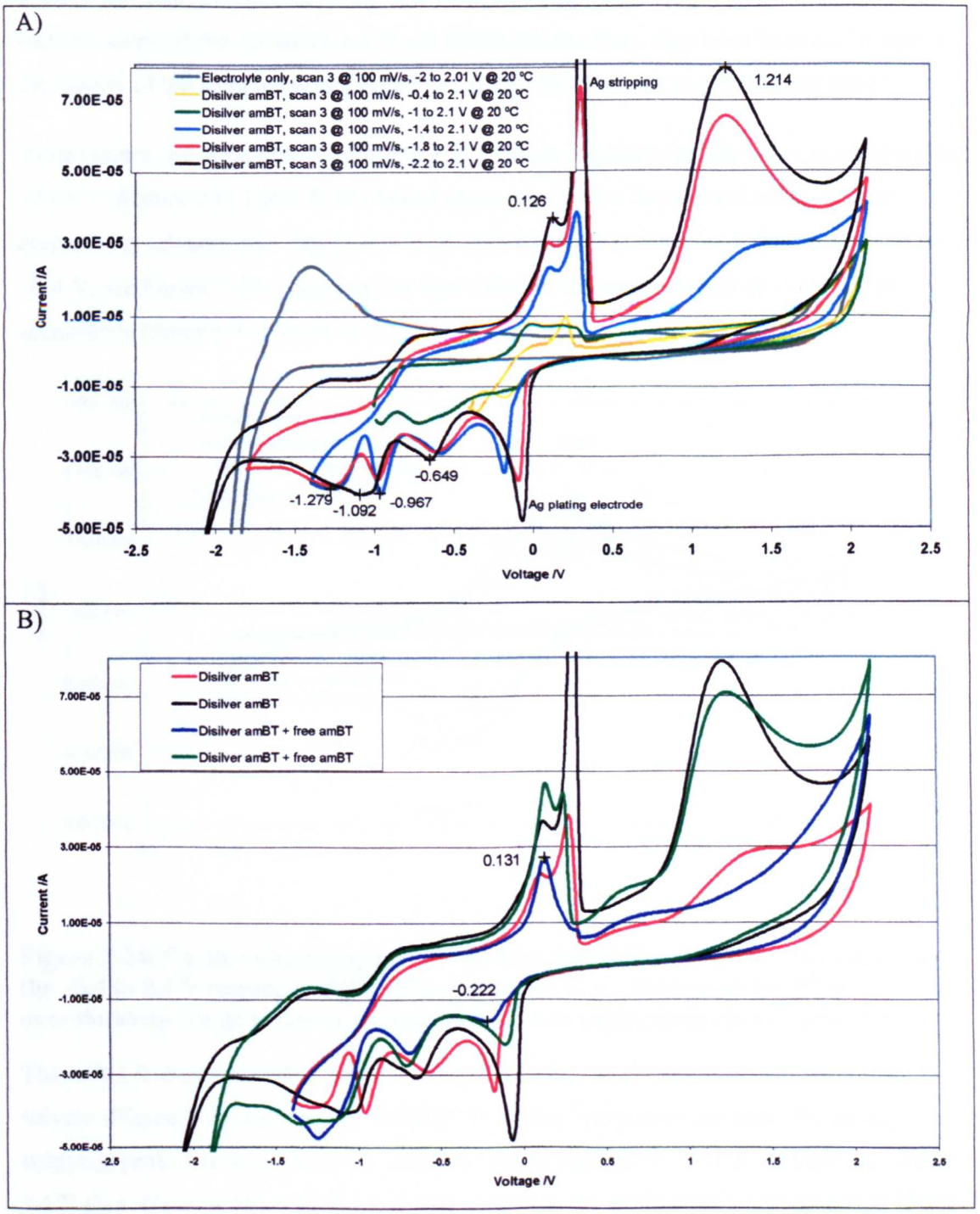

Figure 2-23: Voltammograms for disilver amBT in acetonitrile, A) compared to pure electrolyte, and B) showing the effect of adding excess free ligand.

Stripping did not affect voltammograms in propylene carbonate as severely as in the nitrile solvents, however attempts to completely avoid the effect by running at low temperature resulted in a similar diminution of faradaic current, so scans run at room temperature provided the most useful information.

Many of the observed features were similar to those of simple silver salts, indicating that dissociation and solvent effects are contributing to the complexity of the voltammograms, and that some of the variation in CVs on different occasions may have been due in part to the quality of the sample (which could not always be obtained in a crystalline form).

Nevertheless, we were able to reproducibly measure a quasireversible wave centred around –0.03 V (feature *e* in Table 2-17), which appears to derive from redox of the disilver cryptate (as solvated Ag+ shows no electroactivity when scanned over the region –0.4 to +0.4 V, see Figure 2-24). This may be equivalent to the wave centred at –0.046 V in acetonitrile (feature *b* in Table 2-17).

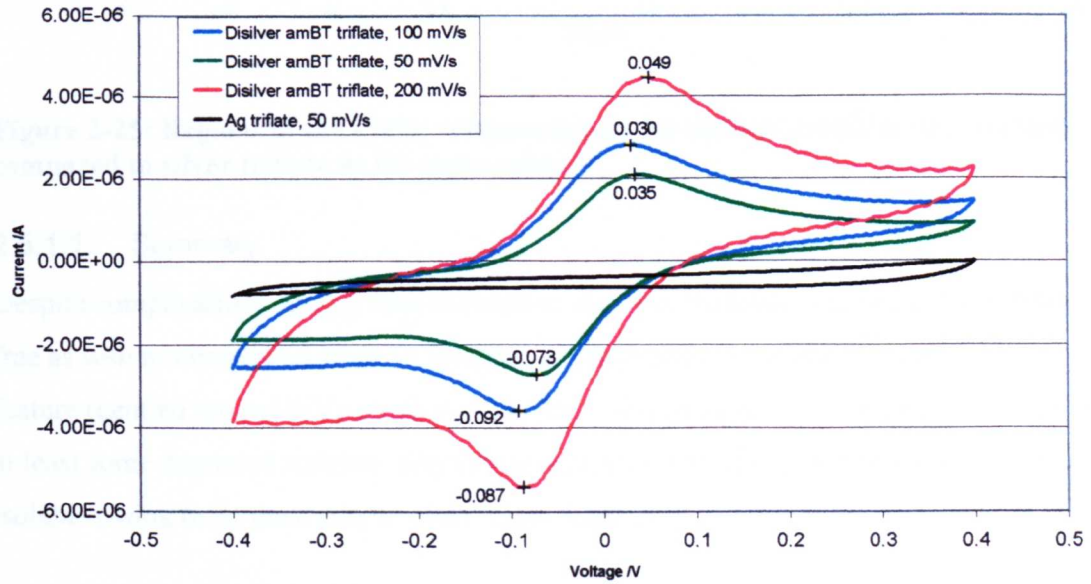

Figure 2-24: Cyclic voltammograms for disilver amBT in propylene carbonate over the –0.4 to 0.4 V region, at different scanning rates. A voltammogram of silver triflate over the same range is shown for comparison, and peak potentials are indicated.

The redox feature centred at –0.03 V can also be observed when butyronitrile is used as solvent (Figure 2-25, feature *f* in Table 2-17), and is better resolved from the strong stripping peak than in acetonitrile. Another feature centred at –0.71 V (feature *g* in Table 2-17) also relates to the cryptate, and may represent the second reduction proposed above (feature *d* in Table 2-17), a very weak oxidation at –0.58 V may be a corresponding feature.

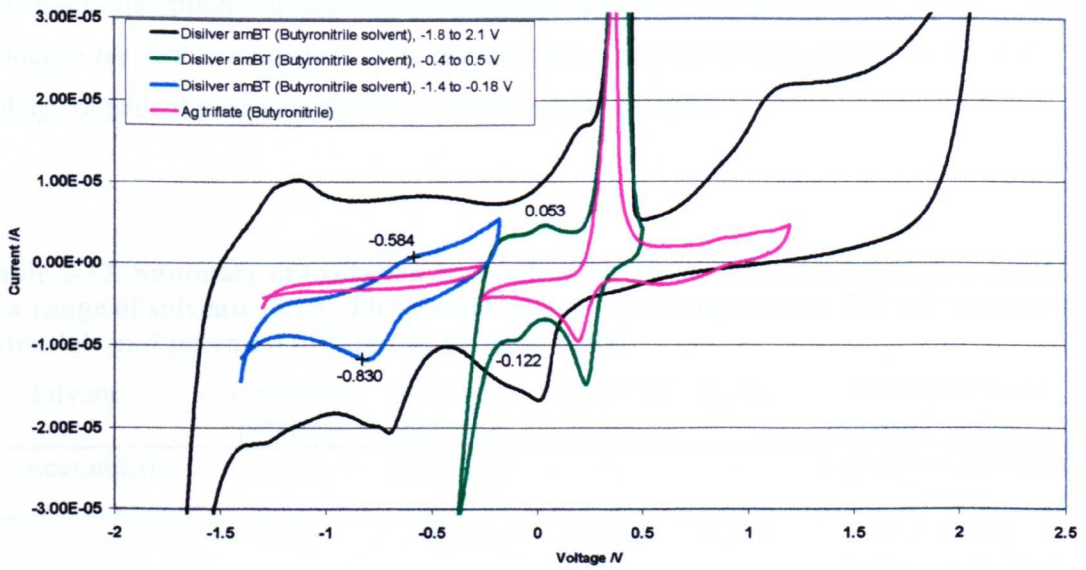

Figure 2-25: Regions of the cyclic voltammogram for disilver amBT in butyronitrile, compared to silver triflate in the same solvent.

2.5.1.1. Summary

Despite complications arising from adsorption onto the electrode, and from the presence of free as well as complexed silver in solution, we have observed a quasireversible redox feature (centred around 0 V) which may be due to the generation of a $Ag^{I}Ag^{0}$ cryptate with at least some degree of stability, although it seems unlikely that this redox state will be isolable owing to its proximity to other redox features.

An irreversible reduction at more reducing voltage (feature *d* in Table 2-17) may represent transformation to an unstable $Ag^{0}Ag^{0}$ state, which decomposes releasing silver from the crypt. This is consistent with the observation that voltammograms extending to or below this voltage are more strongly affected by stripping. A similar observation was made in a different disilver cryptate by Takemura et al (their ligand incorporated a tertiary amine bridgehead, with pyridine spacers, (21)), who noted the growth of a stripping process only after free silver was generated by an irreversible reduction occurring at –1.20 V vs $Ag/AgNO_3$. In their case, this generated a stable monosilver complex (previously isolated), which could not be further reduced at attainable potentials.

In our system, a broad adsorption related oxidation wave at 1.21 V is dependent on a species generated by reduction below –1.1 V, and the large separation between these features leads us to believe that these transformations must relate to a chemical transformation of the ligand, although the exact nature of the species generated is not clear.

When the adsorption is avoided by keeping the minimum voltage above −1 V, there was no evidence for further oxidation of the cryptate, the Ag(I)Ag(II) state apparently lies at a voltage outside the range attainable in these solvent systems.

Table 2-17: Summary of oxidation and reduction waves observed for disilver amBT in a range of solvents (0.1M TBAP electrolyte, room temperature, 100 mV/s scan rate, potentials and potential differences given in volts).

	Solvent	Oxidation potential	Reduction potential	Centre of feature	E_A-E_C	Description and proposed assignment
a	Acetonitrile	1.214	−1.092 to −1.279	-	-	Ligand ↔ Adsorbed species
b		0.131	-0.222	-0.046	0.353	Irreversible $Ag^IAg^I \leftrightarrow Ag^IAg^0$
c		-	-0.649	-	-	Irreversible $2H_2O \rightarrow H_2 + 2OH^-$?
d		-	-0.967	-	-	Irreversible $LAg^IAg^0 \rightarrow L + 2Ag^0$
e	Propylene carbonate	0.030	-0.092	-0.031	0.122	Quasireversible $Ag^IAg^I \leftrightarrow Ag^IAg^0$
f	Butyronitrile	0.053	-0.122	-0.034	0.175	Irreversible $Ag^IAg^I \leftrightarrow Ag^IAg^0$
g		-0.584	-0.830	-0.707	0.246	Irreversible $LAg^IAg^0 \leftrightarrow L + 2Ag^0$

2.5.2. Disilver(I) imBT

Disilver imBT voltammograms were broadly similar to the reduced ligand analogue, also being affected by stripping and adsorption phenomena.

In butyronitrile the majority of the redox features observed in the full range cryptate voltammogram (Figure 2-26 A) could be attributed to either electrolyte, ligand (green line) or silver stripping (the size of the stripping oxidation increased throughout the procedure, and the corresponding plating reduction was broader than in previous experiments). An irreversible oxidation at 0.80 V is assigned to ligand oxidation, presumably electron loss from a π bond. A weak oxidation (0.18 V) on the side of the stripping peak was similar to that observed for the disilver cryptate of the reduced ligand, and corresponds to the reduction at 0.05 V (feature h in Table 2-18). Addition of excess free ligand to the solution enhanced this feature, although the ligand itself was shown to be inactive in this region. These observations are consistent with the known decomplexation behaviour in solution

(6) – the addition of more ligand resulting in an increased concentration of the electrochemically active species. This could occur via the equilibrium suggested in the discussion of ^{1}H NMR evidence above (section 2.1.2), *i.e.*

$$Ag^{I}{}_2L \leftrightarrow Ag^{I}L + Ag^{I}{}_{(solution)} \qquad \textbf{Equation 2-1}$$

addition of free ligand resulting in uptake of solvated silver, shifting the equilibrium towards the RHS, and increasing the concentration of mono-silver complex. Thus the observed redox process could represent $Ag^{I}L \leftrightarrow Ag^{0}L$. Whilst this explanation is consistent with the observations in butyronitrile, a mono-silver complex has never been isolated, and this hypothesis does not explain the voltammograms recorded in propylene carbonate (see below). We therefore propose an alternative explanation: if the equilibrium;

$$Ag^{I}{}_2L \leftrightarrow L + 2Ag^{I}{}_{(solution)} \qquad \textbf{Equation 2-2}$$

was present, addition of free ligand would shift the equilibrium towards the LHS, thus causing an increase in the disilver cryptate concentration – this is also consistent with electrochemical observations in butyronitrile, in this case the redox process could be described as $Ag^{I}{}_2L \leftrightarrow Ag^{I}Ag^{0}L$.

Unlike butyronitrile, voltammograms with electrolyte in propylene carbonate were generally free from stripping phenomena. The full scan voltammograms contained several broad irreversible features probably due to solvent and ligand effects. Scanning within the region of –0.5 to +0.5 V revealed more detail, (Figure 2-26 B) and in this case, *two* redox pairs, one irreversible (centred at 0.05 V, feature j in Table 2-18), and one quasireversible (centred at 0.24 V, feature k in Table 2-18) were observed, both of which were enhanced by the addition of free ligand. The more positive quasireversible redox process is probably the same as the feature observed in butyronitrile, whilst the second may represent $Ag^{I}Ag^{0}L \leftrightarrow Ag^{0}Ag^{0}L$.

Thus, it is possible that we have observed the complete $Ag^{I}Ag^{I}L \rightarrow Ag^{I}Ag^{0}L \rightarrow Ag^{0}Ag^{0}L$ sequence, the proximity of the two redox features suggesting that there is a small extent of interaction between the two nuclei (which are not bridged, and are only separated by 2.83 Å in the solid state (4)). The mixed valence region is short, and given the irreversible nature of the redox process, and the propensity of this system for decomplexation, it seems unlikely that a $Ag^{I}Ag^{0}$ cryptate would be isolable.

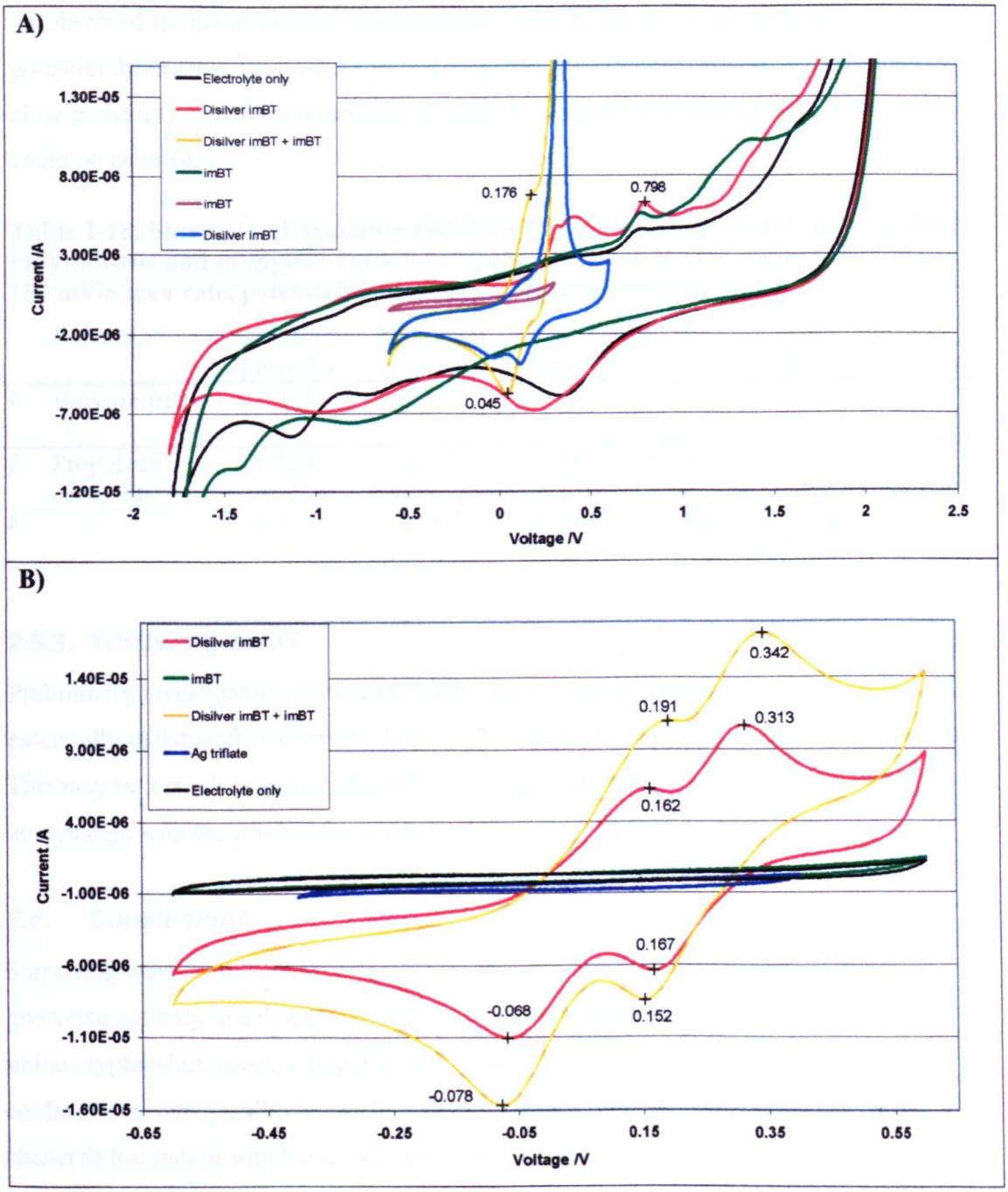

Figure 2-26: Comparison of cyclic voltammograms for disilver imBT and free imBT ligand, in A) butyronitrile, and B) propylene carbonate solvent.

2.5.2.1. Summary

The electrochemistry of disilver imBT has features in common with the disilver cryptate of the reduced ligand, and is subject to similar interferences. A pair of oxidation/reduction waves (summarised in Table 2-18) centred at 0.24 V has been assigned to the $Ag^{I}Ag^{I}L \leftrightarrow Ag^{I}Ag^{0}L$ redox couple, and a second overlapping pair centred at 0.05 V may represent $Ag^{I}Ag^{0}L \leftrightarrow Ag^{0}Ag^{0}L$.

As observed for the analogous aminocryptate, none of the redox features had peak potential differences consistent with reversibility, and this observation, together with the close proximity of several redox waves, leads us to doubt that reduced disilver cryptates could be isolated.

Table 2-18: Summary of oxidation and reduction waves observed for disilver imBT in butyronitrile and propylene carbonate (0.1M TBAP electrolyte, room temperature, 100 mV/s scan rate, potentials and potential differences given in volts).

	Solvent	Oxidation potential	Reduction potential	Centre of feature	E_A-E_C	Description and proposed assignment
h	Butyronitrile	0.176	0.045	0.110	0.131	Quasireversible $Ag^IAg^IL \leftrightarrow Ag^IAg^0L$
j	Propylene carbonate	0.162	-0.068	0.047	0.230	Irreversible $Ag^0Ag^0L \leftrightarrow Ag^IAg^0L$
k		0.313	0.167	0.240	0.146	Quasireversible $Ag^IAg^0L \leftrightarrow Ag^IAg^IL$

2.5.3. Trisilver(I) amBT

Preliminary investigations of trisilver amBT gave voltammograms (in acetonitrile) essentially indistinguishable from those of disilver amBT recorded on the same occasion. This may be a result of contamination of the sample with the disilver cryptate, or of interchange with the (thermodynamically disfavoured) disilver cryptate.

2.6. Conclusions

Surprising behaviour is observed for silver with the small, yet flexible amBT ligand. It gives rise not only to a dinuclear complex with a similar structure to the corresponding imino cryptate but, given a longer period of time in solution, a change in ligand conformation occurs, allowing a *third* silver to coordinate. An asymmetric triangular cluster is formed, in which each silver ion lies in a face of the ligand. Preliminary modelling studies suggested that in the solid state, the ligand conformation in the trisilver cryptate is even more strained than the disilver cryptate. The driving force for coordination of the third silver therefore appears to be the formation of closer Ag-N contacts, and of two additional close silver-silver contacts in the triangular array of silver ions.

The degree of stabilisation which appears to result from the proximity of three, positively charged, full shell ions is at first surprising. The "aurophilic" effect is well known and accepted for gold, where relativistic contraction of the s orbitals allows them to mix more easily with the outer d orbitals, however the silver nucleus is too light to accelerate

electrons to relativistic speeds. The existence of an analogous "argentophilic" (and cuprophilic, see chapter 3) effect has been debated in the literature over several decades, however the weight of evidence in favour of such an effect is now overwhelming. A variety of synthetic/structural studies (*e.g.* (14-16, 19, 21-25)), modelling studies (12, 26) as well as observations reported in this work (this chapter, and chapter 5) support the hypothesis that close approach of silver(I) ions can stabilise a complex, in a manner consistent with the formation of a metal-metal bond of sorts, or at least a strong van der Waals interaction. Our observation of a decreased internuclear separation in a disilver(I) cryptate (tren caps with m-xylyl spacers) compared to the analogous dicopper(I) cryptate (see chapter 5), is similar to observations made by other workers, and strongly suggests an attractive interaction between the d^{10} ions. A recent synthetic and DFT study by Drew and coworkers (12) on this system concluded that a silver-silver interaction is indeed responsible for the internuclear contraction.

Triangular silver clusters with short (~2.8 Å, less than the separation in metallic silver) to relatively long (3.3-3.5 Å) internuclear separations are found many times in the literature, and there are several instances of dimers of such triangular arrangements with close Ag-Ag contacts (*e.g.* (14, 22)), and also of linear arrangements with short distances (25).

Systems studied by Singh, Angaridis, and Burrows (14, 22, 23) contain examples of silver-silver contacts which are unsupported by other ligands. The imidazole system studied by Eastland (16) is particularly notable, containing six Ag(I) ions, with three relatively close silver-silver contacts, none of which are bridged or otherwise supported.

In our system, we believe that the argentophilic effect leads to distortion of the amBT ligand to facilitate an increase in the number of silver-silver contacts. Argentophilicity would also account for a similar observation by Takemura (21), where a ligand was distorted in order to accommodate a second Ag(I) ion.

The cryptates formed do not exhibit the high degree of symmetry observed for many other cryptates, the disilver cryptate with its folded A-frame type structure contains two similar strands, and one quite different strand (giving rise to fiendishly complicated NMR spectra), and even the trisilver cryptate, with one ion in each face of the ligand is asymmetrical, containing an isosceles rather than equilateral triangle of ions. Solid state NMR studies confirm the asymmetry in the trisilver cryptate, as two ^{109}Ag resonances are observed,

presumably relating to the pair of ions at the base of the triangle, and the ion at the apex (*i.e.* C_{2v} rather than D_{3h} point symmetry).

Solution NMR studies on the disilver imBT and disilver amBT systems have shown that they are both affected by dissociation, although the degree of this effect is dependent on solvent, temperature, and counterion. A disilver amBT cryptate with benzoate counterion shows less tendency to dissociate in methanol than with triflate counterion, although, as with other related cryptates (19) exchange processes of some kind are obviously occurring, as the NMR spectrum does not show conformational freezing until –45°C. Electrochemical investigations of these systems were also affected by dissociation, leading to interference from free solvated silver. The influence of solvent and temperature were again demonstrated here, and we have proposed that a mixed valence Ag^0Ag^I amBT complex is generated in a quasireversible process at reduction potential close to 0 V.

Electrochemical studies of a disilver iminocryptate (Ag-Ag 2.83 Å) with a conformation similar to the disilver aminocryptate (Ag-Ag 2.81 Å) revealed successive redox waves that may represent the sequence $Ag^IAg^IL \rightarrow Ag^IAg^0L \rightarrow Ag^0Ag^0L$. The two features are separated by 0.193 V, and if our assignment of these features is correct, then this potential difference is related to the stabilisation afforded by the silver-silver contact. Unfortunately, we doubt that any of these states will be isolable, owing to their poor reversibility, proximity to other redox processes, and the known dissociation equilibria in these systems.

Attempts to control dissociation and exchange processes by coordinating auxiliary ligands to the exposed silver ions in the disilver imBT and amBT cryptates met with little success. Exchanging the counterion for ions with a greater chance of coordinating was the most successful strategy, cyanide and benzoate were both successfully employed, although results of electrochemical studies on these products are not yet available. Neutral ligands either did not coordinate, or else stripped the metal from the crypt, showing that the balance to be achieved between binding to silver but not abstracting it, is very fine.

Cyclic voltammetry of the cryptates with cyanide or benzoate counterions may reveal additional detail of redox processes. Perhaps more importantly however, if the mixed valence region of the voltammogram is sufficiently wide and free of decomposition effects, it may prove possible to generate quantities of mixed valence species sufficient for isolation, or at least for *in situ* study, using for example a combined electrochemical/ESR cell.

Electrochemical studies of the trisilver cryptate will also be of interest, especially in comparison to the silver imidazole structure (16), where radiolytic oxidation resulted in no evidence for delocalisation.

2.7. References

1. Hunter, J., J. Nelson, C. Harding, M. McCann, and V. McKee, Journal of the Chemical Society: Chemical Communications, 1990: p. 1148-1151.

2. Dietrich, B., J.-M. Lehn, J. Guilhem, and C. Pascard, Tetrahedron Letters, 1989. **30**(31): p. 4125-4128.

3. Smith, P.H., M.E. Barr, J.R. Brainard, D.K. Ford, H. Freiser, S. Muralidharan, S.D. Reilly, R.R. Ryan, L.A.I. Silks, and W.-h. Yu, Journal of Organic Chemistry, 1993. **58**: p. 7939-7941.

4. Coyle, J.L., V. McKee, and J. Nelson, Chemical communications, 1998: p. 709-710.

5. Solomons, T.W.G., *Organic Chemistry*. 6th ed. Vol. 1. 1996, New York: John Wiley and Sons Inc.

6. Apperley, D., W. Clegg, S. Coles, J. Coyle, N. Martin, B. Maubert, V. McKee, and J. Nelson, Journal of the Chemical Society: Dalton Transactions, 1999(2): p. 229-236.

7. Soma, T. and T. Iwamoto, Inorganic Chemistry, 1996. **35**: p. 1849-1856.

8. Britton, D., Acta Crystallographica Section C - Crystal Structure, 1990. **46**: p. 2297-2299.

9. Nelson, J., Personal Communication, 1998.

10. Nelson, J., V. McKee, and G. Morgan, Progress in Inorganic Chemistry, 1998. **47**: p. 167-316.

11. McKee, V., J. Nelson, D.J. Speed, and R.M. Town, Journal of the Chemical Society: Dalton Transactions, 2001: p. 3641-3646.

12. Drew, M., D. Farrell, G. Morgan, V. McKee, and J. Nelson, Journal of the Chemical Society-Dalton Transactions, 2000. **9**: p. 1513-1519.

13. Che, C.M., H.K. Yip, V.W.W. Yam, P.Y. Cheung, T.F. Lai, S.J. Shieh, and S.M. Peng, Journal of the Chemical Society-Dalton Transactions, 1992(3): p. 427-433.

14. Burrows, A.D., M.F. Mahon, and M.T. Palmer, Journal of the Chemical Society-Dalton Transactions, 1998(12): p. 1941-1942.

15. Amoroso, A.J., J.C. Jeffery, P.L. Jones, J.A. McCleverty, E. Psillakis, and M.D. Ward, Journal of the Chemical Society-Chemical Communications, 1995(11): p. 1175-1176.

16. Eastland, G., M. Mazid, D. Russell, and M. Symons, Journal of the Chemical Society: Dalton Transactions, 1980: p. 1682-1687.

17. Thompson, J.A., M.E. Barr, D.K. Ford, L.A. Silks, J. McCormick, and P. Smith, Inorganic Chemistry, 1996. **35**: p. 2025-2031.

18. Fijolek, H., T. Oriskovich, A. Benest, P. Gonzalez-Duarte, and M. Natan, Inorganic Chemistry, 1996. **35**(4): p. 797-799.

19. Howarth, O., G. Morgan, V. McKee, and J. Nelson, Journal of the Chemical Society-Dalton Transactions, 1999. **12**(June 21): p. 2097-2102.

20. Gosser, D., *Cyclic voltammetry : simulation and analysis of reaction mechanisms*. 1993, New York: Wiley.

21. Takemura, H., N. Kon, K. Tani, K. Takehara, J. Kimoto, T. Shinmyozu, and T. Inazu, Journal of the Chemical Society: Perkin Transactions, 1997: p. 239-246.

22. Singh, K., J. Long, and P. Stavropoulos, Journal of the American Chemical Society, 1997. **119**: p. 2942-2943.

23. Angaridis, P., P. Baran, R. Raptis, C. Raptopolou, and A. Terzis, Unpublished data, 2000.

24. Baenziger, N. and A. Struss, Inorganic Chemistry, 1976. **15**(8): p. 1807-1809.

25. Hartshorn, C. and P. Steel, Inorganic Chemistry Communications, 2000. **3**: p. 476-481.

26. Pyykko, P., Chemical Reviews, 1997. **97**: p. 597-636.

3. Investigation of a possible copper(I)–copper(I) interaction

The dicopper imBT system has been studied in great depth because it includes the first manmade example of the intermediate redox state dicopper(1.5), which has been described as average valence dicopper, rather than mixed valence (which refers to localised Cu(I)Cu(II)) (1). This type III site (according to the Robin and Day classification (2)) is similar to that observed in the active sites of some biomolecules. The related dicopper(I) cryptate has a very similar solid state configuration, with a copper-copper separation only slightly longer (see Figure 3-1 a and b). The small (less than 0.07 Å) change in internuclear separation on one-electron reduction raises the question, is there also a degree of copper-copper interaction in dicopper(I) imBT? Such an interaction between two, formally d^{10}, cations is well known for gold, where it is accounted for by relativistic contraction of the outer s orbitals. There is also strong evidence for a similar affect with silver (3), where relativistic effects are not strong enough to explain the phenomenon (see also discussion in chapters 2 and 5). The presence (4-6), or lack of (7, 8), interaction between d^{10} copper(I) ions has been argued for many years, and the unambiguous confirmation of such an interaction would be of considerable interest. This chapter describes attempts to investigate this (ESR silent) molecule by crystallographic measurement of the electron density distribution between the copper(I) ions.

In order to make the detailed measurement of electron density required to determine whether a copper-copper interaction exists or not, a crystal of very high quality is required, ideally incorporating a small, high symmetry anion (such as perchlorate). Phenomena resulting in convolution of crystallographic data, such as racemic twinning, are therefore particularly undesirable in this situation.

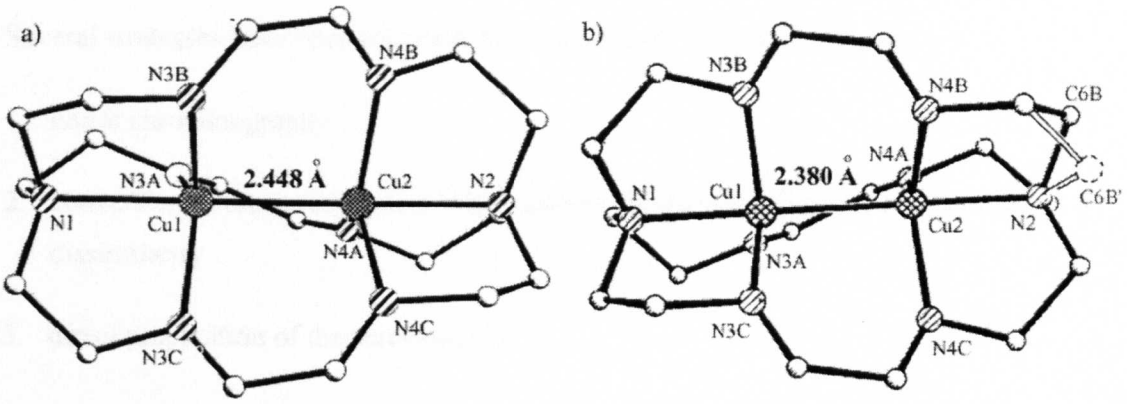

Figure 3-1: Comparison of crystal structures (1, 9) of a) dicopper(I) imBT, and b) dicopper(1.5) imBT, showing the slight reduction in copper-copper separation. Also note the chirality of the molecules, resulting from the helical twist: these two molecules are of opposite handedness.

It is a well-known yet little investigated property of cryptands and cryptates that they are chiral. This arises from the helical nature of the structures which may be formed (see Figure 3-1). The imBT and amBT systems are both subject to this effect as are other cryptates such as the imino-cryptand whose crystal structure is reported in section 9.2.1 (the unusual ligand conformations of the di- and trisilver cryptates discussed in Chapter 2 are approximately ahelical).

The two conformations (denoted M and P according to CIP notation, (10)) are expected to form in equal amounts during encapsulation of the guest ion(s), and are both observed in the crystal structure of the solid (although not in equal proportions, see discussion below). This leads to the aforementioned phenomenon of racemic twinning, and it results in the superimposition of diffraction data from the two distinct species present in the single crystal. Not surprisingly, this can lead to significant difficulties for the crystallographer. The effect of racemic twinning can be accounted for by including a factor known as the Flack parameter in the model, to describe the extent of twinning. However, this factor cannot be independently measured, and is adjusted during refinement of the model in order to optimise the fit of the model to the observed data. The empirical nature of this correction makes it impossible to make the most detailed calculations (*i.e.*, electron density) with the required degree of certainty. Resolution of the enantiomers, and preparation of an optically pure crystal of high quality will therefore be required in order to obtain the desired electron density information.

Several strategies have been successfully used to resolve racemic mixtures:

1. chiral chromatography
2. conversion to diastereoisomers, which can be separated owing to their chemical dissimilarity
3. direct preparation of diastereoisomers
4. enantiopure crystallisation

Chiral chromatography involves the use of a chiral stationary phase, with or without a chiral eluent. Sephadex resins are commonly used, and an attempt to use this method is described in section 3.1.3.

For conversion of a cationic enantiomer to a diastereoisomer, a common procedure is to couple it with an enantiomeric counterion, such as antimonyl tartrate (which has been successfully applied to a different triple helix system (11, 12)), and attempts to perform this transformation using this, and related reagents, are described in section 3.1.4.

An alternative route to the diastereoisomers, is to prepare them directly by reaction of an enantiomeric salt (*e.g.* a copper tartrate) with the free ligand, and attempts to perform this procedure are described in section 3.1.5.

Some enantiomers are known to have different crystalline forms, and racemic mixtures of such compounds can be resolved by physical separation of the crystals. The observation of variable Flack parameters in different crystals of dicopper(I) imBT leads us to believe that by careful adjustment of the conditions of crystallisation, or by crystallisation in the presence of an appropriate agent, it may be possible to obtain crystals of sufficient optical purity for electron density studies. Section 3.1.6 describes the results from attempts to obtain resolved crystals via crystallisation.

3.1. Dicopper(I) imBT

3.1.1. Free imBT

The free ligand was prepared according to literature methods (13), a reference infrared spectrum has been previously given (see Figure 2-2).

3.1.2. Dicopper(I) imBT perchlorate

The dicopper (I) complex was prepared using $Cu^{I}(MeCN)_4ClO_4$ (see section 9.2.2) and free imBT ligand, following the published procedure (1), in 75 % yield.

Large hexagon shaped crystals were obtained by recrystallising the solid from a 50:50 mixture of acetonitrile/water, which was left to stand on the bench for 12 hours. Smaller, X-ray quality crystals were obtained by the slow evaporation of a solution in acetonitrile from a vessel with a punctured lid.

The elemental analysis (Table 3-1) of a non-crystalline sample was only in rough agreement, but was somewhat improved by including one equivalent of water (as observed in the NMR, see Figure 3-4) in the calculation.

Table 3-1: Elemental analysis of (non-crystalline) dicopper(I) imBT perchlorate.

Analysis	%C	%H	%N
Predicted (Cu_2 imBT $(ClO_4)_2$):	31.59	4.42	16.37
Predicted (Cu_2 imBT $(ClO_4)_2$)·H_2O:	30.78	4.59	15.95
Found (non-crystalline sample):	31.04	4.01	15.21

FAB mass spectrometric analysis (Table 3-2) was consistent with the determined structure. Weak peaks relating to a proposed tetracopper 6+4 macrocycle (see chapter 7) were also observed.

Table 3-2: FAB mass spectrum of dicopper imBT perchlorate (EPSRC service, NOBA matrix, L=imBT, L*=possible 6+4 ligand, see chapter 7).

m/z	Abundance /%	Identity	m/z	Abundance /%	Identity
421	97	Cu L	684	6	Cu_2 L $(ClO_4)_2$
484	62	Cu_2 L	1170	0.5	Cu_4 L* $(ClO_4)_2$
585	100	Cu_2 L ClO_4	1270	3	Cu_4 L* $(ClO_4)_3$

The IR spectrum (Figure 3-2) is dominated by the strong perchlorate bands at 1096 and 622 cm^{-1}, while the imine stretch at 1656 cm^{-1} appears weak in relation. CH and fingerprint region peaks similar to those of the free ligand are also observed.

^1H NMR spectra were obtained in deuterated water (Figure 3-3), and deuterated methanol (Figure 3-4). The spectrum is simple in both solvents, and the peak positions resemble

those of the free ligand, since the configuration of this cryptate is similar to the shape of the free ligand. It is noteworthy that the cap protons in the cryptate both give rise to triplets, showing that the ligand conformation is not "frozen". In a rigid cryptate conformation, axial and equatorial protons are non-equivalent, and a more complicated NMR spectrum is expected. Comparison of the cryptate spectrum (Figure 3-4 B) to the free ligand (Figure 3-4 A), and a mixture containing free ligand and cryptate (Figure 3-4 C) shows that the two spectra are additive, with no signs of the time averaging effect observed for the disilver system where addition of free ligand results in changes in the observed spectrum (see discussions in Chapter 2). On the NMR timescale, Cu_2 imBT cation and imBT ligand are distinct species, this is consistent with the observed structure, with its fully encapsulated copper ions, isolated from the solvent by the surrogate "solvation sphere" of the cryptand.

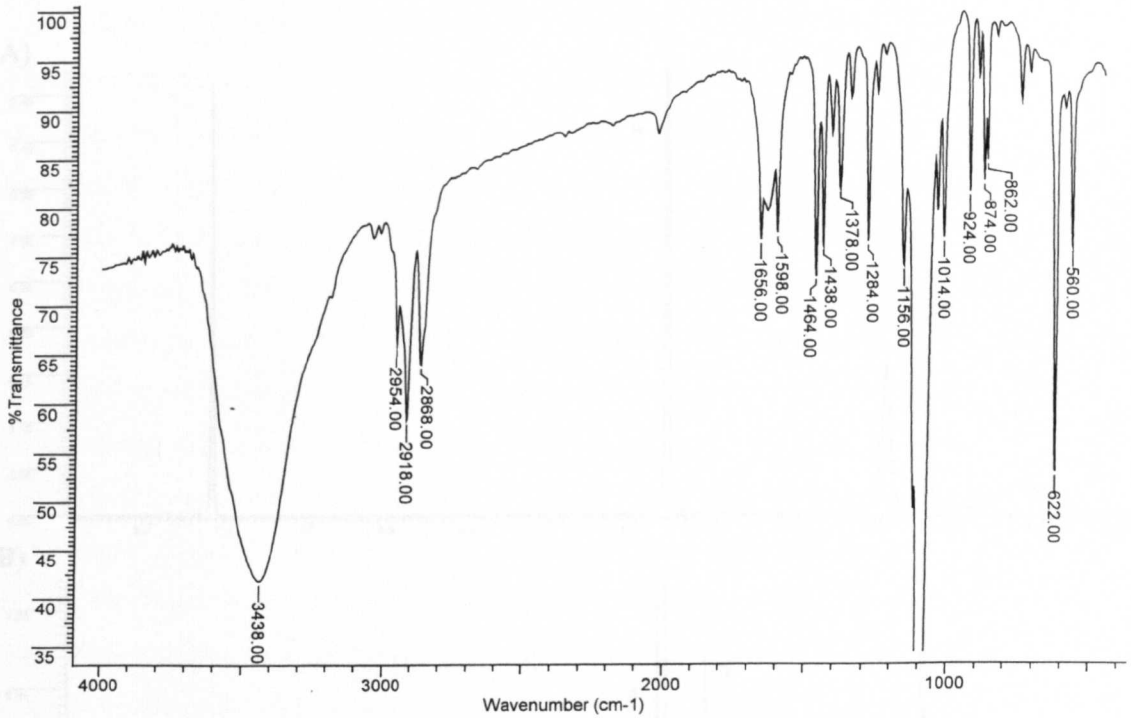

Figure 3-2: Infrared spectrum of $Cu(I)_2$ imBT ClO_4 (KBr disk).

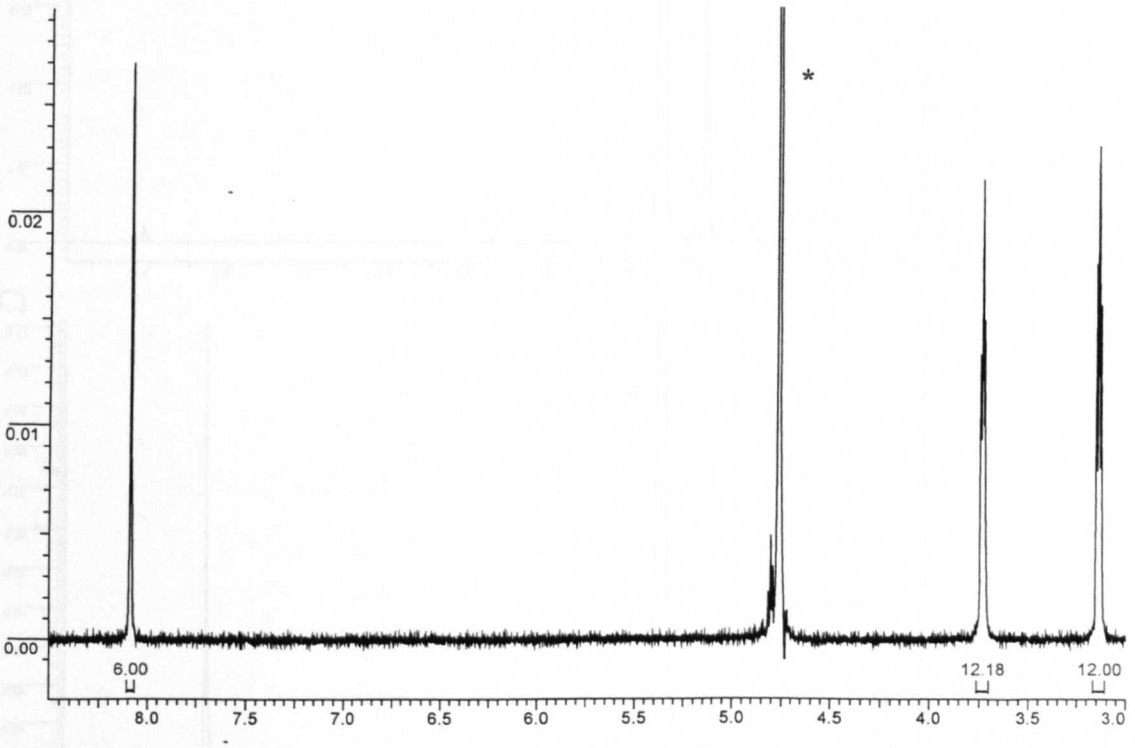

Figure 3-3: ^1H NMR spectrum of $Cu(I)_2$ imBT ClO_4 in D_2O (room temperature) consisting of a singlet at 8.1 ppm owing to the imine protons, and triplets at 3.7 and 3.15 ppm from the cap protons (* water).

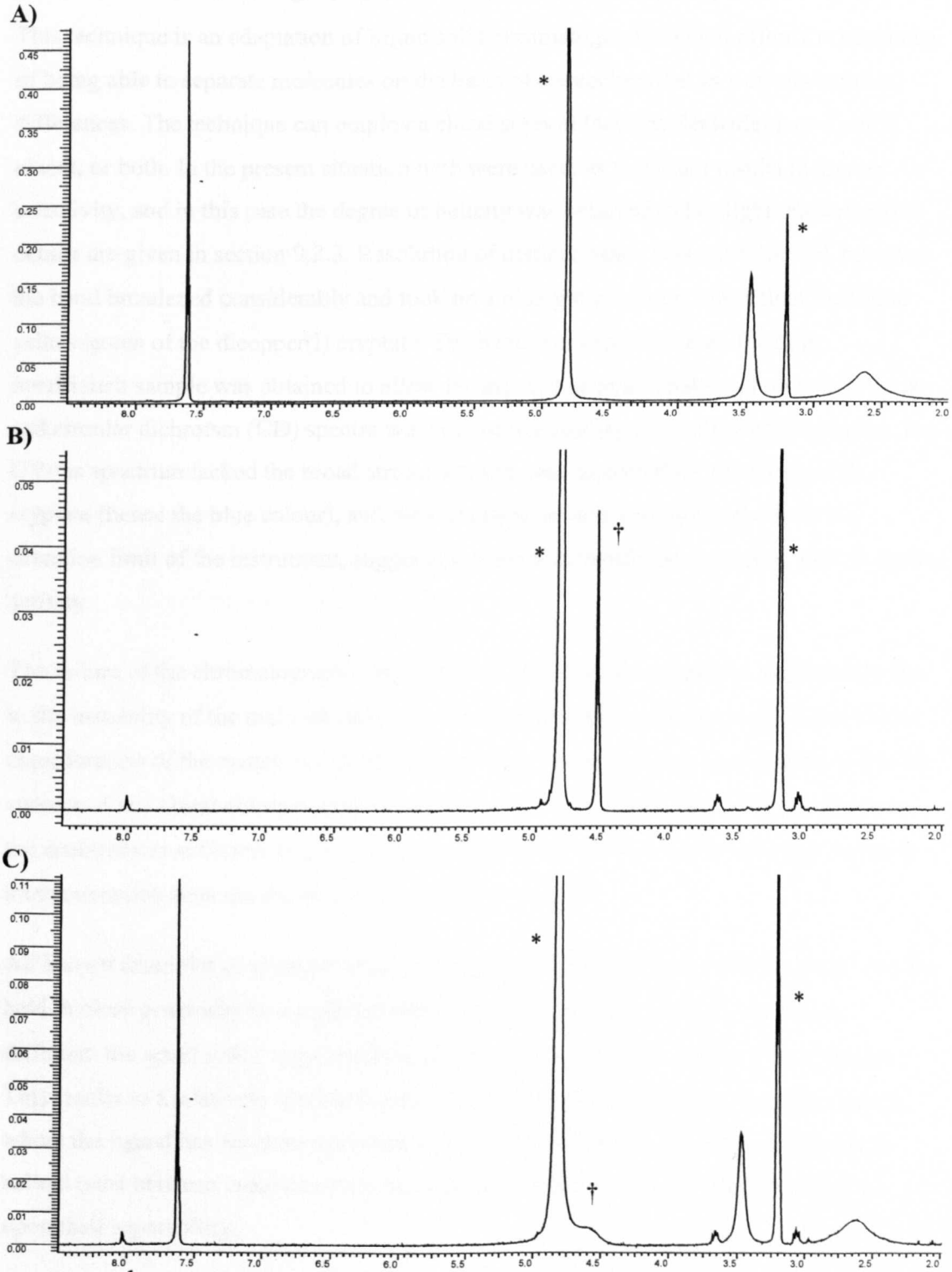

Figure 3-4: ^{1}H NMR in CD_3OD of A) imBT, B) Cu_2 imBT, and C) Cu_2 imBT with free ligand added. Solvent features are marked (* methanol, † water).

3.1.3. Chiral chromatography for resolution of dicopper(I) imBT

This technique is an adaptation of liquid/solid chromatography which offers the advantage of being able to separate molecules on the basis of stereochemical as well as chemical differences. The technique can employ a chiral support (such as Sephadex), or a chiral eluent, or both. In the present situation both were used, as this often results in greater selectivity, and in this case the degree of helicity was believed to be slight. Experimental details are given in section 9.2.3. Resolution of distinct bands was not achieved, however the band broadened considerably and took on a blue/green colour, rather than the initial yellow/green of the dicopper(I) cryptate. The band was eluted in three fractions, insufficient sample was obtained to allow for infrared or other analysis, however UV/vis and circular dichroism (CD) spectra were run on the leading and tailing edge samples. The UV/vis spectrum lacked the broad strong 400 nm peak expected for the dicopper(I) cryptate (hence the blue colour), and the CD spectrum was very noisy and near the detection limit of the instrument, suggesting either a racemate, or a material with no optical activity.

The failure of the chromatographic separation in this instance appears to be primarily due to the instability of the material under the chromatographic conditions used. Upon further consideration of the matter, we identified two other issues that may significantly affect the success of any chiral chromatographic separation of cryptates: is the difference between the enantiomers sufficient to give chromatographic resolution? And what is the barrier to interconversion between the two enantiomers in solution?

All known examples of average valence dicopper occur in situations where copper ions are held in close proximity by a rigid coordination sphere, and the current system is no different: the small imBT crypt enforces an uncomfortably close copper-copper distance. This results in a relatively smaller degree of helical twist than observed in other systems where the ligand has freedom to collapse about the guest ion(s). Thus the difference in helical twist between enantiomers in this system is relatively small, which may impact upon their separability.

Also, in such a strained system, it is not difficult to envisage a relatively facile flipping between the M and P helices, and this speculation is borne out by the observed equivalence of the cap protons in the solution ^{1}H NMR (Figure 3-3 and Figure 3-4). Thus, a continual process of racemisation occurring in solution may prevent chromatographic separation.

The introduction of chemical dissimilarity via preparation of a diastereoisomer may yet overcome this conundrum by giving rise to "favoured" and "un-favoured" conformations of the cryptate, *i.e.* a relatively better, or worse correspondence between the fixed stereochemistry of the chiral anion, and the interchangeable stereochemistry of the cryptate. This would be expected to lead to the enrichment of one diastereoisomeric form, however conversion of a diastereoisomer back to the perchlorate cryptate would remove the potential barrier to racemisation. The next two sections deal with attempts to prepare diastereoisomers of the dicopper(I) cryptate.

3.1.4. Chiral counterions for resolution of dicopper(I) imBT

Attempts to resolve the two enantiomers were made by pairing them with a chiral counterion, in the hope of enriching one diastereoisomeric form. Resolution of a triple helical cobalt(III) complex was performed via such a method by Sargeson's group (11, 12) using antimonyl tartrate (Figure 3-5 (A)), and this counterion was employed in the present situation, together with tartrate, and dibenzoyl tartrate (Figure 3-5 (B) and (C)).

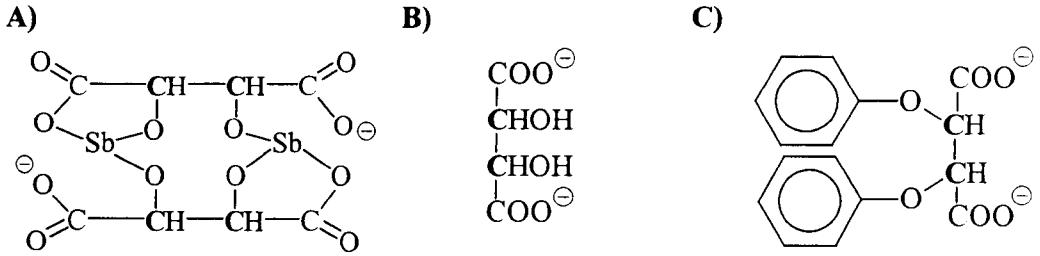

Figure 3-5: The three chiral counterions used: A) antimonyl tartrate, B) tartrate, and C) dibenzoyl tartrate. The chiral centres in each molecule are in bold.

The usual procedure for exchanging a counterion involves treating the alcoholic cryptate with a potassium salt of the tartrate, and simply removing the insoluble potassium perchlorate. In the present situation this was prevented by the insolubility of the tartrates in organic solvents, the only practical solvent was water, and the solubility of potassium perchlorate in this medium was apparently sufficient to prevent its isolation as a precipitate. Additionally, procedures in aqueous solutions are often slower and more laborious, the solubility of the copper(I) imBT complex in water is relatively low, and we believe that the cryptand and cryptate are susceptible to oxidation and ring opening reactions in water.

A large number of attempts to exchange the counterion were made using different solvent systems (aqueous and non-aqueous acetonitrile and methanol), different temperatures, and

different reaction times. In the majority of cases these merely resulted in the regeneration of the dicopper(I) perchlorate cryptate, the identity of which was easily confirmed by the presence of ClO_4 peaks and the absence of any carbonyl peak in the infrared spectrum.

Using a tartrate salt under more forcing conditions (excess reagent at reflux), it was also possible to isolate a blue/green glass with infrared characteristics of tartrate but not of the cryptand. This is likely to be a copper(II) tartrate complex. In light of the pH dependent equilibrium in which copper(II) tartrates exist, and the stability of the complexes (14) it is not so surprising to have obtained a tartrate complex without the cryptand. The antimonyl tartrate counterion also gave rise to similar products after extended reaction times. These observations could be explained as the result of hydrolysis of the imine bonds, exposing the oxidisable copper(I) to tartrate in solution, where copper(II) tartrates would be the preferred product.

Products isolated after a short reaction time with antimonyl tartrate were dicopper(I) cryptates with perchlorate counterion, and generally of high crystalline quality. Several of these crystals were characterised by X-ray crystallography, which revealed that the extent of racemic twinning was not a constant throughout the batch. This implies that: in the solid state, no interconversion between P and M forms can occur (otherwise the extent of twinning would always be the same, 50% of each enantiomer); and during the crystallisation process some enrichment of a particular enantiomer must occur. Section 3.1.6 explores this phenomenon and attempts to exploit it to obtain an optically pure crystal.

3.1.5. Direct preparation of diastereoisomeric cryptate

Since attempts to resolve the enantiomers of dicopper(I) imBT by exchanging the counterion had failed, an attempt was made to directly prepare a diastereoisomeric copper cryptand using free ligand and a copper tartrate. Attempts to prepare copper(I) tartrate by treating copper(I) perchlorate with potassium D-tartrate resulted in the immediate formation of a blue colour suggestive of copper(II), and indeed no mention of a copper(I) tartrate is found in the literature. However, treatment of the amino ligand amBT with copper(II) perchlorate leads to formation of the average valence cryptate, dicopper(1.5) amBT, and we hoped that the copper(II) tartrate may give a similar product, which could then be investigated for chirality and eventually reduced to dicopper(I).

3.1.5.1. Dicopper(1.5) amBT D-tartrate

Copper(II) tartrate was prepared by the reaction of D-tartaric acid with copper(II) carbonate (details in section 9.2.5). The product of the reaction of the tartrate salt with free amBT ligand in acetonitrile was a deep blue solid. The solid was insoluble in organic solvents, but soluble in water, and slow diffusion of methanol resulted in the isolation of small, intensely blue crystals. These proved unsuitable for X-ray structural characterisation, giving no diffraction pattern, despite being of apparently good quality – this may be a result of high solvent disorder within the crystal. The infrared spectra of the crude product and crystals were similar, lacking any clear features attributable to tartrate. The FAB mass spectrum of the crystals (Table 3-3) contained peaks consistent with the dicopper cryptate, but not a tartrate counterion. Peaks consistent with chloride were observed however, and we speculate that traces of chlorine, perhaps from glassware washing or in the water used for recrystallisation have been incorporated into the solid in preference to tartrate.

Table 3-3: FAB mass spectrum of blue crystals (NOBA matrix, EPSRC service).

m/z	Abundance /%	Identity	m/z	Abundance /%	Identity
371	10%	L	530	2%	Cu_2 L Cl
433	5%	Cu L	566	1.8%	Cu_2 L Cl_2
495	4%	Cu_2 L			

Infrared spectra were broad and ill defined, consistent with extensive solvation. Various preparative attempts resulted in either no reaction, or a solid with infrared characteristics of a podate (resulting from opening of the cryptand) but with no features attributable to tartrate.

3.1.6. Crystallisation techniques and crystallographic screening

Since it is suspected that the dicopper cryptate undergoes racemisation in solution, a solid state technique was preferred to determine absolute configuration. The excellent but time-consuming technique of X-ray crystallography was employed, and determined that the extent of racemic twinning varied from crystal to crystal (see section 3.1.4).

The inference was also made that racemisation does not occur in the solid state, and that there must be some preference for enantiomers of like handedness to crystallise together. By adjusting conditions to favour slow crystallisation, and by keeping a salt of fixed

chirality in solution (antimonyl tartrate or tartrate), it was hoped to encourage the selective crystallisation of a particular enantiomer. Experimental details are given in section 9.2.4, and a summary of the results is given in Table 3-4.

Table 3-4: Summary of Flack parameters (extent of racemic twinning) for crystals of dicopper(I) imBT perchlorate screened by X-ray crystallography. A number of the earliest determinations were performed by Prof Vickie McKee, and the datasets discarded once it was clear that they were twinned. An estimate of the Flack parameter is given for these, but no R-value.

Flack parameter (SD)	R-value for refinement	Instrument used
0.2	*Not available*	QUB Smart
0.2	*Not available*	QUB Smart
0.5	*Not available*	QUB Smart
0.1	*Not available*	Daresbury synchrotron
0.0	*Not available*	Daresbury synchrotron
0.48(12)	0.0866	QUB Smart
0.59(7)	0.0796	QUB Smart
0.34(9)	0.0893	QUB Smart
0.70(8)	0.0889	QUB Smart
0.23(9)	0.0989	QUB Smart
0.76(11)	0.138	QUB Smart

One fully resolved crystal was discovered during a session at the Daresbury synchrotron, however on this occasion the instrument's cryostat was faulty. At room temperature vibrational effects make it impossible to obtain sufficiently detailed diffraction data for measurement of electron density, so this promising experiment had to be abandoned.

3.1.7. Dicopper(I) imBT tetrafluoroborate

The dicopper cryptate with tetrafluoroborate counterion was directly prepared from copper(I) tetrafluoroborate and free ligand using a method analogous to that for copper(I) perchlorate cryptate (1). The cryptate was easily oxidised in the presence of water or alcohol, and crystallisation was more difficult than with perchlorate counterion. Yellow/brown blocks were obtained by the slow diffusion of ether into a solution in acetonitrile, and one of these was used for crystallographic studies. Experimental details are given in section 9.2.6.

A graphical representation of the structure is shown in Figure 3-6, the asymmetric unit (Figure 3-6 A) is fully ordered, and contains a 20% occupancy water molecule, whose

protons could not be directly located. The copper ions have trigonal pyramidal geometry, and lie below the equatorial plane.

The most remarkable and interesting feature of this crystal, is that no twinning is present, and the refinement has given a very good R factor of 4.4%. This observation with an achiral counterion is unexpected, although fluorine is known to exert a strong directing influence in crystal structures (15), and may have caused a change in packing sufficient to make racemic twinning undesirable.

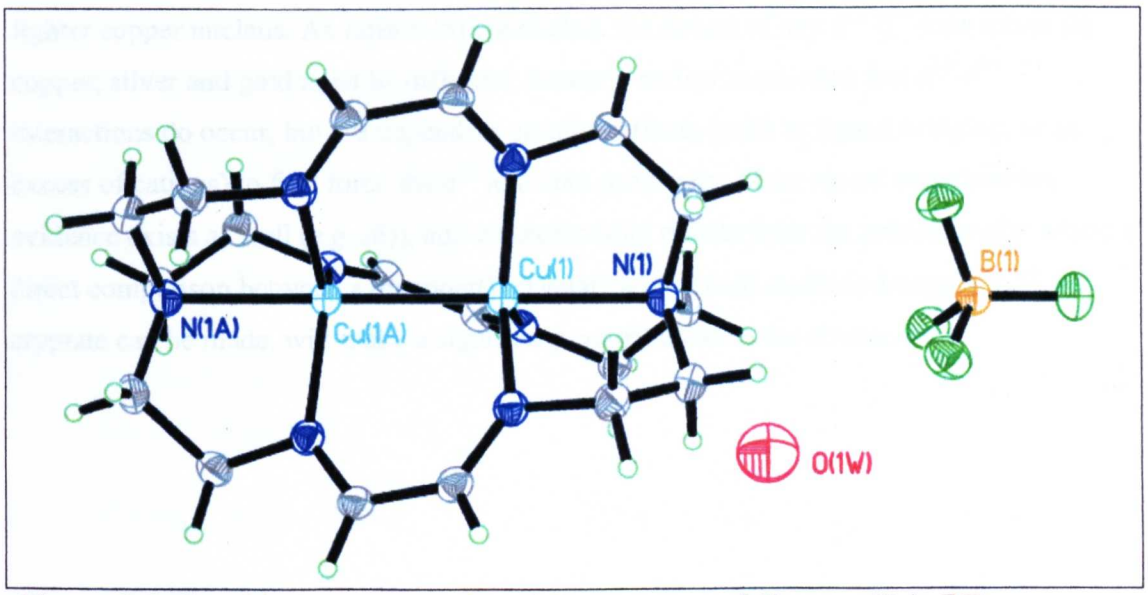

Figure 3-6: Graphical representation of the structure of dicopper(I) imBT tetrafluoroborate. Space group R-3c, cell dimensions a = b = 8.5992(5) Å, c = 61.387(5) Å, R = 0.0436.

3.2. Conclusions

Solution NMR studies suggest that racemisation is occurring in solution, but the observation that the extent of twinning in crystals is variable shows that the conformation is not exchanging in the solid state. Exchanging the perchlorate counterion for tartrate, as well as direct preparation of copper tartrate diastereoisomers proved very difficult, possibly due to the intrinsic stability of copper tartrates, making a pure tartrate complex a more favoured product.

The variable extent of twinning did by random selection yield a non-twinned crystal with perchlorate anion, however the electron density studies could not be performed at the time, and long term crystal stability was insufficient to allow the studies to be completed on the same sample at a later date. Preparation of a cryptate with tetrafluoroborate counterion

yielded a non-twinned crystal which diffracts well, and which we hope will lead to completion of the studies on this system, although this data is not at present available.

This result may help to resolve the long-standing debate over whether a cuprophilic effect (similar to the well known aurophilic effect, and the increasingly well-accepted argentophilic effect) exists in some molecules. Theoretical arguments proposing a hybrid s-d orbital model for the effect were proposed in 1958 by Orgel (4), although Cotton in 1998 (7) claimed that cuprophilicity was impossible on theoretical grounds. Certainly the relativistic mechanism advanced to explain the aurophilic effect cannot operate for the far lighter copper nucleus. As Jansen (5) concluded, the nature of any d^{10}-d^{10} interaction for copper, silver and gold must be different. Jansen's review concluded that d^{10}-d^{10} interactions do occur, but are dependent on other effects (such as ligand bridging, or an excess of cations) to first force the d^{10} ions into proximity. More recent experimental evidence exists as well (*e.g.* (6)), and we expect that results from the present study, where a direct comparison between a dicopper(I) cryptate and a (well studied) dicopper(1.5) cryptate can be made, will make a significant contribution to the debate.

3.3. References

1. Al-Obaidi, A., G. Baranovic, J. Coyle, C.G. Coates, J.J. McGarvey, V. McKee, and J. Nelson, Inorganic Chemistry, 1998. **37**: p. 3567-3574.

2. Robin, M.B. and P. Day, Advances in Inorganic Radiochemistry, 1967. **10**: p. 247-405.

3. Drew, M., D. Farrell, G. Morgan, V. McKee, and J. Nelson, Journal of the Chemical Society-Dalton Transactions, 2000. **9**: p. 1513-1519.

4. Orgel, L., Journal of the Chemical Society, 1958: p. 4186.

5. Jansen, M., Angewandte Chemie, 1987. **26**: p. 1098-1110.

6. Che, C.-M., Z. Mao, V. Miskowski, M.-C. Tse, C.-K. Chan, K.-K. Cheung, D. Phillips, and K.-H. Leung, Angewandte Chemie, 2000. **39**(22): p. 4084-4088.

7. Cotton, F., X. Feng, M. Matusz, and R. Poli, Journal of the American Chemical Society, 1998. **110**: p. 7077-7083.

8. Poblet, J. and M. Benard, Chemical Communications, 1998: p. 179-180.

9. Nelson, J., V. McKee, and G. Morgan, Progress in Inorganic Chemistry, 1998. **47**: p. 167-316.

10. Cahn, R.S., C.K. Ingold, and V. Prelog, Angewandte Chemie International Edition, 1966. **5**(4): p. 385-415.

11. Charbonnière, L., G. Bernardinelli, C. Piguet, A.M. Sargeson, and A.F. Williams, J. Chem. Soc. Chem. Comm, 1994: p. 1419-1420.

12. Sargeson, A., Personal communication, 1995.

13. Smith, P.H., M.E. Barr, J.R. Brainard, D.K. Ford, H. Freiser, S. Muralidharan, S.D. Reilly, R.R. Ryan, L.A.I. Silks, and W.-h. Yu, Journal of Organic Chemistry, 1993. **58**: p. 7939-7941.

14. Ramasubramanian, M., B.N. Popov, R.E. White, and K.S. Chen, Journal of Applied Electrochemistry, 1998. **28**(7): p. 737-743.

15. Row, T., Coordination Chemistry Reviews, 1999. **183**: p. 81-100.

4. Podands and macrocycles incorporating substituted glyoxals

The derivatisation of existing macrocycles by adding substituent groups is of interest for several reasons. There is potential for increasing the number of donor groups, and thereby increasing the stability of complexes, or opening a route to higher nuclearity complexes. Stability of some cryptates could also be enhanced by substitution of a bulky, or hydrophobic group to prevent an encapsulated guest from interacting with its environment.

Methods for derivatising cryptands could also be of use in more specialised applications, for example, to allow attachment of a fluorescent group, or a substrate molecule for imaging/drug delivery purposes.

This chapter presents attempts to derivatise the imBT ligand, with the primary aim of providing additional stability to the disilver cryptate, as well as the multinuclear cryptates of the corresponding reduced ligand. ImBT contains three different carbon atoms susceptible to derivatisation. The present study deals with attempts to functionalise the C_A position (Figure 4-1). Addition of a substituent group could be performed either before, during, or after formation of the cage, and we adopted the "before" approach, by using a substituted diketone in place of glyoxal.

A wide variety of linker units belonging to the family shown in Figure 4-2 A is conceivable, however the keto-enol tautomerism will affect all of them to a greater or lesser extent. In the case of 2,4 pentanedione (used in the preparation of the trac ligand, see

Chapter 6) 76% of the compound is in the enol form under standard conditions (1). Despite this, the Schiff base condensation can be performed under somewhat forcing conditions, and for the glyoxal group of compounds as well, the tautomerism should not be an insurmountable barrier to Schiff base formation. In the case of phenyl glyoxal no β-H is present, and an enol configuration cannot be attained.

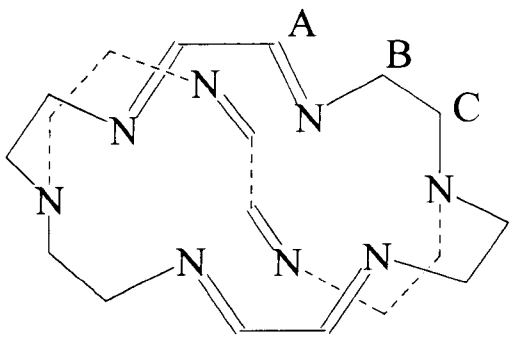

Figure 4-1: The imBT ligand, with the three different carbon atoms indicated. Substitution of C_A, derived from the glyoxal spacer, is the subject of this chapter.

The substituted glyoxals investigated in this work contain both an aldehyde and a ketone. The ease of Schiff base formation will be affected both by steric factors (a bulky substituent will tend to hinder reaction at the adjacent carbonyl), and electronic effects (an electron donating group, such as a methyl will tend to disfavour nucleophilic attack at the adjacent carbonyl). Thus for methyl glyoxal, both electronic and steric effects make reaction at the aldehyde position more likely, but the case is not so clear for either glyoxylic acid or phenyl glyoxal. Conjugation (to the phenyl ring) and resonance effects (the second pi bond in glyoxylic acid is shared over two oxygens) will also operate, tending to weaken the carbonyl (and thus favour imine formation), in contrast to steric and electronic effects (hydroxyl is a strong, and phenyl a weak electron donating group).

The difference in reactivity for the two carbonyls means that isolation of a podand is likely, and reaction with a second molecule of tetraamine to form a crypt may require more forcing conditions than the related glyoxal system.

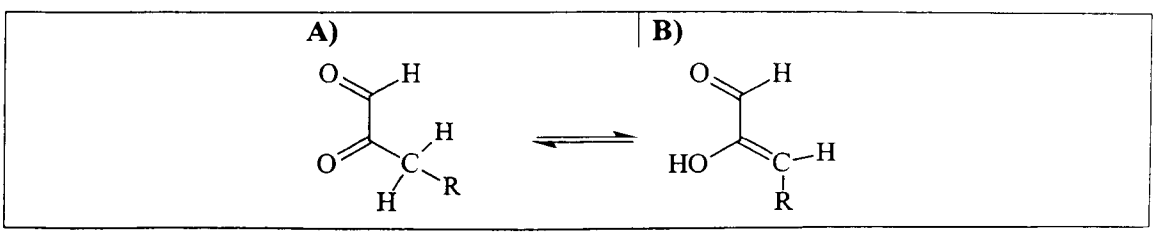

Figure 4-2: The keto-enol tautomerism is expected to affect substituted glyoxals, such as methyl glyoxal (R=H).

A more serious problem however, may be side reactions between separate glyoxal molecules. The aldol reaction has potential to interfere, especially as it is base catalysed and therefore more likely in the presence of the tetraamine. Products of this reaction may take the form shown in Figure 4-3.

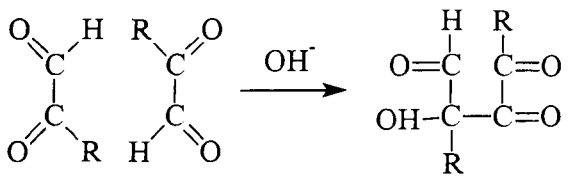

Figure 4-3: The base catalysed aldol reaction has potential to disrupt Schiff base formation.

Hemiacetals and acetals can also be formed via the reaction of a ketone with an alcohol (present as a solvent, or via aldol reaction or the keto-enol tautomerism) resulting in a product which cannot form a Schiff base macrocycle at normal pH (see Figure 4-4).

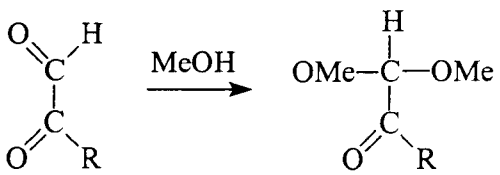

Figure 4-4: Formation of an acetal from a substituted glyoxal.

Thus even before the Schiff base reagents have been combined there is potential for the existence of a complex mixture of addition, polymerisation, and tautomerisation products, whose formation may be enhanced in the presence of base. Competition with the desired reaction outcome will ensue.

Reactions between an amine and carbonyl other than by Schiff base chemistry are also possible, for example if nucleophilic attack at a carbonyl results in addition across the carbonyl, rather than condensation (as observed in the reaction of phenyl glyoxal with diethylamine (2)). The product of such a reaction would therefore contain oxygen, in the form of a hydroxyl group.

Therefore, combination of a tripodal amine with a dicarbonyl allows for a great variety of possible products, from podands and cryptands to polymers. Even if a straightforward Schiff base reaction does occur, a wide range of products is conceivable, and some of the possible outcomes are summarised in Scheme 4-1 below. If reaction occurs along only one

or two strands (Scheme 4-1 A & B), a macrocycle or chelate could be obtained (expect to observe both imine and amine infrared resonances). Alternatively (Scheme 4-1 C) a podand with one or more pendant carbonyls can form, and (Scheme 4-1 D) a similar process can occur for a chelate or macrocycle. An infrared spectrum in this case would show amine, imine and carbonyl peaks. Intramolecular cyclisation is also a possibility in many systems (Scheme 4-1 E), as is reaction with another amine molecule (Scheme 4-1 F) which can lead on to polymerisation. Formation of the desired cryptand (Scheme 4-1 G) is only one of the possible reaction outcomes.

Despite the complexity of the system, and the known side reactions, Schiff base chemistry is well documented for many related systems (including phenyl glyoxal, in its reaction with primary amines such as propylamine and 1,2 diaminoethane (3-5)), presumably where competing reactions are slow, or where equilibrium effects ensure a sufficient supply of the glyoxal.

Trials in the present study were made using both templating and non-templating procedures. Bulkier substituents, such as the phenyl group, were most desirable in terms of increased steric protection at the cavity, however attempts to incorporate smaller methyl and hydroxy substituents were also made. The results of these investigations are described below.

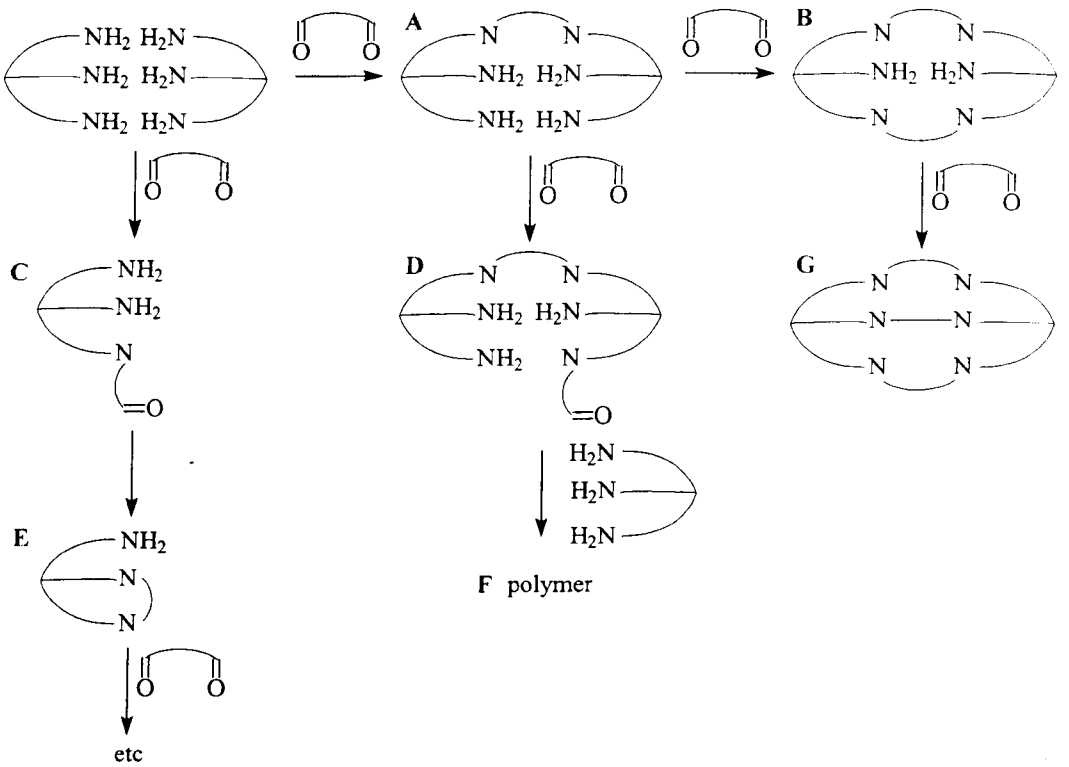

Scheme 4-1: Some of the possible outcomes of Schiff-base reactions in a triamine/dialdehyde mixture.

4.1. Phenyl substitution at C_A

A range of template and non-template methods were essayed in attempts to prepare the phenyl substituted crypt, or a podand. Phenyl glyoxal is commercially available as a monohydrate, with the synonym 2,2 dihydroxy acetophenone (Figure 4-5). Inspection of the ^{1}H NMR of the starting material (Figure 4-6) shows that in chloroform solution at room temperature, no more than one quarter of the material exists as an aldehyde.

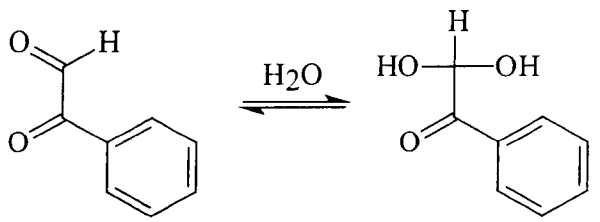

Figure 4-5: The equilibrium between phenylglyoxal and 2,2 dihydroxy acetophenone.

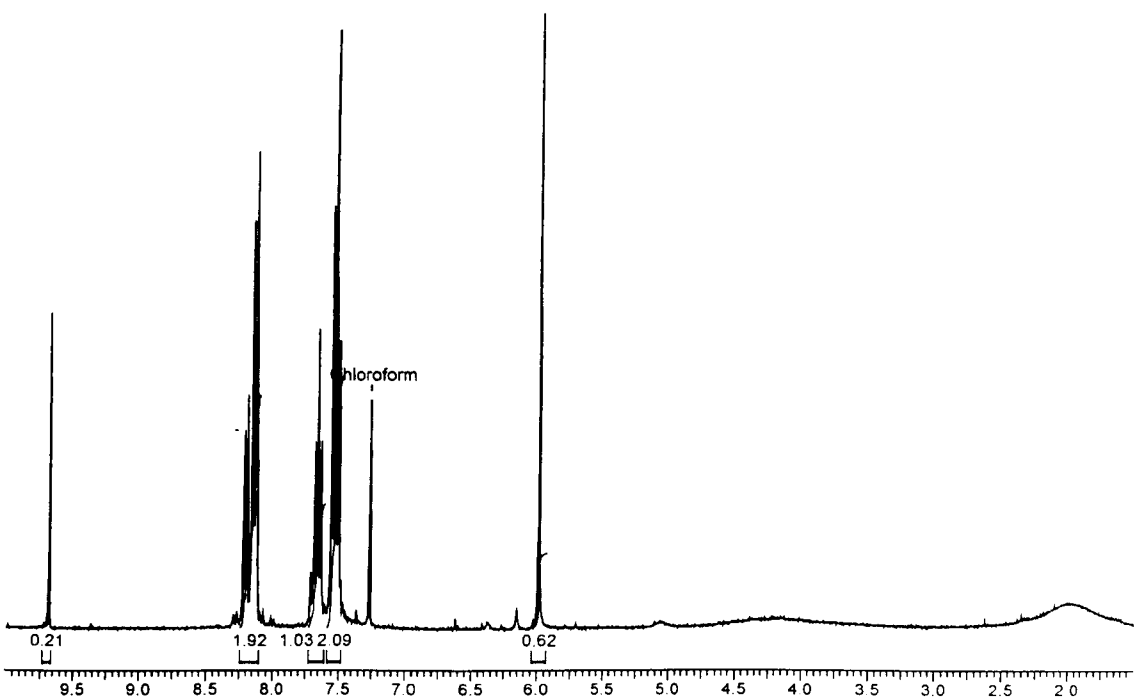

Figure 4-6: ^{1}H NMR of phenyl glyoxal hydrate starting material. The 9.7 ppm peak is attributed to the proton in the aldehyde form, and the 6 ppm peak to the dihydroxy form; showing that a roughly 1:3 ratio exists between the two states under these conditions (deuterated chloroform at room temperature).

4.1.1. Template synthesis of cryptate

Strontium perchlorate was added to a solution of phenyl glyoxal with the aim of templating the crypt, and tren solution added dropwise. A sticky orange solid was obtained, which

despite having some solubility in polar organic solvents, could not be crystallised. Treatment of a solution (acetonitrile) of the solid with tetraphenylborate generated a yellow microcrystalline solid, however X-ray quality crystals could not be obtained. The IR spectra before and after counterion exchange were similar, although sharper with tetraphenylborate (Figure 4-7). A feature consistent with either a carbonyl or imine is present at lower frequency than in phenyl glyoxal (where it lies at 1696 cm^{-1}). Only partial exchange of counterion appears to have occurred however, as perchlorate features are still present. An aromatic C-H stretch at 3064 cm^{-1}, consistent with inclusion of phenyl glyoxal was observed for the perchlorate only material, however it is presumably obscured by tetraphenylborate peaks in Figure 4-7. There is no sign of amine stretches, and this suggests that reaction has occurred at each of the primary amines, with formation of either a cryptate or a podate (possibly with terminal acetal or di-hydroxy groups).

Even with the more soluble perchlorate salt, the FAB mass spectrum was very weak. A few peaks were observed in low abundance, which could not be assigned to complexes containing cryptand, podand, or starting materials.

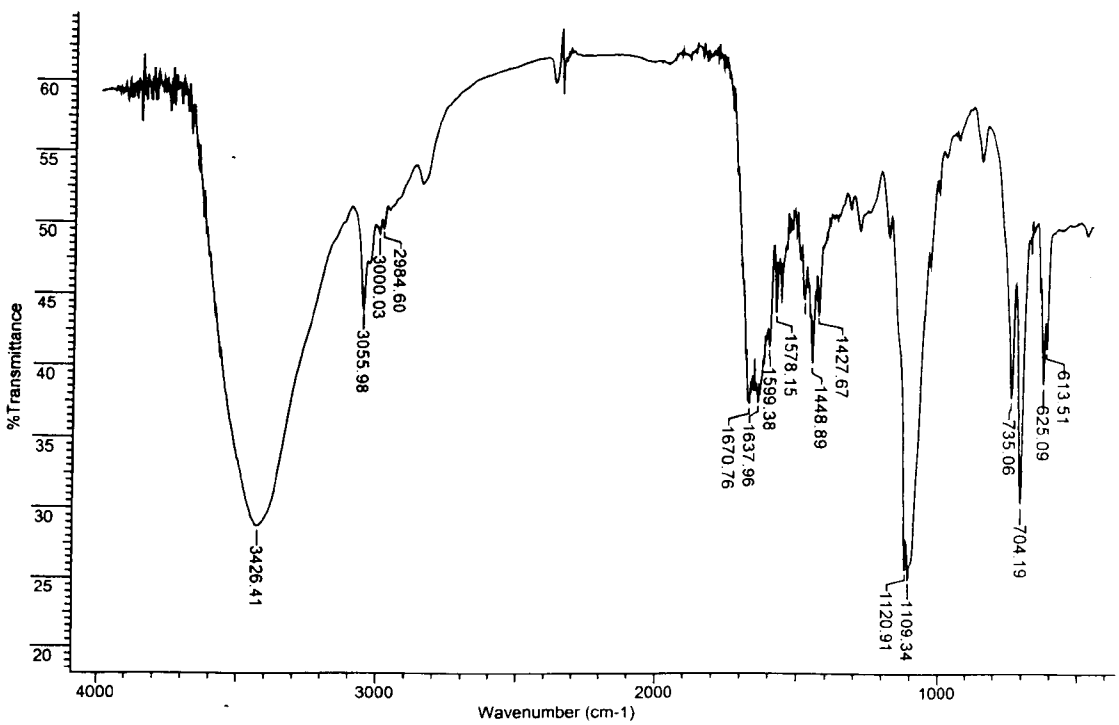

Figure 4-7: Infrared spectrum of the yellow solid obtained by treatment of the perchlorate material with tetraphenylborate, which could be consistent with the formation of a cryptate or podate. The carbonyl frequency observed for phenyl glyoxal (1696 cm^{-1}) is absent.

4.1.2. Synthesis of free podand

The procedure used for preparation of trac (see Chapter 6, and reference (6)) was modified for phenyl glyoxal, full details are given in section 9.3.1.1. The infrared spectrum of the product, a red glass, is shown in Figure 4-8. The 1600-1700 cm^{-1} peak in the IR spectrum may contain an imine stretch overlaid by the strong carbonyl vibration. It is also noteworthy that amine resonances are no longer present.

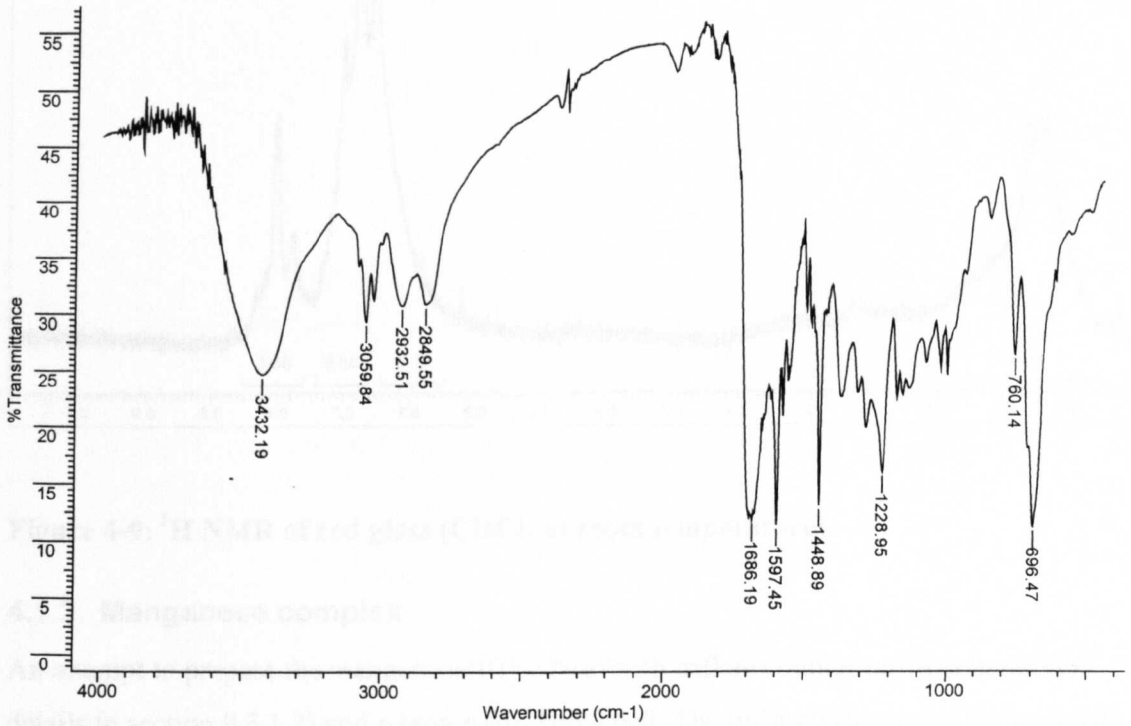

Figure 4-8: Infrared spectrum of the red glass.

The NMR spectrum at room temperature (Figure 4-9) shows poorly resolved aromatic (7-7.6 ppm) and imine (~8 ppm) CH resonances, and a broad feature at 2.3 ppm with an integral broadly consistent with the number of cap protons (12 cap:15 aromatic:3 imine). The only clear features in the ^{13}C spectrum were aromatic carbons at 129 and 128 ppm, other features were not resolved from the background.

Elemental analysis showed the presence of ~10% nitrogen, however percentage C, H, and N were all much lower than predicted, suggesting that chloroform was strongly retained in the glass. Mass spectra (FAB, ES, and EI attempted) did not contain any peaks which could be assigned to Schiff base products.

Despite a promising NMR spectrum, the identity of the product remains ambiguous, and attempts were made to prepare complexes in the hope of obtaining a better characterised product.

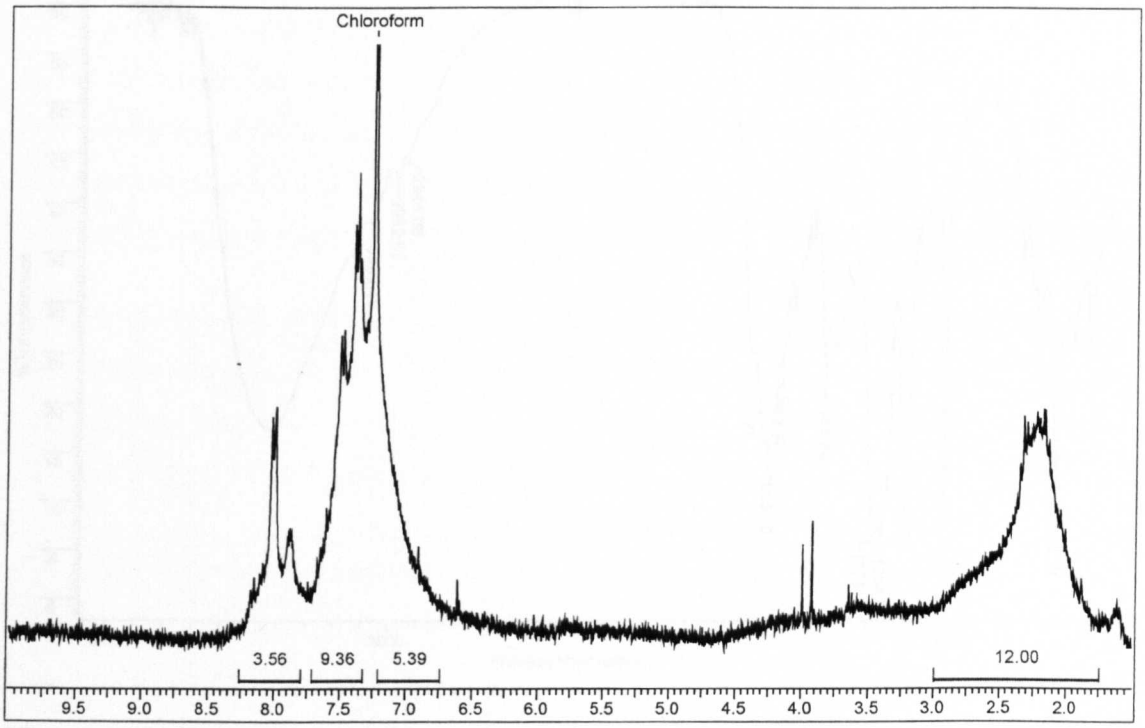

Figure 4-9: ^{1}H NMR of red glass ($CDCl_3$ at room temperature).

4.1.3. Manganese complex

An attempt to prepare the manganese(II) podate (with triflate counterion) was made (full details in section 9.3.1.2) and a brown solid obtained. The infrared spectrum (Figure 4-10) shows triflate features, together with absorptions in the imine/carbonyl region, which are different from those of phenylglyoxal starting material (1696 cm^{-1}). Elemental analysis (Table 4-1) was not in accordance with predicted values, and the FAB mass spectrum did not contain peaks which could be assigned to a Schiff base podand.

Subsequent LCMS studies (7) showed that the material was not pure, and there is little evidence for the formation of a podate.

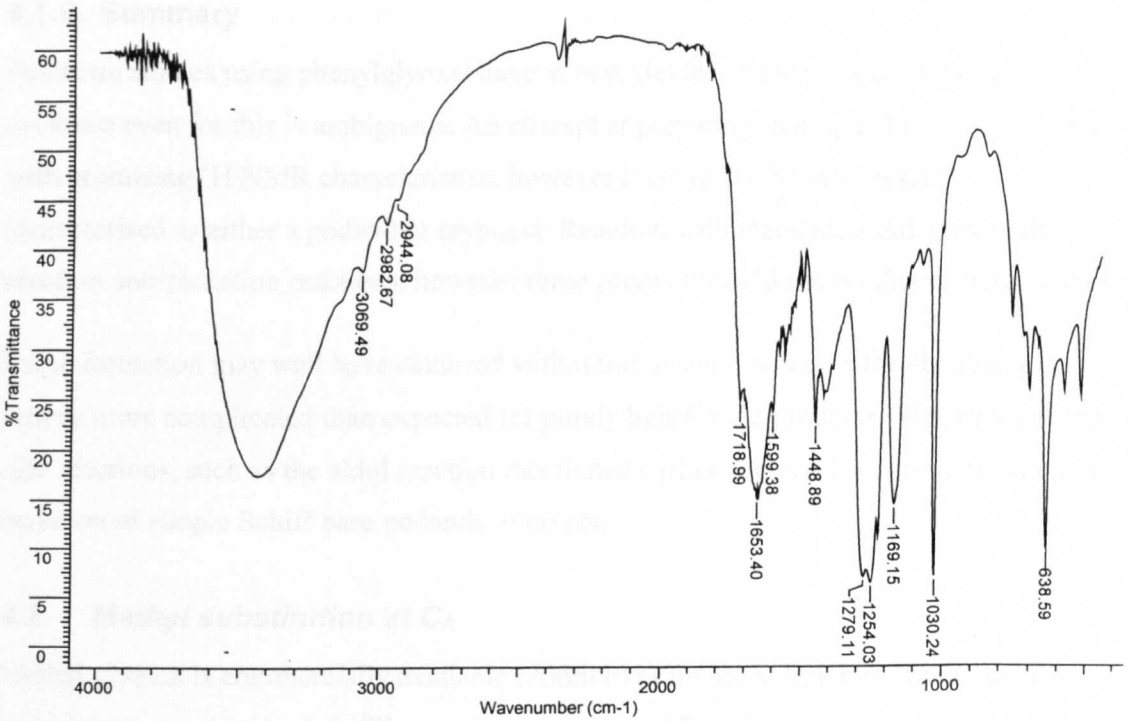

Figure 4-10: IR spectrum of the product obtained from reaction of Mn(II) triflate with the possible podand discussed in the previous section.

Table 4-1: Elemental analysis of the brown solid obtained from reaction of Mn(II) triflate with the possible podand discussed above.

Analysis	%C	%H	%N
Predicted Mn $C_{30}H_{30}N_4O_3$ triflate:	45.34	3.57	6.61
Predicted Mn $C_{22}H_{26}N_4O_2$ triflate (two imines formed):	39.41	3.58	7.66
Found:	37.19	3.71	6.57

4.1.4. Other complexes

Attempts were made to prepare podates using copper(I) and copper(II) perchlorate, barium perchlorate, calcium nitrate, zinc perchlorate, strontium nitrate, at room temperature under nitrogen, or at reflux if no complex appeared to be formed under milder conditions. The products obtained were characterised by infrared, elemental analysis, FAB mass spectrometry, and NMR for copper(I). The IR features were generally very similar to the product obtained with manganese triflate (above), and whilst all of the elemental analyses showed the presence of nitrogen, none of the elemental ratios could be satisfactorily explained. The mass spectra were generally weak, and none contained peaks consistent with any Schiff base ligand complexes.

4.1.5. Summary

Synthetic studies using phenylglyoxal have at best yielded crude podates, although evidence even for this is ambiguous. An attempt at preparing free ligand yielded a product with promising ^{1}H NMR characteristics, however it could not be satisfactorily characterised as either a podand or cryptand. Reaction with metal salts did apparently result in complexation reactions, however these products could not be characterised either.

Imine formation may well have occurred within this system, however the chemistry is clearly more complicated than expected for purely Schiff base products. We speculate that side reactions, such as the aldol reaction mentioned earlier (Figure 4-3), are preventing the isolation of simple Schiff base podands or crypts.

4.2. Methyl substitution at C_A

Methyl glyoxal is commercially available (Aldrich) as a 40% solution in water, and this material was used in the Schiff base reaction. The enol form is expected to be present in significant concentrations for this molecule (Figure 4-2 A), and the complexity of the ^{1}H NMR of a chloroform extract of the aqueous solution (Figure 4-11, four aldehyde resonances are observed rather than the expected one) shows that more than one form is indeed present.

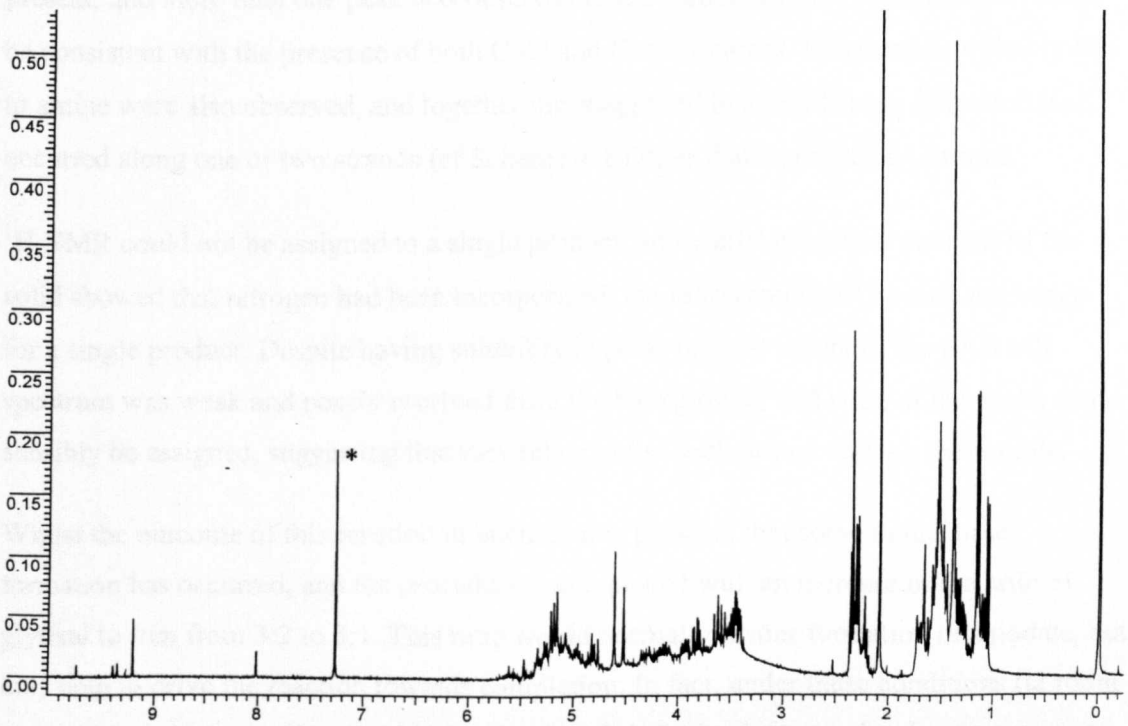

Figure 4-11: Methyl glyoxal in $CDCl_3$ at room temperature. The complexity of the spectrum shows that more than one tautomer is present, and that interchange is slow on the NMR time scale.

Whilst this was discouraging, we and others have observed Schiff base chemistry with other dicarbonyls significantly affected by keto-enol tautomerism (see Chapter 6) and reference (6). Therefore we made a number of attempts using progressively stronger conditions to try and drive the reaction.

4.2.1. Synthesis of free cryptand

Direct synthesis (details in section 9.3.2.1) failed to yield a cryptand, and template methods were subsequently investigated with the aim of prearranging reactants into a configuration amenable to crypt formation. Precoordination of the dicarbonyl may also provide a means of altering the degree of keto-enol tautomerism, possibly favouring the reactive keto form.

4.2.2. Template synthesis of cryptate

The important factors for selection of a templating ion are its size, lability, geometric preferences, and donor-type preferences. Strontium has been previously used for the imBT system, and since the cavity size of a substituted analogue is not expected to differ significantly, it was again chosen for the present situation (details are given in section 9.3.2.2).

IR analysis of the product showed that perchlorate – and presumably the metal ion – was present, and more than one peak was observed in the carbonyl/imine region, which could be consistent with the presence of both C=N and C=O stretches. Resonances probably due to amine were also observed, and together this suggested that Schiff base formation had occurred along one or two strands (cf Scheme 4-1 D), or that a podate had formed.

^{1}H NMR could not be assigned to a single product, and whilst elemental analysis of the solid showed that nitrogen had been incorporated, the ratios could not be well explained for a single product. Despite having solubility in polar organic solvents, the FAB MS spectrum was weak and poorly resolved from the background, and none of the peaks could sensibly be assigned, suggesting that they relate to the background and not the sample.

Whilst the outcome of this reaction in unclear, it is possible that some Schiff base formation has occurred, and the procedure was repeated with an increase in the ratio of glyoxal to tren from 3:2 to 3:1. This ratio would normally favour formation of a podate, but may help to drive the reaction towards completion. In fact, under these conditions (at room temperature) the intensely coloured red/brown solid obtained appeared to be even more polymeric in nature: it was completely insoluble in all available solvents, with a broad and

relatively simple IR spectrum containing fingerprint, OH (probably water), CH peaks, and perchlorate features. The 1638 cm^{-1} peak was stronger than expected for a water bend, and could be a carbonyl or imine, however the general broadness of the spectrum was certainly consistent with polymerisation. The elemental analysis (Table 4-2) again confirmed the inclusion of nitrogen, but has a higher proportion of C, H, and N than expected, which could indicate less than one metal ion occurring per tren unit.

Table 4-2: Elemental analysis of the insoluble reaction product.

Analysis	%C	%H	%N
Predicted Sr $[C_{15}H_{24}N_4O_3]$ $(ClO_4)_2$:	30.28	4.07	9.42
Predicted Sr $[C_{15}H_{24}N_4O_3]_2$ $(ClO_4)_2$:	39.89	5.36	12.41
Predicted Sr $[C_{15}H_{24}N_4O_3]_3$ $(ClO_4)_2$:	41.22	5.53	12.82
Found:	43.28	6.27	14.79

4.2.3. Direct synthesis of podand

An attempt to prepare free podand was made (details in section 9.3.2.3). The IR spectrum of the product (a yellow oil, Figure 4-12) contained features suggesting a mixture of materials. A sharp resonance at 1675 cm^{-1} is in the right region for an imine and is different both from the carbonyl of unreacted glyoxal (which is also present at 1734 cm^{-1}), and from the amine bend of tren (1595 cm^{-1}). Weak resonances at 3092 and 3037 cm^{-1} are likely to be aromatic protons in benzene residue. The unusually strong feature at 2800-3000 cm^{-1} resembles the CH region of methyl glyoxal.

The FAB mass spectrum did not reveal any peaks which could be assigned either to starting materials, or to podand, macrocycle or crypt products. The ^1H NMR spectrum was complex (Figure 4-13), peaks between 2 and 4 ppm may be from cap protons, and a single peak at 7.6 ppm may be due to an imine, and/or residual benzene (normally expected at 7.36, (8)). However, this spectrum could also be explained as a mixture of unreacted tren and methyl glyoxal, with benzene impurity, thus explaining the 7.6 ppm peak and the broad and complicated spectrum at lower chemical shift.

Even if this peak is an imine however, the integral is far smaller than the expected 4:1 cap to imine ratio, and it is clear that a Schiff base macrocycle or podand has not been formed.

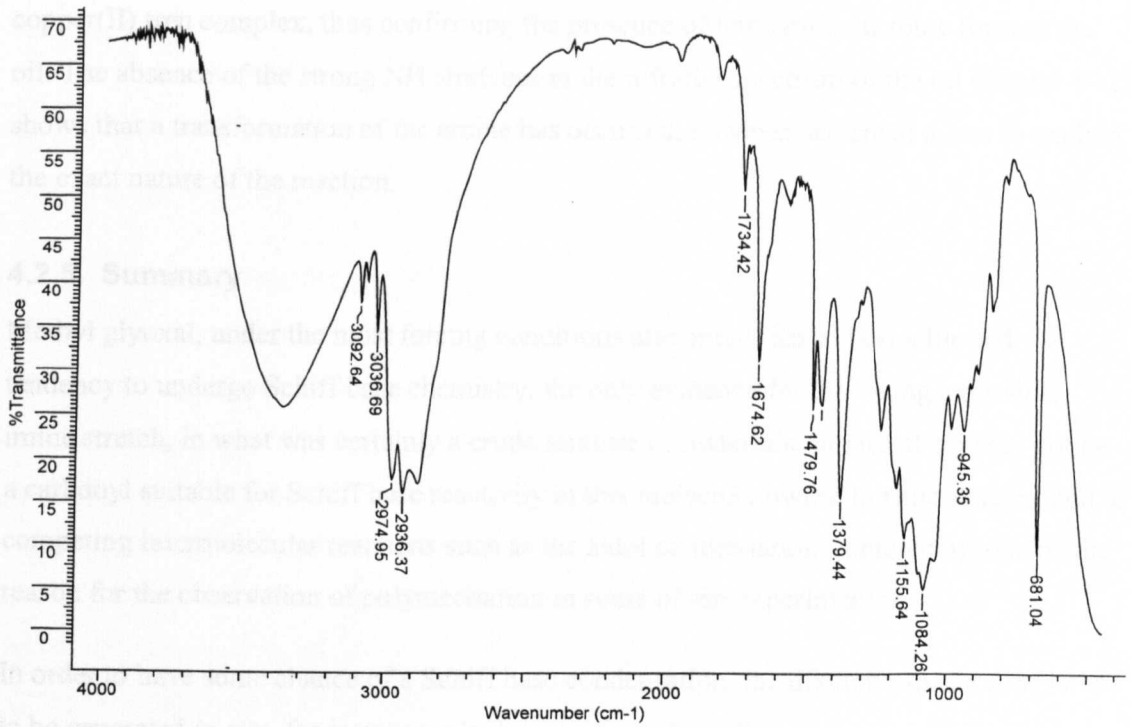

Figure 4-12: The infrared spectrum of the oil (on NaCl plates).

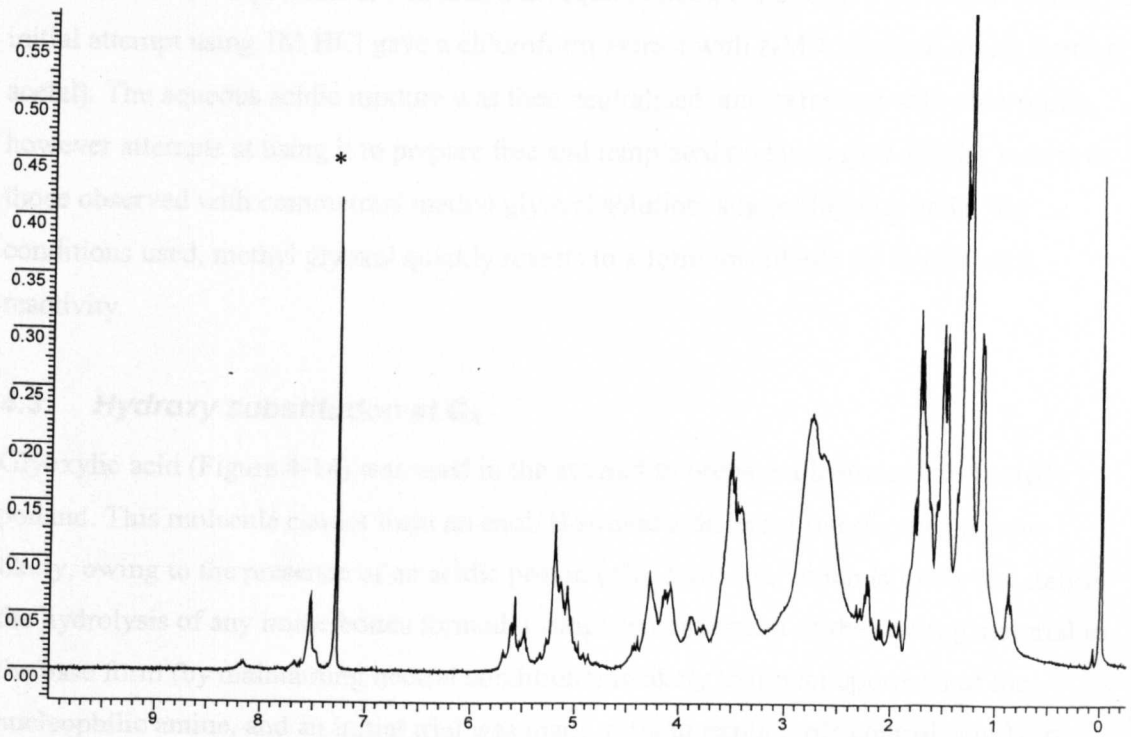

Figure 4-13: ^{1}H NMR of the oil in $CDCl_3$ (marked *) at room temperature.

4.2.4. Synthesis of copper(I) podate

An attempt to form a copper(I) complex using the oil (details in section 9.3.2.4) gave a glassy product which resembled (by its colour, IR spectrum, and elemental analysis) a

copper(II) tren complex, thus confirming the presence of tetraamine in some form in the oil. The absence of the strong NH stretches in the infrared spectrum of the oil (Figure 4-12) shows that a transformation of the amine has occurred, however we are at a loss to explain the exact nature of the reaction.

4.2.5. Summary

Methyl glyoxal, under the most forcing conditions attempted, has at best a limited tendency to undergo Schiff base chemistry, the only evidence for this being a possible imine stretch, in what was certainly a crude mixture of materials. In fact, there may not be a carbonyl suitable for Schiff base reactivity in this molecule, owing to tautomerism, and to competing intermolecular reactions such as the aldol condensation (which may also be the reason for the observation of polymerisation in some of the experiments).

In order to have some chance of a Schiff base condensation, the diketone spacer may have to be generated *in situ*, for instance, via deprotection of the dimethyl acetal of methyl glyoxal. Only preliminary investigations (not reported) were made using this starting material, and the deprotection was found to require strong conditions (4M HCl at reflux, an initial attempt using 1M HCl gave a chloroform extract with NMR identical to the starting acetal). The aqueous acidic mixture was then neutralised, and extracted with chloroform, however attempts at using it to prepare free and templated podands gave similar results to those observed with commercial methyl glyoxal solution, suggesting that under the conditions used, methyl glyoxal quickly reverts to a form unsuitable for Schiff base reactivity.

4.3. Hydroxy substitution at C_A

Glyoxylic acid (Figure 4-14) was used in the attempt to prepare a hydroxy substituted podand. This molecule cannot form an enol. However a different interference is now likely, owing to the presence of an acidic proton (pK_a 3.18) (9), which is likely to catalyse the hydrolysis of any imine bonds formed. Complete conversion of the starting material to the base form (by maintaining neutral conditions) is likely to hinder approach of the nucleophilic amine, and an initial trial was made without explicit pH control simply to observe whether any imine formation occurred.

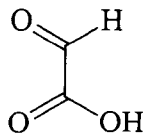

Figure 4-14: Glyoxylic acid

4.3.1. Template synthesis of cryptate

A strontium template was used (details in section 9.3.3.1), and exchange of the perchlorate counterion for tetraphenylborate resulted in precipitation of a brown solid, whose IR spectrum (Figure 4-15 A) was sharper than that of the oil, but apart from tetraphenylborate peaks was otherwise similar. There are strong similarities to the spectrum of protonated tren (Figure 4-15 B), especially in the broad amine and OH region. Features in the carbonyl/imine region are different from those of glyoxylic acid (1760, 1830 cm^{-1}), and could represent imines, but are also in the appropriate area for amine bends. The FAB mass spectrum (Table 4-3) of the perchlorate supports the identification of the material as a protonated tren complex, although a peak was observed which could be representative of a small amount of a ligand where one imine bond has formed.

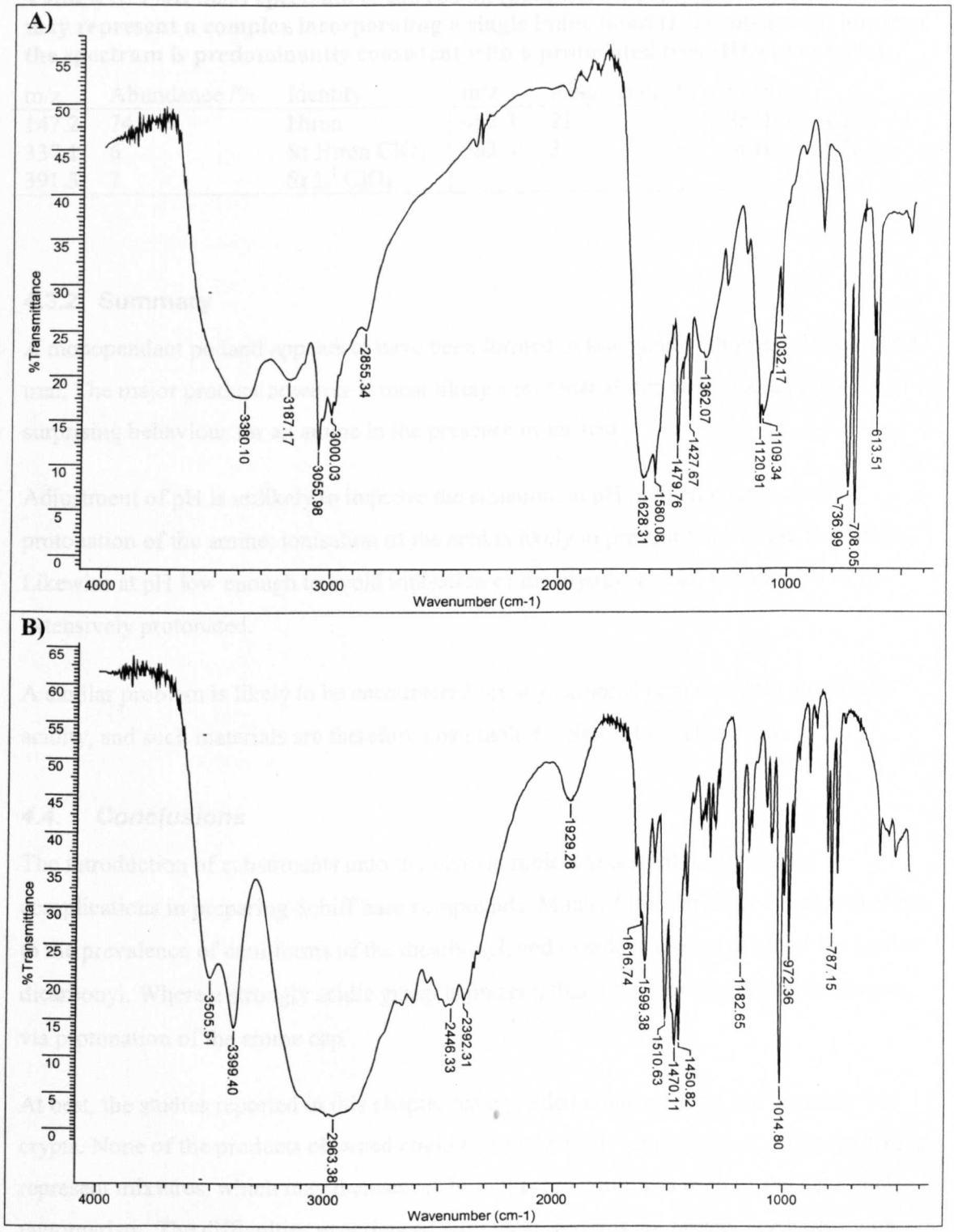

Figure 4-15: Infrared spectra of A) the solid precipitated by addition of sodium tetraphenylborate, apparently a mixed perchlorate/ tetraphenylborate complex and B) tren hydrochloride.

Table 4-3: FAB mass spectrum of the red oil (perchlorate complex). A peak which may represent a complex incorporating a single imine bond (L^1) is observed, however the spectrum is predominantly consistent with a protonated tren (Htren) complex.

m/z	Abundance /%	Identity	m/z	Abundance /%	Identity
147.2	74	Htren	483.3	21	Sr $Htren_2$ ClO_4
337.1	6	Sr Htren ClO_4	583.3	3	Sr $Htren_2$ $(ClO_4)_2$
391.3	7	Sr L^1 ClO_4			

4.3.2. Summary

A monopendant podand appears to have been formed in low yield with glyoxylic acid and tren. The major product however is most likely a protonated tren complex, and this is not surprising behaviour for an amine in the presence of an acid.

Adjustment of pH is unlikely to improve the situation: at pH high enough to avoid protonation of the amine, ionisation of the acid is likely to prevent Schiff base formation. Likewise at pH low enough to avoid ionisation of the glyoxylic acid, the amine will be extensively protonated.

A similar problem is likely to be encountered for any carbonyl complex with significant acidity, and such materials are therefore unsuitable for Schiff base chemistry.

4.4. Conclusions

The introduction of substituents onto the glyoxal molecule has led to significant complications in preparing Schiff base compounds. Much of the difficulty appears to relate to the prevalence of enol forms of the dicarbonyl, and to side reactions of either the enol or dicarbonyl. Where a strongly acidic group is present, this interferes in a different manner, via protonation of the amine cap.

At best, the studies reported in this chapter have yielded crude podates, but certainly no crypts. None of the products obtained could be satisfactorily characterised, and most likely represent mixtures, which may themselves be subject to equilibria such as the keto-enol tautomerism. The difficulties experienced with these systems are largely consistent with the literature, where searches have not discovered reports of Schiff base chemistry for known for methyl glyoxal (including the dimethyl acetal) or glyoxylic acid, although there were numerous examples for phenyl glyoxal reacting at either or both ketones (3-5).

We conclude that the use of a substituted glyoxal to achieve substitution of the C_A position in imBT is not appropriate, and suggest that a different approach is required. Use of nucleophilic substitution chemistry, by replacing the glyoxal spacer with an analogous dibromo spacer may be a suitable alternative. This would avoid the complications experienced by the dicarbonyls studied in this work, and allow access to C_A substituted analogues of *amBT*, which could then be oxidised to the iminocryptand, if required. This chemistry has been exploited in the preparation of podands (see Figure 4-16) by Melhado and Gutsche (10), and is similar to (poorly yielding) preparations performed by Lehn (11).

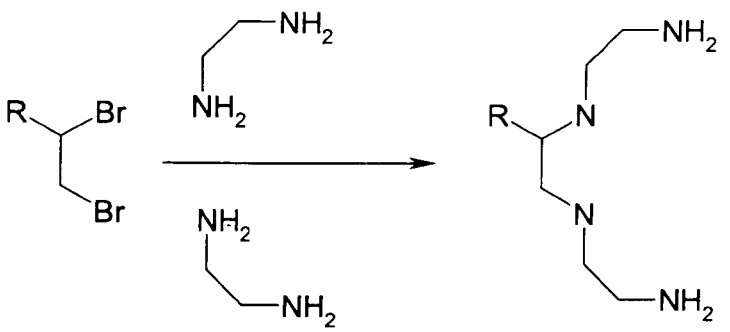

Figure 4-16: Nucleophilic substitution of bromine by primary amine.

Thus, whilst the concept of "building in" substitution in the starting materials is valid, the application of it requires development. A number of potentially important applications can be envisaged, such as the introduction of steric hindrance, or attachment of a pendant arm with functionalities for subsequent binding or substitution.

4.5. References

1. Solomons, T.W.G., *Organic Chemistry*. 6th ed. Vol. 1. 1996, New York: John Wiley and Sons Inc.

2. Boehme, H. and Y. Sadanandam, Archives of pharmacology, 1973. **306**: p. 227-236.

3. Alcaide, B., G. Escobar, R. Perez-Ossorio, J. Plumet, and S. Dionisia, Journal of Chemical Research, 1984. **5**: p. 1466-1488.

4. Ohta, A., T. Watanabe, A. Yasuo, M. Yoshida, and S. Toda, Journal of Heterocyclic Chemistry, 1982. **19**: p. 1061-1067.

5. Ferguson, G., Journal of the American Chemical Society, 1949. **71**: p. 633-637.

6. Smith, A., S.J. Rettig, and C. Orvig, Inorganic Chemistry, 1988. **27**: p. 3929-3934.

7. Bligh, A., Personal Communication, 2002.

8. Gottlieb, H.E., V. Kotlyar, and A. Nudelman, Journal of Organic Chemistry, 1997. **62**(21): p. 7512-7513.

9. Lide, D., ed. *CRC Handbook of Chemistry and Physics*. 77th ed. . Vol. 1. 1996, CRC Press: Boca Raton.

10. Melhado, L. and C. Gutsche, Journal of the American Chemical Society, 1978. **100**(6): p. 1850-1856.

11. Lehn, J.M., Science, 1985. **227**: p. 849-856.

5. Asymmetric tetraamine caps

In general, the coordination properties of cryptands may be altered and tuned in many respects: the number of donors and the type in both strands and caps; the length of the strands (*i.e.* for Schiff base cryptands the cap and spacer size); the number, degree of aromaticity, and rigidity of the strands are some of the variables which have been adjusted to achieve particular goals.

The imBT copper system is an example of adjustment of the cavity size, to enforce a small copper-copper separation, which creates the conditions appropriate to formation of the average valence complex. The adjustment is achieved in this case by selection of a small cap (tren, tris (2-aminoethyl) amine) and a small spacer (glyoxal, giving a 2 carbon bridge). The preparation of the related trpn (tris (2-aminopropyl) amine) cryptand, and tren/three carbon spaced cryptand, which have now been achieved, allows comparison of metal-metal interactions within a somewhat larger cavity size (*i.e.*, potentially larger copper-copper separation).

This chapter presents studies aimed at increasing the degree of control over strand length, and therefore the cavity size. This could be achieved by sacrificing the internal symmetry, and changing each strand individually: in the case of Schiff base cryptands, an elegant method of achieving this would be to use an asymmetric cap unit.

Our specific aim was to investigate the effect of slight variations in cavity size on the average valence dicopper imBT system, and we therefore chose two cap units similar to the tren cap of imBT. These were the 2,2,3 tetraamine, bis (2-aminoethyl) 3-aminopropyl

amine (abbreviated baep), and the 3,3,2 tetraamine, 2-aminoethyl bis (3-aminopropyl) amine (abbreviated abap). A summary of the various spacer:cap combinations investigated during the development of this methodology is given in Table 5-1 and Scheme 5-1.

Table 5-1: Cap and spacer combinations together with section numbers in which they are discussed.

Spacer unit	Cap unit	
	abap 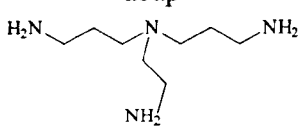	baep 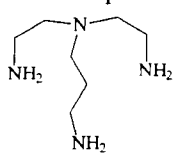
Glyoxal 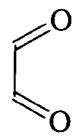	ABimBT (2 isomers) 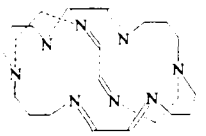 Section 5.1.2	BAimBT (2 isomers) 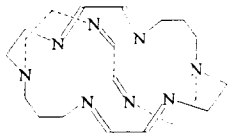
Isophthaldehyde 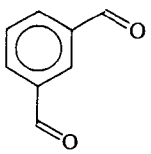	AB3Bm (2 isomers) 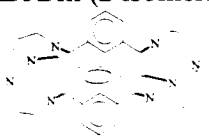 Section 5.1.1	BA3Bm (2 isomers) 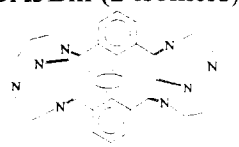 Section 5.2.2
Benzaldehyde 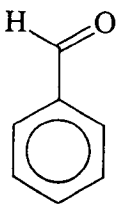		BAbenz 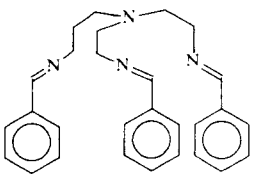 Section 5.2.2

It is worth noting that the stepwise Schiff base condensation which ultimately results in a cryptand, can, in the case of asymmetric caps, lead to two different isomers. Scheme 5-1 illustrates the situation for two abap caps. The isomer in Scheme 5-1 (A) is formed when long strands couple with opposing long strands, and the short strands couple to each other, and is referred to by the LLSS designation elsewhere in this chapter. The molecules shown in Scheme 5-1 (B) and (C) are identical, and are formed when only one long strand couples to a long strand, and the remaining long strands couple to the opposing short strands. This isomer is given the LSSL designation, and on purely statistical grounds is expected to be formed at twice the rate of the LLSS isomer, as it results from two possible combinations,

rather than only one. At first glance, the complementary long-short, short-long pairing appears to result in a slightly smaller cavity size.

A computer model was prepared for the ABimBT cryptand (glyoxal spacer with abap cap, see Table 5-1), using MM2 theory to compare LLSS and LSSL isomers. The bridgehead nitrogen separation was measured as a basic index of cavity size, and this also suggested that the LSSL pairing would give a smaller cavity: 5.83 Å N_{br}–N_{br} compared to 6.42 Å for the LLSS isomer.

A template preparative method involving a large ion may therefore tend to favour the LLSS isomer. If a significant difference in cavity size does exist, then this may also lead to differences in the ligand conformation of cryptates of the isomers.

For cryptands incorporating the baep cap, a similar situation exists, in this case formation of the LSSL isomer is also statistically favoured.

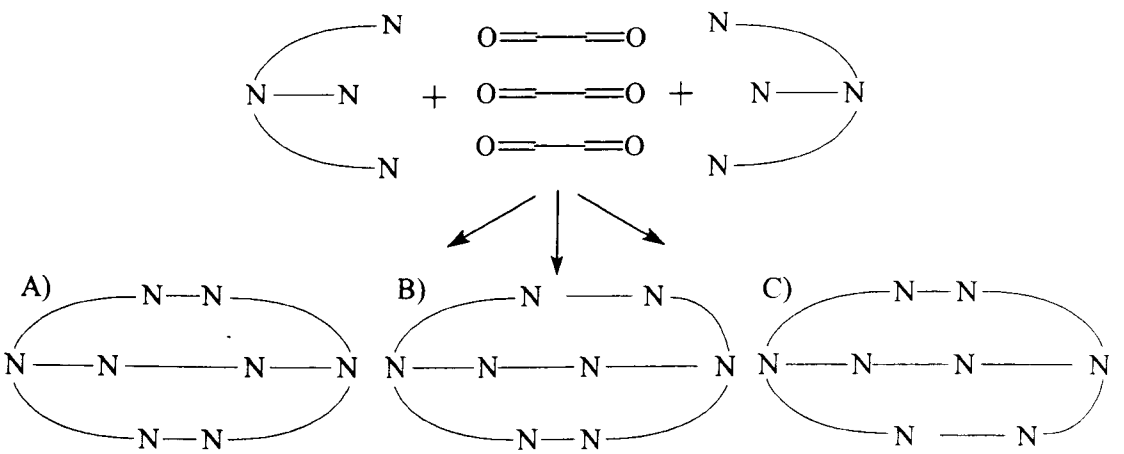

Scheme 5-1: Schiff base condensation involving two asymmetric caps can lead to more than one cryptand. *N.B.* B) and C) are identical but can be formed via two routes compared to one, and are thus statistically favoured.

5.1. Complexes incorporating a 3,3,2 tetraamine cap (abap)

Preparative methods reported by (1) and (2) were used in the preparation of abap, the exact procedure is described in the experimental section (section 9.4.1).

The procedure (Scheme 5-2) involved protection of the primary amine groups of dipropylenetriamine with phthalimide groups, following by a condensation reaction between the secondary amine and a phthalimide protected bromo-amine. The phthalimide

protecting group is selective for primary amines as it forms a ring incorporating the amine nitrogen, and thus very effectively blocks any reaction at this centre.

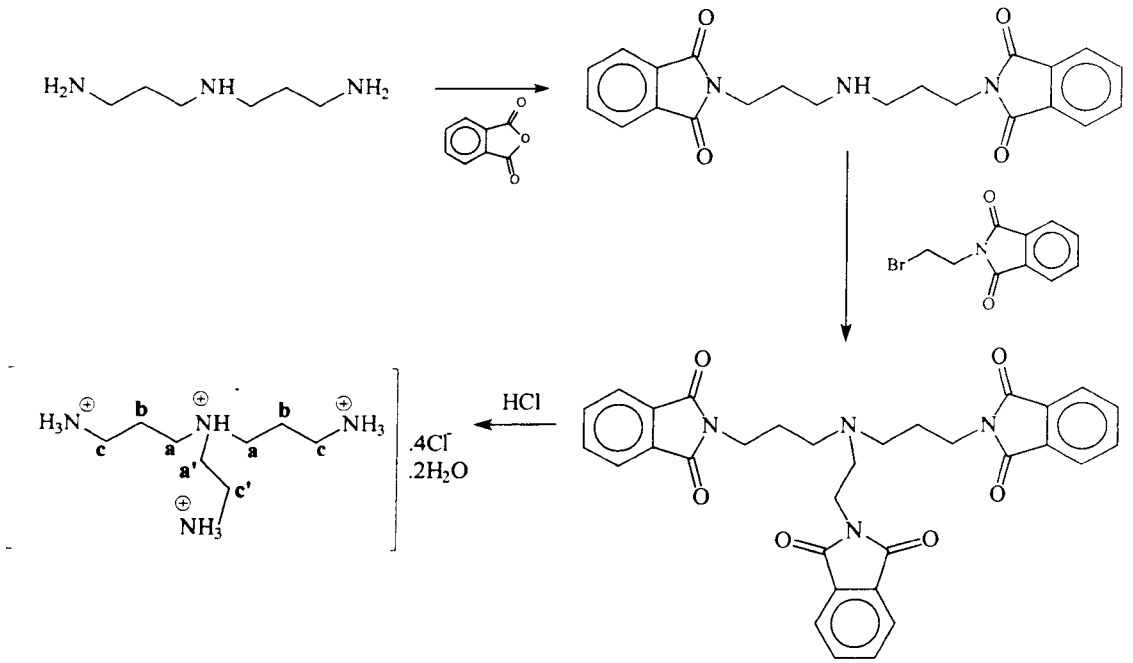

Scheme 5-2: Reaction scheme for the preparation of the 3,3,2 tetraamine cap, abap. The hydrogen positions in the final product have been labelled a, b, c, a' and c', corresponding to the NMR spectrum assignment below.

The procedure is somewhat unusual, as it does not require any solvent. During both the addition of the protecting groups, and the formation of the new C-N bond the reagents are simply melted and stirred together. Removal of the protecting groups is achieved by refluxing the solid in concentrated HCl, and the final product is isolated as a hydrochloride salt (see section 9.4.1 for full experimental details).

The ^{1}H NMR is shown in Figure 5-1, peaks have been assigned according to the numbering scheme shown in Scheme 5-2, and with reference to the NMR spectrum of tris-3-aminopropylamine (trpn) assigned by Dietrich (3). The absence of any aromatic protons (see inset) shows that the protecting group has been fully removed.

The infrared spectrum is consistent with the product, showing evidence of strong H-bonding as expected for an amine salt (see Figure 5-2). Elemental analysis was not consistent with the pure hydrochloride salt (Table 5-2), but suggests that residual bromide has been incorporated into the product, resulting in a mixed hydrochloride/hydrobromide salt.

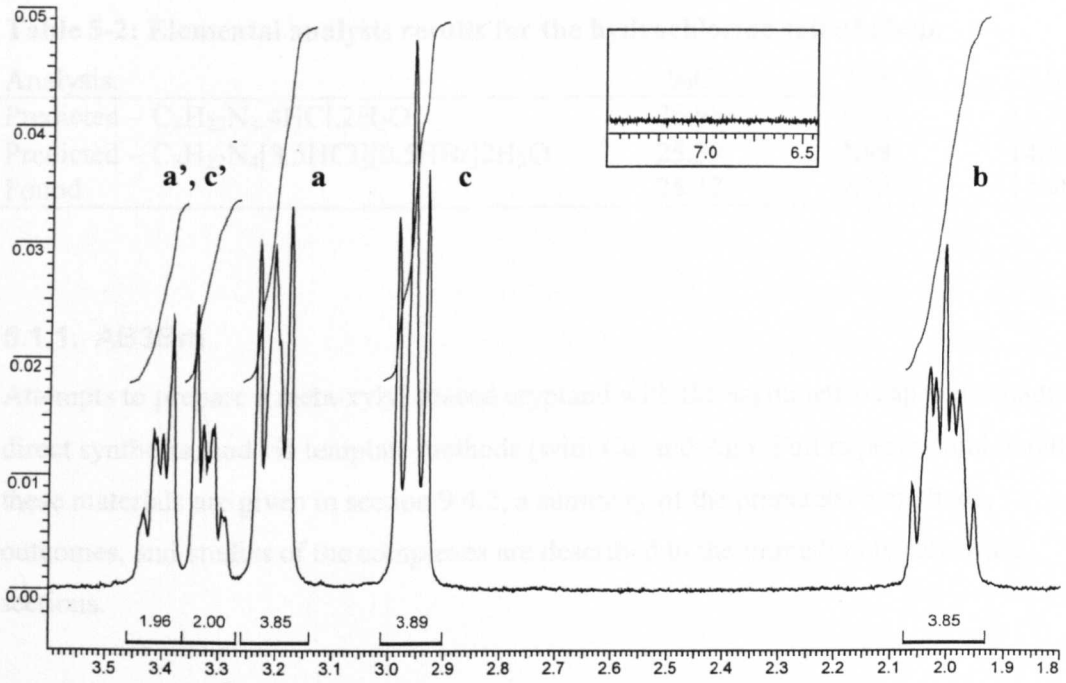

Figure 5-1: ^{1}H NMR of abap.4HCl.2H$_2$O in D$_2$O at room temperature. Peak labelling corresponds to Scheme 5-2, and the inset contains the aromatic region of the spectrum, showing clearly that the phthalimide protecting group has been fully removed.

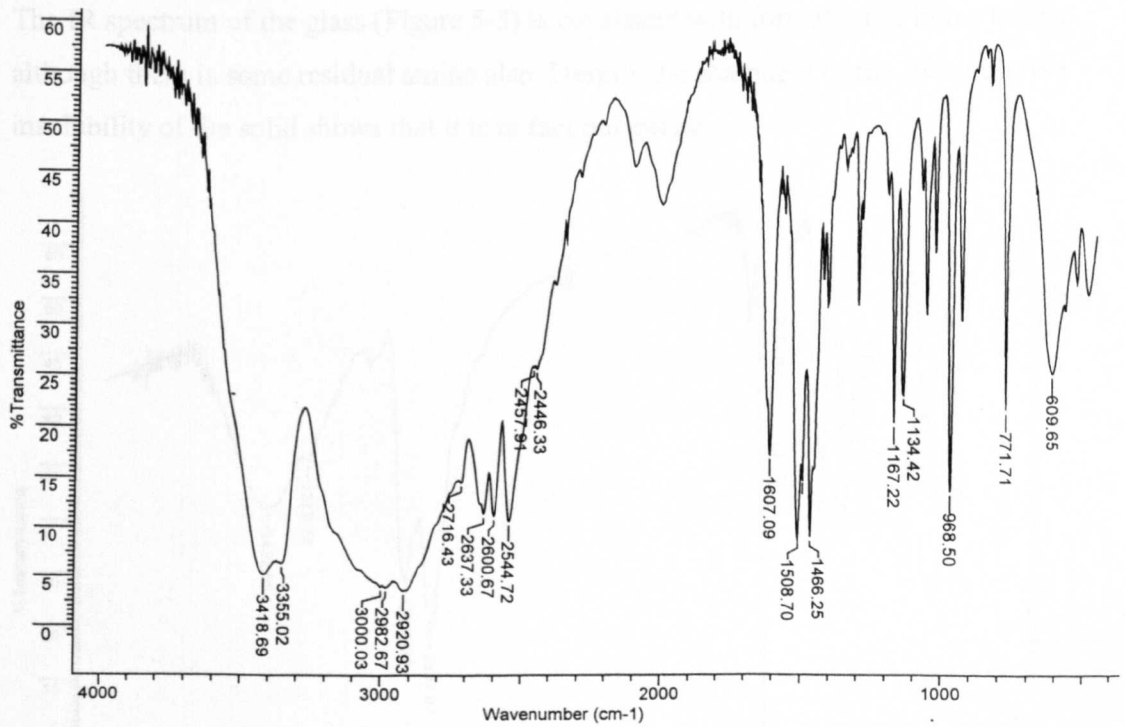

Figure 5-2: IR spectrum of a KBr disk of abap.4HCl.2H$_2$O. The amine stretches (3419 and 3355 cm^{-1}) and bend (1607 cm^{-1}) are easily distinguished, and the strong broad feature between 2700-3200 cm^{-1} is consistent with the existence of extensive hydrogen bonding.

Table 5-2: Elemental analysis results for the hydrochloride salt of abap.

Analysis:	%C	%H	%N
Predicted – $C_8H_{22}N_4.4HCl.2H_2O$	26.98	8.49	15.73
Predicted – $C_8H_{22}N_4[3.5HCl][0.5HBr]2H_2O$	**25.39**	**7.99**	**14.81**
Found	25.32	7.76	14.40

5.1.1. AB3Bm

Attempts to prepare a meta-xylyl spaced cryptand with the asymmetric cap were made via direct synthesis, and via template methods (with Cu^I and Ag^I). Full experimental details for these materials are given in section 9.4.2, a summary of the preparative methods, outcomes, and studies of the complexes are described in the immediately following sections.

5.1.1.1. Free cryptand

Dropwise addition of the free amine to 1.5 equivalents of isophthalaldehyde in refluxing methanol gave an insoluble, rubbery, yellow film (full details are given in section 9.4.2.1). The IR spectrum of the glass (Figure 5-3) is consistent with formation of imine bonds, although there is some residual amine also. Despite the sharpness of the spectrum, the insolubility of the solid shows that it is in fact polymeric.

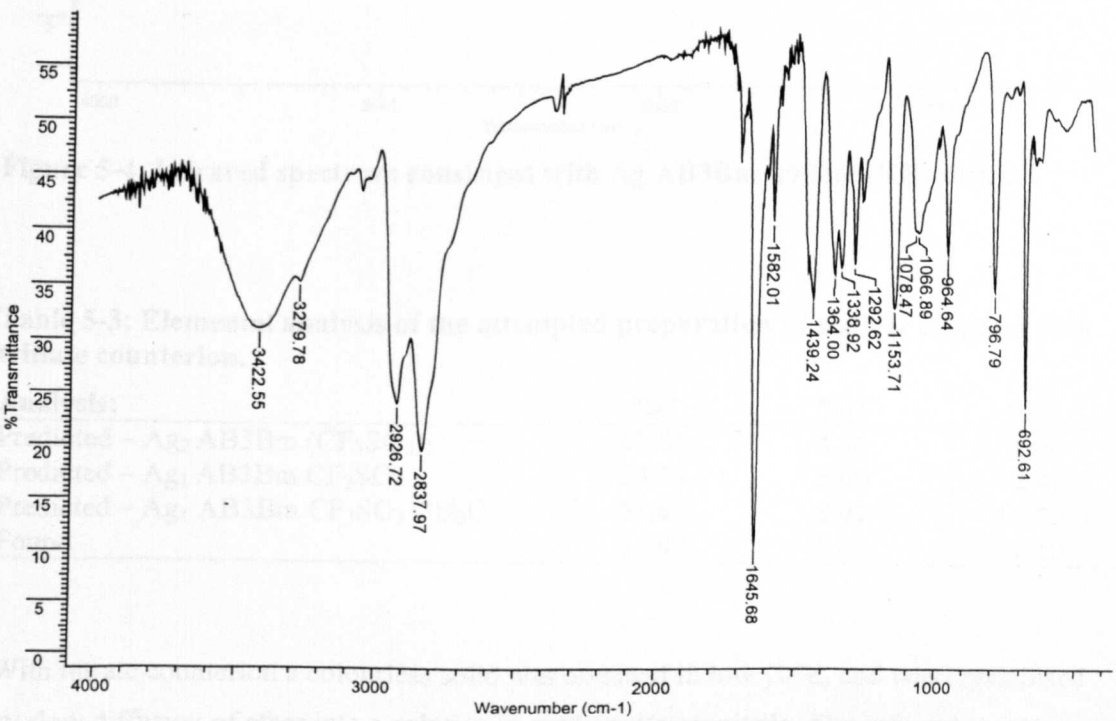

Figure 5-3: IR spectrum of the yellow rubbery solid, showing a strong imine stretch at 1645 cm^{-1} (KBr disk).

5.1.1.2. Silver(I) cryptate

The method described for the free ligand above was repeated with a templating ion (full details in section 9.4.2.2). Whilst the solution was refluxing (in a foil covered vessel), 1 equivalent of solid silver triflate was added to the yellow solution, yielding a powdery white solid whose IR spectrum (Figure 5-4) is consistent with an imine bonded complex, containing triflate anion. The elemental analysis suggests a mononuclear cryptate, however in light of the later preparation of a dinuclear cryptate, this could also be explained as a mixture of disilver cryptate and free ligand.

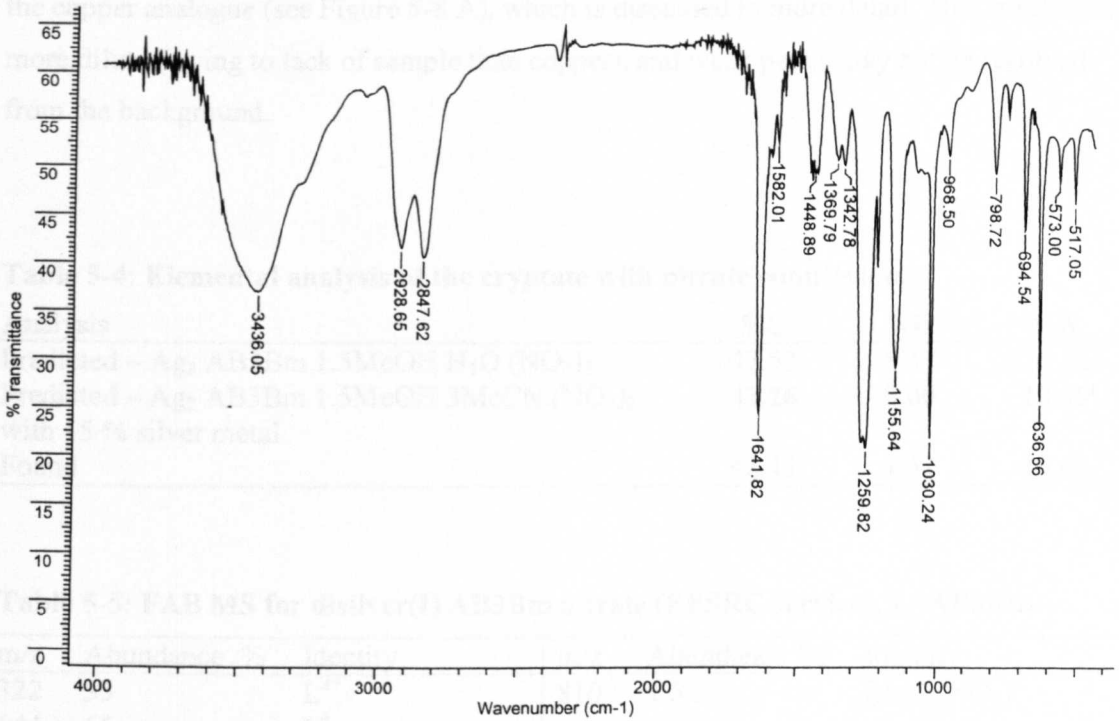

Figure 5-4: Infrared spectrum consistent with Ag AB3Bm triflate (KBr disk).

Table 5-3: Elemental analysis of the attempted preparation of a silver cryptate with triflate counterion.

Analysis:	%C	%H	%N
Predicted – Ag_2 AB3Bm $(CF_3SO_3)_2$	43.61	4.36	9.69
Predicted – Ag_1 AB3Bm CF_3SO_3	54.73	5.60	12.45
Predicted – Ag_1 AB3Bm $CF_3SO_3 \cdot 3H_2O$	**51.63**	**5.92**	**11.75**
Found	51.47	5.83	12.10

With nitrate counterion a colourless solid was obtained in low yield, and was crystallised by slow diffusion of ether into a solution in methanol/acetonitrile. The infrared spectrum, and structure of these crystals are given in Figure 5-5 and Figure 5-7. The elemental

analysis (Table 5-4) was not in agreement with the observed crystal structure (which incorporates one full and one half occupancy methanol, and one water molecule), however the sample submitted for analysis was a grey non- crystalline powder, and the analysis could be explained by the presence acetonitrile (from initial recrystallisation attempts) and silver. The FAB mass spectrum was weak, most likely owing to low solubility, however it did show peaks clearly related to the cryptate (Table 5-5). ^{1}H NMR (Figure 5-6) was complex, and contains peaks in regions consistent with imine, aromatic, and cap protons. The spectrum appeared broader with a slightly lesser number of individual resonances than the copper analogue (see Figure 5-8 A), which is discussed in more detail. This spectrum is more dilute (owing to lack of sample than copper), and weak peaks may not be resolved from the background.

Table 5-4: Elemental analysis of the cryptate with nitrate counterion.

Analysis	%C	%H	%N
Predicted – Ag_2 AB3Bm 1.5MeOH H_2O $(NO_3)_2$	47.53	5.57	13.36
Predicted – Ag_2 AB3Bm.1.5MeOH 3MeCN $(NO_3)_2$ with 15 % silver metal	**42.26**	**5.00**	**13.49**
Found	42.48	4.52	13.63

Table 5-5: FAB MS for disilver(I) AB3Bm nitrate (EPSRC service), L=AB3Bm.

m/z	Abundance /%	Identity	m/z	Abundance /%	Identity
322	35	L^{2+}	810	1.5	$[Ag\ L\ NO_3]^+$
644	65	L^+			

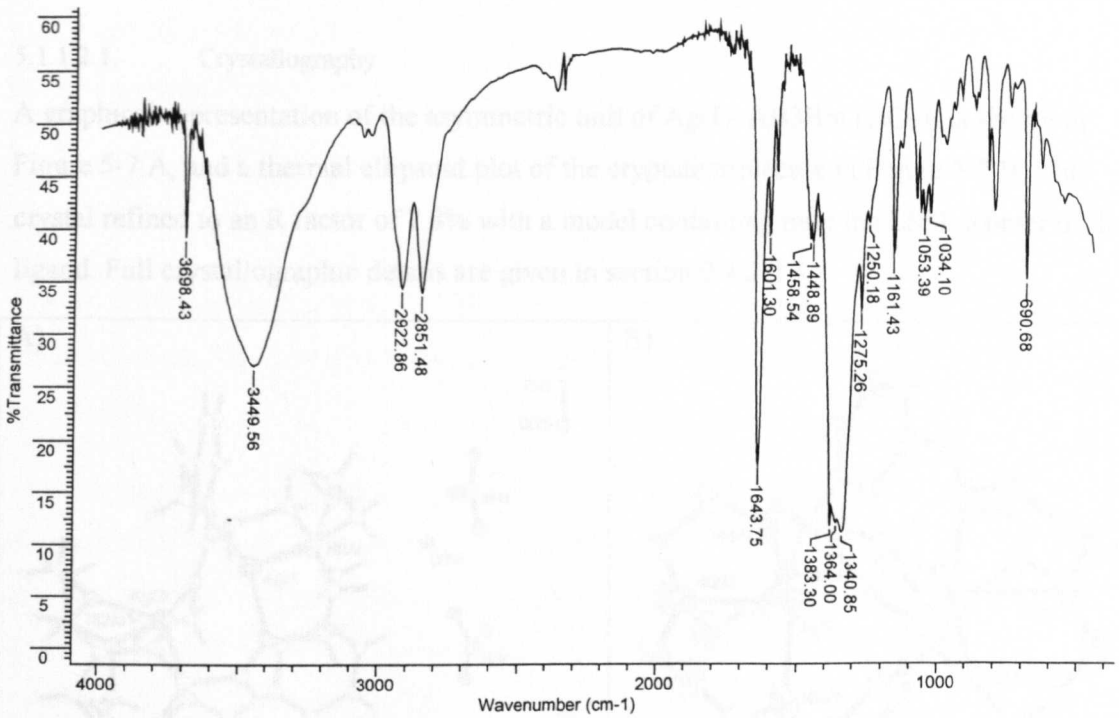

Figure 5-5: Infrared spectrum of Ag_2 AB3Bm $(NO_3)_2$ (KBr disk). NO_3 peaks are observed at 691 and 1364 cm^{-1}, and a strong imine peak at 1644 cm^{-1}. The identity of the unusually strong peak at 3698 cm^{-1} may be due to the OH stretch of methanol in the sample.

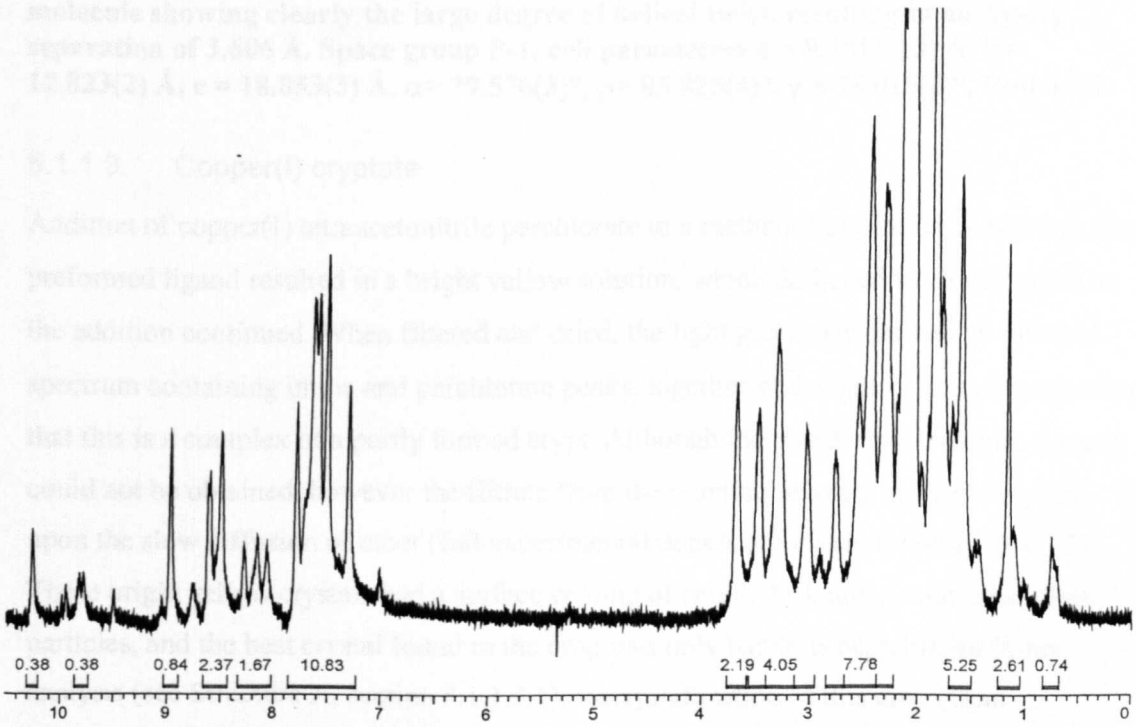

Figure 5-6: ^1H NMR spectrum of Ag_2 AB3Bm $(NO_3)_2$ (CD_3CN at room temperature, integrals indicated beneath the peaks).

5.1.1.2.1. Crystallography

A graphical representation of the asymmetric unit of $Ag(I)_2$ AB3Bm $(NO_3)_2$ is shown in Figure 5-7 A, and a thermal ellipsoid plot of the cryptate molecule in Figure 5-7 B. This crystal refined to an R factor of 7.8% with a model containing only the LSSL isomer of the ligand. Full crystallographic details are given in section 9.4.2.2.3.

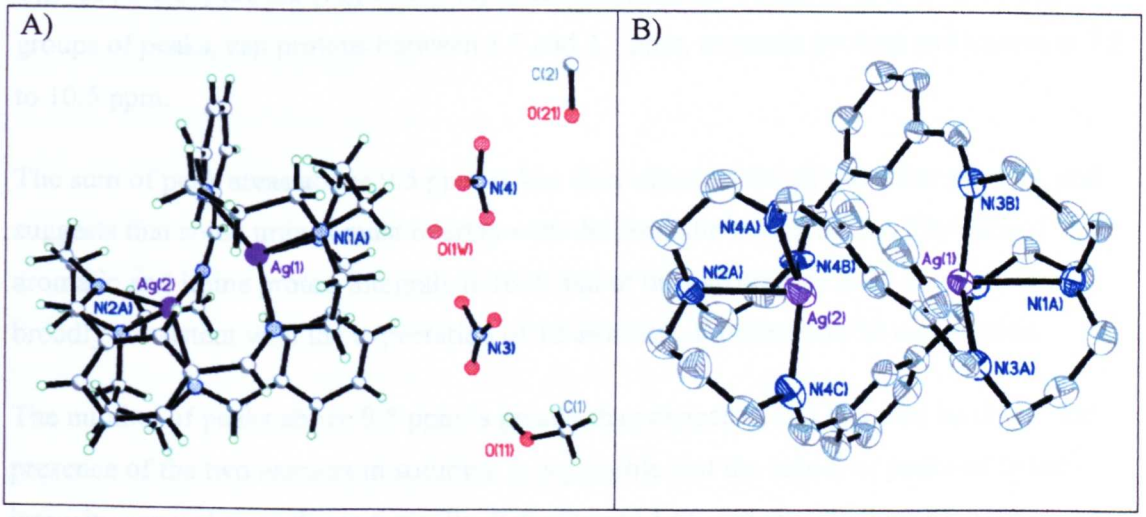

Figure 5-7: Graphical representation of the structure of Ag_2 AB3Bm $(NO_3)_2$, A) the cryptate in relation to the counterions and solvent molecules, and B) the cryptate molecule showing clearly the large degree of helical twist, resulting in an Ag-Ag separation of 3.606 Å. Space group P-1, cell parameters a = 9.5814(13) Å, b = 12.823(2) Å, c = 18.853(3) Å, α= 79.576(3)°, β= 85.825(4)°, γ = 78.016(4)°, R=0.0787.

5.1.1.3. Copper(I) cryptate

Addition of copper(I) tetraacetonitrile perchlorate to a methanolic solution containing the preformed ligand resulted in a bright yellow solution, which darkened to cloudy green as the addition continued. When filtered and dried, the light green powder had an infrared spectrum containing imine and perchlorate peaks, together with signs of amine, suggesting that this is a complex of a partly formed crypt. Although the powder was soluble, crystals could not be obtained, however the filtrate from the reaction mixture did yield crystals upon the slow diffusion of ether (full experimental details are given in section 9.4.2.3). These bright yellow crystals had a surface coating of small, dark green, non-crystalline particles, and the best crystal found in the crop was only barely acceptable for X-ray analysis (see Structure A, section 5.1.1.3.1). Recrystallisation of this crop (from acetonitrile with slow diffusion of ether) resulted in good quality crystals (Structure B, section 5.1.1.3.2) whose asymmetric unit contained a single cryptate cation with two perchlorate anions and an acetonitrile molecule. The elemental analysis (Table 5-6) of the recrystallised crop suggests the presence of water and/or another impurity not evident in

the crystal structure, which may be evidence of partial decomposition, possibly hydrolytic, whilst the sample was awaiting analysis.

FAB MS for the recrystallised material (Table 5-7) was consistent with the crystal structure.

The ^{1}H NMR spectrum (Figure 5-8 A) of the complex shows three apparently distinct groups of peaks, cap protons between 1.5 and 3.5 ppm, aromatic protons and imines at 7.5 to 10.5 ppm.

The sum of peak areas above 9.5 ppm is less than expected for all six imine protons, and suggests that some imines must overlap with the aromatic region below. The sum of aromatic and imine proton integrals is 16.2, and of the cap protons is 33.8, which is broadly consistent with the expectation of 12 aromatic, 6 imine, and 32 cap protons.

The number of peaks above 9.5 ppm is greater than expected, and this may be due to the presence of the two isomers in solution. It is possible that the subset of peaks of lower intensity may relate to the statistically disfavoured LLSS isomer. The overall complexity and sharpness of the spectrum shows that there is no conformational change occurring on the NMR timescale, however no attempt was made to assign the extremely complex and overlapped cap proton region. In comparison, the disilver cryptate, for which only one isomer was present in the solid state, has an apparently simpler spectrum (Figure 5-6), however this may be due purely to a relatively dilute sample.

The dicopper ^{1}H NMR is consistent with the ^{13}C spectrum (Figure 5-8 B), where imine carbons are between 166 and 161 ppm, aromatic carbons 136 to 121 ppm, and cap carbons lie between 27 and 63 ppm, being split into two separate groups. The lower group presumably relates to N-C-**C**-C-N, of which each cryptate molecule contains four. The other group of cap carbons then should contain resonances for three times as many carbons (12 in each molecule), and this is broadly consistent with observations. There are however 8 separate signals in the lower group, and at least 16 in the upper group (overlapping is likely in this area), showing that if each strand is different, then at least two different isomers or conformations must exist.

The imine carbon region (6 in each molecule) also appears too complicated for a single conformation or isomer. At least nine separate peaks are present, which, allowing for overlapping, is likely to represent at least 2 isomers or conformations. 26 separate aromatic

carbons (18 in each molecule) can be identified, and in this relatively noisy spectrum the quaternary carbons (6 in each molecule) may not be resolved from background.

Thus is appears highly likely that the NMR spectra represent a mixture of the LSSL and LLSS isomers, as was observed in the original crystal structure (structure A, see section 5.1.1.3.1), probably with a larger proportion of one isomer. A full assignment of the spectra for this cryptate was not attempted, however initial NOE experiments (Figure 5-9) showed the pair of peaks at 9.49 (integral 0.25) and 9.92 ppm (integral 1.01) to mutually interact through space, as well as the pair at 9.65 (integral 0.79) and 10.17 ppm (integral 0.34). The difference in integral within each pair is unexpected, and may also be a consequence of the presence of more than one isomer or conformation in solution: a minor component which displays the through-space coupling, and a major component whose peaks partly overly the other spectrum. Comparison with the crystal structure suggests that each of these pairs may represent an imine proton with its nearest aromatic neighbour (*e.g.* C4A and C6A, see section 9.4.2.3.2), which are coplanar, and within 2.4 Å of each other. If this is the case however, the same coupling would be expected for all imine protons, and in all conformations, owing to the rigid conjugated arrangement. A full set of NOE experiments may help to resolve this conundrum, however given the complex and overlapping nature of the spectrum a full assignment is likely to be unachievable.

Despite the observation of so many distinct imine protons, splitting of the imine resonance cannot clearly be observed in the infrared spectrum (Figure 5-10), although this could be due to insufficient instrument resolution, or simply the relatively high background in this spectrum.

Table 5-6: Elemental analysis of the bright yellow dicopper(I) AB3Bm perchlorate.

Analysis	%C	%H	%N
Predicted – Cu_2 AB3Bm MeCN $(ClO_4)_2$	49.95	5.29	12.48
Predicted – Cu_2 AB3Bm MeCN $(ClO_4)_2.2H_2O$	48.23	5.49	12.05
Found – Initial sample (structure A)	52.10	5.93	11.93
Found – After recrystallisation (structure B)	48.43	5.00	11.38

Table 5-7: FAB MS for dicopper(I) AB3Bm perchlorate (EPSRC service, L = AB3Bm).

m/z	Abundance /%	Identity	m/z	Abundance /%	Identity
705	9	Cu L	805	7	Cu L ClO_4
768	18	Cu_2 L	869	12	Cu_2 L ClO_4

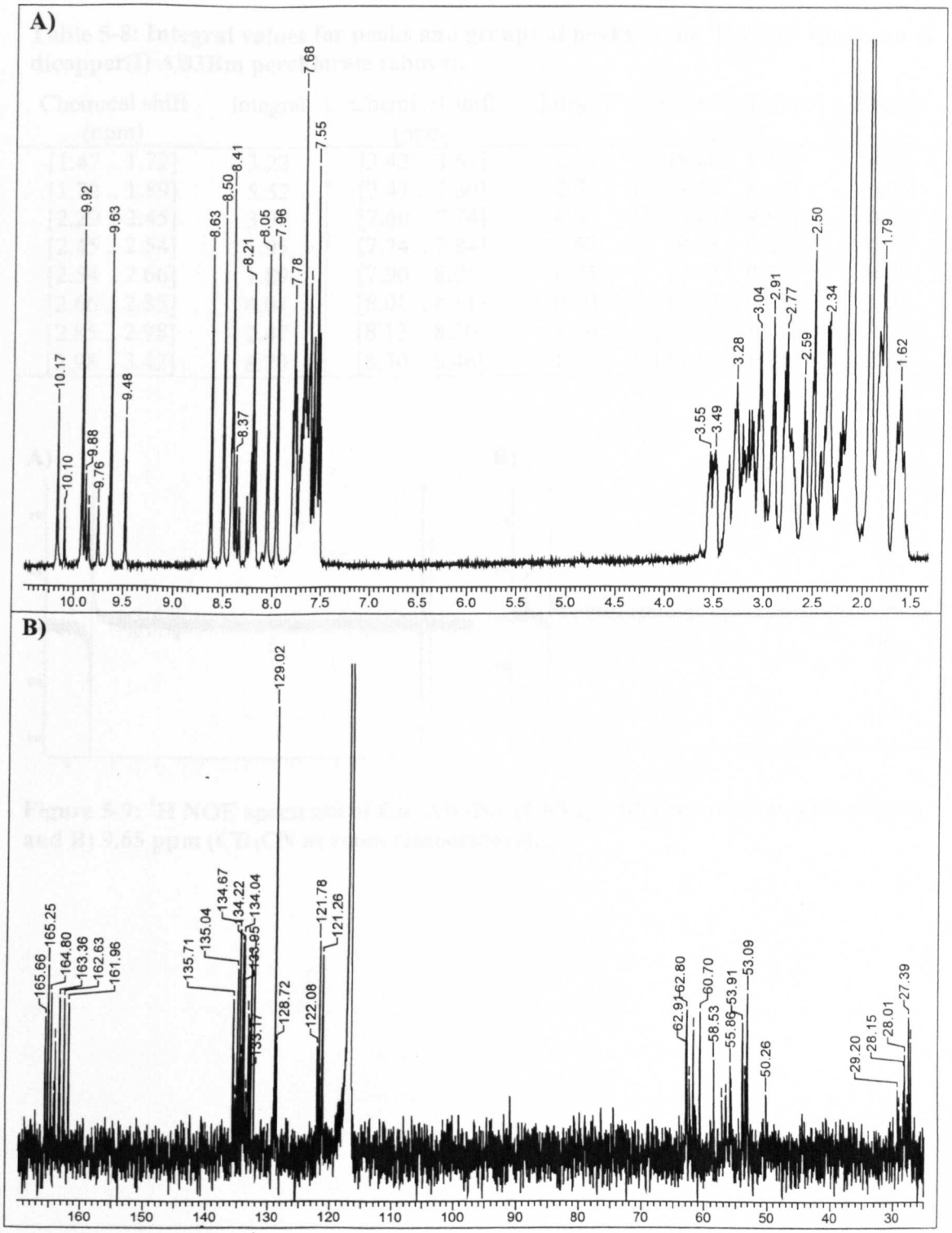

Figure 5-8: A) ^{1}H and B) ^{13}C NMR spectra of Cu_2 AB3Bm $(ClO_4)_2$ in CD_3CN at room temperature. As far as possible the chemical shifts are indicated, and proton spectrum shifts and integrals are in the table below.

Table 5-8: Integral values for peaks and groups of peaks in the ^{1}H NMR spectrum of dicopper(I) AB3Bm perchlorate (above).

Chemical shift (ppm)	Integral	Chemical shift (ppm)	Integral	Chemical shift (ppm)	Integral
[1.47 .. 1.72]	3.22	[3.42 .. 3.61]	2.11	[8.48 .. 8.52]	0.73
[1.72 .. 1.89]	5.52	[7.47 .. 7.60]	2.31	[8.59 .. 8.66]	0.65
[2.29 .. 2.45]	3.92	[7.60 .. 7.74]	4.36	[9.43 .. 9.53]	0.25
[2.45 .. 2.54]	1.95	[7.74 .. 7.84]	1.67	[9.58 .. 9.69]	0.79
[2.54 .. 2.66]	1.89	[7.90 .. 8.01]	0.73	[9.72 .. 9.80]	0.06
[2.66 .. 2.85]	4.01	[8.01 .. 8.11]	0.70	[9.83 .. 9.95]	1.01
[2.85 .. 2.98]	2.47	[8.13 .. 8.30]	1.34	[10.05 .. 10.12]	0.03
[2.98 .. 3.42]	8.70	[8.30 .. 8.46]	1.57	[10.14 .. 10.22]	0.34

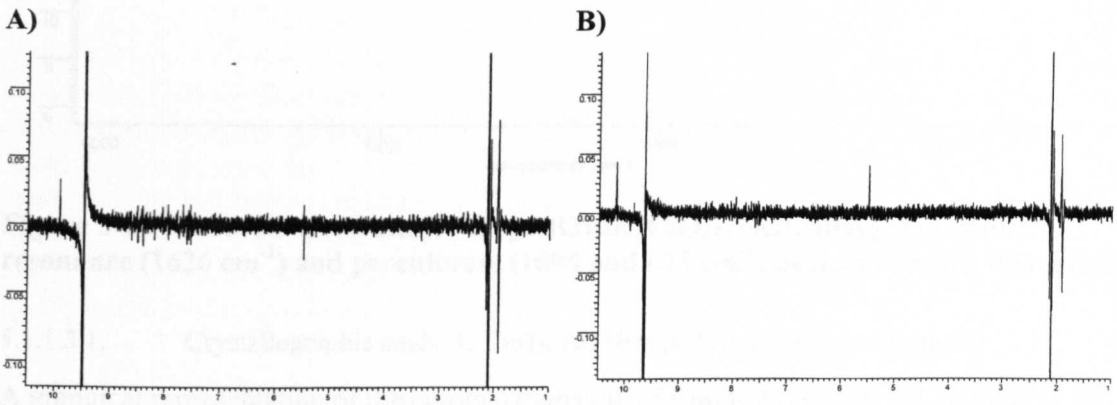

Figure 5-9: ^{1}H NOE spectrum of Cu_2 AB3Bm $(ClO_4)_2$ with excitation at A) 9.49 ppm, and B) 9.65 ppm (CD_3CN at room temperature).

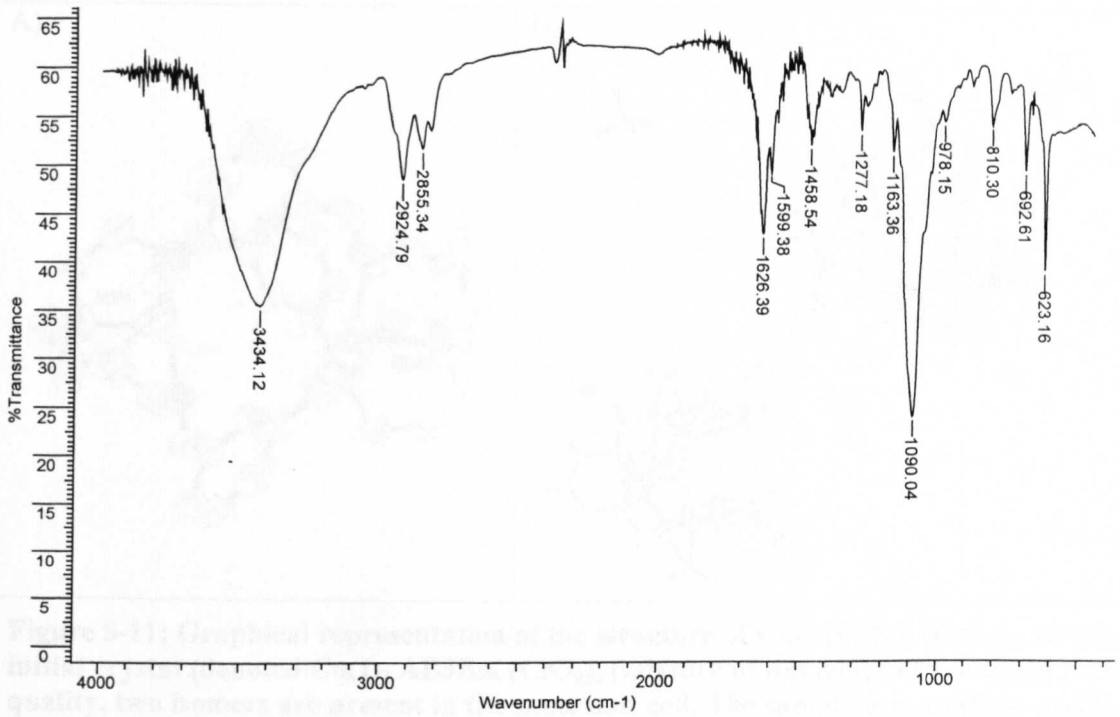

Figure 5-10: Infrared spectrum for Cu_2 AB3Bm $(ClO_4)_2$ (KBr disk). The imine resonance (1626 cm^{-1}) and perchlorate (1090 and 623 cm^{-1}) peaks are easily discerned.

5.1.1.3.1. Crystallographic study A: $Cu(I)_2$ AB3Bm $(ClO_4)_2$ (mixture of isomers)

A graphical representation of the cryptate molecule of $Cu(I)_2$ AB3Bm $(ClO_4)_2$ (mixture of isomers) is shown in Figure 5-11 A, and the asymmetric unit in Figure 5-11 B. Full crystallographic details are given in section 9.4.2.3.1.

This crystal diffracted relatively weakly, and was not expected to refine to a very low R factor, however it is reported here as it contained a slightly different configuration from the second structure (see section 5.1.1.3.2 below). Significant disorder is evident in this structure from the elongated ellipsoids as illustrated for one molecule in Figure 5-11 (a). Ellipsoids extending across the direction of the strands, as well as along the strands are observed, suggesting disorder of two different types: two alternative positions for the strands, and disorder of 3-carbon and 2-carbon cap strands over the same position (as modelled for $Cu(I)_2$ AB3Bm $(ClO_4)_2$ (single isomer) below). Since the second crystal was of far superior quality, a detailed model incorporating the extensive disorder in the present crystal was not constructed. Figure 5-11 (b) shows the unit cell incorporating two cryptate molecules, one LSSL isomer (upper right), and one LLSS (lower left). A molecule of acetonitrile is present, together with four perchlorate ions.

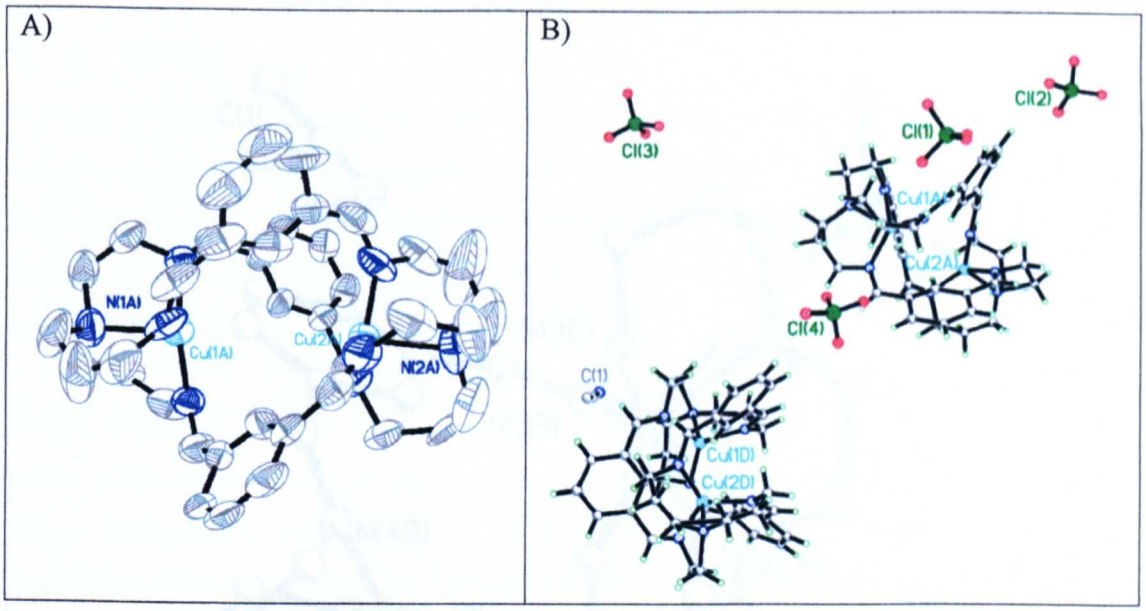

Figure 5-11: Graphical representation of the structure of Cu_2 AB3Bm $(ClO_4)_2$. In this initial crystal (denoted $Cu(I)_2$ AB3Bm $(ClO_4)_2$ (mixture of isomers)), of relatively poor quality, two isomers are present in the same unit cell. The sample was a yellow needle with some green non-crystalline particulates adhering to the surface, data collected at -120°C. Space group P2(1)/c, unit cell dimensions A 9.688 Å, B 25.334 Å, C 36.55 Å, α 90°, β 97.47°, γ 90°. The Cu-Cu distances are: for the LSSL isomer 4.5467 (0.0039) Å; and for the LLSS isomer 4.5971 (0.0040) Å.

5.1.1.3.2. Crystallographic study B: $Cu(I)_2$ AB3Bm $(ClO_4)_2$ (single isomer)

A graphical representation of the asymmetric unit of $Cu(I)_2$ AB3Bm $(ClO_4)_2$ (single isomer) is shown in Figure 5-12 A, and the cryptate molecule in Figure 5-12 B. Full crystallographic details are given in section 9.4.2.3.2.

The Cu-Cu distance of 4.4356(10) Å is similar to that observed with the symmetric trpn cap (3 carbon cap strands), and is more than 0.8 Å longer than the internuclear separation in the disilver cryptate, despite the smaller size of the copper(I) ion – an effect which mirrors that observed for the tren and trpn capped systems ((4), see section 5.1.4 for a discussion of this observation).

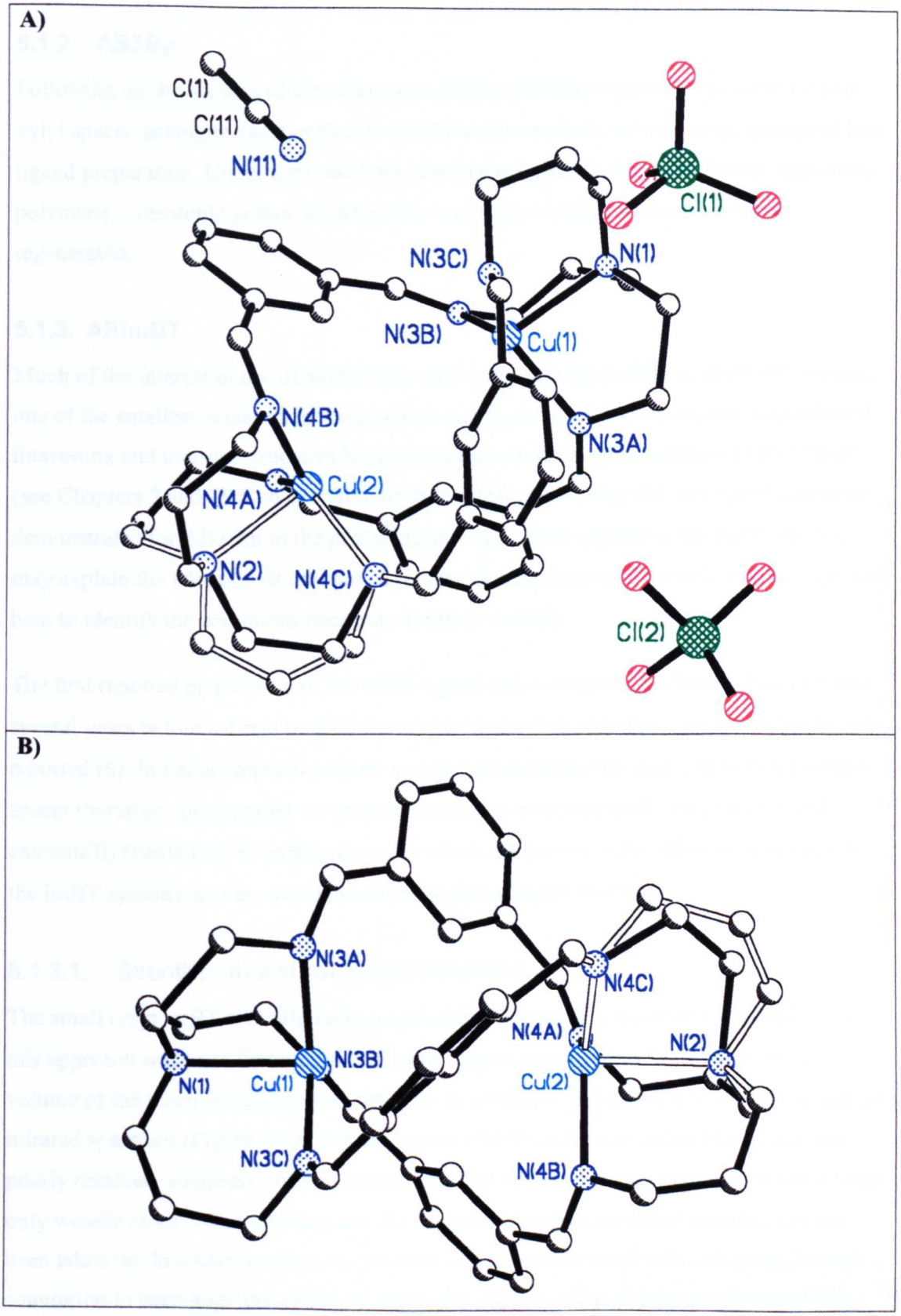

Figure 5-12: Graphical representation of the structure of Cu_2 AB3Bm $(ClO_4)_2$ (single isomer), A) asymmetric unit and B) cryptate molecule. Space group P2(1)/c, cell dimensions a = 14.5958(14) Å, b = 11.8877(11) Å, c = 25.470(2) Å, β= 94.309(2)°, R=0.0628.

5.1.2. AB3Bp

Following on the success of the meta-xylyl spacer, attempts were made to form the para-xylyl spaced analogue using copper(I) and silver(I) templates, as well as an attempted free ligand preparation. Under the conditions used the only products obtained were apparently polymeric – insoluble yellow brown solids, and some crystals of metal salt were regenerated.

5.1.3. ABimBT

Much of the interest in use of asymmetric caps is in their application to the imBT system, one of the smallest octaazacryptands, which incorporates a 2-carbon spacer. A number of interesting and unusual structures have been discovered for the complexes of this ligand (see Chapters 2 and 3). Consideration of the control over cavity size and ligand geometry demonstrated for AB3Bm in the preceding sections, when applied to the imBT system, may explain the adoption of unusual structures such as those in Figures 2-15 and 2-20, and help to identify the conditions necessary for their stability.

The first reported preparation of the imBT ligand was a template synthesis (5), and it was several years before a direct method for preparing the free ligand in a one-pot reaction was reported (6). Initial attempts to prepare a crypt incorporating the abap cap with a 2-carbon spacer therefore concentrated on template syntheses with copper(I), strontium(II) and calcium(II) (labile ions of appropriate size, which are known to be effective templates for the imBT system), and are summarised in the following sections.

5.1.3.1. Strontium(II) and calcium(II) templates

The small crypt imBT was originally prepared in the form of a strontium(II) template, so this approach was tried first with the (slightly larger) asymmetric amine abap. When the volume of the reaction mixture was reduced, an insoluble yellow solid was isolated, whose infrared spectrum (Figure 5-13) was consistent with formation of imine bonds, but was poorly resolved, suggestive of polymerisation. The normally strong perchlorate peaks were only weakly observed, suggesting that the strontium perchlorate metal template has not been taken up. In a later attempt, the reaction mixture was treated with tetraphenylborate counterion to encourage precipitation. When the volume of the filtrate was reduced, this led to the isolation of a few crystals from the filtrate, although in insufficient yield for infrared analysis. X-ray crystallographic investigation proved these to be merely tetraphenylborate salts however.

Calcium perchlorate also appeared to be unsuitable as a template, a precipitate from the reaction mixture turned out to be merely the metal salt, and an insoluble solid was again obtained from the reduced filtrate, suggesting that polymerisation had occurred.

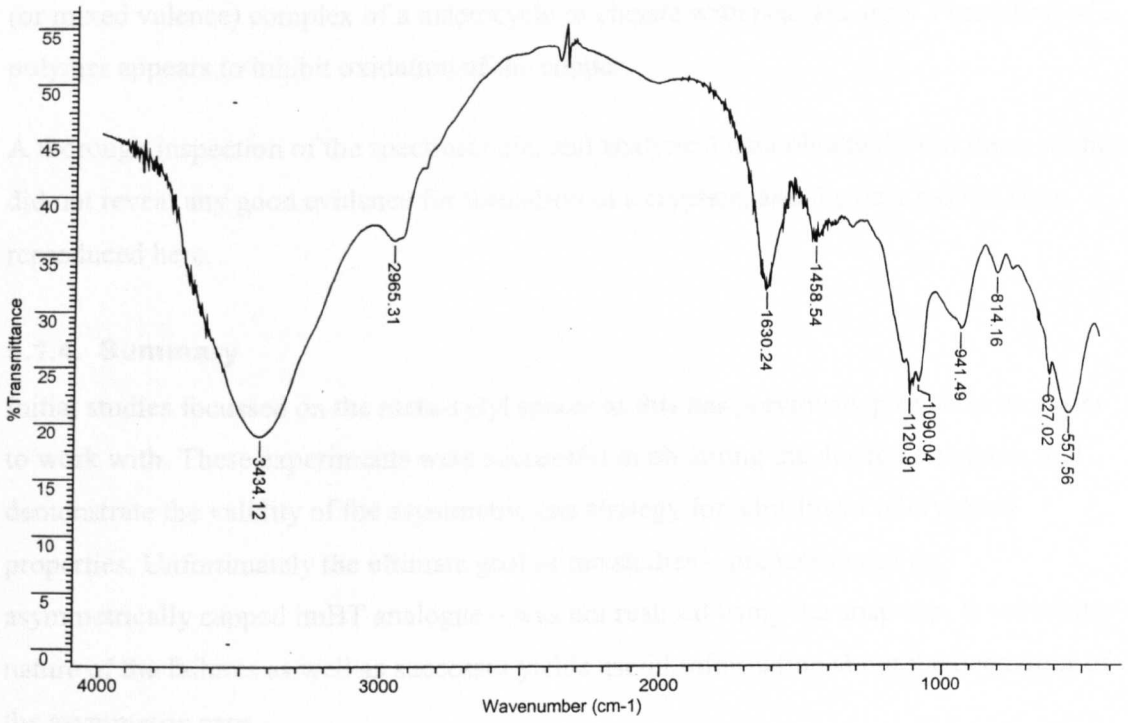

Figure 5-13: Infrared spectrum of the solid obtained from the attempted strontium template preparation.

5.1.3.2. Copper(I) template

Template syntheses were carried out using Cu(I) $(MeCN)_4$ ClO_4 in degassed solvents, under an inert atmosphere. Several variations on the method were attempted, including addition of glyoxal solution to a copper/tren solution, addition of tren to a copper/glyoxal solution, at different temperatures, dilution and addition rates, however no conclusive evidence for the isolation of the ABimBT ligand was obtained. Variable results were observed from the reactions, some suggestive of oxidation to copper(II) (blue or green solutions), and some yellow/brown solids, which were either insoluble, or else were oils which could not be induced to yield a solid.

Infrared spectra of many of the products (not shown) contained peaks consistent with the formation of imine bonds, however many of these also contained amine resonances, and many were broad and ill-defined, suggestive of polymerisation.

The imBT system is somewhat strained, and it appears that alteration of the cap characteristics in this case has disrupted the alignment necessary for stability of the

product. Oxidation of copper(I) to copper(II), concurrent with cleavage of imine bonds has been observed in related systems where internal strain is present (7, 8). This may explain the present situation: any product formed is immediately cleaved, resulting in a copper(II) (or mixed valence) complex of a macrocycle or chelate with pendant arms. Formation of a polymer appears to inhibit oxidation of the copper.

A thorough inspection of the spectroscopic, and analytical data obtained from these studies did not reveal any good evidence for formation of a cryptate, and the data has not been reproduced here.

5.1.4. Summary

Initial studies focussed on the meta-xylyl spacer as this has previously proven to be easier to work with. These experiments were successful in obtaining the desired cryptates, and demonstrate the validity of the asymmetric cap strategy for adjustment of cryptand properties. Unfortunately the ultimate goal of the studies – preparation of an asymmetrically capped imBT analogue – was not realised using the abap cap, however the nature of the failures as well as successes yields useful information about the behaviour of the asymmetric caps.

Synthesis of the – once-elusive – uncomplexed imBT cryptand has now been optimised to provide yields in excess of 50% (6) by careful adjustment of the reaction conditions. Incorporation of an asymmetric cap was expected to further complicate the system, and it is apparent that the different spatial and steric demands of abap disrupt the balance optimal to formation of the product.

The crystal structures obtained of the AB3Bm cryptates clearly demonstrate one of the complications of the asymmetric cap system – the possibility of forming more than one isomer of the cryptand, the LLSS and LSSL isomers. In the case of the dicopper(I) complex, a crystal apparently containing both isomers was isolated, however the weakness of data for this specimen, and the crystallographic disorder make it unwise to draw conclusions. Recrystallisation yielded a specimen containing the LSSL isomer, although the nature of the disorder in this case suggests that the crystal may have contained a proportion of the other isomer, occupying the same position in the lattice.

The disilver cryptate was better ordered in the solid state, and only the LSSL isomer was present. Despite the larger size of the ions in this case, the internuclear separation is less

than for copper (see Table 5-9), at first sight a somewhat surprising observation, but one which nevertheless mirrors the situation in tren and trpn capped cryptates.

Table 5-9: Variation in M-M separation for the metaxylyl spaced crypt series.

	tren (222) cap	abap (332) cap	trpn (333) cap
Cu-Cu distance /Å	4.23	4.4356(10)	4.44
Ag-Ag distance /Å	3.449	3.6062(15)	3.775

Synthetic and modelling studies by Drew et al (4) show that this effect is due to an interaction between the two (closed shell, d^{10}) silver ions.

5.2. Complexes incorporating a 2,2,3 tetraamine cap (baep)

5.2.1. Preparation of the cap (baep.4HCl.2H$_2$0)

A preparation reported by Dittler-Klingemann (9) was initially investigated for the preparation of baep (Figure 5-14), however an adaptation of the method used for abap (described above) was found to be simpler, and to avoid the use of hazardous reagents such as liquid ammonia, and potassium cyanide. The modified procedure was analogous to that described in Scheme 5-2, and involved protection of the primary amine groups of diethylenetriamine with phthalimide groups. Full experimental details are given in section 9.4.3.

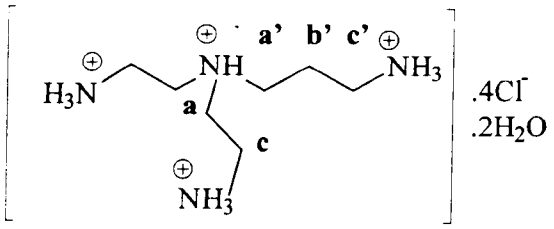

Figure 5-14: The tripodal amine baep.4HCl.2H$_2$O

The infrared and ^{1}H NMR spectra of the product are shown in Figure 5-15 and Figure 5-16. The infrared spectrum is very similar to that of abap (Figure 5-2), with notable differences in the number of amine stretches and bends (3410 cm^{-1}, only single peak; 1597 and 1624 cm^{-1}, two peaks now observed). Protons on the short strands are not resolved in the ^{1}H NMR as they were for abap, and result in a large overlapped feature at 3.3 ppm. Other protons are well resolved and easily identified, and the integrals agree with the expected ratio of 6 (long strand) to 8 (two short strands). The protons have been assigned by comparison to the NMR spectrum of tris-3-aminopropylamine (trpn) assigned by (3). The elemental analysis (Table 5-10) is in close agreement with expected ratios.

Table 5-10: Elemental analysis for baep.4HCl.2H$_2$O.

Analysis:	%C	%H	%N
Predicted – $C_7H_{20}N_4$.4HCl.2H$_2$O	24.57	8.25	16.38
Found	24.83	8.25	16.12

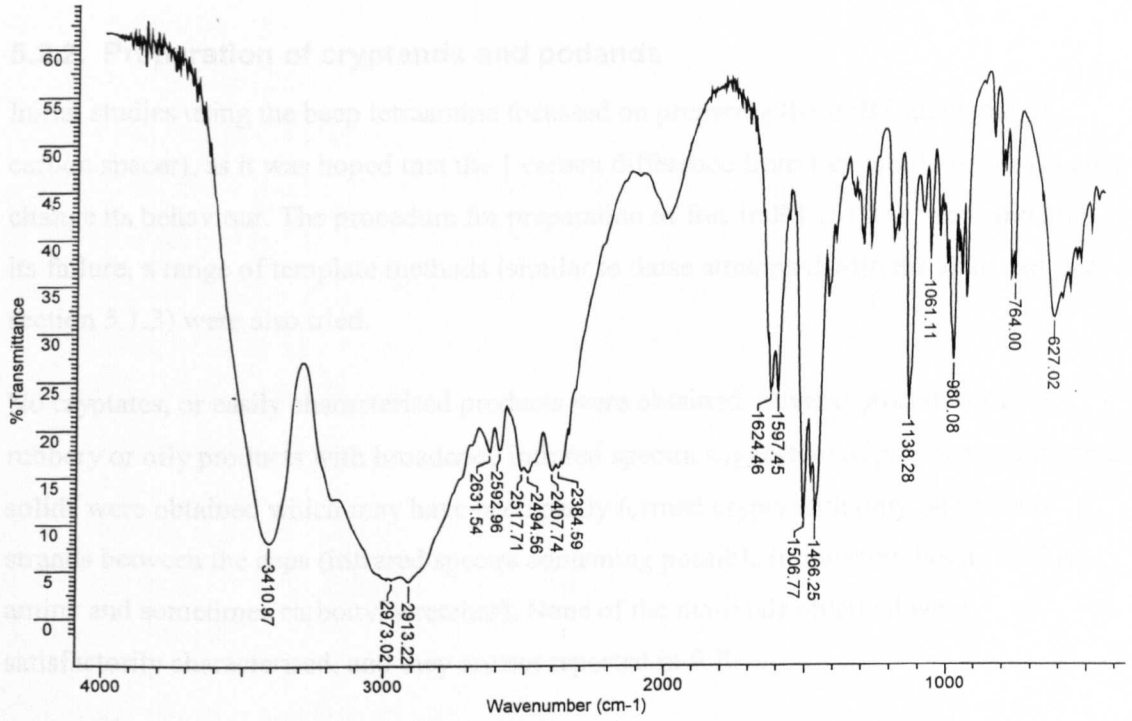

Figure 5-15: Infrared spectrum of baep.4HCl.2H_2O (KBr disk).

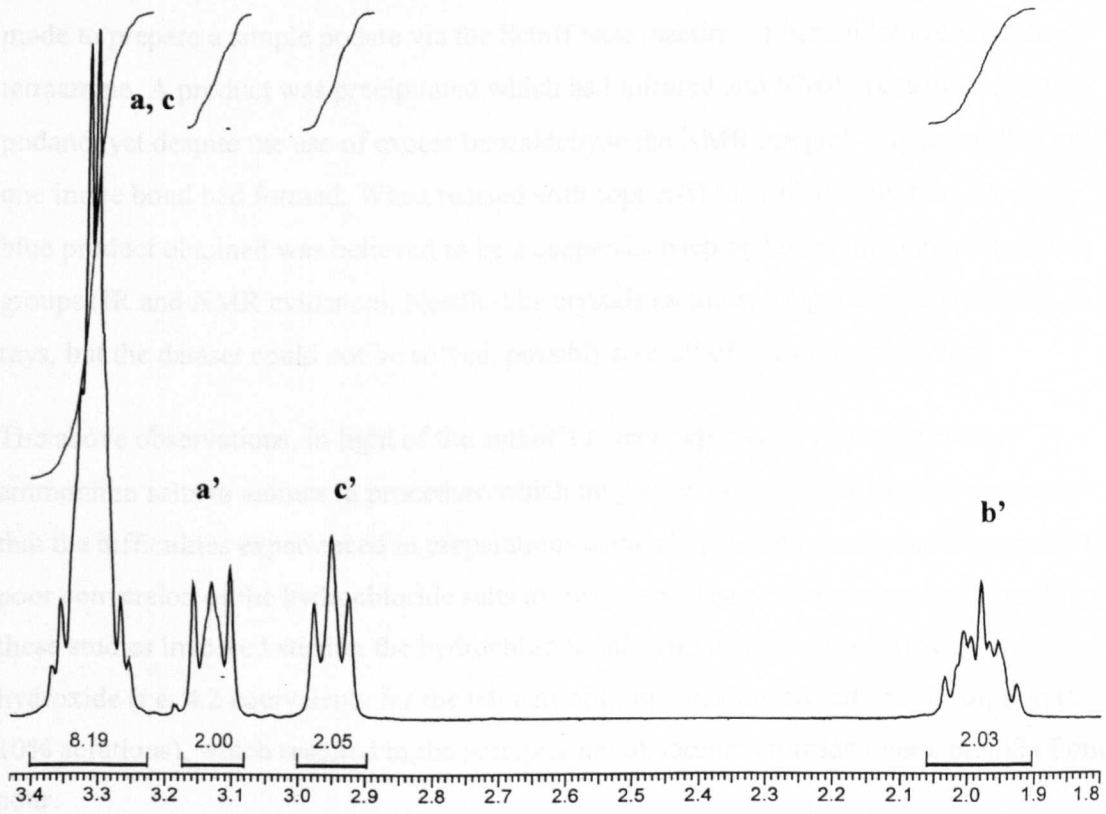

Figure 5-16: ^{1}H NMR of baep.4HCl.2H_2O (D_2O, at room temperature). The peaks are labelled following the numbering set out in Figure 5-14.

5.2.2. Preparation of cryptands and podands

Initial studies using the baep tetraamine focussed on preparing the imBT analogue (2-carbon spacer), as it was hoped that the 1 carbon difference from tren would not drastically change its behaviour. The procedure for preparation of free imBT (6) was used, and after its failure, a range of template methods (similar to those attempted with the abap cap, see section 5.1.3) were also tried.

No cryptates, or easily characterised products were obtained. Several procedures gave rubbery or oily products with broadened infrared spectra suggestive of polymers, and some solids were obtained which may have been partly formed crypts with only one or two strands between the caps (infrared spectra containing possible imine stretches as well as amine and sometimes carbonyl stretches). None of the materials obtained were satisfactorily characterised, and they are not reported in full.

Despite having good spectroscopic and analytical results for the hydrochloride salt of the tetraamine, we began to wonder whether the cap itself was suspect, and attempts were made to prepare a simple podate via the Schiff base reaction of benzaldehyde with the tetraamine. A product was precipitated which had infrared and NMR characteristics of a podand, yet despite the use of excess benzaldehyde the NMR integrals suggested that only one imine bond had formed. When reacted with copper(I) $MeCN_4$ perchlorate, the deep blue product obtained was believed to be a copper(II) baep podate containing no benzene groups (IR and NMR evidence). Needle-like crystals (actually long plates) did diffract X-rays, but the dataset could not be solved, possibly a result of extensive solvation.

The above observations, in light of the author's recent experience with converting ammonium salts to amines (a procedure which may occur surprisingly slowly) suggests that the difficulties experienced in preparations using abap and baep may have been due to poor conversion of the hydrochloride salts to free bases. The procedure normally used in these studies involved stirring the hydrochloride salt with a slight excess of sodium hydroxide (*i.e.* 4.2 equivalents for the tetraamines), in concentrated ethanolic solution (5-10% solutions), which resulted in the precipitation of sodium chloride over a period of one hour.

Apparently the time given for the reaction to occur was insufficient to free all four amine groups, and this corresponds with the commonly observed result of only partial formation of a crypt.

5.3. Conclusions

The studies presented in this chapter have shown that the approach of using an asymmetric cap is a valid means of introducing slight changes in strand length, cavity size, and donor distribution. The cryptates prepared in this study using asymmetric tetraamines with 2 and 3 carbon strands, have physical properties (such as internuclear separation) intermediate between the symmetric 2 carbon, and 3 carbon cap cryptates. The disilver cryptate is of particular interest, as surprisingly, it has a smaller internuclear separation than the dicopper cryptate, an effect which has been attributed to a closed shell silver-silver interaction in the related (symmetric) tren and trpn capped systems (4).

The introduction of asymmetry to the cap leads to the possibility of more than one isomer, and in the solid state, the statistically favoured "LLSS" isomer was indeed observed in greatest abundance.

Unfortunately, we were unable to successfully apply this methodology to the 2 carbon spaced imBT cryptand using either of the asymmetric tetraamines, from either template procedures, or direct preparations of the ligand. The original (strontium template) synthesis of this cryptand was not facile, and preparation of the three-carbon cap, two carbon spaced cryptand (10) was even more difficult. It therefore appears that the increased cap strand length disfavours the formation of a crypt, possibly via change in the hydrogen bonding pattern in the tetraamine. Another possible cause of the problems experienced in obtaining crypts or podands is poor conversion of hydrochloride salts to the free bases, a transformation which has been observed to occur surprisingly slowly in other systems (more than 48 hours for complete conversion of an ammonium salt in one extreme case (11)). This would explain a number of attempted preparations which appeared to have formed incomplete crypts, and it is also possible that it could have led to a greater likelihood of polymerisation, which was another reaction outcome often observed.

A more rigorous procedure for obtaining the free base may therefore allow the preparation of a greater range of cryptands and cryptates with the asymmetric cap, and we believe that this will prove to be a useful tool in the development and fine tuning of cryptands. For example, the recently elucidated Cu_Z site (12) is now the subject of modelling studies, and the methodology presented in this work may be applicable in the fine tuning of the nitrogen donor ligands which will be required for an appropriate model.

The ability to tune cavity size and donor distribution has important implications for binding coefficients, and may allow development of ligands with increased selectivity and

decreased lability. These would be desirable effects in many applications, such as the encapsulation of paramagnetic ions for MRI contrast agents (see following chapter), extraction of toxic or precious metals, or preparation of more robust sensors.

5.4. References

1. Fanshawe, R.L. and A.G. Blackman, Inorganic Chemistry, 1994. **34**(2): p. 421-423.

2. Streater, M., P. Taylor, R. Hider, and J. Porter, Journal of Medicinal Chemistry, 1990. **33**(6): p. 1749-1755.

3. Dietrich, B., D.L. Fyles, T.M. Fyles, and J.-M. Lehn, Helvetica Chimica Acta, 1979. **62**(8): p. 2763-2787.

4. Drew, M., D. Farrell, G. Morgan, V. McKee, and J. Nelson, Journal of the Chemical Society-Dalton Transactions, 2000. **9**: p. 1513-1519.

5. Hunter, J., J. Nelson, C. Harding, M. McCann, and V. McKee, Journal of the Chemical Society: Chemical Communications, 1990: p. 1148-1151.

6. Smith, P.H., M.E. Barr, J.R. Brainard, D.K. Ford, H. Freiser, S. Muralidharan, S.D. Reilly, R.R. Ryan, L.A.I. Silks, and W.-h. Yu, Journal of Organic Chemistry, 1993. **58**: p. 7939-7941.

7. Harding, C.J., Q. Lu, J.F. Malone, D.J. Marrs, N. Martin, V. McKee, and J. Nelson, Journal of the Chemical Society-Dalton Transactions, 1995(10): p. 1739-1747.

8. Nelson, J., Personal Communication, 1998.

9. Dittler-Klingemann, A.M. and F.E. Hahn, Inorganic Chemistry, 1996. **35**: p. 1996-1999.

10. Martin, N., *Azacryptand hosts for transition, main group, and lanthanide cations* PhD Thesis. 1996: Queen's University Belfast.

11. Speed, D.J., Author's unpublished data, 2002.

12. Brown, K., M. Tegoni, M. Prudencio, A.S. Pereira, S. Besson, J.J. Moura, I. Moura, and C. Cambillau, Nature Structural Biology, 2000. **7**(3): p. 191-195.

6. Manganese cryptates and podates for MRI trials

Interest in the development of new and improved contrast agents for MRI has in recent times turned to manganese, which in its high-spin II oxidation state has 5 unpaired electrons, together with a long relaxation time. Although not as paramagnetic as gadolinium (7 unpaired electrons), the lower toxicity and cost of manganese make it worth investigation. In fact, in 1997 FDA approval was given to a manganese contrast agent for clinical use. In this material (marketed as Teslascan by Amersham), manganese is encapsulated by a vitamin B6 analogue, and the complex is preferentially taken up by the liver, leading to applications in the diagnosis of hepatic disorders.

This chapter describes the preparation and characterisation of some candidate manganese(II) cryptates and podates, together with preliminary investigations of their suitability for MRI contrast agents. Development of different hosts for the paramagnetic ion will allow different organs to be targeted, and thus extend the usefulness of the technique.

The desirable characteristics for an MRI contrast agent have been discussed in Chapter 1, but to recap, the complex must have: high paramagnetism, good water solubility and stability at physiological pH (precipitation in the blood stream can cause serious problems), a high relaxivity for associated water (which is normally enhanced if the metal actually coordinates water molecules). It is believed to be necessary that water should be associated with the paramagnetic ion, either by direct coordination or second-shell effects, such as H-bonding to the ligand, for the paramagnetic relaxation to be experienced by target tissue. Associated water should also be in rapid exchange with the bulk solvent.

The solubility issue was addressed by using trifluoromethane sulfonate counterion ($CF_3SO_3^-$, triflate, known for its high solubility) wherever possible. Cryptates are more

likely than podates or chelates to form stable complexes with the paramagnetic ion, however due to the more total encapsulation the guest may not coordinate additional water molecules so easily. Both cryptates and podates were investigated for this reason.

6.1. Preparation of Mn(II) cryptates and podates

6.1.1. Mn(II) amBT

The mononuclear amBT (Figure 6-1 B) cryptate was prepared by reaction of the manganese(II) perchlorate salt with the free ligand in denatured EtOH ((1) details in section 9.5.1), and recrystallised by the slow diffusion of ether into a solution in acetonitrile. The infrared spectrum (Figure 6-2) was consistent with the desired product, showing NH, counterion and cryptate fingerprint bands as expected. The elemental analysis agreement (Table 6-1) was improved by inclusion of half an equivalent of water, which may be indicative of water in the lattice, although the reported crystal structure (1) did not include this in the model.

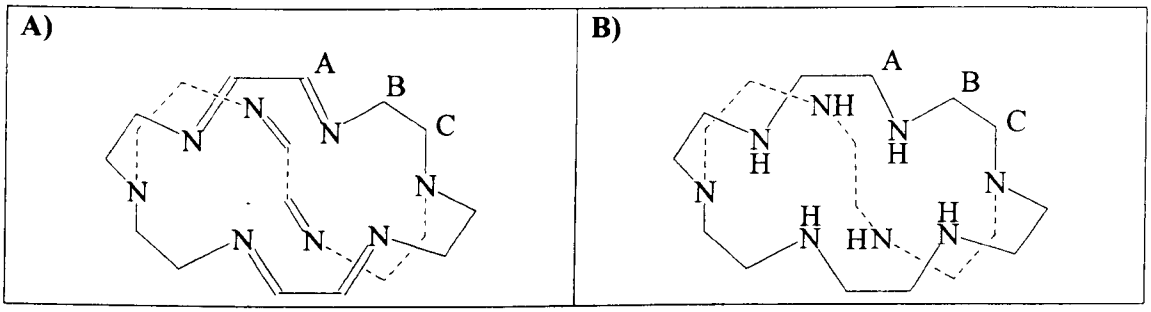

Figure 6-1: The ligands A) imBT and B) amBT which incorporate a two carbon spacer, with a tren-derived cap.

A rough estimate of the water solubility of the cryptate was made by adding a known weight of the solid to 25 ml of water, and mixing thoroughly. The undissolved residue was filtered, dried and weighed. Calculation by difference showed the solubility to be in the order of 0.44 g l^{-1} (0.7 mM).

It was noted during recovery of the sample used for solubility determination that some brown precipitate – possibly MnO_2 – formed when the solution was allowed to concentrate in air. It appears that this basic ligand is mediating oxidation of the guest, which suggests that the stability of the complex may be insufficient for *in vivo* use.

The triflate cryptate was also prepared using a similar method, however this appeared even more susceptible to decomposition, forming a large amount of brown precipitate during the preparative procedure. The elemental analysis (Table 6-2) was again consistent with the

presence of about half an equivalent of water, and the FAB mass spectrum contained peaks related to the cryptate (Table 6-3).

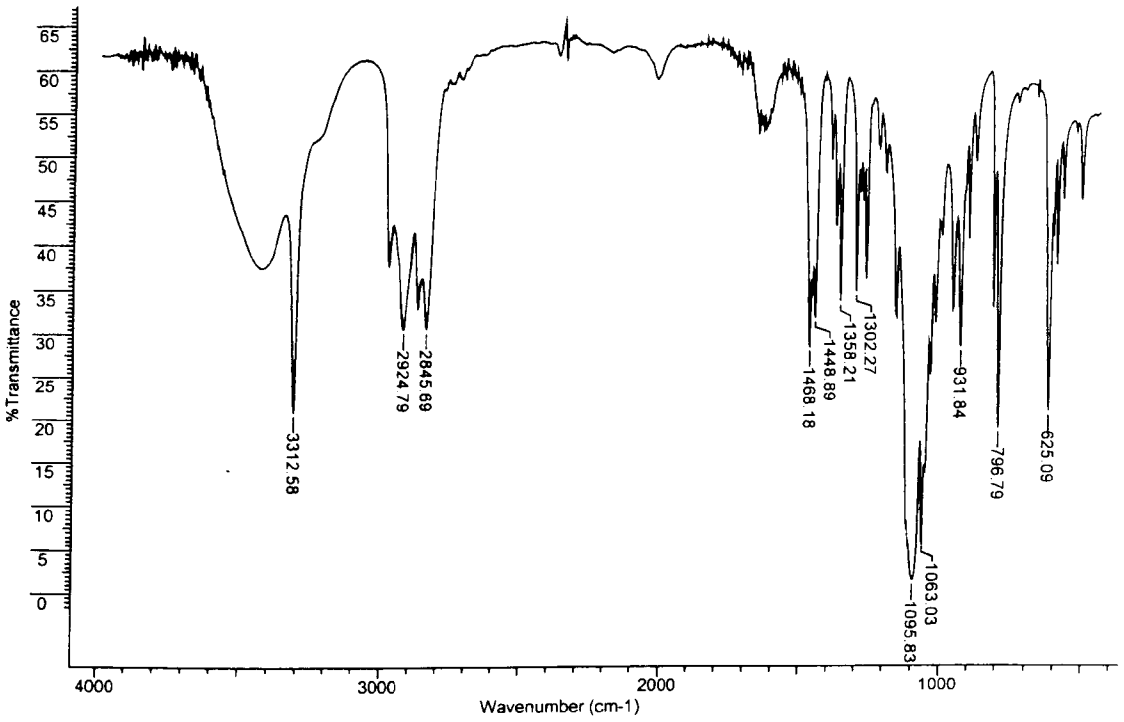

Figure 6-2: Infrared spectrum of the Mn(II) amBT cryptate, showing clear evidence for the presence of ligand (NH at 3313 cm^{-1}, as well as CH stretches and fingerprint region stretches) and counterion (especially the intense 1096 cm^{-1} absorption).

Table 6-1: Elemental analysis of Mn(II) amBT perchlorate.

Analysis	%C	%H	%N
Predicted – $C_{18}H_{42}N_8MnCl_2O_8$	34.62	6.78	17.95
Predicted – $C_{18}H_{42}N_8MnCl_2O_8 \cdot 0.5\ H_20$	**34.13**	**6.84**	**17.69**
Found	34.05	6.84	17.65

Table 6-2: Elemental analysis of Mn(II) amBT triflate.

Analysis	%C	%H	%N
Predicted – $C_{20}H_{42}N_8MnF_6S_2O_6$	33.20	5.85	15.48
Predicted – $C_{20}H_{42}N_8MnF_6S_2O_6 \cdot 0.5\ H_20$	**32.79**	**5.92**	**15.29**
Found	32.85	5.88	14.84

Table 6-3: FAB mass spectrum (EPSRC service) of Mn(II) amBT triflate. A heavy mass peak, m/z 1245 may relate to the proposed 6+4 cryptate (see Chapter 7).

m/z	Abundance /%	Identity	m/z	Abundance /%	Identity
371	8	amBT	724	1.2 %	Mn_2 amBT $(CF_3SO_3)_2$
423	35	Mn amBT	1245	0.2 %	Mn (6+4 amBT) ?? $(CF_3SO_3)_3$ (weak)
573	100	Mn amBT CF_3SO_3			

6.1.2. Mn(II) imBT

A perchlorate complex of imBT (Figure 6-1 A) was prepared by combination of the salt with free ligand in ethanol. Evaporation of an acetonitrile solution overnight yielded large, hexagonal, orange, single crystals which proved suitable for X-ray structure determination (see section 9.5.2). The infrared spectrum (Figure 6-3) was consistent with the desired product, the imine peaks (1675 and/or 1624 cm^{-1}) are sharply defined although of lesser intensity than observed in other complexes of this ligand. Weak peaks around 3300 cm^{-1} are in the region associated with amines, and may be indicative of some opening of the cryptand in this sample, although LCMS analysis of the material used for MRI trials confirmed that it was of high purity.

The elemental analysis (Table 6-4) was also consistent with the desired product, but gave no indication of water content.

The water solubility was estimated as described for manganese(II) amBT above, and determined to be approximately 1.3 g l^{-1}, (2.2 mM).

The analogous triflate cryptate was prepared by substituting a triflate salt for the perchlorate. Elemental analysis was again consistent with the product, (see Table 6-5), and again gave no clear indication for the presence or absence of water. The entire sample used for estimation of water solubility dissolved, showing the aqueous solubility to be at least 11 g l^{-1} (15 mM).

6.1.2.1. Dissociation and stability study

Results from the MRI trials generated concern that significant concentrations of free manganese may have been available in the later samples used. A study of the UV/visible absorption characteristics in the same 60:40 acetonitrile:water mixture was made (neutral pH), experimental details are given in section 9.5.2.1.

The results of this investigation suggest that dissociation is not significant in the short term, however there appears to be slow hydrolysis of the cryptand and cryptate in the 60:40 MeCN:H_2O mixture, an effect previously encountered for other cryptates (2) and suggested for this system (1).

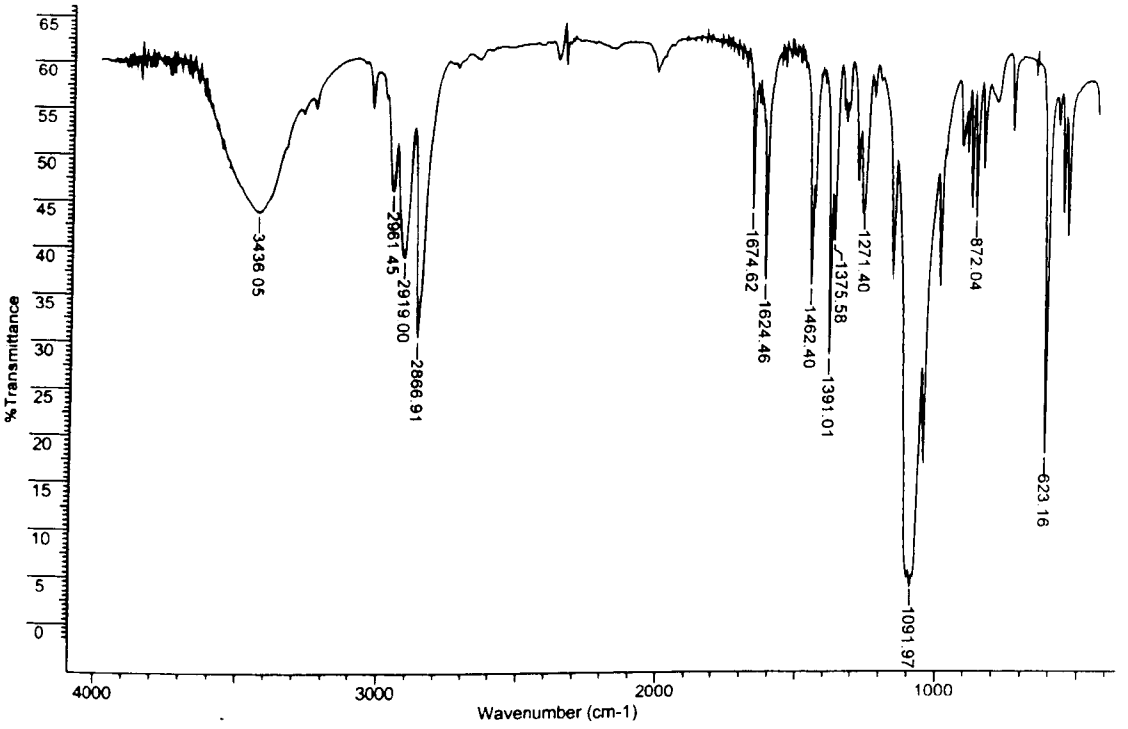

Figure 6-3: Infrared spectrum of Mn(II) imBT cryptate.

Table 6-4: Elemental analysis of Mn(II) imBT perchlorate.

Analysis	%C	%H	%N
Predicted – $C_{18}H_{30}N_8MnCl_2O_8$	35.31	4.94	18.30
Predicted – $C_{18}H_{30}N_8MnCl_2O_8 \cdot 0.5\ H_2O$	34.80	5.03	18.03
Found	35.23	5.07	18.22

Table 6-5: Elemental analysis of Mn(II) imBT triflate.

Analysis	%C	%H	%N
Predicted – $C_{20}H_{30}N_8MnF_6S_2O_6$	33.76	4.25	15.75
Predicted – $C_{20}H_{30}N_8MnF_6S_2O_6 \cdot 0.5\ H_2O$	33.34	4.34	15.55
Found	33.49	4.19	15.67

6.1.2.2. Crystallographic study – perchlorate anion

The formula unit for Mn(II) imBT perchlorate is shown in Figure 6-4 (A), and a thermal ellipsoid plot of the cryptate is shown in Figure 6-4 (B). Full crystallographic details are given in section 9.5.2.2.

Considering the intensity of diffraction exhibited by this sample, it is surprising that the model could not be refined to an R factor much below 10%, and the structure of the same complex with triflate counterion was determined in the hope that it would refine more precisely.

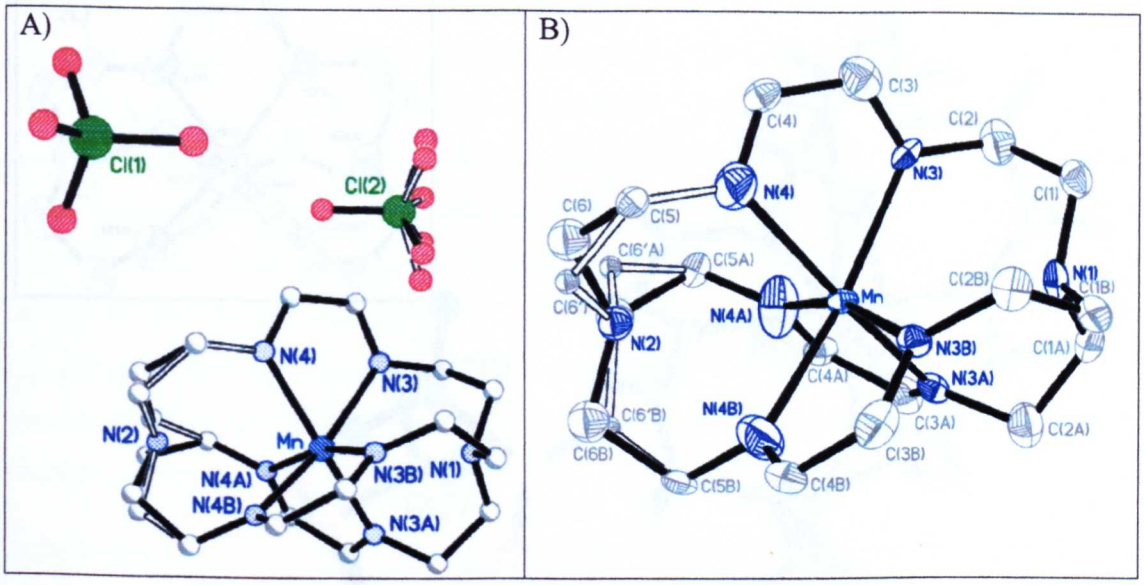

Figure 6-4: Graphical representation of the crystal structure of Mn(II) imBT perchlorate. A) Formula unit, containing one ordered and one disordered perchlorate, and the cryptate with disorder in one end of the cage. B) 40% thermal ellipsoid diagram of the cryptate, distended ellipsoids for N4 and its symmetry equivalents show that this atomic coordinate is not well defined. Space group P6(3), cell dimensions a = 9.0593(6) Å, b = 9.0593(6) Å, c = 17.8254(16) Å, R=0.0971.

6.1.2.3. Crystallographic study – triflate anion

The formula unit for Mn(II) imBT triflate is shown in Figure 6-5, full crystallographic details are given in section 9.5.2.3. Despite being fully encapsulated by the cryptand, the manganese ion is still relatively easily accessible by, for instance, water molecules (see Figure 6-5 B). Although no water molecules were located in the structure, this does not rule out the possibility of diffuse water in the lattice, and this may even be responsible for the somewhat poor R factors obtained for these strongly diffracting crystals.

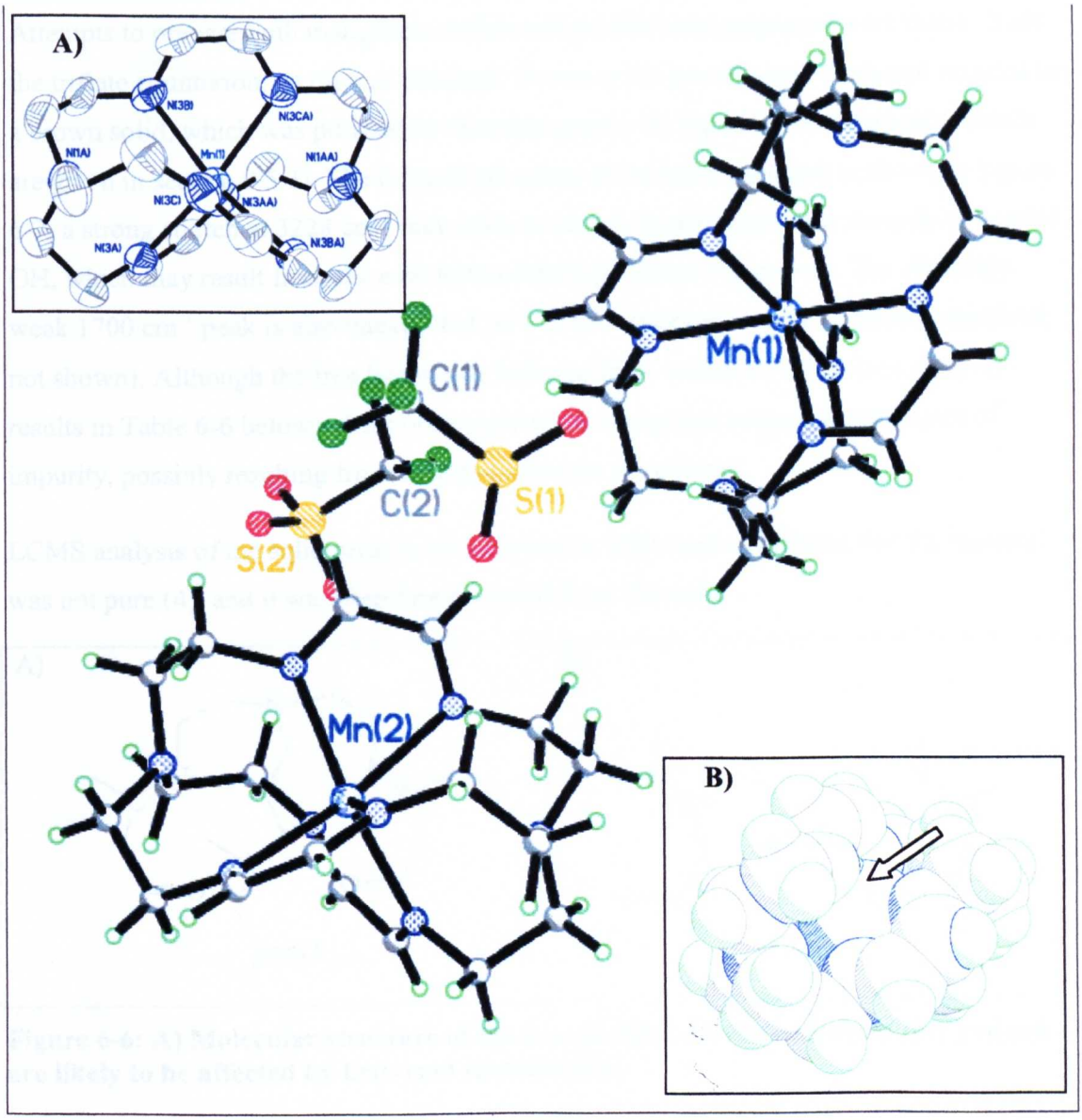

Figure 6-5: Graphical representation of the crystal structure of Mn(II) imBT triflate (Mn(II) imBT triflate). The unit cell contains two cryptate molecules, and four triflate anions (two symmetry equivalents not shown). Inset A) 40% thermal ellipsoid diagram of one cryptate molecule, and B) a space filling diagram of the same molecule showing that despite its octahedral coordination sphere, the manganese is still accessible by the external environment. Space group p2/c, cell parameters a = 18.3987(12) Å, b = 9.1306(6) Å, c = 20.3105(18) Å, β= 117.3190(10)°, R=0.0807.

6.1.3. Mn(II) trac

Trac was prepared according to literature methods (3), and elemental analysis (Table 6-6) of the product suggested that this dense oil was partially hydrated, most likely with between 1 and 2 equivalents of water.

Attempts to prepare both manganese triflate and perchlorate complexes were made. With the triflate counterion, an oil was obtained. However the perchlorate counterion resulted in a brown solid, which was purified by chromatography on sephadex (experimental details are given in section 9.5.3). The infrared spectrum of the brown product is shown in Figure 6-7, a strong stretch at 3228 cm^{-1} may relate to amine, or alternatively a strongly H-bonded OH, which may result from the enol form of the ligand (see Figure 6-6). The relatively weak 1700 cm^{-1} peak is also unexpected, as it is not observed in the free ligand (spectrum not shown). Although the free ligand was believed to be reasonably pure (see analysis results in Table 6-6 below), these observations taken together suggest some degree of impurity, possibly resulting from decomposition on the column.

LCMS analysis of the solid prior to its inclusion in MRI trials confirmed that the material was not pure (4), and it was therefore excluded from the trials.

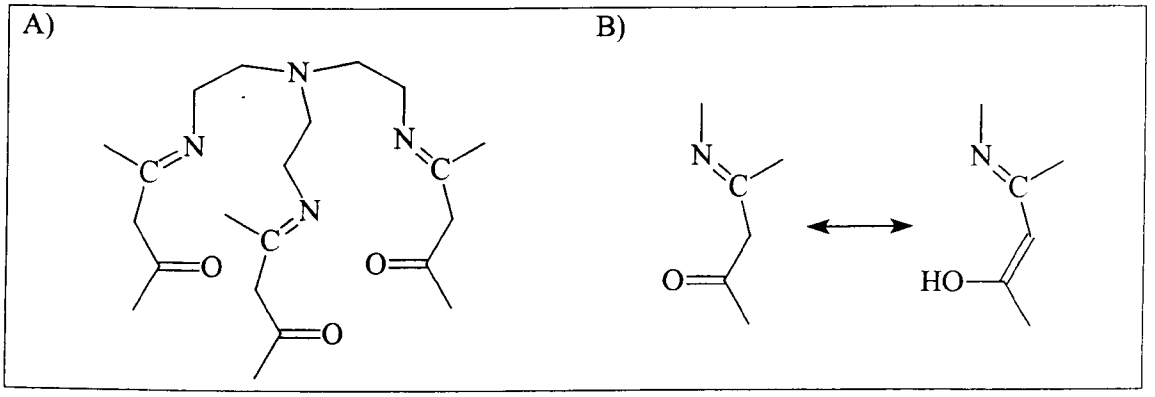

Figure 6-6: A) Molecular structure of the trac podand, B) the strands of this podand are likely to be affected by keto-enol tautomerism.

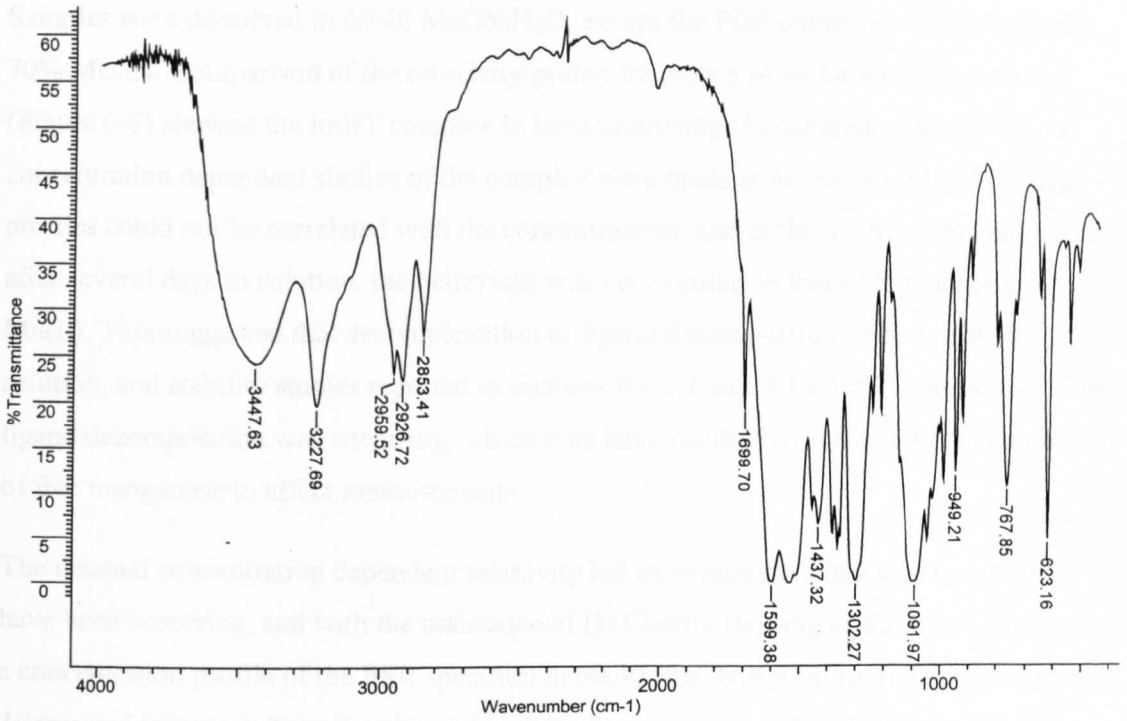

Figure 6-7: Infrared spectrum of manganese(II) trac complex after chromatographic cleanup.

Table 6-6: Elemental analysis of the free trac ligand.

Analysis	%C	%H	%N
Predicted – $C_{21}H_{36}N_4O_3$	64.26	9.24	14.27
Predicted – $C_{21}H_{36}N_4O_3 \cdot 1.2\ H_2O$	60.90	9.35	13.53
Found	60.63	8.97	13.55

6.1.4. Mn(II) PGP triflate

The phenyl substituted podand described in Chapter 4 (here denoted as PGP) was used to prepare a Mn(II) complex. The preparation of both the free ligand and the podate are described in section 4.1.2.1.

Whilst LCMS analysis showed that this material was not pure (4), it was nevertheless included in the trials.

6.2. *Results of MRI trials*

Dr Annie Bligh of the University of North London carried out studies on the two cryptates and a (poorly characterised) podate (Mn(II) PGP triflate).

Samples were dissolved in 60:40 MeCN:H_2O, except the PGP complex which required 70% MeCN. Comparison of the relaxivity/proton frequency plots for the three species (Figure 6-8) showed the imBT complex to have promising characteristics for MRI, and concentration dependent studies of the complex were made at 40 mM to 0.1 mM. These profiles could not be correlated with the concentrations, and at the 0.1 mM concentration after several days in solution, the behaviour was very similar to that of free aqueous Mn(II). This suggested that decomplexation or ligand decomposition is occurring in solution, and stability studies reported in sections 6.1.2.1 and 9.5.2.1 did suggest that slow ligand decomposition was occurring, which may have resulted in sufficient concentrations of free manganese to affect measurements.

The unusual concentration dependent relaxivity led us to speculate that aggregation may have been occurring, and with the assistance of Dr Charlie Harding of the Open University, a concentration profile of the ESR spectrum in 60:40 MeCN:H_2O at room temperature was determined (Figure 6-9), and compared to that of a manganese salt (Mn(II) nitrate, data not shown) under the same conditions.

The salt revealed the 6 line pattern expected for high spin Mn(II) at concentrations from 0.1 mM up to 100 mM, with hyperfine components of 30-35 G, showing that over this range there is no internuclear interaction. At 500 mM there was perceptible line broadening, indicating that some internuclear interaction was beginning to occur.

For the cryptate (Figure 6-9), the line width of each component is 50 to 60 G, and additional components of the fine structure are apparent at the 0.1mM and 1 mM concentrations. These could be caused by forbidden transitions (5) or be the result of the non-octahedral manganese site in this molecule, in contrast to the symmetric octahedral site for hydrated Mn(II) nitrate. At 10mM, the lines have broadened, and the spectrum takes the form of a simple 6-line pattern. This loss of fine structure suggests that internuclear interaction is beginning to occur, possibly via a perturbation of the coordination sphere of the manganese ion. It is impossible to state whether the onset of this interaction occurs at a lower concentration than for the hydrated ion, since the hydrated ion did not display the additional fine structure.

However, the observation of this magnetic interaction leads us to speculate that it may be involved with the surprising enhancement of relaxivity observed for the Mn(II) imBT cryptate.

Determination of the magnetic susceptibility for Mn(II) imBT with both perchlorate and triflate counterion was performed (Table 6-7) and showed that both solids exist as high spin d^5 at ambient and low temperature. A better fit to theoretical values was observed when one equivalent of water was included in the calculation for Mn(II) imBT triflate, suggesting that the bulk sample may be a hydrate. Despite further investigation of the crystal structure refinement, and the application of tools for modelling diffuse solvent (Platon (6) and SWAT (7)) no water molecules could be located, and allowance for diffuse solvent gave no improvement in the refinement of the model. The presence of water in the crystal therefore remains unproven.

The – superficially simple – Mn(II) imBT cryptate clearly has a complex behaviour in solution, however it is the apparently poor stability of the compound over time which is the single greatest barrier to its use as a MRI contrast agent. The enhanced relaxivity of the iminocryptate over the amino analogue is surprising, given amBT's superior hydrogen bonding ability, its known lability, and its ability to undergo exchange with water (8).

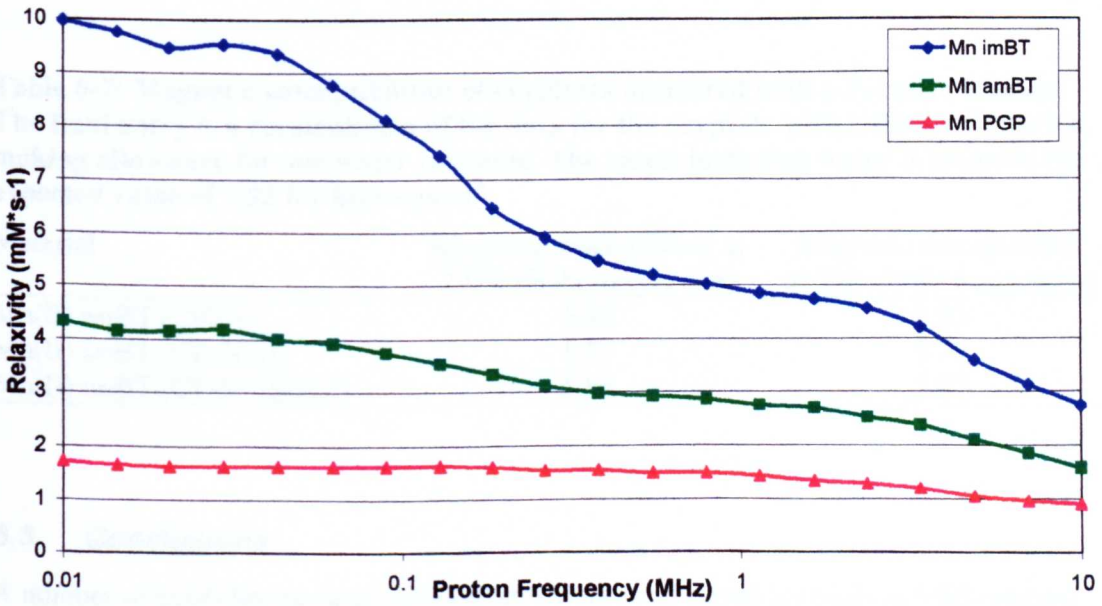

Figure 6-8: Plot of relaxivity vs proton frequency for the imBT and amBT cryptates, and the PGP podate.

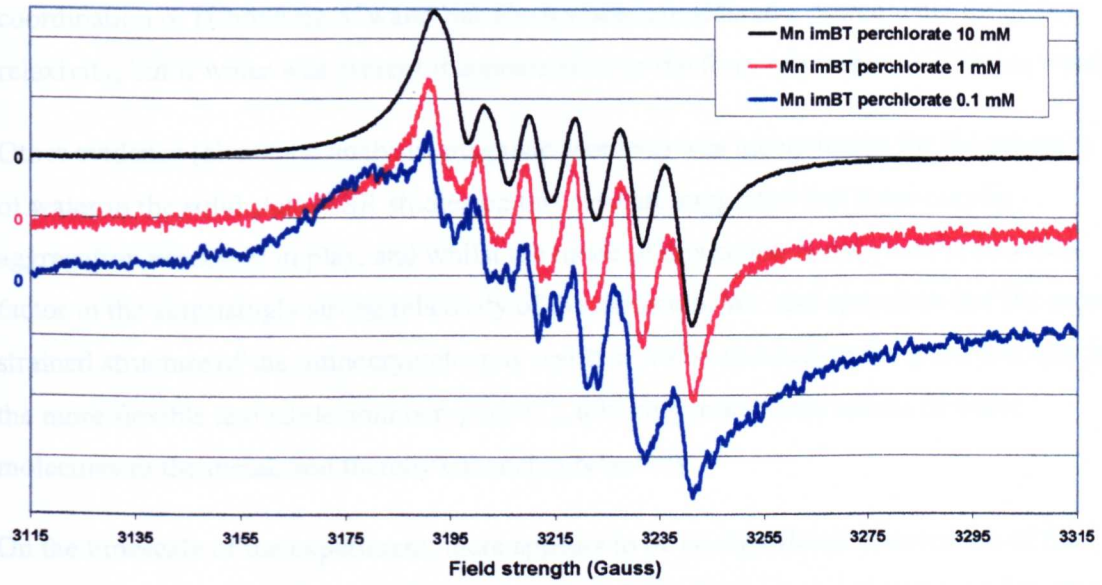

Figure 6-9: Concentration profile of the ESR spectrum of Mn(II) imBT perchlorate (60:40 MeCN:H_2O, recorded at ambient T in a flat cell). The three spectra have been offset on the vertical axis for clarity.

Table 6-7: Magnetic susceptibilities of cryptates measured with a Faraday balance. The final entry is a recalculation of the data for the cryptate with triflate counterion, making allowance for one water molecule. The result including water is closer to the expected value of 5.92 for high spin d^5.

Material	Magnetic susceptibility at 295K (Bohr magnetons)	Magnetic susceptibility at 80K (Bohr magnetons)
Mn(II) imBT $(ClO_4)_2$	5.92	5.92
Mn(II) imBT $(CF_3SO_3)_2$	5.77	5.79
Mn(II) imBT $(CF_3SO_3)_2 \cdot H_2O$	5.85	5.87

6.3. Conclusions

A number of candidate podates and cryptates were synthesised for trials as MRI contrast agents. Unfortunately they could not all be supplied in a pure form within the available time, however two cryptates and one podate were eventually used in relaxivity experiments.

The podate proved to be a weak relaxer, and the aminocryptate (expected to be more favourable in terms of H-bonding, and interaction with water) only showed moderate relaxivity, with the iminocryptate proving to have a very strong relaxivity, making it an attractive candidate for further studies. This finding is extremely interesting, as

coordination or H-bonding of water has always been considered a prerequisite for strong relaxivity, but if water was present it appears to be in the form of weakly held lattice water.

Other evidence (elemental analysis, magnetic moment) was inconclusive for the presence of water in the solid state. ESR studies on this cryptate suggested that there may be aggregation processes in play, and whilst the mode of this action is not clear, it may be a factor in the surprisingly strong relaxivity of the molecule. We also speculate that the more strained structure of the iminocryptate may result in wider channels to the guest ion than in the more flexible and labile aminocryptate (1), allowing more facile access of water molecules to the metal, and thereby enhancing relaxivity.

On the timescale of the experiment, there appears to be no significant dissociation of the cryptate, however slow decomposition of the ligand may become significant over longer periods of time. For a material to be used *in vivo*, stability is a critical parameter as decomplexation can lead to serious side effects such as precipitation within the tissue. The relative rates of clearance from the body, and decomposition of the cryptate would therefore be of importance in this case.

Whilst this particular cryptate may therefore be unsuitable as a MRI contrast agent, these studies have confirmed the viability of manganese(II) for this use, even where the Mn(II) ion has 6 strong donors and no 1^{st} or 2^{nd} sphere site for water. This brings into question the need for stable coordinated water in the complex, an attribute which has previously been considered necessary to achieve the degree of relaxivity to be useful for MRI. It appears sufficient to provide a conformation open enough to permit access of water molecules to the metal cation in solution.

6.4. References

1. Coyle, J.L., M.G.B. Drew, C.J. Harding, J. Nelson, and R.M. Town, Journal of the Chemical Society, Dalton Transactions, 1997: p. 1123-1125.

2. Harding, C.J., Q. Lu, J.F. Malone, D.J. Marrs, N. Martin, V. Mckee, and J. Nelson, Journal of the Chemical Society-Dalton Transactions, 1995(10): p. 1739-1747.

3. Smith, A., S.J. Rettig, and C. Orvig, Inorganic Chemistry, 1988. **27**: p. 3929-3934.

4. Bligh, A., Personal Communication, 2002.

5. Goodman, B. and J. Raynor, *ESR of transition metal complexes*, in *Advances in Inorganic Chemistry and Radiochemistry*. 1970. p. 200-221.

6. Spek, A.L., *PLATON, A Multipurpose Crystallographic Tool* 1998: Utrecht University Utrecht, The Netherlands.

7. Sheldrick, G.M., *SHELX97 [Includes SHELXS97, SHELXL97, CIFTAB (and SHELXA)] - Programs for Crystal Structure Analysis* 97-2. 1998: Institüt für Anorganische Chemie der Universität, Tammanstrasse 4, D-3400 Göttingen, Germany.

8. DeSantis, G., L. Fabbrizzi, A. Perotti, N. Sardone, and A. Taglietti, Inorganic Chemistry, 1997. **36**: p. 1998-2003.

7. 6+4 Macrobicycles for tetranuclear cryptates

Preparation of cryptand ligands via the Schiff base coupling of "cap" and "spacer" units can have a number of outcomes, including polymerisation, intramolecular ring closure, as well as formation of higher oligomers. Scheme 7-1 outlines possible outcomes for the combination of tripodal caps with dialdehyde linker units being studied in this work.

The preparation of imBT described by (1) is an excellent example of the use of dilution, solvent, temperature, addition and stirring rates to influence the outcome of such a reaction. Nevertheless, a soxhlet extraction is required in the final stage to remove the desired ligand from the mass of polymer which also forms. It seems reasonable that if the reaction mixture contains the 3 spacer/2 cap addition compound (denoted "3+2 cryptand") together with larger polymeric structures, then it may also contain intermediate sized oligomers, such as the 6 spacer/4 cap compounds ("6+4 cryptands") suggested in Scheme 7-1. FAB MS analysis of imBT cryptates (see section 7.1) has on occasion shown mass peaks consistent with these heavier cryptands, and this section describes attempts to study and isolate these, potentially very interesting and useful, cryptands.

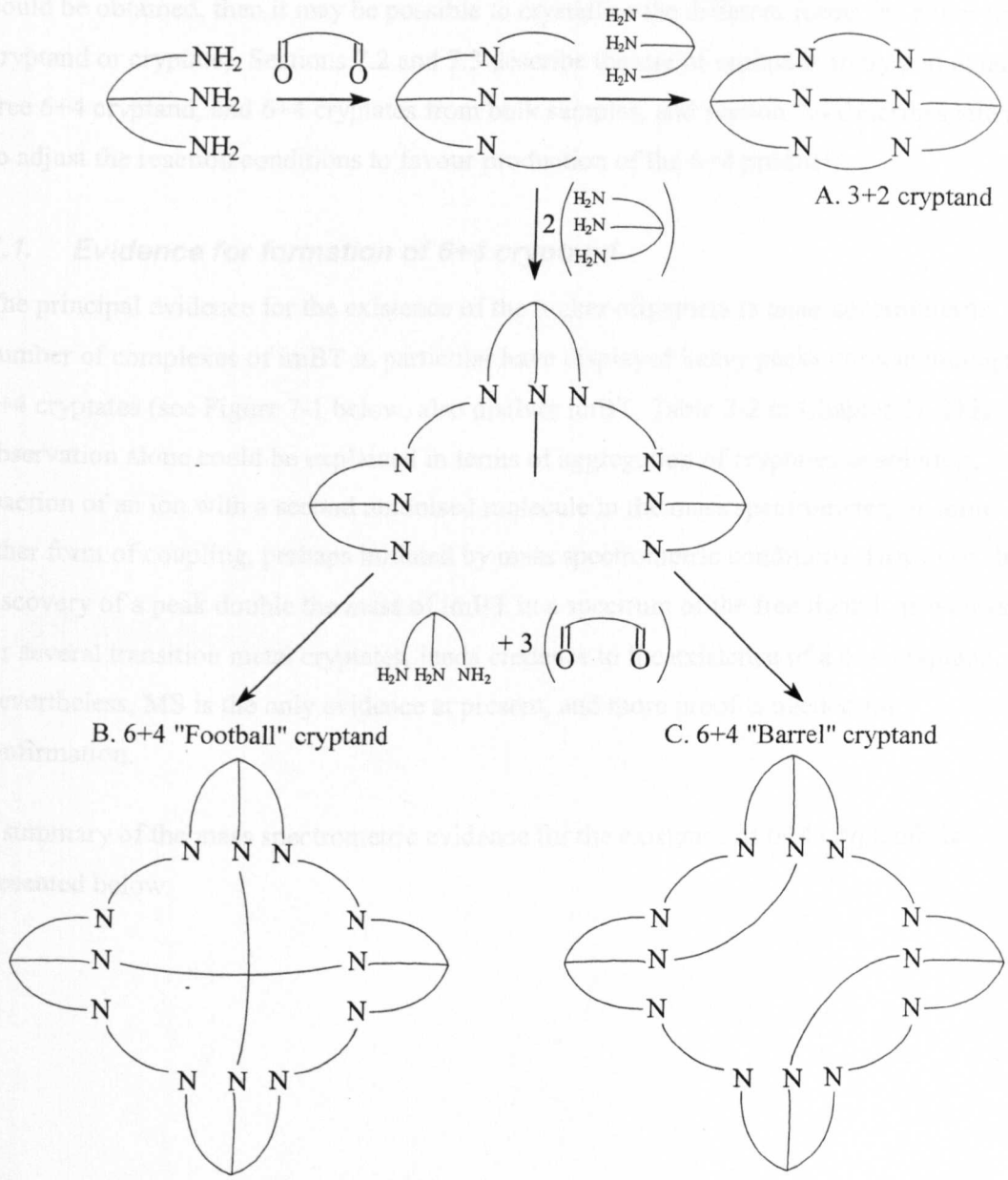

Scheme 7-1: Schiff base condensation of a tripodal amine with dialdehyde can result in a range of products ranging from polymers and incompletely closed crypts (see also Scheme 4-1) to (A) 3+2 closed crypts and (B, C) 6+4 "footballs" and "barrels".

From the similar chemical nature of the 3+2 and 6+4 cryptands, it is perhaps not surprising that they display similar solubilities (as evidenced by their presence in the soxhlet extract, and their persistence throughout cryptate preparative procedures). The larger size of the 6+4 cryptands will render them less volatile. However their mass is too great for gas chromatographic separation. Thin layer chromatography on silica could not resolve separate spots, however size exclusion chromatography is more suited to this situation and investigations were made using this medium. If a sample enriched in the higher oligomer

could be obtained, then it may be possible to crystallise the different forms (as either free cryptand or cryptate). Sections 7.2 and 7.3 describe the use of sephadex to try and obtain free 6+4 cryptand, and 6+4 cryptates from bulk samples, and section 7.4 describes attempts to adjust the reaction conditions to favour production of the 6+4 product.

7.1. Evidence for formation of 6+4 cryptand

The principal evidence for the existence of the higher oligomers is mass spectrometric. A number of complexes of imBT in particular have displayed heavy peaks corresponding to 6+4 cryptates (see Figure 7-1 below, also disilver imBT, Table 2-2 in Chapter 2). This observation alone could be explained in terms of aggregation of cryptates in solution, reaction of an ion with a second unionised molecule in the mass spectrometer, or some other form of coupling, perhaps initiated by mass spectrometric conditions. However, the discovery of a peak double the mass of imBT in a spectrum of the free ligand, as well as for several transition metal cryptates, lends credence to the existence of a 6+4 cryptand. Nevertheless, MS is the only evidence at present, and more proof is needed for confirmation.

A summary of the mass spectrometric evidence for the existence of 6+4 cryptands is presented below.

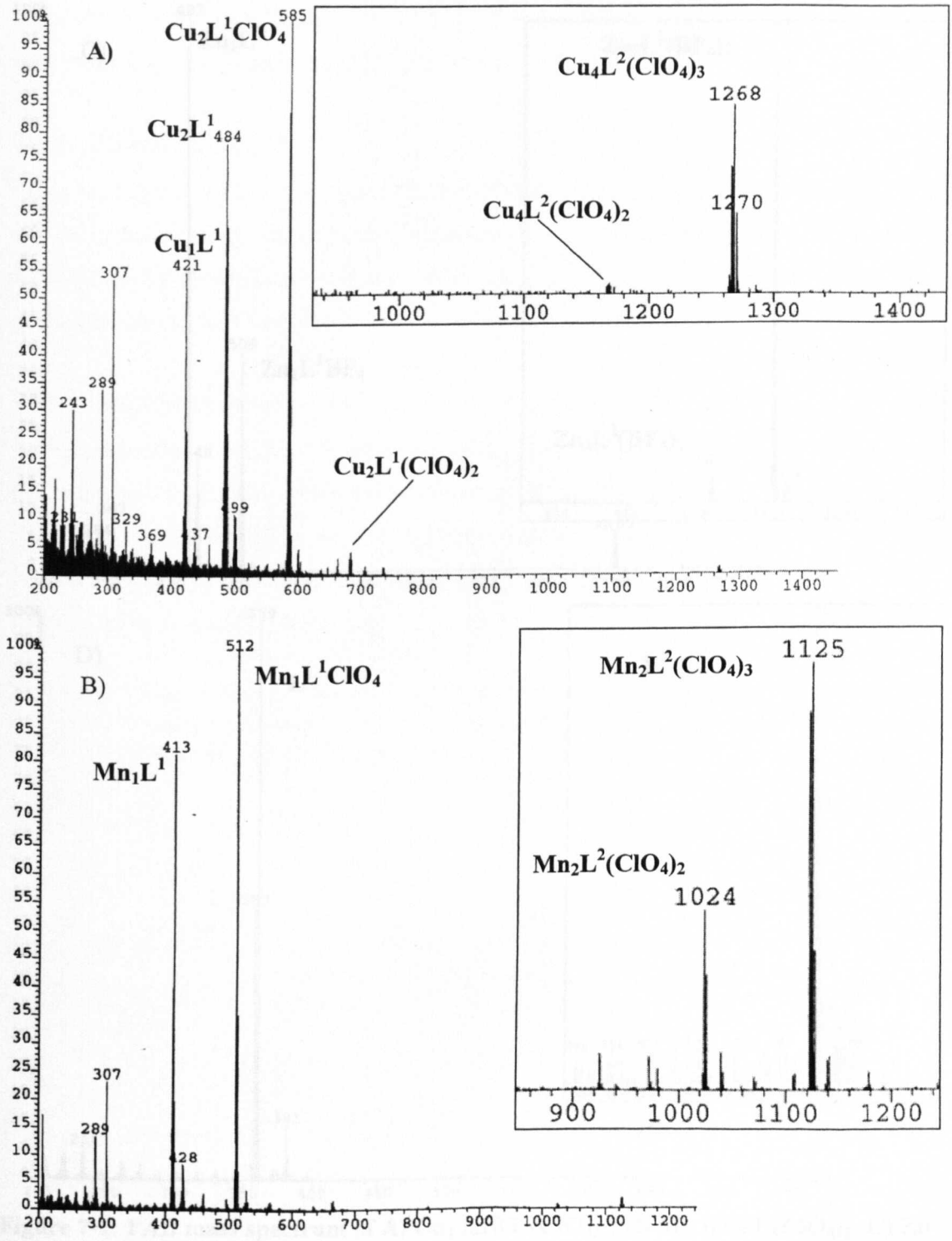

Figure 7-1: continued over page

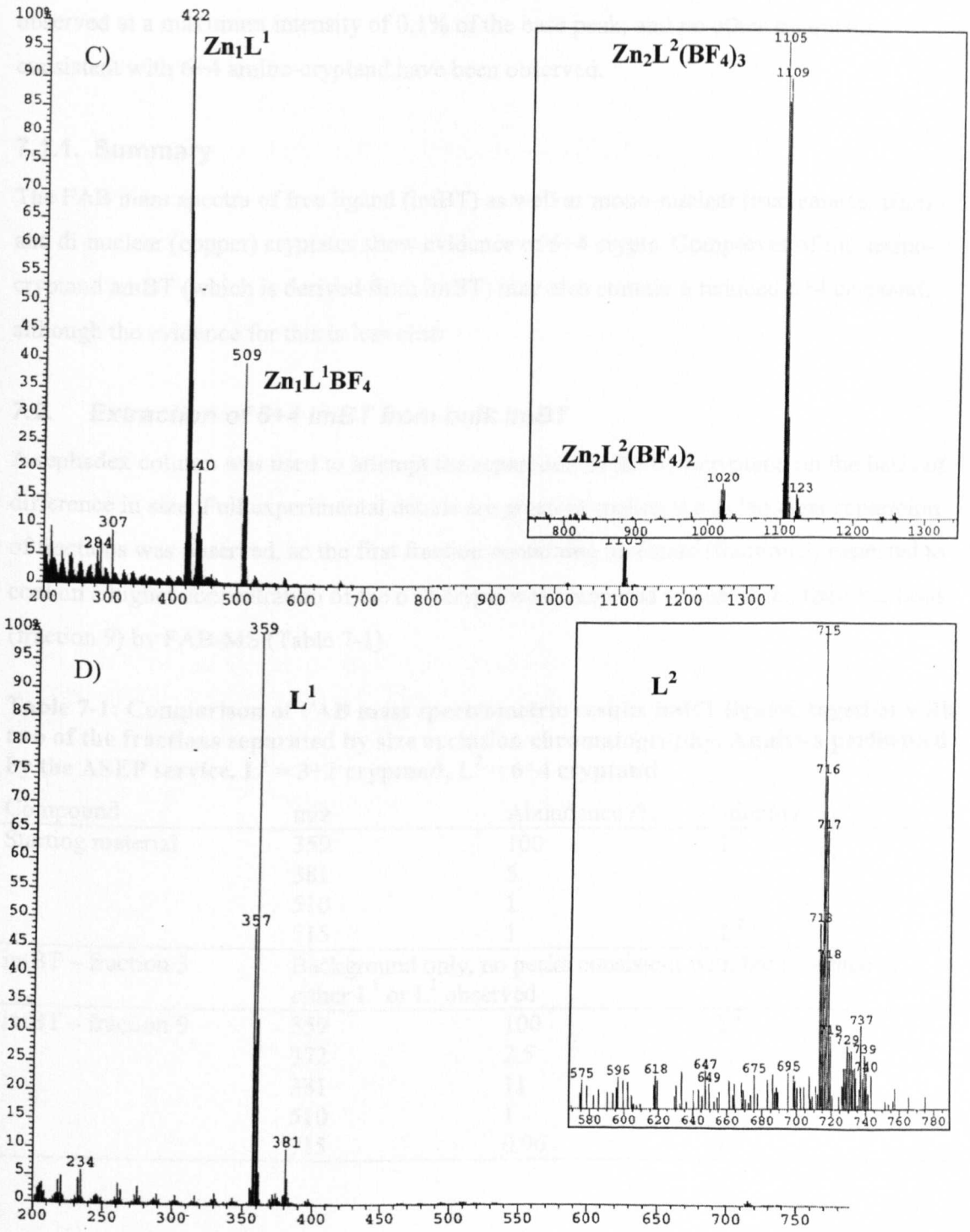

Figure 7-1: FAB mass spectrum of A) Cu_2 imBT $(ClO_4)_2$; B) Mn imBT $(ClO_4)_2$; C) Zn imBT $(BF_4)_2$; D) imBT ligand. Inset figures show enlargements of the heavier mass regions. All analyses performed by the ASEP MS service. Legend: L^1 3+2 cryptand, L^2 6+4 cryptand.

Cryptates of the amBT ligand (which is prepared by reduction of free imBT) have also on occasion shown a peak consistent with a 6+4 amino-cryptand (L^3). A peak at m/z 1105 has been observed in samples of Ag_2 amBT triflate analysed by both the EPSRC and ASEP services. This peak could be explained as Ag_2 L^3 CF_3SO_3, however it has only been

observed at a maximum intensity of 0.1% of the base peak, and no other fragments consistent with 6+4 amino-cryptand have been observed.

7.1.1. Summary

The FAB mass spectra of free ligand (imBT) as well as mono-nuclear (manganese, zinc) and di-nuclear (copper) cryptates show evidence of 6+4 crypts. Complexes of the amino-cryptand amBT (which is derived from imBT) may also contain a reduced 6+4 cryptand, although the evidence for this is less clear.

7.2. *Extraction of 6+4 imBT from bulk imBT*

A sephadex column was used to attempt the separation of the 6+4 cryptand on the basis of difference in size. Full experimental details are given in section 9.6.1. No clear separation of fractions was observed, so the first fraction containing an eluate (fraction 3, expected to contain a higher concentration of the 6+4 crypt) was compared to one of the final fractions (fraction 9) by FAB-MS (Table 7-1).

Table 7-1: Comparison of FAB mass spectrometric results imBT ligand, together with two of the fractions separated by size exclusion chromatography. Analysis performed by the ASEP service. L^1 = 3+2 cryptand, L^2 = 6+4 cryptand

Compound	m/z	Abundance /%	Identity
Starting material	359	100	L^1
	381	5	
	510	1	
	715	1	L^2
imBT – fraction 3	Background only, no peaks consistent with the presence of either L^1 or L^2 observed		
imBT – fraction 9	359	100	L^1
	372	2.5	
	381	11	
	510	1	
	715	0.96	L^2

7.2.1. Summary

The initial fraction obtained by size exclusion chromatography contained insufficient material to give a mass spectrum. In one of the final fractions (fraction 9), FAB MS showed both 6+4 and 3+2 cryptand to be present. The 6+4 molecular ion having approximately 1% of the abundance of the 3+2 molecular ion – similar to the starting material. The presence of both ligands towards the end of the elution, and in similar ratios

as before the procedure, suggests that no significant separation has occurred, and so the intermediate fractions were not analysed.

7.3. Extraction of 6+4 imBT cryptate from bulk cryptate

Samples of zinc(II) cryptate whose FAB mass spectrum showed peaks consistent with 6+4 cryptate, and dicopper(I) cryptate prepared as described in section 7.4.1 were run on a size exclusion chromatography column containing 50 g of sephadex G50, cleaned according to the regime described in section 9.6.1, and soaked in acetonitrile before loading the column.

7.3.1. Separation of Zinc(II) cryptate

The yellow mono-zinc(II) cryptate was run through a sephadex column using acetonitrile as the mobile phase. Two main fractions were collected: the first comprised all of the eluent before the main coloured band, and the second fraction comprised the bulk of the broad yellow band of cryptate.

Table 7-2: Comparison of the FAB mass spectra (EPSRC service) of the initial fractions eluted from the column. The first sample gave a weak spectrum, with many peaks only slightly above background level. L^1 = 3+2 cryptand, L^2 = 6+4 cryptand.

m/z	Abundance /%	Identity	m/z	Abundance /%	Identity
Zn(II) imBT $(ClO_4)_2$, 1st fraction – note poor resolution from background					
413	78.6 %		1048	6.9 %	$Zn_2L^2(ClO_4)_2$
424	45.2 %	ZnL^1	1114	6.7 %	$L^2(ClO_4)_4$
515	100.0 %		1146	5.5 %	$Zn_2L^2(ClO_4)_3$
647	23.8 %		1179	5.0 %	$ZnL^2(ClO_4)_4$
680	23.8 %		1191	5.5 %	
719	23.8 %	L^2	1213	5.7 %	
758	23.8 %		1240	6.7 %	
816	7.6 %	L^2ClO_4	1248	6.2 %	$Zn_2L^2(ClO_4)_4$
845	8.1 %	Zn_2L^2	1262	5.5 %	
873	7.9 %		1276	5.5 %	
952	6.7 %		1301	4.5 %	
986	5.5 %	$ZnL^2(ClO_4)_2$	1360	4.3 %	
1002	11.9 %		1392	3.8 %	
1011	5.5 %		1422	3.8 %	
1039	6.4 %	$L^2(ClO_4)_3$	1458	3.6 %	
Zn(II) imBT $(ClO_4)_2$, 2nd fraction					
422	100.0 %	ZnL^1	766	22.7 %	
458	13.6 %	L^1ClO_4	902	11.4 %	
522	22.7 %	ZnL^1ClO_4	920	13.6 %	
557	11.4 %	$L^1(ClO_4)_2$	958	9.1 %	
623	11.4 %	$ZnL^1(ClO_4)_2$	1154	9.1 %	
749	13.6 %				

Several attempts were made to crystallise the first fraction with no success. The mass spectrum was weak, and although peaks consistent with the 6+4 cryptand are present, they are only slightly stronger than the average background. The peak diagnostic for 6+4 cryptand seen in greatest intensity in the starting material (molecular ion less one counterion, m/z 1146 in this case) did not stand out in the eluted fraction, and the base ions were also different in each fraction, making the identity of the product less certain. The 2nd fraction however gave a good spectrum consistent with only 3+2 cryptand, which tends to suggest that the heavier cryptate has indeed eluted earlier, and also that the observation of a m/2 peak for the 6+4 compound is not an artefact of the MS technique.

7.3.2. Separation of dicopper(I) cryptate

A sample of dicopper(I) imBT perchlorate was prepared from the same sample of ligand used for the investigation of zinc above. A similar chromatographic separation was performed using acetonitrile eluent, however smaller fractions were collected this time. The first product fraction collected yielded X-rayable crystals, which were determined to have the same unit cell as $Cu(I)_2$ imBT $(ClO_4)_2$, and a full dataset was therefore not collected.

Mass spectrometry (ASEP service) confirmed the absence of 6+4 cryptand peaks from both the earliest and latest product fractions, however it also showed that the starting material contained no 6+4 cryptand. It is possible that the heavier cryptate was lost during preparation of the starting material.

7.3.3. Summary

There is tentative evidence that separation of zinc cryptate has enriched the 6+4 cryptate content of the material, however it has proven impossible to verify this by an independent method.

The copper(I) cryptate used for size exclusion chromatography was later determined to contain no 6+4 crypt in the starting material, even though the free ligand used to prepare the cryptate was known to contain 6+4 cryptand. Whilst this was disappointing, the lack of observed 6+4 cryptand peaks in this particular sample helped to convince us that the heavy peaks being observed in other samples were not simply artefacts of the mass spectrometer.

7.4. Direct preparation of 6+4 cryptand

Bharadwaj (2) describes the influence of temperature, solvent, and concentration on the formation of 1+1 versus 2+2 cryptates in a tripodal coupling reaction (trialdehyde with triamine). In his case, formation of the small cage is favoured by lower temperature (which he believes is due to slower movement of tripod arms, and reduced chance of polymerisation), and lower concentration (less chance of polymerisation). The solvent used also has a marked affect on the reaction outcome, however the relationship between solvent and reaction result is not simple.

We believe that imBT prepared via the method of Smith (1) contains 6+4 cryptand as a minor impurity, and several variations on the reaction were made in an attempt to increase the yield of the larger cryptand.

- use of a different solvent in place of isopropanol (other conditions the same)
- use of a preformed trialdehyde (see Scheme 7-1, obtained by adding a low concentration of tren to a high concentration of glyoxal to encourage the formation of a trialdehyde) followed by further addition of tren.

These two strategies are discussed in detail in sections 7.4.1 and 0.

7.4.1. Influence of solvent on 6+4 addition

The imBT preparation reported by Smith (1) was performed using methanol in place of isopropanol, with reaction conditions otherwise the same. The reaction appeared to proceed in a similar manner as for isopropanol, and the yield obtained from the final soxhlet extraction was similar (35%) to that usually obtained with isopropanol.

Table 7-3: Elemental analysis results for imBT prepared using methanol solvent.

Analysis	%C	%H	%N
Predicted: imBT	60.31	8.43	31.26
Predicted: imBT.H_2O	57.42	8.57	29.76
Found:	59.12	8.58	29.97

The elemental analysis (Table 7-3) was close to theory values, and was consistent with the presence of less than one equivalent of water.

FAB MS of the product (Table 7-4) resulted in a base peak corresponding to the molecular ion of the 3+2 crypt, however a molecular ion for the 6+4 crypt was also present, although at only 0.3% abundance – less than that observed for cryptand prepared in isopropanol (about 1%, see section 7.2)

Table 7-4: FAB MS results for imBT prepared using methanol solvent (ASEP service). L^1 = 3+2 cryptand, L^2 = 6+4 cryptand

m/z	Abundance /%	Identity	m/z	Abundance /%	Identity
359	100	L^1	510	1	
371	3		620	0.3	
381	9	Na L^1	648	0.2	
465	4		663	0.2	
478	4		716	0.3	L^2

7.4.2. 6+4 "barrel" preparation via trialdehyde

Reaction conditions were adjusted to encourage the formation of a trialdehyde, which was then added to more triamine, in an attempt to encourage the formation of larger crypts and discourage the stepwise formation of the smaller 3+2 crypt (see Scheme 7-2). We proposed that the longer strands of the trialdehyde would disfavour reaction with one equivalent of tetraamine, and favour formation of larger compounds. By performing the reaction at a higher temperature (room temperature, instead of 0°C) we inferred that the temperature effect proposed by Bharadwaj (2) would also favour the larger products. It is also anticipated that a much larger amount of polymer will be formed via this procedure. Experimental details are given in section 9.6.2, and include the attempted preformation of trialdehyde, which was then divided into two fractions and reacted with further tetramine under both high and low dilution conditions, yielding soluble and insoluble fractions (which were soxhlet extracted).

The four samples obtained were submitted for FAB mass spectrometric analysis (Table 7-5). The material obtained from extraction of the insoluble polymer (samples A1 and B1) were poorly soluble, no spectrum was detected at all for B1, however A1 contained a strong peak consistent with the 3+2 cryptand, but no sign of 6+4 cryptand. Both of the chloroform soluble fractions (A2 and B2) showed peaks consistent with formation of the 6+4 cryptand, however the relative intensity of these was no greater than that observed in samples of imBT prepared by the method of (1).

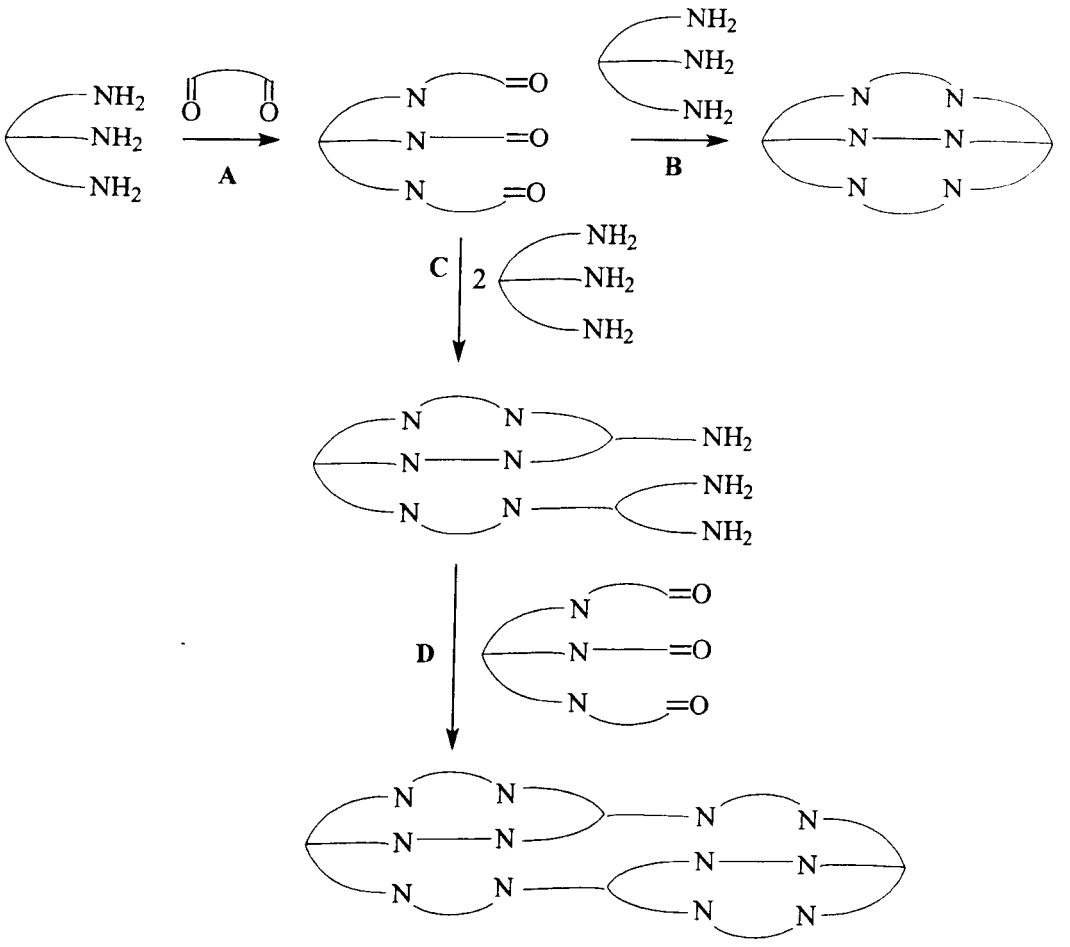

Scheme 7-2: Outline of a modified reaction scheme to favour the formation of 6+4 cryptand. A) Addition of tren to a concentrated solution of glyoxal should encourage formation of a trialdehyde intermediate, which when added to a solution of tetraamine could react B) with one equivalent of tetraamine to form a normal 3+2 cryptand, or C) with two equivalents to form a 6+4 – or larger – product.

The cryptands A2 and B2 were also used to prepare dicopper(I) cryptates via literature methods (3) (Table 7-6), and the mass spectra of both showed evidence of 6+4 cryptates. For A2 the relative intensity (1% for the m/z 1268 ion corresponding to 6+4 cryptate – ClO_4) was similar, or slightly less than that observed in other dicopper imBT cryptates (*e.g.* Figure 7-1 A, approx 1.4%), however for B2 it was present at 2.2% abundance. This increase in abundance of the 6+4 cryptate ion using ligand B2 may be evidence of a greater concentration of the 6+4 cryptand in this ligand sample, although we note that slight variations in peak intensities in other cryptates have been observed on different occasions.

The possibility of changing the 6+4 ligand concentration during complexation also exists. For example, in the presence of a lewis acidic ion, hydrolysis and reformation of the imine bond may be promoted, which could lead to an increase in the 6+4 ligand concentration especially if excess amine and/or aldehyde was present.

Table 7-5: FAB MS results (ASEP service) for the various attempts at preparing 6+4 barrel cryptands. L^1 = 3+2 cryptand, L^2 = 6+4 cryptand

m/z	Abundance /%	Identity	m/z	Abundance /%	Identity
A1, weak spectrum					
221	100		369	77	
262	31		401	16	
281	70		465	15	
293	25		530	12	
327	24		631	46	
359	72	L^1			
A2					
220	6		534	0.4	
234	4		551	0.2	
359	100	L^1	577	0.15	
381	10	Na L^1	647	0.2	
427	0.36		663	0.23	
465	0.5		715	0.75	L^2
494	0.6		731	0.1	
510	1		737	0.08	Na L^2
524	0.36				
B1					
Insufficient solubility, no spectrum observed					
B2					
234	6		511	0.65	
359	100	L^1	532	0.36	
381	10	Na L^1	550	0.15	
411	0.4		715	1	L^2
465	0.4		729	0.12	
494	0.55		737	0.16	Na L^2

Table 7-6: FAB MS results for dicopper(I) cryptates prepared from the ligands discussed above. Legend: L^1 = 3+2 cryptand, L^2 = 6+4 cryptand.

m/z	Abundance /%	Identity	m/z	Abundance /%	Identity
Cryptate from ligand A2					
243	30		585	100	$Cu_2 L^1 ClO_4$
289	34		601	4	
307	53		647	1.5	
329	9		664	2	
369	5		684	3	$Cu_2 L^1 (ClO_4)_2$
421	54	$Cu L^1$	707	1.5	
437	5		736	1.5	
460	5		1168	0.04	$Cu_4 L^2 (ClO_4)_2$
484	78	$Cu_2 L^1$	1268	1	$Cu_4 L^2 (ClO_4)_3$
499	10				
Cryptate from ligand B2					
243	34		601	4	
289	27		684	5	$Cu_2 L^1 (ClO_4)_2$
307	48		706	2	
329	7		738	2	
421	58	$Cu L^1$	747	0.5	
437	5		891	0.2	
460	4		1170	0.3	$Cu_4 L^2 (ClO_4)_2$
484	77	$Cu_2 L^1$	1268	2.2	$Cu_4 L^2 (ClO_4)_3$
601	10		1368	0.05	$Cu_4 L^2 (ClO_4)_4$
585	100	$Cu_2 L^1 ClO_4$			

7.4.3. Summary

Whilst samples of cryptand prepared via the various routes described above have been shown to yield FAB MS peaks consistent with 6+4 cryptand, the intensity of these peaks has not been significantly higher than observed in imBT prepared by the method of Smith (1). The trialdehyde route, which is expected to favour formation of the "barrel" form, likewise did not show a significant increase in abundance of 6+4 fragment ions in either the free ligand, or in a dicopper cryptate prepared from the ligand. Dicopper cryptates prepared from ligand prepared by the "one-pot" reaction with methanol solvent did not show fragment ions consistent with *any* 6+4 cryptate content.

This may suggest that the "football" form – which is more likely to be formed in the one-pot reaction than it is via trialdehyde – displays significantly different chemical coordination characteristics. Given the low abundance of these ions any conclusions from these observations must be considered tentative.

7.5. Conclusions

FAB MS has revealed ions of charge/mass ratio consistent with 6+4 cryptands and cryptates. The imBT system in particular regularly shows 6+4 peaks in both the free ligand, as well as in cryptates of zinc(II), manganese(II), copper(I) and silver(I) (see Chapter 2), where higher nuclearity is also observed – dinuclear zinc and manganese, and up to *tetra*nuclear copper(I).The amBT ligand, formed by reduction of imBT has also exhibited a similar peak in its disilver cryptate.

Variability in the abundance of the 6+4 ions in the cryptate mass spectra may be due simply to the concentration of the 6+4 cryptand in the ligand sample used, however it is also possible that enrichment of the large crypts may occur via a chemical process such as imine hydrolysis and reformation, mediated by a lewis acidic metal ion.

Currently the only evidence for the presence of the large crypts is mass spectrometric, although the presence of this form has been independently verified on two different instruments. The heavy crypt has also been shown to be absent in some samples, showing that it is unlikely to be merely an artefact formed within the mass spectrometer (which would be expected to be present consistently).

Preliminary efforts to increase the yield of the 6+4 crypt with respect to the 3+2 version have so far met with little success, and owing to the close chemical similarity, good separation of the small fraction of heavy crypt has proven difficult. Nevertheless, a mono-zinc cryptate subjected to size-exclusion chromatography may have an enriched 6+4 content, although this is not firmly established owing to low recovery and possibly poor solubility as well.

The only crystalline products obtained from the various preparations have proven to be simple 3+2 cryptates.

Whilst there is a significant amount of mass spectrometric evidence for the existence of 6+4 cryptates, this is the only technique which has given any evidence so far, and some other verification is desired. Initial concerns that the 6+4 peaks resulted from a rearrangement within the spectrometer appear unfounded, given that on some occasions no heavy peaks were observed.

We therefore believe that this is a useful area for investigation, especially given the current interest in cryptands capable of coordinating up to 4 guests, for models of the tetracopper

Cu_Z site. Although tetracopper molecules have been reported in the literature (*e.g.* 4-8), none presents features to recommend it as a model for Cu_Z. If a rational synthesis or enrichment of the 6+4 cryptates could be developed, then this may provide a useful starting point for tetracopper models, and methodologies such as those presented in chapters 4 and 5 may be of use in developing the system.

7.6. References

1. Smith, P.H., M.E. Barr, J.R. Brainard, D.K. Ford, H. Freiser, S. Muralidharan, S.D. Reilly, R.R. Ryan, L.A.I. Silks, and W.-h. Yu, Journal of Organic Chemistry, 1993. **58**: p. 7939-7941.

2. Bharadwaj, P., *Laterally Non-Symmetric Aza-Cryptands*, in *Progress in Inorganic Chemistry*, K.D. Karlin, Editor. 2002, John Wiley & Sons, Inc.

3. Al-Obaidi, A., G. Baranovic, J. Coyle, C.G. Coates, J.J. McGarvey, V. McKee, and J. Nelson, Inorganic Chemistry, 1998. **37**: p. 3567-3574.

4. Kumar, M., V.J. Aran, and P. Navarro, Tetrahedron Letters, 1995. **36**(12): p. 2161-2164.

5. Maekawa, M., M. Munakata, T. Kuroda-Sowa, Y. Suenaga, and K. Sugimoto, Inorganica Chimica Acta, 1999. **290**: p. 153-158.

6. Motoda, K.I., H. Sakiyama, N. Matsumoto, H. Okawa, and D.E. Fenton, Journal of the Chemical Society-Dalton Transactions, 1995(20): p. 3419-3425.

7. Ziessel, R. and M.-T. Youinou, Angewandte Chemie, 1993. **32**(6): p. 877-880.

8. McKillop, K.P., S.M. Nelson, J. Nelson, and V. McKee, Journal of the Chemical Society: Chemical Communications, 1988: p. 387-389.

8. Conclusions

Silver cryptates

Detailed studies on the silver(I) cryptates of imBT and amBT show that these ligands are capable of some surprising behaviour.

amBT gives rise to a disilver(I) cryptate with a distorted "A-frame" conformation similar to the corresponding imBT cryptate, but rearranges in solution over time to give a *tri*silver(I) cryptate, implying that this is the thermodynamically favoured product. An asymmetric triangular cluster is formed, in which each silver ion lies in a face of the ligand. Preliminary modelling studies suggested that in the solid state, the ligand conformation in the trisilver(I) cryptate is even more strained than the disilver(I) cryptate. The driving force for coordination of the third silver therefore appears to be the formation of closer Ag-N contacts, and of two additional close silver-silver contacts in the triangular array of silver ions. Solid state NMR studies confirm the asymmetry in the trisilver cryptate, as two ^{109}Ag resonances are observed, presumably relating to the pair of ions at the base of the triangle, and the ion at the apex (*i.e.* C_{2v} rather than D_{3h} point symmetry).

This cryptate probably represents an argentophilic interaction, of similar nature to that observed in the disilver(I) cryptate of AB3Bm, which was prepared using an asymmetric tetraamine cap. With this ligand the disilver cryptate contains a smaller internuclear separation than the dicopper(I) cryptate, an effect which was demonstrated in the related symmetrically capped ligands to be due to a argentophilic interaction.

Silver cryptate NMR

The disilver amBT cryptate with its folded A-frame type structure gives rise to very complicated, temperature and solvent dependent solution NMR spectra, which show behaviour consistent with dissociation. Attempts to stabilise the cryptate by attaching auxiliary ligands to the exposed silver faces met with little success, although cryptates with cyanide and benzoate counterions were obtained. A crystal structure of the benzoate cryptate indicates that some weak Ag-O interactions may exist, and the solution NMR spectrum is somewhat simpler, consistent with a smaller degree of dissociation. Results of structural and spectroscopic studies on the cyanide cryptate are not yet available.

Another strategy attempted to stabilise the silver cryptates was to sterically hinder the cavity via the introduction of substituents onto the glyoxal spacer molecule used in preparation of the ligand. This led to significant complications in preparing Schiff base

compounds, much of the difficulty appearing to relate to the prevalence of enol forms of the dicarbonyl, and to side reactions of either the enol or dicarbonyl.

At best, these studies yielded crude podates, but certainly no crypts. We conclude that the use of a substituted glyoxal to achieve substitution of the C_A position in imBT is not appropriate, and suggest that a different approach is required. Use of nucleophilic substitution chemistry, by replacing the glyoxal spacer with an analogous dibromo spacer may be a suitable alternative. This would avoid the complications experienced by the dicarbonyls studied in this work, and allow access to C_A substituted analogues of amBT, which could then be oxidised to the iminocryptand, if required.

Silver cryptate electrochemistry

Electrochemical investigations of the silver imBT and amBT systems were also affected by dissociation, leading to interference from free solvated silver. The influence of solvent and temperature were again demonstrated here, and we have proposed that a mixed valence Ag^0Ag^I amBT complex is generated in a quasireversible process at reduction potential close to 0 V.

Cyclic voltammetry of a disilver iminocryptate (Ag-Ag 2.83 Å) with a conformation similar to the disilver aminocryptate (Ag-Ag 2.81 Å) revealed successive redox waves that may represent the sequence $Ag^IAg^IL \rightarrow Ag^IAg^0L \rightarrow Ag^0Ag^0L$. The two features are separated by 0.193 V, and if our assignment of these features is correct, then this potential difference is related to the stabilisation afforded by the silver-silver contact. Unfortunately, we doubt that any of these states will be isolable, owing to their poor reversibility, proximity to other redox processes, and the known dissociation equilibria in these systems.

Cyclic voltammetry of the cryptates with cyanide or benzoate counterions may reveal additional detail of redox processes. Perhaps more importantly however, if the mixed valence region of the voltammogram is sufficiently wide and free of decomposition effects, it may prove possible to generate quantities of mixed valence species sufficient for isolation or at least *in situ* study, using for example a combined electrochemical/ESR cell.

Copper cryptates

Our studies on the dicopper(I) imBT system were directed at determining whether a d^{10}-d^{10} interaction exists between the copper ions, which are only slightly further apart than in the related average valence dicopper(1.5) cryptate, which contains a fully delocalised electron.

The challenge was to obtain X-ray diffraction data of sufficient quality to determine the electron density distribution, a goal which required the preparation of a non-racemically-twinned crystal. Solution NMR studies suggest that racemisation is occurring in solution, but the observation that the extent of twinning in crystals was variable showed that the conformation was not exchanging in the solid state. Attempts to exchange the perchlorate counterion for tartrate, or to directly prepare copper tartrate diastereoisomers failed, possibly due to the intrinsic stability of copper tartrates, making a pure tartrate complex a more favoured product.

The variable extent of twinning did, by random selection, yield a non-twinned crystal with perchlorate anion, however the electron density studies could not be performed at the time, and long term crystal stability was insufficient to allow the studies to be completed on the same sample at a later date. Preparation of a cryptate with tetrafluoroborate counterion yielded a non-twinned crystal which diffracts well, and which we hope will lead to completion of the studies on this system. This result may help to resolve the long-standing debate over whether a cuprophilic effect (similar to the well known aurophilic effect, and the increasingly well-accepted argentophilic effect) exists in some molecules.

Our attempts to incorporate an asymmetric tetraamine cap into cryptates met with success when using the meta-xylyl spacer, and yielded dicopper and disilver cryptates with features intermediate between the tren and trpn capped analogues. Unfortunately the desired imBT analogues could not be obtained. These cryptands would have slightly larger cavity sizes than imBT, and the effect on the character of the dicopper(1.5) and dicopper(I) cryptates could yield useful information on the nature of copper-copper interactions.

The failure to obtain an asymmetric imBT cryptand may relate to the increase in cap strand length favouring the formation of a polymer rather than a crypt (possibly as a result of a different hydrogen bonding pattern in the tetraamine), or simply to poor conversion of the tetraamine hydrochloride to the free base, a transformation which has been observed to occur surprisingly slowly in other systems. A more rigorous procedure for obtaining the free base may therefore allow the preparation of a greater range of cryptands and cryptates with the asymmetric cap, and we believe that this will yield useful results when applied to average valence copper systems, as well as providing a useful tool in the development and fine tuning of other cryptands.

Manganese cryptates

Manganese(II) imBT and amBT cryptates, as well as trac and PGP podates were synthesised for trials as MRI contrast agents, although purity problems meant that the trac podate was excluded from relaxivity experiments.

The PGP podate proved to be a weak relaxer, and the aminocryptate (expected to be more favourable in terms of H-bonding, and interaction with water) only showed moderate relaxivity, with the iminocryptate proving to have a very strong relaxivity, making it an attractive candidate for further studies. This finding is extremely interesting, as coordination or H-bonding of water has always been considered a prerequisite for strong relaxivity, but if water was present it appears to be in the form of weakly held lattice water.

Other evidence (elemental analysis, magnetic moment) was inconclusive for the presence of water in the solid state. ESR studies on this cryptate suggested that there may be aggregation processes in play, and whilst the mode of this action is not clear, it may be a factor in the surprisingly strong relaxivity of the molecule. We also speculate that the more strained structure of the iminocryptate may result in wider channels to the guest ion than in the more flexible and labile aminocryptate, allowing more facile access of water molecules to the metal, and thereby enhancing relaxivity.

On the timescale of the experiment, there appears to be no significant dissociation of the cryptate, however slow decomposition of the ligand was observed, and thus the relative rates of clearance from the body, and decomposition of the cryptate would be critical in deciding whether this cryptate had potential for *in vivo* use.

These studies have shown that cryptates of manganese(II) can show the strong relaxivity required for a MRI contrast agent, and brings into question the need for stable coordinated water in the complex, an attribute which has previously been considered necessary to achieve the degree of relaxivity to be useful for MRI.

Larger cryptates

Investigations of heavy ions in the FAB mass spectra of imBT and amBT cryptates revealed that these are consistent with "6+4" cryptands and cryptates (incorporating 6 spacer and 4 cap molecules rather than 3 and 2 as in the normal crypts). The imBT system in particular regularly shows 6+4 peaks in both the free ligand, as well as in cryptates of zinc(II), manganese(II), copper(I) and silver(I), where higher nuclearity is also observed –

dinuclear zinc and manganese, and up to *tetra*nuclear copper(I).The amBT ligand, formed by reduction of imBT has also exhibited a similar peak in its disilver cryptate.

Preliminary efforts to increase the yield of the 6+4 crypt with respect to the 3+2 version have so far met with little success, and owing to the close chemical similarity, separation of the small fraction of heavy crypt has proven difficult. Nevertheless, a mono-zinc cryptate subjected to size-exclusion chromatography may have an enriched 6+4 content, although this is not firmly established.

The investigation of tetranuclear cryptates is of particular interest at present, when efforts are being directed towards modelling the tetracopper Cu_Z site, and if a rational synthesis or enrichment of the 6+4 cryptates could be developed, then we believe that these molecules may be useful as 1st approximation models for the Cu_Z system.

9. Experimental methods

9.1. Experimental details for Chapter 2

9.1.1. Disilver(I) imBT

The yield of this preparation was maximised by performing the reaction at high concentration; by stirring the solution overnight in the dark, and filtering the product off the following morning. Good quality crystals (yellow needles) were obtained by slow diffusion of ether into an acetonitrile solution of the crude product.

9.1.1.1. Preparation of disilver(I) imBT cyanide

Despite the insolubility of silver cyanide, a bright yellow colour developed when a methanolic solution of ligand was added to two equivalents of the solid salt under a nitrogen atmosphere. This colour faded quickly as the suspension was stirred, and a mixture of pale yellow and black (silver oxide) precipitates was obtained. The infrared spectrum of the mixture (not shown) contained only CN peaks, showing that the ligand had remained in solution. Attempts to obtain a solid from the solution by evaporating it further, or by diffusion of ether resulted in the formation of a silver mirror.

Whilst no cryptate was obtained from this procedure, the colour change, and the formation of a silver mirror from the solution suggests that the ligand is involved in the reaction, although the only solid isolated is a free cyanide salt.

The procedure described above was repeated, and after the bright yellow colour had appeared, and before trying to isolate any solid, one equivalent of solid potassium dicyanoargentate was added to the solution. A pale yellow precipitate formed, whose infrared spectrum is shown in Figure 9-1.

The solid was only very slightly soluble in acetonitrile or DMSO, and could not be crystallised.

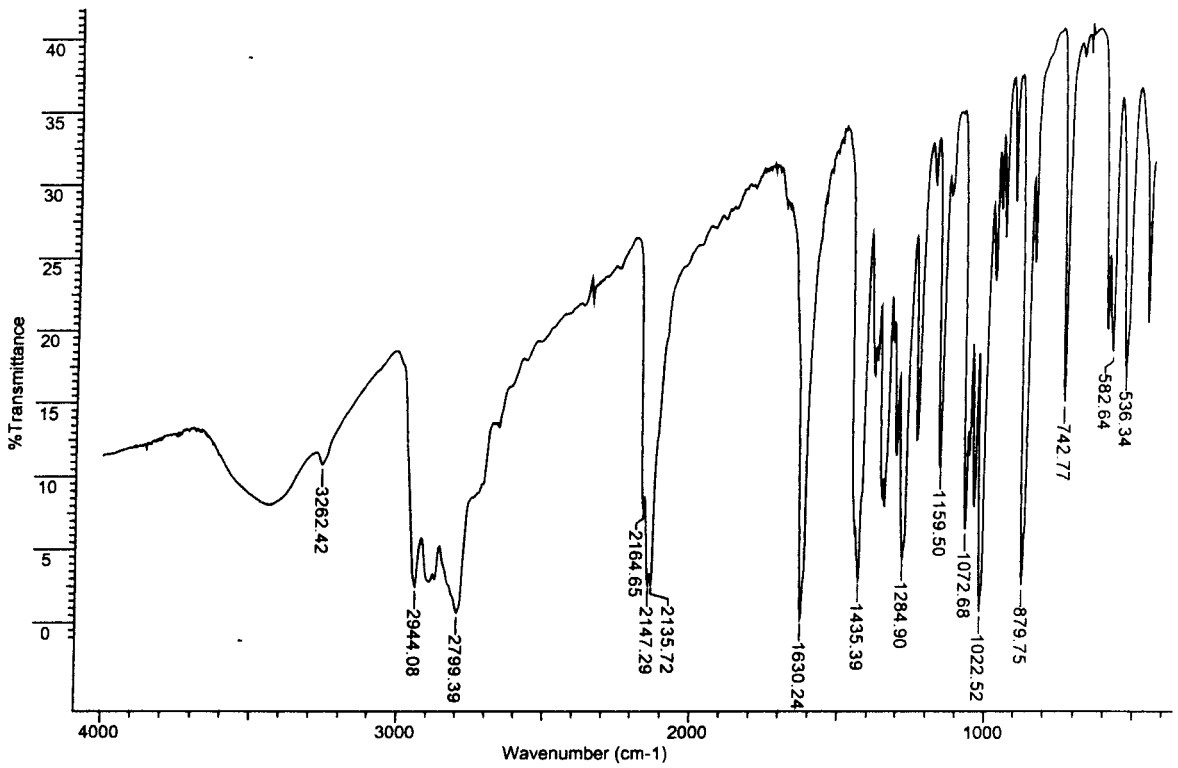

Figure 9-1: Infrared spectrum of the yellow solid obtained by addition of dicyanoargentate to a suspension of silver cyanide in a solution of imBT.

9.1.2. Substitution ligands for disilver imBT

9.1.2.1. Triphenylphosphine

Treatment of Ag_2 imBT with triphenylphosphine does not result in any visible reaction, even after reflux and stirring for 12 hours. The crude product obtained when the solvent is removed is of a yellow hue similar to the starting cryptate, and when redissolved in acetonitrile leaves a white residue, with an infrared spectrum matching that of the phosphine. Slow diffusion of ether into the solution results in the formation of small yellow needles, together with an orange/brown amorphous solid. The needles proved unsuitable for X-ray structure determination, no unit cell could be determined, which is most likely due to disorder within the crystal. However, their infrared spectrum (not

shown) and elemental analysis (Table 9-1) strongly suggest that they are merely the starting cryptate.

Table 9-1: Elemental analysis of yellow crystals obtained by slow diffusion of ether into a solution in acetonitrile.

Analysis	%C	%H	%N
Predicted: Ag_2 imBT $(ClO_4)_2 \cdot 2PPh_3$	49.98	4.66	8.63
Predicted: Ag_2 imBT $(ClO_4)_2$	27.96	3.91	14.49
Found:	28.73	3.48	14.29

The infrared spectrum of the orange/brown solid (Figure 9-2) was more interesting however, with peaks similar to both the phosphine (1480, 1437, 696, 520 cm^{-1}) and the starting cryptate (2925, 2853, 1636, 1459, 1376 cm^{-1}). The FAB mass spectrum has similar characteristics to that of the starting complex, but also a peak with m/z corresponding to $Ag(PPh_3)_2^+$. Another peak with m/z 618 could correspond to PPh_3 + imBT, however a peak with this mass was also observed for the starting complex, where it was attributed to inclusion of the matrix – NOBA – in the complex. No fragment corresponding to an ion containing all 3 species (Ag, PPh_3 and imBT) was observed.

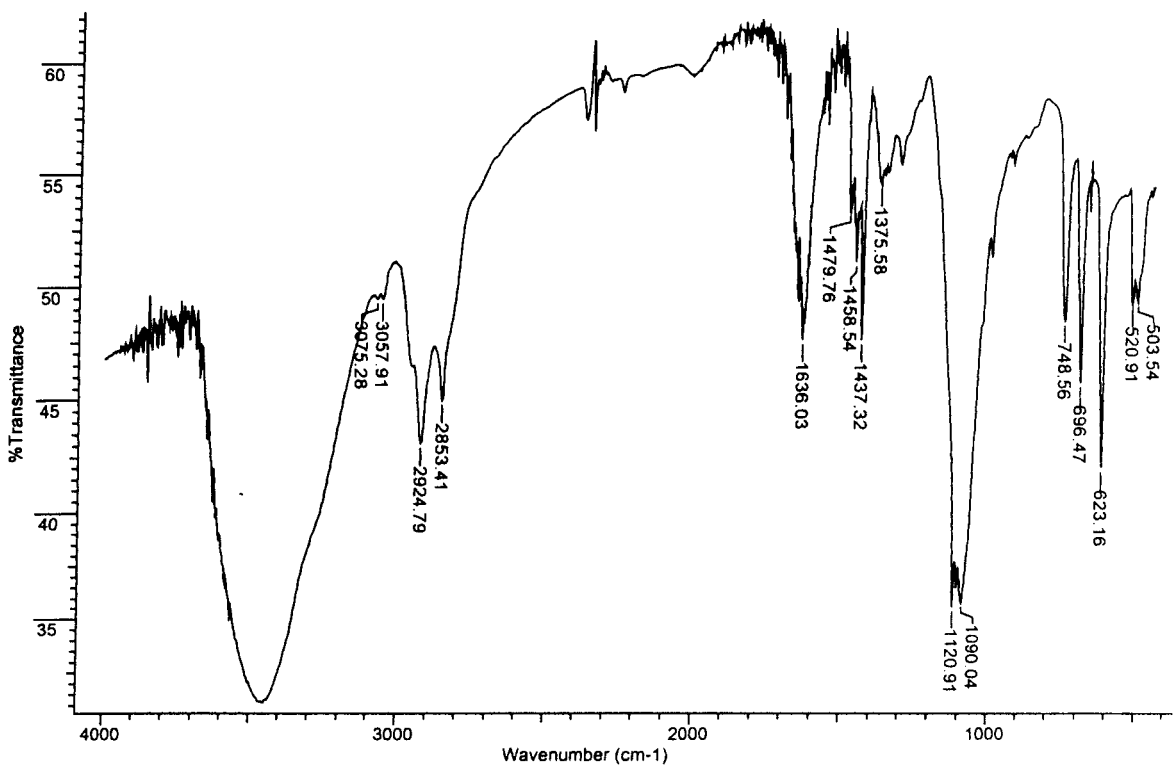

Figure 9-2: Infrared spectrum of a KBr disk of the orange/brown solid obtained by diffusion of ether into a solution in acetonitrile.

Table 9-2: FAB mass spectrum of the orange/brown solid resulting from reaction of Ag_2 imBT with triphenylphosphine (EPSRC service, L = imBT)

m/z	Abundance /%	Identity	m/z	Abundance /%	Identity
273	12		566	1.5	Ag L ClO_4
359	10	L	618	9	L PPh_3 or Ag L NOBA?
391	7		635	2	Ag $(PPh_3)_2$
467	34	Ag L	773	1.5	Ag_2 L $(ClO_4)_2$

The material obtained in this preparation appears to be a mixture of 2 or more species. Several attempts to prepare a PPh_3/imBT species, as was speculated to account for the m/z 618 peak in the FAB spectrum, were unsuccessful, lending further support to the theory that this ion relates to the starting complex and not a derivative.

No direct evidence for the formation of a cryptate with extraneous P-donors exists, and it seems, perhaps for steric reasons, that the triphenylphosphine ligand cannot bind to the exposed silver sites. The presence of a silver phosphine peak in the mass spectrum can be rationalised by considering that in solution an equilibrium is believed to exist between solvated and cryptated silver; free silver in solution may then react with the phosphine in a normal manner, to form a stable complex.

9.1.2.2. Diphos

The diphos ligand, containing two phosphorous donors has potential to cross-link two cryptate molecules, or even to form a –diphos–cryptate–diphos–cryptate– polymer. A similar set of reaction conditions were used as for triphenylphosphine in the preceding section. The (yellow) crude product was redissolved, and white diphos (determined by infrared), together with some solid black material (probably Ag(0) or Ag oxide) was filtered from the solution. Slow diffusion of ether resulted in a mixture of yellow and brown solids after 2 days, this solid was redissolved in acetonitrile and allowed to concentrate in the dark, leaving a yellow glass with infrared spectrum identical to Ag_2 imBT $(ClO_4)_2$.

As for triphenylphosphine, it appears that this P-donor fails to form a stable bond with the di-silver cryptate. A number of variations on the diphos ligand exist, however given the lack of affinity for the two phosphines used to date, these were not pursued any further.

9.1.2.3. Sodium diethyl-dithiocarbamate

No visible reaction occurs immediately between Ag_2 imBT and diethyl-dithiocarbamate, however a precipitate formed after two hours stirring at room temperature. The infrared spectrum (Figure 9-3) of this precipitate is identical to that of a separately prepared silver diethyl-dithiocarbamate complex (Figure 9-8 B), with no definite sign of any crypt-related absorbance.

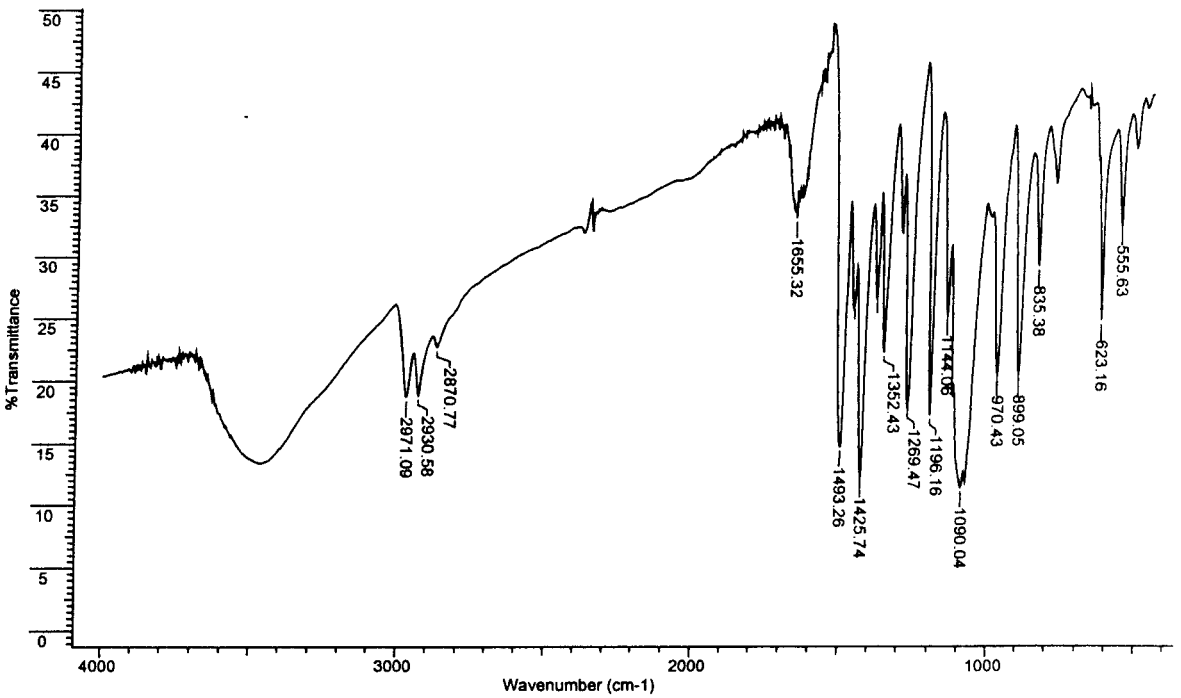

Figure 9-3: Infrared spectrum of the yellow precipitate obtained by reaction of disilver imBT with sodium diethyl dithio carbamate. The spectrum is the same as that of the silver diethyl-dithiocarbamate triflate complex described in section 9.1.4.4, with perchlorate peaks instead of triflate. The broad peak at 1655 cm^{-1} is probably OH bend owing to the presence of water in the sample.

9.1.2.4. Thiophenol

Reaction of thiophenol with the cryptate results in the immediate formation of a yellow precipitate of silver(I) thiophenol perchlorate (confirmed by comparison to a sample of authentic thiophenol complex prepared in the absence of imBT). Removing the solvent from the filtrate resulted only in the recovery of unreacted Ag_2 imBT $(ClO_4)_2$. In the case of thiophenol therefore, it appears that the S-donor ligand has too great an affinity for silver(I), resulting in abstraction of silver ions from the cryptate.

9.1.2.5. Maleic anhydride

This anhydride was slow to react, but yielded a white/yellow precipitate after 5 hours, which darkened when exposed to air. Yellow needle shaped crystals were obtained from the filtrate by slow diffusion of ether, however their infrared spectrum and elemental analysis were consistent with the starting cryptate, with no IR frequencies attributable to free or complexed carbonyl.

The IR spectrum (Figure 9-4) of the initial precipitate however, has three distinct peaks at 1580, 1632 and 1714 cm^{-1} which appear to be superimposed on a broad feature in the imine/carbonyl region. This suggests a complex incorporating the anhydride, with shifted carbonyl frequencies – as expected if the carbonyls are involved in coordination. The perchlorate peak is surprisingly weak however, suggesting that this counterion may have been replaced by another, such as the diacid form of the anhydride. Although neither partial nor full replacement of perchlorate was consistent with the analytical results however (Table 9-3). These show that nitrogen is present, consistent with the presence of an azacryptand (or acetonitrile), but no reasonable match for any combination of silver, anhydride, acid, crypt and perchlorate could be found. The mass spectrum was too weak to allow for sensible interpretation. The darkening of the solid, together with the poor analysis and mass spectrum suggest that a process such as reduction of silver(I) to silver(0) and oxidation of the crypt/anhydride may be occurring.

It is evident from the instability of this compound (or mixture of compounds) that a significant change has occurred in the silver environment. Whether a cryptate incorporating the anhydride, or a mixture of different components has been formed has not been established, however the obvious instability of the material makes it a low priority for further investigation in this study.

Table 9-3: Analytical results for the precipitate obtained from the reaction of maleic anhydride with the disilver cryptate.

Analysis	%C	%H	%N
Predicted: Ag_2 imBT maleic anhydride $(ClO_4)_2$	30.33	3.70	12.86
Predicted: Ag maleic anhydride$(MeCN)_4$ ClO_4	30.69	3.00	11.93
Predicted: Ag [maleic anhydride][maleic acid]	39.61	4.60	14.21
Found:	38.56	5.21	9.01

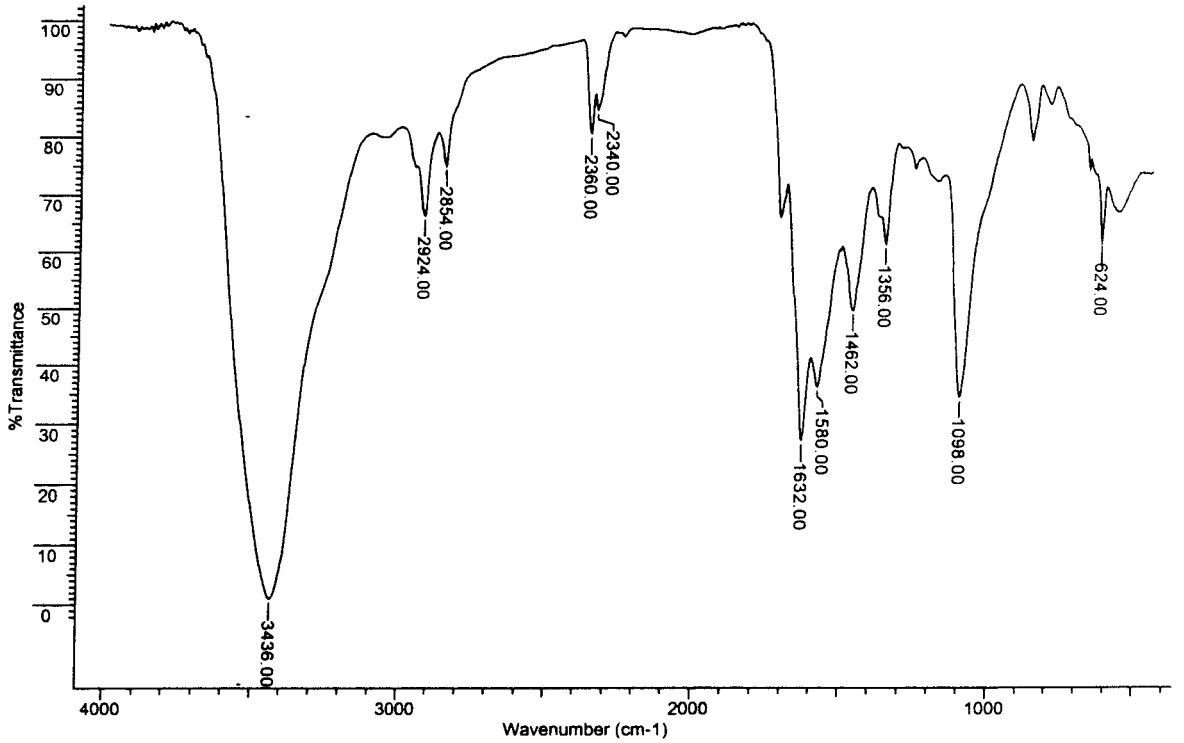

Figure 9-4: Infrared spectrum of the product of the reaction of maleic anhydride with Ag_2 imBT (KBr disk).

9.1.2.6. Succinic acid

Succinic acid behaved in a similar manner to maleic anhydride (described in the previous section), reacting slowly to give an orange/brown precipitate after one day, the filtrate yielding a small amount of yellow solid by diffusion of ether.

The solids obtained were once again sensitive to air/light, and the solid received by the mass spectrometric service was too weakly ionised to give a spectrum, possibly owing to decomposition in transit. Elemental analysis of the product obtained by diffusion of ether confirms the presence of nitrogen, but no reasonable match to the experimental result could be devised. Infrared spectra (the spectrum of the initial precipitate is shown in Figure 9-5) showed no traces of carbonyl peaks in either sample, but neither did they resemble the spectrum of the starting cryptate, and seem most likely to be breakdown products.

Analysis	%C	%H	%N
Predicted: Ag_2 imBT -OOC-C_2H_4-COO-	38.28	4.96	16.23
Found:	28.70	4.47	12.96

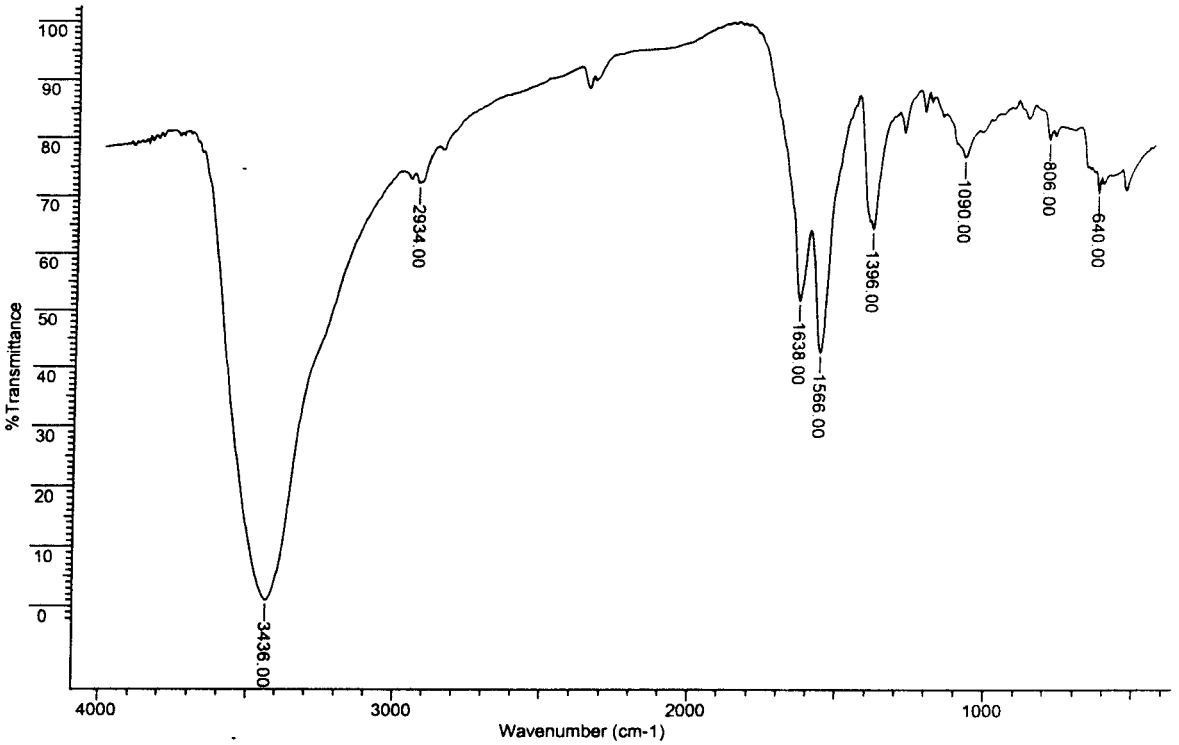

Figure 9-5: Infrared spectrum of the initial product of the reaction of succinic acid with Ag_2 imBT (KBr disk). 1638 cm^{-1} is within the window for an imine or carbonyl, however in this case it is more likely to be the water bend corresponding to the strong stretch in the 3000-4000 cm^{-1} range. The lack of clear CH, perchlorate, or fingerprint region peaks suggest that this is a breakdown product of the cryptate and/or carboxylic acid.

9.1.2.7. Adipic acid

No reaction was immediately visible, but a mixture of brown and orange precipitates formed after 1 day. The orange/yellow filtrate from this mixture yielded pale yellow needles mixed with a spongy yellow solid by slow diffusion of ether. The spongy solid has an infrared spectrum similar to the first precipitate, and is believed to be a further yield of the same material.

The elemental analysis of the initial precipitate showed a very low nitrogen content, and no perchlorate or carbonyl peaks were present in its infrared spectrum (Figure 9-6). A weak peak suggestive of imine is present, possibly owing to a small percentage of crypt, or to water content. These results are consistent with a breakdown product similar to that observed for the previous carboxylic acids used.

The elemental analysis and infrared spectrum of the crystals were very similar to the starting cryptate, with no sign of carbonyl frequencies.

Table 9-4: Elemental analysis results for the products of reaction of adipic acid with Ag_2 imBT.

Analysis	%C	%H	%N
Predicted (Ag_2 imBT adipate):	40.13	5.33	15.60
Found (precipitate):	25.56	3.20	2.68
Predicted (Ag_2 imBT perchlorate):	27.96	3.91	14.49
Predicted (Ag_2 imBT perchlorate:0.5 Et_2O):	**29.65**	**4.35**	**13.83**
Found (crystals):	29.54	4.55	13.81

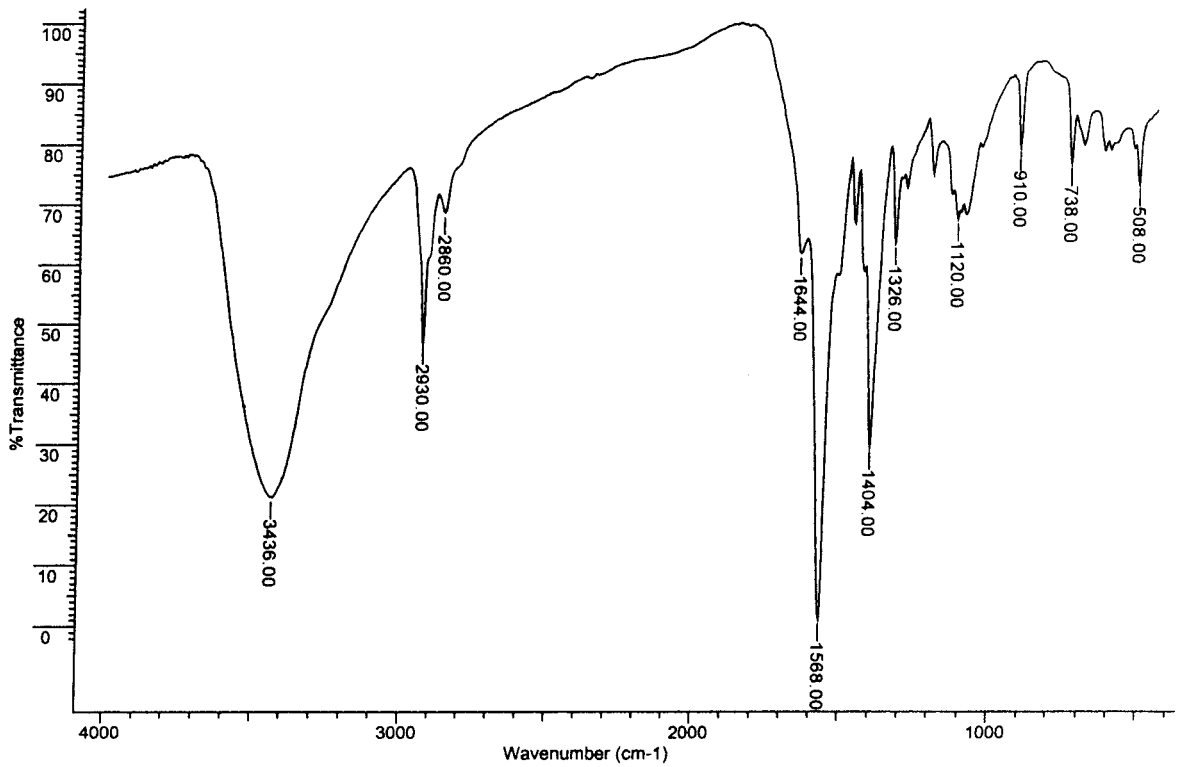

Figure 9-6: Infrared spectrum of the orange/brown precipitate obtained by reaction of Ag_2 imBT with adipic acid.

9.1.2.8. Disodium terephthalate

A small amount of water was required to bring the terephthalate salt into solution, before adding it to the cryptate solution in acetonitrile. No reaction occurred immediately, however after several hours a white precipitate formed, with an infrared spectrum identical to the terephthalate salt and no peaks suggesting presence of the crypt.

Small yellow needles with infrared and FAB mass spectra consistent with the starting cryptate were obtained by slow diffusion of ether into the filtrate.

The poor solubility of this salt in organic solvents has complicated its handling, as the disilver cryptate decomposes in the presence of water. Nevertheless, the small amount of water required in this preparation has not caused decomposition, and there has been no

interaction between the carboxylate and the cryptate, use of a free acid seems unlikely to bring any improvement.

9.1.2.9. 3-methylglutaric acid

Reaction of 3-methylglutaric acid with the cryptate yields an orange/brown precipitate after several hours, which turns black within a day, suggesting decomposition to silver(0). Slow diffusion of ether into the yellow solution remaining results in the formation of yellow needle shaped crystals, identical in appearance and infrared absorption to that of the starting complex.

The FAB mass spectrum of the initial precipitate only showed peaks associated with the NOBA matrix, consistent with the suggestion of decomposition of the product.

9.1.2.10. Glutaric anhydride

An orange/brown precipitate forms from the reaction of glutaric anhydride with the cryptate after several hours. The infrared spectrum (Figure 9-7) although weak and broadened, resembles the starting cryptate. An additional small peak in the carbonyl region, and a broad feature extending from 1600 to 1750 cm^{-1} underlying the imine peak are suggestive of the presence of anhydride. The solid was submitted for FAB mass spectrometry to determine whether a complex or a mixture was present, and a weak spectrum with peaks relating only to the starting cryptate was observed.

Slow diffusion of ether into the filtrate yielded a dark yellow solid with infrared spectrum identical to the starting cryptate (no sign of the new features mentioned above), and elemental analysis suggestive of an impure sample of the starting cryptate, possibly containing solvent (isopropanol) and inorganic silver impurities.

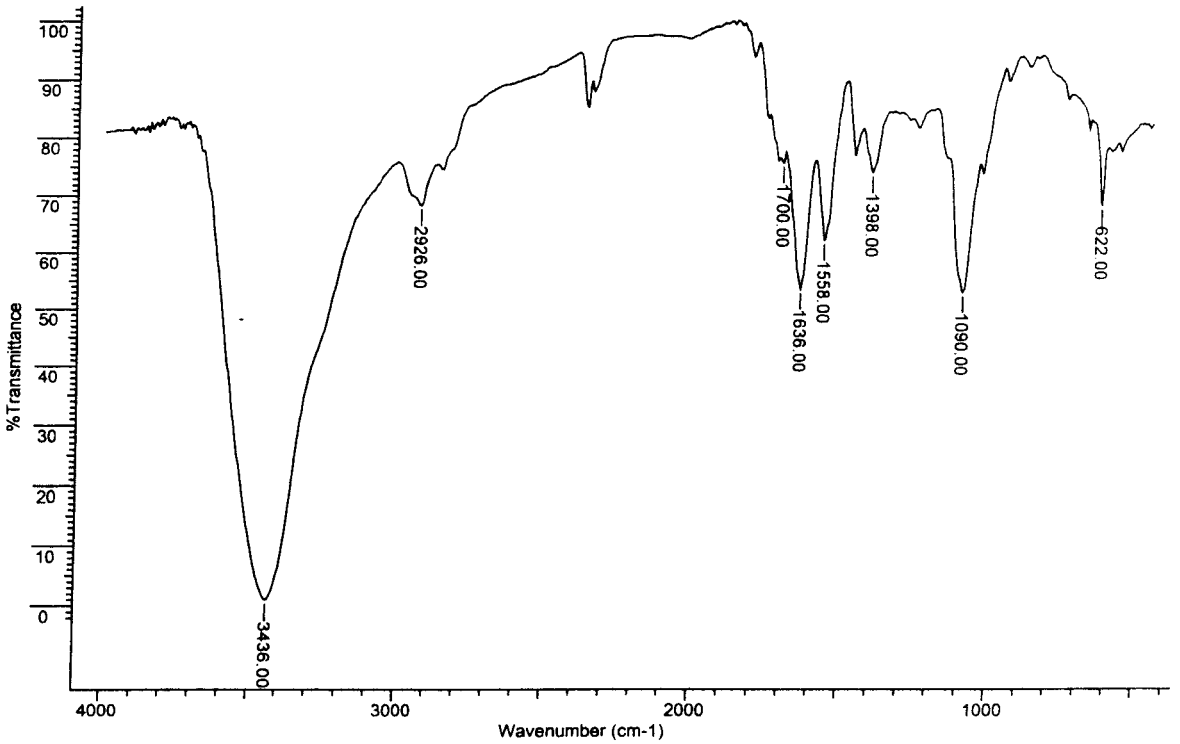

Figure 9-7: Infrared spectrum of the orange/brown precipitate formed by the reaction of glutaric anhydride with disilver imBT.

9.1.2.11. Acetylene dicarboxylic acid

Attempts to derivatise the cryptate were made using both the free acid and a potassium salt. Using an aqueous solution of the salt resulted initially in the formation of a yellow precipitate, as well as yellow crystals by diffusion of ether into the filtrate. The precipitate, which had an infrared spectrum that resembled the breakdown products observed from previous experiments with carboxylates, was too insoluble to give a FAB mass spectrum.

The crystals had intense perchlorate infrared absorptions, but only weak CH and fingerprint region peaks. A matrix of X-ray diffraction data was collected for crystals from two different preparations using the dicarboxylate salt, and the cell parameters were determined to be consistent with silver(I) perchlorate. Closer inspection of the crystals under a microscope revealed that they are in fact colourless, with a coating of yellow non-crystalline solid, presumably of the same identity as the initial precipitate.

Reaction of one equivalent of the free acid with the cryptate gave an orange precipitate after one hour, which quickly turned brown. The initial orange material proved impossible to isolate in repeated attempts. The brown solid is insoluble, and has a weak infrared spectrum with a suggestion of perchlorate peaks but no other discernible features, suggesting that it is largely composed of breakdown products, including silver(0) or silver

oxide. The elemental analysis (Table 9-5) could not be rationalised in terms of a cryptate. Slow diffusion of ether into the yellow filtrate gave large yellow needle shaped crystals (similar in appearance to starting material), with an infrared spectrum and crystal unit cell consistent with the starting cryptate.

Table 9-5: Elemental analysis results of the brown solid precipitated from the reaction of disilver imBT with acetylene dicarboxylic acid.

Analysis	%C	%H	%N
Predicted – Ag_2 $C_{18}H_{30}N_8$ $C_2(CO_2)_2$	38.5	4.41	16.33
Found	27.4	3.84	11.08

9.1.2.12. Pyridine and related N-donor ligands

A range of N-donor ligands (see Table 2-3) were investigated, and since the behaviour of this entire group was very similar, they are discussed under the same heading.

Addition of a solution of each N-donor ligand to a solution of the cryptate did not result in any visible reaction, and there was no obvious change even after several days. The yellow solution obtained in each case was placed in an ether jar, and crystals of the starting cryptate were obtained, the auxiliary ligand remaining in solution.

This group of ligands appear to have too little affinity for the cryptated silver(I), and do not interact in any way.

9.1.3. Disilver(I) amBT

140 mg (0.38 mmol) of amBT was dissolved in 5 ml of degassed isopropanol, and the solution placed in an aluminium foil covered vessel under a nitrogen atmosphere. 400 mg (1.56 mmol) of solid silver triflate was added, resulting in an immediate formation of a pale yellow solution, and a large amount of black precipitate. This mixture was stirred in the fully foil covered vessel for another 30 minutes, the vessel was then sealed, and allowed to rest overnight. The pale yellow supernatant was transferred to a clean vial, and crystals were obtained by the slow diffusion of ether into the solution. Yield 182 mg (54 %).

9.1.4. Stabilisation ligands for disilver amBT

9.1.4.1. Silver amBT benzoate

100 mg (0.27 mmol) of amBT was dissolved in 2 ml of isopropanol, in a darkened vessel with a nitrogen atmosphere. 146 mg (0.64 mmol) of silver benzoate was added as a solid. The mixture immediately turned dark brown, and was left in a sealed vessel in the dark overnight. A dark brown precipitate (mainly unreacted benzoate salt) was filtered off the following day, and white crystals were obtained by diffusion of ether into the yellow filtrate after two days.

9.1.4.1.1. Crystallographic study of disilver(I) amBT benzoate

Data for disilver amBT benzoate was collected by Prof Vickie McKee on a Bruker SMART 1000. Details of the data collection and refinement are given in Table 9-6. The structure was solved using direct methods, and refined with assistance from Prof Vickie McKee using full matrix least-squares on F^2, using SHELXTL (13). Data beyond 50° was omitted from the refinement. Non-hydrogen atoms were refined with anisotropic atomic displacement parameters. Hydrogen atoms were inserted at calculated positions with isotropic displacement parameters riding on U_{ij} of their carrier atoms.

The asymmetric unit is fully ordered, and contains a disilver cryptate molecule of similar conformation to that seen with BF_4^- counterion, together with two benzoate ions, a water molecule, and a carbonate or bicarbonate ion. This unexpected component could result from atmospheric uptake of CO_2, or else from partial breakdown of benzoate, or an impurity in the silver benzoate used for cryptate preparation. In order to achieve charge balance, it is clear that two protons must be inserted into the model. The position of the carbonate ion with two of its oxygen atoms near, and in a similar plane to a benzoate suggests that a proton may in fact bridge each carbonate/benzoate oxygen pair. The distances separating these oxygen pairs are 2.63 and 2.61 Å (see Table 9-8), which is consistent with strong H-bonding. Close examination of the Fourier maps (F observed) did not reveal any electron density consistent with bonding between these oxygens, however this does not disprove our hypothesis, as protons could not be directly located elsewhere in the structure either.

Selected bond lengths and angles are given in Table 9-7, as well as a comparison of the bond lengths in the tetrafluoroborate variant on this structure. Bond lengths in the cryptate

molecules are broadly similar, however silver to benzoate oxygen distances are shorter than the silver to fluorine distances, which may suggest some degree of interaction.

Table 9-6: Crystal data and structure refinement for the disilver amBT benzoate complex.

Identification code	Disilver amBT benzoate	
Empirical formula	C33 H56 Ag2 N8 O8	
Formula weight	908.60	
Temperature	150(2) K	
Wavelength	0.71073 Å	
Crystal system	Monoclinic	
Space group	P2(1)/c	
Unit cell dimensions	a = 11.847(2) Å	α= 90°
	b = 16.981(4) Å	β= 93.014(4)°
	c = 19.117(4) Å	γ = 90°
Volume	3840.4(13) $Å^3$	
Z	4	
Density (calculated)	1.571 Mg/m^3	
Absorption coefficient	1.078 mm^{-1}	
F(000)	1872	
Crystal size	0.35 x 0.32 x 0.17 mm^3	
Theta range for data collection	1.60 to 25.00°	
Index ranges	-14<=h<=14, -20<=k<=20, -22<=l<=22	
Reflections collected	36856	
Independent reflections	6751 [R(int) = 0.0944]	
Completeness to theta = 25.00°	100.0 %	
Refinement method	Full-matrix least-squares on F^2	
Data / restraints / parameters	6751 / 0 / 460	
Goodness-of-fit on F^2	0.949	
Final R indices [I>2sigma(I)]	R1 = 0.0485, wR2 = 0.1149	
R indices (all data)	R1 = 0.0789, wR2 = 0.1288	
Largest diff. peak and hole	1.517 and -1.527 $e.Å^{-3}$	

Table 9-7: Selected bond lengths and angles for disilver amBT benzoate. A comparison of bond lengths in the tetrafluoroborate variant is also made.

Bond length /Å		BF_4 bond lengths /Å		Bond angle /°
Ag(1)-N(3C)	2.258(4)	*2.338(13)*	N(3C)-Ag(1)-N(4A)	145.85(15)
Ag(1)-N(4A)	2.308(4)	*2.343(11)*	N(3C)-Ag(1)-N(3A)	114.59(15)
Ag(1)-N(3A)	2.406(4)	*2.377(12)*	N(4A)-Ag(1)-N(3A)	78.44(15)
Ag(1)-N(1)	2.627(4)	*2.465(12)*	N(3C)-Ag(1)-N(1)	75.91(14)
Ag(1)-Ag(2)	2.7937(8)	*2.8167(14)*	N(4A)-Ag(1)-N(1)	137.45(14)
Ag(1)-O(21)	3.716(4)	*4.64 (F13)*	N(3A)-Ag(1)-N(1)	72.63(15)
Ag(1)-O(22)	3.757(4)		N(4C)-Ag(2)-N(3B)	152.29(15)
Ag(2)-N(4C)	2.250(4)	*2.270(12)*	N(4C)-Ag(2)-N(4B)	119.46(15)
Ag(2)-N(3B)	2.292(4)	*2.34(2)*	N(3B)-Ag(2)-N(4B)	78.11(15)
Ag(2)-N(4B)	2.420(4)	*2.418(11)*	N(4C)-Ag(2)-N(2)	75.23(14)
Ag(2)-N(2)	2.668(5)	*2.604(10)*	N(3B)-Ag(2)-N(2)	132.40(14)
Ag(2)-O(11)	3.614(4)	*3.99 (F21)*	N(4B)-Ag(2)-N(2)	72.41(15)
Ag(2)-O(12)	3.836(4)			
Ag(2)-O(32)	3.842(4)			
Ag(2)-O(31)	4.614(4)			
Ag(2)-O(33)	5.357(4)			

Table 9-8: Hydrogen bonds for disilver amBT benzoate. Although no hydrogens could be located for the neighbouring benzoate and carbonate molecules, the oxygen-oxygen separation (see lower section of table) is consistent with the presence of a strong H-bond between them.

D-H...A	d(D-H) /Å	d(H...A) /Å	d(D...A) /Å	<(DHA) /°
N(4C)-H(4C)...O(12)	0.94	2.07	2.955(6)	158.3
N(3C)-H(3C)...O(21)	0.99	1.92	2.882(6)	162.6
N(3B)-H(3B)...O(1W)#1	0.92	2.17	3.068(6)	164.3
N(4B)-H(4B)...O(32)	1.00	2.07	3.029(6)	160.4
O(1W)-H(1WB)...O(31)#2	0.79	2.07	2.824(5)	160.0
O(1W)-H(1WA)...O(21)	0.77	2.02	2.768(5)	162.9
O(11)-H...O(32)			2.631(5)	
O(31)-H...O(12)			2.610(5)	

Symmetry transformations used to generate equivalent atoms:

#1 -x+1,y-1/2,-z+1/2 #2 x-1,y,z

9.1.4.2. Triphenylphosphine

No visible reaction occurs between the cryptate and triphenylphosphine, and in a similar fashion to the imBT cryptate, the reactants were apparently recovered separately – the phosphine as a white precipitate from the solution after its volume was reduced, and the cryptate as white needles by slow diffusion of ether into the filtrate. The FAB mass spectrum (Table 9-9) of the crystals did not contain any peaks consistent with a silver phosphine complex, with or without amBT. However, a surprisingly strong peak with m/z consistent with amBT PPh_3 was observed (m/z 632.9). A weak peak with this mass has

been observed in the FAB MS spectrum of the starting cryptate, where it was believed to relate to NOBA internal standard, either in an interaction with the cryptate, or as an aggregate incorporating another moiety such as sodium (*e.g.*, m/z for 4NOBA.Na = 635). Attempts to prepare an amBT/PPh_3 species independently under similar reaction conditions have not had any success, and the assignment of the 632.9 ion to a background artefact seems most probable.

Table 9-9: FAB mass spectrum of crystals isolated from the reaction of triphenyl phosphine with disilver amBT. L = amBT.

m/z	Abundance /%	Identity	m/z	Abundance /%	Identity
371	30	L	735	22	Ag_2 L triflate
477	100	Ag L	775	3	Ag L $triflate_2$
633	37	NOBA artefact or L PPh_3?			

9.1.4.3. Diphos

No visible reaction occurred between diphos and the cryptate, and diffusion of ether into to the solution once again yielded white crystals, mixed with a brown amorphous solid.

The FAB mass spectrum for the crystals obtained has peaks corresponding to Ag amBT, Ag Diphos, Ag_2 amBT triflate, Ag $Diphos_2$, Ag $Diphos_2$ triflate, and Ag_2 $Diphos_2$ triflate, in addition to a number of very weak heavier mass peaks which could not be assigned. The phosphine ligand appears to have partly reacted to form simple silver complexes (without the amBT ligand), mixed with remnants of the disilver cryptate. There is no indication in the FAB MS of a complex containing both amBT and the diphos ligand. Elemental analysis (Table 9-10) results could not be fitted to any of the expected products, and are also likely to be evidence of the presence of a mixture.

Table 9-10: Elemental analysis results product of the reaction of diphos with disilver amBT (predominantly white crystals, with some brown solid).

Analysis	%C	%H	%N
Predicted: 2:1 cryptate:diphos ratio	37.27	4.97	10.23
Predicted: 1:1 cryptate:diphos ratio	43.07	5.19	8.73
Found:	41.88	4.86	7.13

9.1.4.4. Sodium diethyldithiocarbamate

A fine yellow precipitate forms immediately from the reaction of diethyldithiocarbamate with the disilver cryptate. This solid, when dried, proved to be insoluble in a wide range of solvents, and no FAB mass spectrum could be obtained. Its infrared spectrum was compared to that of an authentic sample of silver diethyl-dithiocarbamate complex (prepared by reaction of silver(I) triflate with sodium diethyldithiocarbamate), and the two spectra are identical (Figure 9-8 A and B), showing no sign of any crypt-related absorption. Thus, in a similar manner to the imBT complex, the S-donor ligand has proven too strong, and abstracted silver from the cryptate.

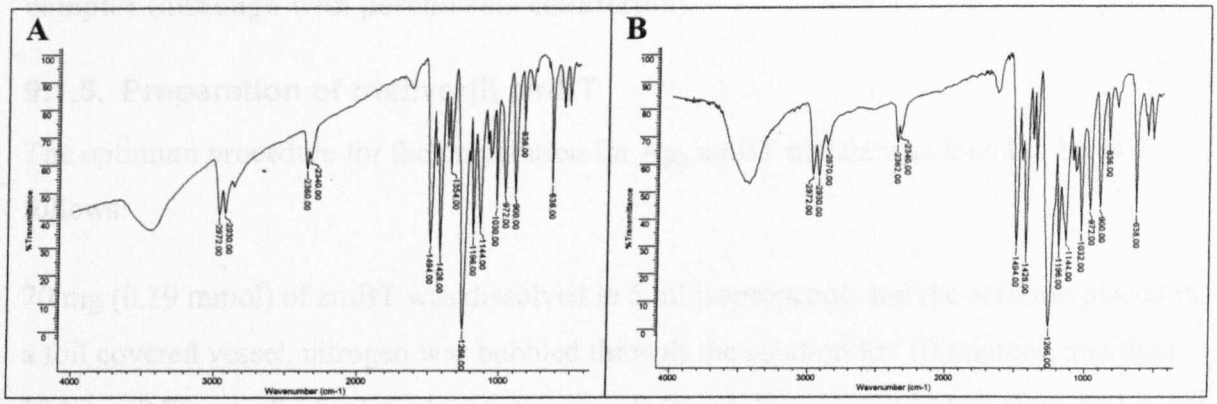

Figure 9-8: Infrared spectra of A) the yellow precipitate from reaction of dithiocarbamate with disilver amBT, and B) authentic silver diethyl-dithiocarbamate complex.

9.1.4.5. Thiophenol

Thiophenol behaved in a similar fashion to diethyl-dithiocarbamate in the previous section, forming a white precipitate of silver thiophenol triflate in a short time. The identity of the product was confirmed by comparison of its infrared spectrum to that of a silver thiophenol complex prepared separately in the absence of any other ligand (Figure 9-9 A and B). Once again, no signs of the key crypt-related peaks, such as NH stretches, were observed in the spectrum.

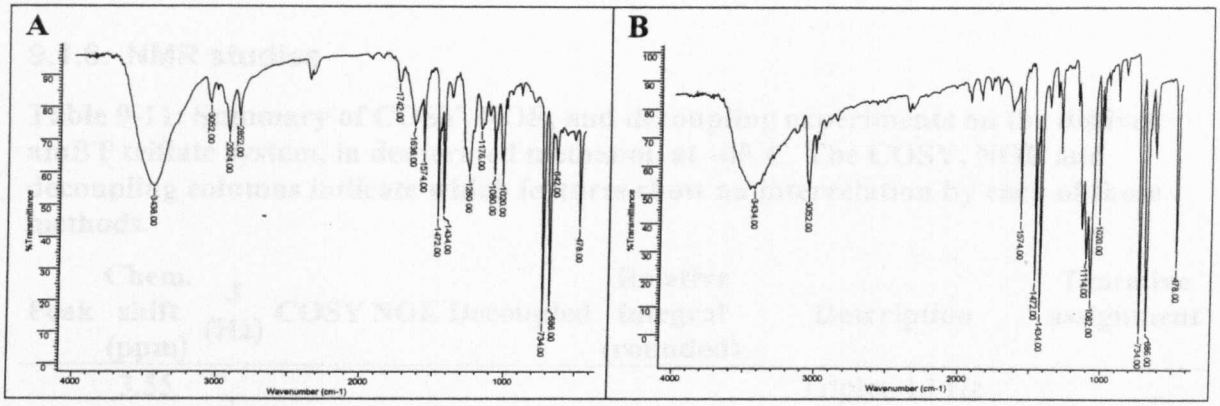

Figure 9-9: Infrared spectra of A) the solid isolated from the reaction of disilver amBT triflate with thiophenol, and B) an authentic sample of a silver thiophenol complex (although with perchlorate counterion).

9.1.5. Preparation of trisilver(I) amBT

The optimum procedure for the preparation for Ag_3 amBT triflate was found to be as follows:

70 mg (0.19 mmol) of amBT was dissolved in 5 ml isopropanol, and the solution placed in a foil covered vessel, nitrogen was bubbled through the solution for 10 minutes, and then 194 mg (0.76 mmol) of solid silver trifluoromethanesulphonate was added, and a foil cover placed over the top of the vessel. The gas flow continued for another 30 minutes, and the vessel was then left sealed in the dark for 9 days. A colourless solution with insoluble black solid was obtained after this time, the supernatant solution was transferred to a clean vial, and crystals were obtained by the slow diffusion of ether into the solution. Yield 56 mg (26 %).

9.1.6. NMR studies

Table 9-11: Summary of COSY, NOE, and decoupling experiments on the disilver amBT triflate system, in deuterated methanol, at –45°C. The COSY, NOE and decoupling columns indicate which features show an interrelation by each of those methods.

Peak	Chem. shift (ppm)	J (Hz)	COSY	NOE	Decoupled	Relative integral (rounded)	Description	Tentative assignment
a	3.55 3.53 3.5	13.5 12.9	h, c	h?	h	1	Triplet, 13 Hz splitting, 1 proton. Couples to part of h, and c, near h and maybe b, c, e, g	HB_{ax}
b	3.37 3.33	19.5	j			1	Doublet? 19.5 Hz splitting, 1 proton. May couple to j, near f/g, j, a	HA (ax or eq)
c	3.24 3.21 3.19	12.2 9.6	a, h, i, e			3	Triplet or overlapping doublets, 9, 12 Hz splittings, 3 protons. Couples to a, h, i, e, near to l, k, a	
d	3.16 3.14 3.11 3.08	14.4 14.7 13	l, h?, i? e?			3	Overlapping doublets, 13-14 Hz splittings, 3 protons. Couples to l, and maybe h, i, e also. Near to j, f/g, h	HC_{ax} lies in this region
e	3.02 3 2.99 2.97 2.95 2.94	8.9 8.3 8.2 8 8.5	k, c, d?, h?, i?			5	Overlapping doublet/triplets, 8-9 Hz splittings, 5 protons. Couples to k and c, and maybe d, h, i. Near to k, j, a, h, f/g	
f	2.82 2.8	9.4	k, i	h?	j, i, e, k?	4	Doublet? 9-10 Hz splitting, 4 protons. Couples to k and i, near to j, h and maybe b, c, d, e.	
g	2.76	10.5	j, i	h?	j, i, e, k?	2	Doublet, 10.5 Hz splitting, 2 protons.	

	2.74						Couples to j and i, near to k, a and maybe b, c, d, e.	
h	2.67 2.65 2.64 2.61	11.5 5.9 12.2	a, c, d?, e?, k		k, a, c	10	Probably 4 or 5 overlapping features, 10 protons. Couplings to a, c, k, and maybe d and e. Near to l, k, j, a, f and maybe d, e	
i	2.53 2.51 2.48 2.46 2.44 2.41	12.6 11.5 10.7 12.6. 11.7	c, f, d?, g, e?			4	Overlapping doublets/triplets 10-12 Hz splittings, 4 protons. Couples to c, f, g, and maybe d and e. Near to k, j.	HB_{eq} lies in this region
j	2.25 2.24 2.22 2.21	7.7 6.9 8	b, g	e, f, g, h	b, g	1	Complex doublet, 7-8 Hz splitting, 1 proton? Couples to b and g, near to f, h, e, and maybe b, d, i, k	HA (ax or eq)
k	2.06 2.04 2.02 1.99	7.8 11.4 11	e, f, h	f, g, h	f, h	3	Complex doublet, 8-11 Hz splitting, 3 protons. Couples to f, h and maybe e, near to l, j, g, h and maybe i, e, c	
l	1.83 1.8	12.6	d			1	Doublet, 12.6 Hz splitting, 1 proton. Couples to d, maybe near to c, k, h	HC_{eq}

9.1.7. Electrochemical studies

Cyclic voltammetric studies of the cryptates were conducted using an Autolab PGSTAT10 potentiostat, with a Ag/AgCl reference electrode and platinum auxiliary electrode, and various working electrodes.

Comparisons with silver, and gold working electrodes were made at the outset of the studies, a comparison of cyclic voltammograms is shown in Figure 9-10 (A). The silver electrode was strongly oxidised under experimental conditions, and the gold electrode also appeared susceptible to this effect as in some initial scans a very marked deposition on the electrode was noted. Platinum appeared not to suffer from this to such a degree, and this electrode was used exclusively thereafter.

0.1 M tetrabutylammonium perchlorate in freshly distilled acetonitrile, anhydrous propylene carbonate (Aldrich, sureseal), propionitrile, or butyronitrile (both Lancaster) was used as electrolyte, and a comparison of the electrolyte only voltammograms is shown in Figure 9-10 (B). Propionitrile was only used on one occasion, and the pure electrolyte voltammogram contained several peaks, which were not removed by cleaning the electrode, or replacing the electrolyte. Since the longer chain butyronitrile gave a comparatively simple electrolyte voltammogram, no further investigations were made using propionitrile.

Choice of a different solvent is expected to affect the observed behaviour of the analyte. Nitrile containing solvents (acetonitrile and butyronitrile) are considered good solvents for both oxidative and reductive processes (17), and have the additional feature that they coordinate relatively well to silver(I), and therefore any redox processes resulting in the production of this ion will be favoured. Other solvents, such as propylene carbonate will not stabilise silver(I), and therefore more detail in other regions of the voltammogram may be observed. Change in solvent will also shift the potential at which redox processes occur, as a result of the change in dielectric constant and in the degree of stabilisation provided by the solvent for the initial and final states of the redox process.

Somewhat variable electrolyte-only voltammograms were observed with propylene carbonate (Figure 9-10 B), suggesting that some of the redox processes are owing to the presence of trace contaminants, such as water. The peaks observed are:

- oxidations at +1.3 V, –0.1 V (weak), and another possible weak oxidation wave at -0.6 V

- reductions at +0.66 V, –0.31 V and –1.3 V, as well as possible weak reduction waves at 0.9 V and 0.2 V

Voltammograms of free ligand are complicated by the fact that the ligand was usually obtained as a hydrate, and water features will therefore overlay the ligand features.

Different behaviour is noted in the different solvents used. The propylene carbonate solution of amBT shows a pair of poorly reversible waves centred at ~ -0.25 V and –0.84 V. Only the more negative of these appears in the acetonitrile solution, and in that case only weakly. The –0.25 V peak appears in Figure 9-10 B for propylene carbonate and propionitrile electrolyte-only voltammograms, and is assigned to solvent or vessel impurity.

A broad poorly defined oxidative feature at ~0.85 V in acetonitrile is not easy to observe in propylene carbonate, because of impurity features close to that potential. This peak may be due to the expected oxidative dehydrogenation of the amine ligand.

The more positive potential feature in propylene carbonate is absent in acetonitrile and blank electrolyte solution, and may come from further ligand oxidation or the oxidation of water.

For silver triflate (Figure 9-10 D):

- an oxidation at –0.1 V, which appears to be dependent on a reduction occurring below –0.8 V (which cannot be discerned, and may coincide with an electrolyte feature). This peak may relate to oxidation of Ag(0) to Ag(I), such as appears in the well-known "stripping" process.

- a split feature around +1.6 V overlying the 1.3 V electrolyte feature. This presumably originates in oxidation of Ag(I), possibly associated with oxidative dehydrogenation of the ligand.

Note that all cyclic voltammograms in this work are shown with increasing positive voltage on the x axis (*i.e.* increasingly oxidative environment) and increasing current on the y axis, with the result that oxidative features appear on the upper portion of the plot, and reductive features on the lower portion. Each voltammogram began with voltage at the

most negative limit, where it was held for 3 seconds to equilibrate the system, before running the oxidation/reduction cycle at least three times. The third scan from each set is reproduced in this section, with the result that oxidation features in these voltammograms may relate to oxidation of a reduced species not originally present, but generated during a prior reduction phase. Except where otherwise noted, voltammograms were recorded at room temperature, with a scan rate of 100 mV/s, and stationary electrode.

Sample solutions were prepared by adding the solid sample directly to the electrolyte solution after the initial pure electrolyte scans had been measured. On each occasion, these scans were compared to previously measured voltammograms, in order to ensure that there was no discrepancy in the electrolyte solution. On some occasions it proved that the electrode required cleaning before the pure electrolyte scan gave an acceptably flat baseline. All measurements were performed after degassing by bubbling nitrogen through the solution, and a nitrogen headspace was maintained above solutions during measurements.

Following the observation that subsequent sets of duplicate scans differed in some respects, a cleaning regime was adopted between each set of 3 scans. This consisted of briefly stirring the working electrode in 10% nitric acid, then deionised water, and blotting dry, then stirring in the electrolyte solution and again blotting dry. The observed discrepancies presumably resulted from accumulation of adsorbed species on the electrode surface, and were significantly reduced with regular cleaning.

Nevertheless, throughout the course of these studies we struggled to overcome other interferences such as silver stripping, and adsorption of other moieties onto the electrode, and various strategies were attempted in order to overcome these (see section 2.5.1).

All voltages reported in this section are given with reference to Ag/AgCl. Scans of ferrocene in the various solvents were made, in order to establish the correction needed for comparison to the standard hydrogen electrode (where ferricinium is reduced to ferrocene at +0.400 V, (18)); and these additive factors are given in Table 9-12.

Table 9-12: Correction factors needed to relate the reported data (which were recorded vs Ag/AgCl) to the standard hydrogen electrode.

Solvent	Correction factor
Acetonitrile	+0.104 V
Butyronitrile	–0.063 V
Propylene carbonate	–0.012 V

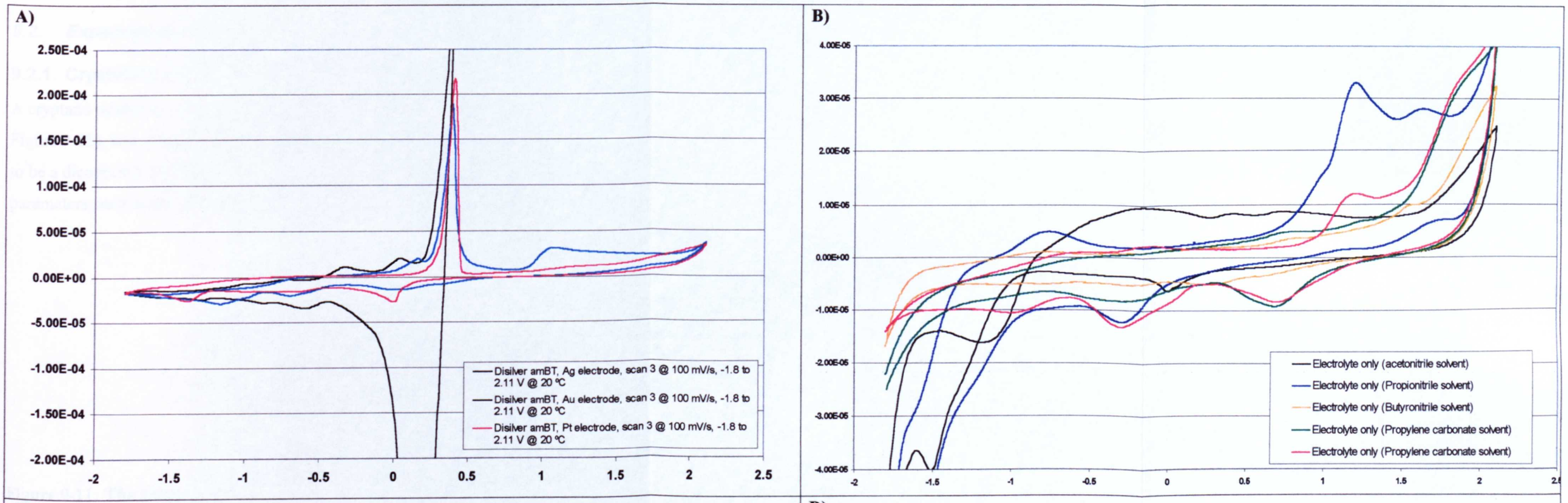

Figure 9-10: A) Comparison of the disilver amBT voltammogram with different electrodes. All three electrodes were affected by stripping, however the silver electrode was continuously oxidised above 0.2 V. B) Comparison of electrolyte only voltammograms in different solvents. Two propylene carbonate voltammograms, recorded on different occasions are presented to show the variability in background. C) Cyclic voltammograms of free ligand compared to pure electrolyte at two different scanning speeds (in propylene carbonate, and acetonitrile, with peak potentials marked). D) Silver triflate voltammograms compared to pure electrolyte (in propylene carbonate).

9.2. Experimental details for Chapter 3

9.2.1. Crystallographic study of dicopper(I) iminocryptate

A cryptand related to the imBT/amBT system, but incorporating a pyridazine spacer (see Figure 9-11), was being studied by Professor Nelson, and the isolation of a crystal believed to be a dicopper(I) cryptate provided an opportunity to directly compare structural parameters such as helicity in relation to a larger metal–metal separation.

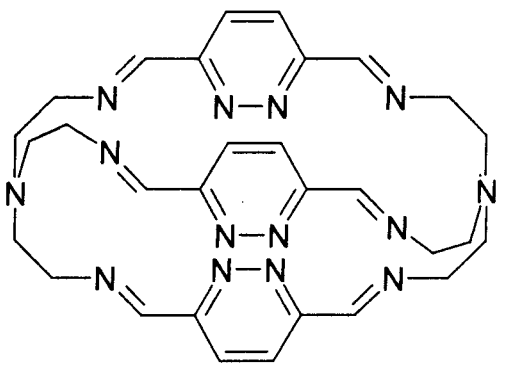

Figure 9-11: The iminocryptand ligand 3pd, incorporating pyridazine spacers with tren caps.

Data for $Cu(I)_2$ 3pd $(BF_4)_2$ was collected by the author on a Bruker SMART 1000. Details of the data collection and refinement are given in Table 9-13. The structure was solved using direct methods, and refined with assistance from Prof Vickie McKee and Dr Sally Brooker using full matrix least-squares on F^2, using SHELXTL (1). Data beyond 50° was omitted from the refinement as well as three reflections which were behind the beam stop. Non-hydrogen atoms were refined with anisotropic atomic displacement parameters. Hydrogen atoms were inserted at calculated positions with isotropic displacement parameters riding on U_{ij} of their carrier atoms.

A graphical representation of the structure is shown in Figure 9-12, the asymmetric unit is fully ordered, one counterion was reasonably well ordered, and the other is modelled as 52% and 48% contributions of two positions resulting from rotation around the central boron. The best refinement was obtained with two pairs of pyridazine nitrogens pointing inwards, and one pair pointing out of the cryptate. Residual electron density of 3.14 e $Å^{-1}$ lies too near to Cu(2) to be chemically sensible.

The copper ions have trigonal pyramidal geometry, are separated by 6.48 Å and lie below the equatorial plane resulting in slightly elongated Cu–N_{ax} distances (2.251 and 2.246 Å, compared to Cu–N_{eq} distances ranging from 1.994 to 2.046 Å, see Table 9-14 for selected

bond lengths and angles). This position for the copper is more likely to result from space constraints within the cap than from any interaction with the inward pointing pyridazine nitrogens (which are more than 3 Å distant). Indeed, the observation that one pair of pyridazine nitrogens is actually pointing outwards suggests that there is no appreciable interaction occurring over this distance.

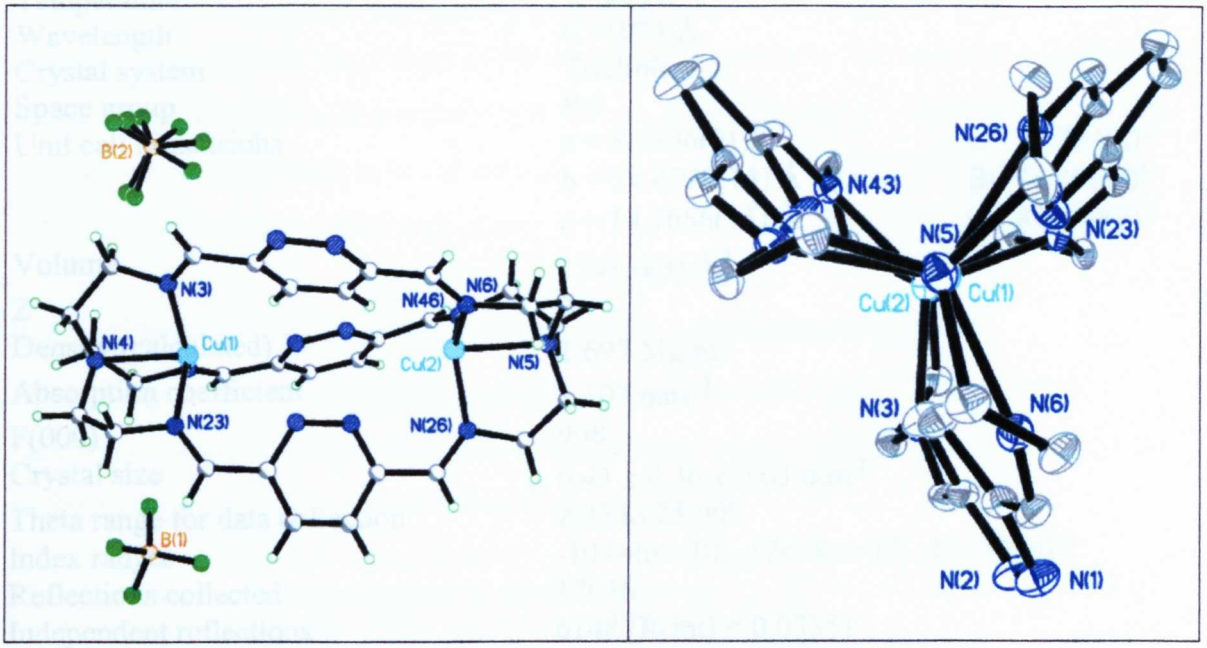

Figure 9-12: A) Perspective view of the cryptate with two BF_4 ions, and B) View along the N-Cu-Cu-N axis with 40% thermal ellipsoids, showing the slight degree of helicity.

Table 9-13: Crystal data and structure refinement for $Cu(I)_2$ 3pd $(BF_4)_2$.

Identification code	$Cu(I)_2$ 3pd $(BF_4)_2$	
Empirical formula	C30 H36 B2 Cu2 F8 N14	
Formula weight	893.43	
Temperature	153(2) K	
Wavelength	0.71073 Å	
Crystal system	Triclinic	
Space group	P-1	
Unit cell dimensions	a = 8.6996(9) Å	α= 77.724(2)°
	b = 14.4770(14) Å	β= 74.268(2)°
	c = 14.7656(15) Å	γ = 85.530(2)°
Volume	1748.6(3) $Å^3$	
Z	2	
Density (calculated)	1.697 Mg/m^3	
Absorption coefficient	1.307 mm^{-1}	
F(000)	908	
Crystal size	0.43 x 0.36 x 0.03 mm^3	
Theta range for data collection	2.25 to 25.00°.	
Index ranges	-10<=h<=10, -17<=k<=17, -17<=l<=17	
Reflections collected	17036	
Independent reflections	6148 [R(int) = 0.0335]	
Completeness to theta = 25.00°	99.7 %	
Absorption correction	Multiscan	
Max. and min. transmission	1.00 and 0.84	
Refinement method	Full-matrix least-squares on F^2	
Data / restraints / parameters	6148 / 6 / 541	
Goodness-of-fit on F^2	0.983	
Final R indices [I>2sigma(I)]	R1 = 0.0554, wR2 = 0.1321	
R indices (all data)	R1 = 0.0760, wR2 = 0.1430	
Largest diff. peak and hole	3.101 and -0.514 $e.Å^{-3}$	

Table 9-14: Selected bond lengths and angles for $Cu(I)_2$ 3pd $(BF_4)_2$.

Bond length /Å		Bond angle /°	
Cu(1)-N(23)	1.998(4)	N(23)-Cu(1)-N(3)	129.64(14)
Cu(1)-N(3)	2.045(4)	N(23)-Cu(1)-N(43)	113.96(14)
Cu(1)-N(43)	2.045(3)	N(3)-Cu(1)-N(43)	112.26(14)
Cu(1)-N(4)	2.247(3)	N(23)-Cu(1)-N(4)	85.01(13)
Cu(2)-N(46)	1.994(3)	N(3)-Cu(1)-N(4)	82.36(13)
Cu(2)-N(6)	2.018(4)	N(43)-Cu(1)-N(4)	82.27(13)
Cu(2)-N(26)	2.033(3)	N(46)-Cu(2)-N(6)	121.48(14)
Cu(2)-N(5)	2.248(3)	N(46)-Cu(2)-N(26)	111.19(14)
		N(6)-Cu(2)-N(26)	123.30(14)
		N(46)-Cu(2)-N(5)	83.79(13)
		N(6)-Cu(2)-N(5)	83.50(14)
		N(26)-Cu(2)-N(5)	82.67(13)

9.2.2. Preparation of copper(I) perchlorate

$Cu^{I}(MeCN)_4ClO_4$ was prepared via the conproportionation of 15.55 g (41.8 mmol) of $Cu^{II}(ClO_4)_2.6H_2O$ with 8 g (130 mmol) of metallic copper powder (cleaned by stirring in acetone/iodine for 15 minutes, then washing with acetone, then 1M HCl, then acetone again, and finally ether) in 100 ml of dried distilled acetonitrile. The mixture (copper solid in a green solution) was stirred overnight, and on the following day the colour had faded and a white powder (with traces of metallic copper) was filtered from the colourless solution on a frit and washed with ether.

9.2.3. Chiral chromatography for resolution of dicopper(I) imBT

The column support used an aqueous suspension of Sephadex SPC25. The sample (aqueous) was pipetted onto to the top of the column, where it adsorbed onto the top layer of Sephadex, resulting in a band about 12 mm thick.

The eluent was aqueous potassium L-dibenzoyl tartrate (0.025 M), which was applied to the top of the column using a peristaltic pump. The dark yellow/green band of sample initially spread out, and separated quickly from a small amount of a green/blue substance, probably the average valence dicopper(1.5) species.

Once the leading edge of the band was nearing the bottom of the (approximately 1 m long) column, the pump setup was rearranged so that the eluent would recirculate. The column was run over a period of a week, during which time the sample band spread out to about 30 cm in length, but showed no sign of separating into two bands. The band was eluted in three fractions, each of approximately 70 ml and having a blue/green colour. The leading and tailing fractions were converted to the PF_6^- salt by adding an excess of KPF_6 to the aqueous eluate, and extracting with dichloromethane. The dichloromethane layers were evaporated, and the finely dispersed solid reconstituted in acetonitrile and allowed to concentrate slowly. The products finally obtained had a definite blue/green (rather than yellow/green) colour, and it is strongly suspected that over the extended period in aqueous solution, oxidation of the copper has occurred, possibly in conjunction with hydrolysis of the ligand, as has been proposed for the manganese(II) cryptate (see Chapter 6, and (2, 3)).

9.2.4. Crystallisation techniques and crystallographic screening

Dicopper(I) imBT perchlorate was dissolved in the minimum volume of acetonitrile, and one equivalent of potassium antimonyl tartrate, or potassium tartrate dissolved in water was added. The solution was placed in a vessel with only a small puncture in the top, and left to stand undisturbed. Crystals began to form after 2 to 3 days, and random samples were taken for crystallographic screening.

9.2.5. Preparation of copper(II) D-tartrate

Copper(II) D-tartrate was prepared by dissolving 1 g of D-tartaric acid in 10 ml of water, and adding 0.823 g of powdered copper(II) carbonate to the solution. A moderately fast effervescence was observed for 15 minutes, although there was no colour change, and no apparent dissolution of the solid. The mixture was heated slightly with stirring once the visible reaction had stopped, but no further effervescence was noted. The stirring continued for a further 3 hours, after which the grey green solid was filtered off and dried.

9.2.6. Crystallographic study of $Cu(I)_2$ imBT $(BF_4)_2$

Data for $Cu(I)_2$ imBT $(BF_4)_2$ was collected by the author on a Bruker SMART 1000. Details of the data collection and refinement are given in Table 9-15. The structure was solved using direct methods, and refined with assistance from Prof Vickie McKee using full matrix least-squares on F^2, using SHELXTL (1). One reflection obscured by the beam stop was omitted from the refinement. Non-hydrogen atoms were refined with anisotropic atomic displacement parameters. Hydrogen atoms were inserted at calculated positions with isotropic displacement parameters riding on U_{ij} of their carrier atoms.

Table 9-16 gives selected bond lengths and angles, the copper-copper separation is very slightly longer than in the cryptate with perchlorate counterion.

Table 9-15: Crystal data and structure refinement for $Cu(I)_2$ imBT $(BF_4)_2$.

Identification code	$Cu(I)_2$ imBT $(BF_4)_2$	
Empirical formula	C18 H30 B2 Cu2 F8 N8 O0.33	
Formula weight	664.53	
Temperature	153(2) K	
Wavelength	0.71073 Å	
Crystal system	Rhombohedral	
Space group	R-3c	
Unit cell dimensions	a = 8.5992(5) Å	α= 90°
	b = 8.5992(5) Å	β= 90°
	c = 61.387(5) Å	γ= 120°
Volume	3931.1(5) $Å^3$	
Z	6	
Density (calculated)	1.684 Mg/m^3	
Absorption coefficient	1.706 mm^{-1}	
F(000)	2020	
Crystal size	0.41 x 0.29 x 0.07 mm^3	
Theta range for data collection	2.81 to 28.65°.	
Index ranges	-10<=h<=11, -11<=k<=11, -79<=l<=79	
Reflections collected	13542	
Independent reflections	1083 [R(int) = 0.0925]	
Completeness to theta = 28.65°	94.9 %	
Absorption correction	Multiscan	
Max. and min. transmission	0.948637 and 0.352525	
Refinement method	Full-matrix least-squares on F^2	
Data / restraints / parameters	1083 / 0 / 61	
Goodness-of-fit on F^2	1.110	
Final R indices [I>2sigma(I)]	R1 = 0.0436, wR2 = 0.1210	
R indices (all data)	R1 = 0.0503, wR2 = 0.1257	
Largest diff. peak and hole	1.366 and -0.363 $e.Å^{-3}$	

Table 9-16: Selected bond lengths and angles for $Cu(I)_2$ imBT $(BF_4)_2$.

Bond length /Å		Bond angle /°	
Cu(1)-N(3)	1.999(2)	N(3)-Cu(1)-N(3)#1	119.206(19)
Cu(1)-N(3)#1	1.999(2)	N(3)-Cu(1)-N(3)#2	119.206(19)
Cu(1)-N(3)#2	1.999(2)	N(3)#1-Cu(1)-N(3)#2	119.206(19)
Cu(1)-N(1)	2.218(4)	N(3)-Cu(1)-N(1)	84.86(6)
Cu(1)-Cu(1)#3	2.4561(10)	N(3)#1-Cu(1)-N(1)	84.86(6)
		N(3)#2-Cu(1)-N(1)	84.86(6)
		N(3)-Cu(1)-Cu(1)#3	95.14(6)
		N(3)#1-Cu(1)-Cu(1)#3	95.14(6)
		N(3)#2-Cu(1)-Cu(1)#3	95.14(6)
		N(1)-Cu(1)-Cu(1)#3	180.0

Symmetry transformations used to generate equivalent atoms:
#1 -y+1,x-y,z #2 -x+y+1,-x+1,z #3 y+1/3,x-1/3,-z+1/6

9.3. Experimental details for Chapter 4

9.3.1. Phenyl substitution at C_A

9.3.1.1. Synthesis of free podand

The procedure used for preparation of trac (see Chapter 6, (4)) was modified for phenyl glyoxal. Four equivalents of phenyl glyoxal were added to a refluxing solution of tren in benzene, with a Dean-Stark trap. The solution gradually darkened from yellow to reddish, and after 12 hours at reflux was evaporated to a red oil. Unreacted glyoxal was removed from the oil by extraction with water from a chloroform solution. This formed a glass when pumped in a vacuum desiccator overnight.

9.3.1.2. Manganese complex

One equivalent of Mn(II) triflate in MeCN was added to a refluxing solution in 50:50 MeCN/EtOH of the red glass discussed above (section 9.3.1). There was no visible reaction, and the reddish solution was evaporated to a brown solid.

9.3.2. Methyl substitution at C_A

9.3.2.1. Synthesis of free cryptand

The direct approach of attempting preparation of the free ligand was carried out by slowly adding methyl glyoxal solution (3 equivalents, 40% aqueous, diluted in isopropanol) to tren (2 equivalents, in isopropanol at 0°C), in an analogous manner to the preparation of imBT (5). ^{1}H NMR of the reaction mixture, after stirring overnight at room temperature and then heating to reflux, showed that no imine protons (indicative of Schiff base formation) were present.

9.3.2.2. Template synthesis of cryptate

One equivalent of strontium perchlorate and three of aqueous methyl glyoxal were dissolved together in isopropanol, then two equivalents of tren in isopropanol added under rate limiting conditions (slow addition of a dilute solution at low temperature). An orange/brown solid formed from the solution, and was proved to be insoluble in water and methanol, however it dissolved well in acetone and acetonitrile.

9.3.2.3. Direct synthesis of podand

Somewhat forcing reaction conditions were used for preparation of a podand. More than 3 equivalents of methyl glyoxal (40% aqueous solution) were added dropwise to tren in

refluxing benzene, with a Dean-Stark trap to collect water generated during the reaction (as well as from the methyl glyoxal solution). A completely insoluble (probably polymeric) solid separated from the mixture, and the solution was reduced to a yellow oil, which was partitioned between chloroform and water to try and remove excess amine and glyoxal.

9.3.2.4. Synthesis of copper(I) podate

An attempt to form a copper(I) complex using the oil (described in section 9.3.2.3) was made by adding solid Cu(I) $(MeCN)_4$ ClO_4 to a methanolic solution of the oil under a nitrogen atmosphere. When the volume of the mixture was reduced, a blue glass was obtained.

9.3.3. Hydroxy substitution at C_A

9.3.3.1. Template synthesis of cryptate

Strontium(II) perchlorate was used as template together with the (50% aqueous) acid in isopropanol. Tren (also in isopropanol) was added dropwise. No reaction was apparent, however after refluxing the solution 1 hour a yellow solution was obtained, which intensified to red overnight. A dark red oil was obtained when the volume was reduced, which could only be redissolved in water. Addition of tetraphenylborate to an aqueous solution resulted in precipitation of a brown solid.

9.4. Experimental details for Chapter 5

9.4.1. Preparation of the cap (abap.4HCl.2$H_2$0)

Preparative methods reported by (6) and (7) were used in the preparation of abap. The primary amine groups of the starting compound dipropylenetriamine were protected using a phthalimide group as follows:

59.3 g of phthalic anhydride was melted at 180°C and 26.3 g of dipropylenetriamine added dropwise with stirring. A vigorous reaction occurred with production of white smoke, and once the reaction had ceased the mixture was poured into a large mortar and allowed to cool. A glassy reddish solid was obtained, which was ground to a powder and recrystallised from ethanol.

27.7 g of the phthalimide protected triamine was melted at 155°C, and 18 g of solid (2-bromoethyl)phthalimide added over a period of 10 minutes. The mixture was stirred at

160-170°C for 45 minutes, poured into a large mortar and allowed to cool. This solid was again ground to a powder, and then refluxed in 8 M HCl for 11 hours.

The dark solution obtained was cooled in ice, and filtered to remove the phthalic acid by-product, and the filtrate was dried in a rotovap. The crude product was purified using the following procedure: The crude was dissolved in the minimum volume of water, filtered through celite, and the filtrate added dropwise to 500 ml of EtOH. The precipitate obtained after standing overnight and cooling in ice was filtered off, and suspended in 300 ml of hot EtOH, and then sufficient water added to just dissolve the solid. A further 300 ml of EtOH was added, and the solution allowed to cool overnight, then further cooled in ice, and the pure off-white crystals obtained filtered off.

9.4.2. AB3Bm

9.4.2.1. Free cryptand

Conversion of abap.4HCl.2H_2O to the free amine was attempted by dissolving 200 mg (3.56 mmol) of KOH in methanol, and adding 250 mg (0.7 mmol) of solid abap.4HCl.2H_2O to the solution, and stirring for 10 minutes at room temperature. The volume of the mixture was reduced to 5 ml using a rotovap (the solvent was not completely removed, to avoid evaporating the amine), and the amine solution obtained filtered to remove solid KCl.

1.5 equivalents (140 mg, 1.05 mmol) of isophthalaldehyde was dissolved in 200 ml of methanol and brought to reflux. The amine solution was added dropwise over a period of 5 minutes: there was no colour change. The solution was refluxed a further 4 hours, and left to sit for one day. The pale yellow solution was evaporated to dryness in a rotovap, and the yellow oil with some white solid was placed in a vacuum dessicator. The following morning a rubbery yellow film was obtained. This solid was insoluble in acetonitrile, methanol, DMF, and water, but very slightly soluble in chloroform. Attempts to recrystallise the solid with chloroform only succeeded in regenerating an oil or glass. An attempt was also made to extract the solid using a soxhlet with hexane/heptane, however no product was recovered.

9.4.2.2. Silver(I) cryptate

9.4.2.2.1. 1st attempt

The method described for the free ligand above was repeated, and 1 equivalent (180 mg) of solid silver triflate was added to the refluxing yellow solution, in a darkened vessel. The solution was stirred at room temperature for one further hour, no visible reaction occurred in this time.

The pale yellow solution was divided into two fractions, and one was rotovaped to dryness in a foil covered flask., giving specks of a brown solid embedded in a grey glass, which was insoluble in methanol, acetonitrile and chloroform, but slightly soluble in DMF, giving a brownish solution. This solution was left to concentrate in the dark for 2 weeks, and then transferred to an ether jar.

The second fraction was placed in a foil covered vessel and left to slowly concentrate in the dark. After four weeks a powdery white solid was observed in the base of the flask, together with a cream coloured solid.

9.4.2.2.2. 2nd attempt

A second preparation was carried out, in this case nitrate anion was used instead of triflate. 1 g (2.8 mmol) of abap·4HCl·$2H_2O$ was converted to the free base using a stoichiometric amount of KOH in 20 ml of MeOH, and the filtrate added to a refluxing solution of 565 mg (4.2 mmol) of isophthalaldehyde in 150 ml of methanol. Some pale yellow solid formed immediately, and after the solution had been refluxed for 3 hours a large amount of an insoluble rubbery yellow solid was present. One half of the remaining solution was treated with 120 mg (0.70 mmol) of solid silver nitrate: there was no visible reaction (the other half was used in the preparation of a copper(I) complex, see section 9.4.2.3 below). The mixture was stirred for 2 hours under nitrogen, and left to concentrate in the dark for 2 days. No solid was obtained after this time, and the solution was dried in a rotovap, and reconstituted in the minimum volume of acetonitrile. After 4 days in an ether jar several colourless crystals (blocks) were obtained, together with some more brown/yellow solid.

9.4.2.2.3. Crystallography

Data for $Ag(I)_2$ AB3Bm $(NO_3)_2$ was collected by the author on a Bruker SMART 1000. Details of the data collection and refinement are given in Table 9-17. The structure was solved by the author using direct methods, and refined with assistance from Prof Vickie

McKee using full matrix least-squares on F^2, using SHELXTL (1). Data beyond 45° was omitted as it was weak. All non-hydrogen atoms in the cryptate were ordered, and were refined with anisotropic atomic displacement parameters. Hydrogen atoms were inserted at calculated positions with isotropic displacement parameters riding on U_{ij} of their carrier atoms.

One nitrate ion (N4) showed slight disorder, and its component atoms were restrained to coplanar geometry. The other nitrate was refined with isotropic atomic displacement parameters and restrained to the same geometry. One full occupancy methanol molecule (C1) was ordered, and its hydrogens were modelled in riding positions. The second half occupancy methanol was restrained to the same C-O distance, and refined with isotropic atomic displacement parameters.

The water-to-nitrate distances (Table 9-19) suggest that the nitrates are bridged via hydrogen bonds with water. The distance between the full occupancy methanol hydroxy oxygen and the nearest nitrate is also consistent with H bonding.

Table 9-17: Crystal data and structure refinement for $Ag(I)_2$ AB3Bm $(NO_3)_2$.

Identification code	Ag(I)2 AB3Bm $(NO_3)_2$
Empirical formula	C41.50 H54 Ag2 N10 O8.50
Formula weight	1044.69
Temperature	153(2) K
Wavelength	0.71073 Å
Crystal system	Triclinic
Space group	P-1
Unit cell dimensions	a = 9.5814(13) Å α= 79.576(3)°
	b = 12.823(2) Å β= 85.825(4)°
	c = 18.853(3) Å γ = 78.016(4)°
Volume	2227.0(6) $Å^3$
Z	2
Density (calculated)	1.558 Mg/m^3
Absorption coefficient	0.943 mm^{-1}
F(000)	1070
Crystal size	0.10 x 0.07 x 0.03 mm^3
Theta range for data collection	1.65 to 22.50°.
Index ranges	-10<=h<=10, -13<=k<=13, -20<=l<=20
Reflections collected	12175
Independent reflections	5785 [R(int) = 0.0936]
Completeness to theta = 22.50°	99.1 %
Absorption correction	Multiscan
Refinement method	Full-matrix least-squares on F^2
Data / restraints / parameters	5785 / 17 / 540
Goodness-of-fit on F^2	1.056
Final R indices [I>2sigma(I)]	R1 = 0.0787, wR2 = 0.1891
R indices (all data)	R1 = 0.1425, wR2 = 0.2311
Largest diff. peak and hole	2.162 and -2.226 $e.Å^{-3}$

Table 9-18: Selected bond lengths and angles for $Ag(I)_2$ AB3Bm $(NO_3)_2$.

Bond length /Å		Bond angle /°	
Ag(1)-N(3A)	2.286(10)	N(3A)-Ag(1)-N(3C)	123.4(4)
Ag(1)-N(3C)	2.310(11)	N(3A)-Ag(1)-N(3B)	120.7(4)
Ag(1)-N(3B)	2.318(10)	N(3C)-Ag(1)-N(3B)	110.7(3)
Ag(1)-N(1A)	2.475(10)	N(3A)-Ag(1)-N(1A)	86.9(3)
Ag(1)- Ag(2)	3.6062(15)	N(3C)-Ag(1)-N(1A)	74.0(3)
Ag(2)-N(4C)	2.264(12)	N(3B)-Ag(1)-N(1A)	86.0(3)
Ag(2)-N(4B)	2.291(12)	N(4C)-Ag(2)-N(4B)	118.9(4)
Ag(2)-N(4A)	2.302(17)	N(4C)-Ag(2)-N(4A)	125.2(5)
Ag(2)-N(2A)	2.455(11)	N(4B)-Ag(2)-N(4A)	111.5(4)
		N(4C)-Ag(2)-N(2A)	86.3(4)
		N(4B)-Ag(2)-N(2A)	84.7(4)
		N(4A)-Ag(2)-N(2A)	78.0(4)

Table 9-19: Hydrogen bonding distances (Å) for $Ag(I)_2$ AB3Bm $(NO_3)_2$.

Donor	Acceptor	Distance /Å
O1W	O31	3.1811 (0.0221)
O1W	O33	2.6703 (0.0251)
O1W	O42	2.8797 (0.0294)
O11	O32	2.8330 (0.0257)
O11	N3	3.4232 (0.0295)

9.4.2.3. Copper(I) cryptate

To approximately 80 ml of a methanolic solution containing not more than 0.7 mmol of AB3Bm (preparation described in section 9.4.2.1 above), 250 mg of $Cu^{I}(MeCN)_4ClO_4$ in MeOH was added, causing an immediate change to a bright yellow solution, and then cloudy green as addition continued. A light green powder was filtered off, its infrared spectrum showed imine and perchlorate peaks, together with signs of amine. The powder, believed to be a partly formed crypt, was soluble in acetonitrile, but could not be crystallised. The filtrate of the reaction mixture was placed in an ether jar, and after 4 days a crop of bright yellow crystals was obtained. When inspected under a microscope the surfaces of these crystals proved to be nearly half covered in small, dark green, non-crystalline particles. The best crystal found in the crop was only barely acceptable for X-ray analysis (see Structure A, section 9.4.2.3.1). Good quality crystals were obtained by slow diffusion of ether into a solution in acetonitrile of the initial crop (see Structure B, section 9.4.2.3.2). The elemental analysis of the recrystallised crop suggests the presence of one equivalent of water.

9.4.2.3.1. Crystallographic study A: Cu(I)2 AB3Bm $(ClO_4)_2$ (mixture of isomers)

Data for Cu(I)2 AB3Bm $(ClO_4)_2$ (mixture of isomers) was collected by the author on a Bruker SMART 1000. Details of the data collection and refinement are given in Table 9-20. The structure was solved by the author using direct methods, and refined with assistance from Prof Vickie McKee using full matrix least-squares on F^2, using SHELXTL (1). Non-hydrogen atoms in the cryptate were refined with anisotropic atomic displacement parameters. Hydrogen atoms were inserted at calculated positions with isotropic displacement parameters riding on U_{ij} of their carrier atoms.

Data beyond 45° was omitted from the refinement, as were three reflections obscured by the beam stop. This crystal diffracted relatively weakly, and was not expected to refine to a

very low R factor, however it is reported here as it contained a slightly different configuration from the second structure (see section 9.4.2.3.2 below).

Table 9-20: Crystal data and structure refinement for $Cu(I)_2$ AB3Bm $(ClO_4)_2$ (mixture of isomers).

Identification code	$Cu(I)_2$ AB3Bm $(ClO_4)_2$ (mixture of isomers)
Empirical formula	C40.30 H49.50 Cl2 Cu2 N8.15 O8
Formula weight	974.06
Temperature	293(2) K
Wavelength	0.71073 Å
Crystal system	Monoclinic
Space group	P2(1)/c
Unit cell dimensions	a = 9.6880(19) Å α= 90°
	b = 25.334(5) Å β= 97.47(3)°
	c = 36.550(7) Å γ = 90°
Volume	8895(3) $Å^3$
Z	8
Density (calculated)	1.455 Mg/m^3
Absorption coefficient	1.136 mm^{-1}
F(000)	4035
Crystal size	0.37 x 0.07 x 0.05 mm^3
Theta range for data collection	1.61 to 22.50°.
Index ranges	-10<=h<=10, -27<=k<=27, -39<=l<=39
Reflections collected	68764
Independent reflections	11639 [R(int) = 0.4629]
Completeness to theta = 22.50°	100.0 %
Absorption correction	Multiscan
Refinement method	Full-matrix least-squares on F^2
Data / restraints / parameters	11639 / 380 / 1094
Goodness-of-fit on F^2	0.887
Final R indices [I>2sigma(I)]	R1 = 0.1131, wR2 = 0.2597
R indices (all data)	R1 = 0.3574, wR2 = 0.3932
Extinction coefficient	0.0155(10)
Largest diff. peak and hole	0.771 and -0.769 $e.Å^{-3}$

Table 9-21: Selected bond lengths and angles for $Cu(I)_2$ AB3Bm $(ClO_4)_2$ (mixture of isomers).

Bond length /Å		Bond angle /°	
Cu(1D)-N(3D)	1.990(19)	N(4E)-Cu(2D)-N(4D)	119.5(8)
Cu(1D)-N(3E)	2.022(18)	N(4E)-Cu(2D)-N(4F)	118.5(8)
Cu(1D)-N(3F)	2.035(19)	N(4D)-Cu(2D)-N(4F)	122.0(8)
Cu(1D)-N(1D)	2.19(2)	N(4E)-Cu(2D)-N(2D)	89.6(10)
Cu(1D)-Cu(2D)	4.597(4)	N(4D)-Cu(2D)-N(2D)	93.6(10)
Cu(2D)-N(4E)	1.98(2)	N(4F)-Cu(2D)-N(2D)	89.3(11)
Cu(2D)-N(4D)	1.979(19)	N(4E)-Cu(2D)-Cu(1D)	91.1(6)
Cu(2D)-N(4F)	2.00(2)	N(4D)-Cu(2D)-Cu(1D)	86.2(6)
Cu(2D)-N(2D)	2.12(2)	N(4F)-Cu(2D)-Cu(1D)	90.2(6)
Cu(1A)-N(3B)	1.961(18)	N(2D)-Cu(2D)-Cu(1D)	179.3(9)
Cu(1A)-N(3C)	2.01(2)	N(3B)-Cu(1A)-N(3C)	121.7(8)
Cu(1A)-N(3A)	2.060(17)	N(3B)-Cu(1A)-N(3A)	128.0(8)
Cu(1A)-N(1A)	2.21(2)	N(3C)-Cu(1A)-N(3A)	110.2(8)
Cu(1A)-Cu(2A)	4.547(4)	N(3B)-Cu(1A)-N(1A)	93.6(9)
Cu(2A)-N(4A)	1.96(2)	N(3C)-Cu(1A)-N(1A)	94.3(10)
Cu(2A)-N(4C)	1.97(2)	N(3A)-Cu(1A)-N(1A)	84.3(8)
Cu(2A)-N(4B)	1.99(2)	N(3B)-Cu(1A)-Cu(2A)	84.8(5)
Cu(2A)-N(2A)	2.17(2)	N(3C)-Cu(1A)-Cu(2A)	89.0(7)
		N(3A)-Cu(1A)-Cu(2A)	94.4(5)
Bond angle /°		N(1A)-Cu(1A)-Cu(2A)	176.7(7)
N(3D)-Cu(1D)-N(3E)	119.7(8)	N(4A)-Cu(2A)-N(4C)	110.6(9)
N(3D)-Cu(1D)-N(3F)	119.7(8)	N(4A)-Cu(2A)-N(4B)	135.9(9)
N(3E)-Cu(1D)-N(3F)	120.6(8)	N(4C)-Cu(2A)-N(4B)	113.4(10)
N(3D)-Cu(1D)-N(1D)	92.6(8)	N(4A)-Cu(2A)-N(2A)	94.4(11)
N(3E)-Cu(1D)-N(1D)	95.4(8)	N(4C)-Cu(2A)-N(2A)	87.9(11)
N(3F)-Cu(1D)-N(1D)	83.7(9)	N(4B)-Cu(2A)-N(2A)	88.1(12)
N(3D)-Cu(1D)-Cu(2D)	92.5(6)	N(4A)-Cu(2A)-Cu(1A)	83.0(6)
N(3E)-Cu(1D)-Cu(2D)	87.9(5)	N(4C)-Cu(2A)-Cu(1A)	96.5(7)
N(3F)-Cu(1D)-Cu(2D)	88.0(6)	N(4B)-Cu(2A)-Cu(1A)	91.2(6)
N(1D)-Cu(1D)-Cu(2D)	171.7(7)	N(2A)-Cu(2A)-Cu(1A)	175.5(9)

9.4.2.3.2. Crystallographic study B: Cu(I)2 AB3Bm $(ClO_4)_2$ (single isomer)

Data for $Cu(I)_2$ AB3Bm $(ClO_4)_2$ (single isomer) was collected by the author on a Bruker SMART 1000. Details of the data collection and refinement are given in Table 9-22. The structure was solved by the author using direct methods, and refined with assistance from Prof Vickie McKee using full matrix least-squares on F^2, using SHELXTL (1). All non-hydrogen atoms were refined with anisotropic atomic displacement parameters. Hydrogen atoms were inserted at calculated positions with isotropic displacement parameters riding on U_{ij} of their carrier atoms.

Two perchlorate anions, and one acetonitrile molecule in this structure are fully ordered.

Disorder in the region of C12C and C13C was evident from large thermal ellipsoids extending along the direction of the bonds – rather than the normal cross-chain alignment of ellipsoids observed for a saturated carbon chain.

Apparent disorder in one strand of the cap was modelled as 60% occupancy of the 2-carbon cap strand (C12C and C13C) and 40% occupancy of a 3-carbon cap strand (C1X, C1Y, C1Z). Although there is suggestion of a similar disorder at the other end of the molecule, the residual electron density is far smaller at this end (peak value 1.34 $eÅ^{-3}$) and this was not included in the model. The remaining 40% of the 2-carbon cap strand is probably divided over the two other 3-carbon cap strands, although this electron density was not explicitly located. This disorder suggests that the crystal contains a mixture of LLSS and LSSL (probably less than 20%) isomers.

The two copper(I) ions are in trigonal pyramidal sites with the metal lying almost exactly in the plane (out of plane distances 0.0065 Å for Cu1, and 0.0397 Å for Cu2) of the three equatorial nitrogens. The M-N_{eq} distances range from 1.982(5) to 2.017(5) Å, and the M-N_{ax} distances are 2.185(5) Å (Cu1) and 2.207(5) Å (Cu2).

Table 9-22: Crystal data and structure refinement for $Cu(I)_2$ AB3Bm $(ClO_4)_2$ (single isomer).

Identification code	$Cu(I)_2$ AB3Bm $(ClO_4)_2$ (single isomer)	
Empirical formula	C42.40 H53.80 Cl2 Cu2 N9 O8	
Formula weight	1015.52	
Temperature	153(2) K	
Wavelength	0.71073 Å	
Crystal system	Monoclinic	
Space group	P2(1)/c	
Unit cell dimensions	a = 14.5958(14) Å	α= 90°
	b = 11.8877(11) Å	β= 94.309(2)°
	c = 25.470(2) Å	γ = 90°
Volume	4406.9(7) $Å^3$	
Z	4	
Density (calculated)	1.531 Mg/m^3	
Absorption coefficient	1.150 mm^{-1}	
F(000)	2109	
Crystal size	0.48 x 0.09 x 0.02 mm^3	
Theta range for data collection	1.40 to 25.00°.	
Index ranges	-17<=h<=17, -14<=k<=14, -30<=l<=30	
Reflections collected	39949	
Independent reflections	7757 [R(int) = 0.1054]	
Completeness to theta = 25.00°	99.9 %	
Absorption correction	Multiscan	
Refinement method	Full-matrix least-squares on F^2	
Data / restraints / parameters	7757 / 26 / 596	
Goodness-of-fit on F^2	1.023	
Final R indices [I>2sigma(I)]	R1 = 0.0628, wR2 = 0.1665	
R indices (all data)	R1 = 0.1064, wR2 = 0.1934	
Largest diff. peak and hole	1.336 and -0.501 $e.Å^{-3}$	

Table 9-23: Selected bond lengths and angles for $Cu(I)_2$ AB3Bm $(ClO_4)_2$ (single isomer).

Bond length /Å		Bond angle /°	
Cu(1)-N(3B)	1.985(5)	N(3B)-Cu(1)-N(3C)	124.51(19)
Cu(1)-N(3C)	1.993(5)	N(3B)-Cu(1)-N(3A)	117.5(2)
Cu(1)-N(3A)	2.013(5)	N(3C)-Cu(1)-N(3A)	117.96(19)
Cu(1)-N(1)	2.185(5)	N(3B)-Cu(1)-N(1)	93.8(2)
Cu(1)-Cu(2)	4.4356(10)	N(3C)-Cu(1)-N(1)	89.3(2)
Cu(2)-N(4A)	1.982(5)	N(3A)-Cu(1)-N(1)	86.08(19)
Cu(2)-N(4B)	1.999(5)	N(4A)-Cu(2)-N(4B)	121.19(19)
Cu(2)-N(4C)	2.017(5)	N(4A)-Cu(2)-N(4C)	121.7(2)
Cu(2)-N(2)	2.207(5)	N(4B)-Cu(2)-N(4C)	116.95(19)
		N(4A)-Cu(2)-N(2)	91.67(19)
		N(4B)-Cu(2)-N(2)	89.33(19)
		N(4C)-Cu(2)-N(2)	85.48(19)

9.4.3. Preparation of the cap (baep.4HCl.2$H_2$0)

The procedure used for preparation of baep was analogous to that described in section 9.4.1.

The primary amine groups of the starting compound diethylenetriamine were protected using a phthalimide group as follows:

59.3 g (0.37 mol) of phthalic anhydride was melted at 180°C and 20.6 g (0.2 mol) of diethylenetriamine added dropwise with stirring. A vigorous reaction occurred with production of white smoke, and once the reaction had ceased the mixture was poured into a large mortar and allowed to cool. A glassy reddish solid was obtained, which was ground to a powder and extracted into ethanol using a soxhlet.

5 g (13.8 mmol) of the red solid obtained by evaporating this solution in a rotovap was added to 5.5 g (20.5 mmol) of (3-bromopropyl)phthalimide, and 3 g (36.1 mmol) of sodium carbonate were melted together at 150-160°C, and stirred under nitrogen for 3-4 hours. The mixture was poured into a large mortar and allowed to cool, and the resulting solid was ground to a powder, and then refluxed in 8 M HCl for 11 hours.

After removing the solvent in a rotovap, the solid was purified in a similar manner as described for abap in section 9.4.1.

9.5. Experimental details for Chapter 6

9.5.1. Mn(II) amBT

Manganese (II) amBT perchlorate: 200 mg (0.540 mmol) of amBT was dissolved in EtOH and 195 mg (1.4 molar equivalents) of solid Mn(II) perchlorate added to the stirring solution. An off-white precipitate formed, which was filtered and recrystallised from acetonitrile to give 121 mg of colourless blocks (36 % yield).

Manganese (II) amBT triflate: 100 mg (0.270 mmol) of amBT was dissolved in denatured ethanol, and 95 mg of solid Mn(II) triflate (1 molar equiv) added. The mixture was stirred at room temperature for 1 hour, and then left for 16 hours. 72 mg of fine white needles were collected (37 % yield).

9.5.2. Mn(II) imBT

Manganese(II) imBT perchlorate: 200 mg of imBT (0.558 mmol) was dissolved in EtOH, and 202 mg (1.4 molar equivalents) of solid Mn(II) perchlorate added to the stirring

solution. A yellow precipitate separated from the solution, which was recrystallised from MeCN, forming 144 mg of large orange hexagonal prisms (42 % yield).

Manganese(II) imBT triflate: 298 mg of imBT (0.831 mmol) was dissolved in 50:50 acetonitrile/ethanol, and 296 mg (1 equiv) of solid Mn(II) triflate added. The solution turned orange, and was stirred for 1 hour, and then for 16 hours. 248 mg of orange solid was collected (42 % yield). X-ray quality crystals were obtained by the slow diffusion of ether into a solution of the cryptate in MeCN.

9.5.2.1. Dissociation and stability study

The spectrum of the free ligand (Figure 9-13 A) contains two absorptions in the 190 to 450 nm range: a $\pi \rightarrow \pi^*$ transition at 271 nm, and a very intense peak (presumably charge transfer) centred at around 203 nm. Measurements in this region were strongly affected by solvent absorption and the $\pi \rightarrow \pi^*$ transition was considered a more reliable parameter to monitor. In the manganese(II) cryptate (Figure 9-13 B) the $\pi \rightarrow \pi^*$ transition is shifted to 336 nm.

In order to check for dissociation phenomena, the spectrum of the cryptate was compared before and after the addition of one equivalent of free ligand. The increase in intensity at 336 nm was consistent with the contribution from ligand absorption, but was not sufficiently enhanced to suggest formation of more manganese(II) cryptate (as would be expected if dissociation was occurring).

In order to check for the possibility of decomposition, UV/visible spectra of free imBT cryptand, Mn imBT cryptate, and a 1:1 mixture of the two were compared over a period of more than a month. The cryptand and cryptate solutions were allowed to stand in stoppered vessels for 5 hours before the first spectra were recorded. 1:1 mixtures were prepared immediately before their spectra were recorded. The solutions were stored in stoppered volumetric flasks at room temperature between measurements.

After one day, the ligand solution showed a slight reduction in the $\pi \rightarrow \pi^*$ transition, and after 6 weeks it was reduced to a weak shoulder, presumably a result of hydrolysis of the imine bonds. The cryptate spectrum appeared identical after one day in solution, however at the end of the period of observation the peak had reduced in intensity, and its position had shifted to 349 nm, which could indicate the presence of hydrated Mn(II).

Two indicative comparisons are shown in Figure 9-13 C and D. The day one comparison shows that the mixed sample spectrum is almost a perfect average of the cryptand and cryptate spectra (some deviation occurs at absorbance>1.4, this is likely due to the non-linear nature of absorbances much greater than 1). After 6 weeks however there is a significant difference between the observed cryptate + cryptand spectrum and the predicted spectrum. The observed peak in the mixed solutions now occurs at 336 nm, the same as the original cryptate, and this may indicate uptake of manganese by the added ligand, resulting in regeneration of the cryptate spectrum.

These observations suggest that dissociation is not significant in the short term, however there appears to be slow hydrolysis of the cryptand and cryptate in the 60:40 MeCN:H_2O mixture, an effect previously encountered for other cryptates (3) and suggested for this system (2).

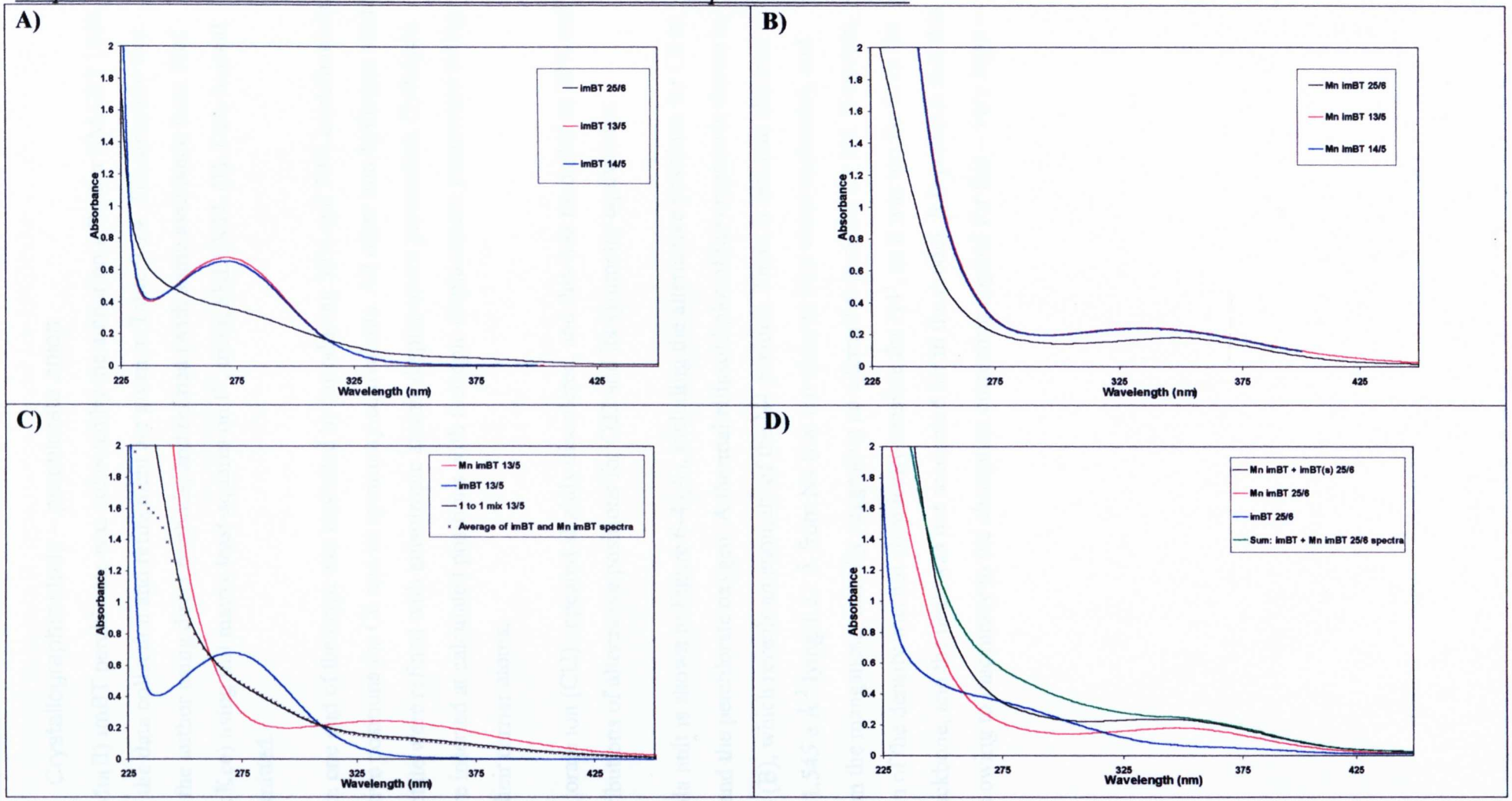

Figure 9-13: Time course of A) imBT and B) Mn imBT UV/Vis absorption. C) shows a comparison of cryptand to cryptate spectra, together with a 1:1 mixture, and the predicted average spectrum (crosses). D) shows the same solutions 6 weeks later, as well as the cryptate solution with one equivalent of solid imBT added, and the predicted spectrum (sum of the cryptand and cryptate spectra).

9.5.2.2. Crystallographic study – perchlorate anion

Data for Mn(II) imBT perchlorate was collected by the author on a Bruker SMART 1000. Details of the data collection and refinement are given in Table 9-24. The structure was solved by the author using direct methods, and refined (with some assistance from Prof Vickie McKee) using full matrix least-squares on F^2, using SHELXTL (1). Data beyond 50° was omitted.

Disorder in one end of the crypt was modelled by introducing 30% and 70% contributions of alternative positions for C6 and its symmetry equivalents. All other non-hydrogen atoms in the cryptate were refined with anisotropic atomic displacement parameters. Hydrogen atoms were inserted at calculated positions with isotropic displacement parameters riding on U_{ij} of their carrier atoms.

One perchlorate ion (Cl2) appeared slightly disordered, and this was modelled as 20% and 80% contributions of alternative positions for O22 and its symmetry equivalents.

The formula unit is shown in Figure 6-4 (A), including the alternative positions for C6 in the crypt, and the perchlorate oxygen. A thermal ellipsoid plot of the cryptate is shown in Figure 6-4 (B), which reveals an anomaly of the N4 position. There is residual electron density of 1.545 e.$Å^{-3}$ lying 1.21 Å from N4 (*i.e.* too close to be a water molecule), and 2.33 Å from the manganese, initially suggesting an alternative position for N4. However, the location of the density was not chemically sensible for N4', as it was too far from the cryptate backbone, and the peak was not accounted for in the model. It is possible that this anomaly is owing to inaccuracy in the absorption correction applied for this – very large – crystal.

Table 9-24: Crystal data and structure refinement for Mn(II) imBT perchlorate .

Identification code	Mn(II) imBT perchlorate	
Empirical formula	C18 H30 Cl2 Mn N8 O8	
Formula weight	612.34	
Temperature	153(2) K	
Wavelength	0.71073 Å	
Crystal system	Hexagonal	
Space group	P6(3)	
Unit cell dimensions	a = 9.0593(6) Å	α= 90°
	b = 9.0593(6) Å	β= 90°
	c = 17.8254(16) Å	γ = 120°
Volume	1266.95(16) $Å^3$	
Z	2	
Density (calculated)	1.605 Mg/m^3	
Absorption coefficient	0.792 mm^{-1}	
F(000)	634	
Crystal size	0.8 x 0.65 x 0.35 mm^3	
Theta range for data collection	2.29 to 24.99°	
Index ranges	-10<=h<=10, -10<=k<=10, -21<=l<=21	
Reflections collected	12175	
Independent reflections	1509 [R(int) = 0.0658]	
Completeness to theta = 24.99°	100.0 %	
Absorption correction	Multiscan	
Max. and min. transmission	0.801279 and 0.548630	
Refinement method	Full-matrix least-squares on F^2	
Data / restraints / parameters	1509 / 1 / 117	
Goodness-of-fit on F^2	1.087	
Final R indices [I>2sigma(I)]	R1 = 0.0971, wR2 = 0.2857	
R indices (all data)	R1 = 0.0973, wR2 = 0.2859	
Absolute structure parameter	0.15(9)	
Extinction coefficient	0.038(11)	
Largest diff. peak and hole	1.545 and -0.780 $e.Å^{-3}$	

Table 9-25: Atomic coordinates and equivalent isotropic displacement parameters.

	x /Å x 10^4	y /Å x 10^4	z /Å x 10^4	U(eq) / $Å^2$x 10^3
Mn	-3333	3333	7495(1)	19(1)
N(1)	-3333	3333	5845(8)	33(4)
C(1)	-2348(14)	5155(14)	5617(6)	33(2)
C(2)	-2560(17)	6261(18)	6183(7)	47(3)
N(3)	-2020(10)	5943(10)	6899(5)	24(2)
C(3)	-646(17)	7136(19)	7188(7)	47(3)
C(4)	-61(12)	6660(12)	7896(6)	30(2)
N(4)	-951(15)	5127(18)	8155(7)	66(4)
C(5)	-400(12)	4763(12)	8858(5)	27(2)
C(6)	-1560(20)	4580(20)	9494(10)	43(4)
N(2)	-3333	3333	9304(10)	28(3)
C(5')	-400(12)	4763(12)	8858(5)	27(2)
C(6')	-1590(30)	3700(40)	9457(14)	14(5)
N(2')	-3333	3333	9304(10)	28(3)
Cl(1)	10000	0	9163(3)	26(1)
O(11)	10000	0	8350(9)	50(4)
O(12)	10844(15)	-860(15)	9430(6)	63(3)
Cl(2)	3333	6667	6730(3)	32(1)
O(21)	3333	6667	7526(12)	54(4)
O(22)	1991(14)	6931(15)	6470(7)	46(3)
O(22')	2950(40)	7920(40)	6479(16)	17(6)

Table 9-26: Selected bond lengths and angles for Mn(II) imBT perchlorate.

Bond length /Å		Bond angle /°	
Mn-N(4)	2.276(12)	N(4)-Mn-N(3)#2	165.2(4)
Mn-N(3)	2.307(9)	N(4)#1-Mn-N(3)#2	93.5(4)
Bond angle /°		N(4)#2-Mn-N(3)#2	71.8(4)
N(4)-Mn-N(4)#1	95.7(4)	N(3)#1-Mn-N(3)#2	100.5(2)
N(4)-Mn-N(4)#2	95.7(4)	N(4)-Mn-N(3)	71.8(4)
N(4)#1-Mn-N(4)#2	95.7(4)	N(4)#1-Mn-N(3)	165.2(4)
N(4)-Mn-N(3)#1	93.5(4)	N(4)#2-Mn-N(3)	93.5(4)
N(4)#1-Mn-N(3)#1	71.8(4)	N(3)#1-Mn-N(3)	100.5(2)
N(4)#2-Mn-N(3)#1	165.2(5)	N(3)#2-Mn-N(3)	100.5(2)

Symmetry transformations used to generate equivalent atoms:

#1 -x+y-1,-x,z #2 -y,x-y+1,z

9.5.2.3. Crystallographic study – triflate anion

Data for Mn(II) imBT triflate was collected by the author on a Bruker SMART 1000. Details of the data collection and refinement are given in Table 9-27. The structure was solved by the author using direct methods, and refined using full matrix least-squares on F^2, using SHELXTL (1). A single reflection obscured by the beamstop, as well as all data beyond 50° (weak) was omitted.

The crypt was fully ordered in this variation of the complex, although distended ellipsoids of the triflate fluorine and oxygen atoms showed the anions to be disordered. The nature of the disorder could not be modelled simply as rotation about the axis, but was more complex, suggestive of two alternative overlapping positions, and was not explicitly dealt with in the model. All non-hydrogen atoms were refined with anisotropic atomic displacement parameters. Hydrogen atoms were inserted at calculated positions with isotropic displacement parameters riding on U_{ij} of their carrier atoms.

The asymmetric unit of this crystal contains two half-cryptate parts, and two triflate anions. Despite the similarity of the two cryptate molecules (see Figure 6-5 and Table 9-28) no missing symmetry elements were discovered by the Addsym function of Platon (8, 9). The cryptate moiety in this crystal is very similar to that observed with perchlorate counterion, and the R factor is slightly improved. Mn-N distances and angles within the octahedral coordination sphere in the two crystals are within experimental error of each other.

Table 9-27: Crystal data and structure refinement for Mn(II) imBT triflate.

Identification code	Mn(II) imBT triflate
Empirical formula	C20 H30 F6 Mn N8 O6 S2
Formula weight	711.58
Temperature	153(2) K
Wavelength	0.71073 Å
Crystal system	Monoclinic
Space group	P2/c
Unit cell dimensions	a = 18.3987(12) Å α= 90°
	b = 9.1306(6) Å β= 117.3190(10)°
	c = 20.3105(18) Å γ = 90°
Volume	3031.4(4) Å^3
Z	4
Density (calculated)	1.559 Mg/m^3
Absorption coefficient	0.659 mm^{-1}
F(000)	1460
Crystal size	0.52 x 0.44 x 0.42 mm^3
Theta range for data collection	2.02 to 25.00°.
Index ranges	-21<=h<=21, -10<=k<=10, -24<=l<=24
Reflections collected	21388
Independent reflections	5339 [R(int) = 0.0245]
Completeness to theta = 25.00°	99.9 %
Absorption correction	Multiscan
Max. and min. transmission	0.801516 and 0.617688
Refinement method	Full-matrix least-squares on F^2
Data / restraints / parameters	5339 / 264 / 389
Goodness-of-fit on F^2	1.057
Final R indices [I>2sigma(I)]	R1 = 0.0807, wR2 = 0.2533
R indices (all data)	R1 = 0.0995, wR2 = 0.2836
Largest diff. peak and hole	1.271 and -1.068 e.Å^{-3}

Table 9-28: Selected bond lengths and angles for Mn(II) imBT triflate.

Bond length /Å		Bond angle /°	
Mn(1)- N(3A)	2.296(4)	N(4D)#2-Mn(2)-N(4E)#2	97.95(14)
Mn(1)- N(3B)	2.258(4)	N(4D)-Mn(2)-N(4E)#2	164.96(16)
Mn(1)- N(3C)	2.310(4)	N(4E)-Mn(2)-N(4E)#2	71.5(2)
Mn(2)-N(3D)	2.271(4)	N(3B)#1-Mn(1)-N(3B)	163.8(2)
Mn(2)-N(4D)	2.285(4)	N(3B)#1-Mn(1)-N(3A)	94.31(15)
Mn(2)-N(4E)	2.292(4)	N(3B)-Mn(1)-N(3A)	98.78(16)
Bond angle /°		N(3B)#1-Mn(1)-N(3A)#1	98.78(16)
N(3D)#2-Mn(2)-N(3D)	165.6(2)	N(3B)-Mn(1)-N(3A)#1	94.30(14)
N(3D)#2-Mn(2)-N(4D)#2	72.25(17)	N(3A)-Mn(1)-N(3A)#1	72.1(3)
N(3D)-Mn(2)-N(4D)#2	97.72(16)	N(3B)#1-Mn(1)-N(3C)#1	96.54(15)
N(3D)#2-Mn(2)-N(4D)	97.72(16)	N(3B)-Mn(1)-N(3C)#1	72.08(16)
N(3D)-Mn(2)-N(4D)	72.25(17)	N(3A)-Mn(1)-N(3C)#1	166.40(16)
N(4D)#2-Mn(2)-N(4D)	94.3(2)	N(3A)#1-Mn(1)-N(3C)#1	98.12(16)
N(3D)#2-Mn(2)-N(4E)	97.33(15)	N(3B)#1-Mn(1)-N(3C)	72.08(16)
N(3D)-Mn(2)-N(4E)	94.35(15)	N(3B)-Mn(1)-N(3C)	96.54(15)
N(4D)#2-Mn(2)-N(4E)	164.96(16)	N(3A)-Mn(1)-N(3C)	98.12(16)
N(4D)-Mn(2)-N(4E)	97.95(14)	N(3A)#1-Mn(1)-N(3C)	166.40(16)
N(3D)#2-Mn(2)-N(4E)#2	94.35(14)	N(3C)#1-Mn(1)-N(3C)	93.0(2)
N(3D)-Mn(2)-N(4E)#2	97.33(15)		

Symmetry transformations used to generate equivalent atoms:

#1 -x,y,-z+1/2 #2 -x+1,y,-z+1/2

9.5.3. Mn(II) trac

309 mg (0.787 mmol) of trac was dissolved in 1:1 EtOH:MeCN, and 285 mg Mn(II) perchlorate (1.4 molar equivalents) added in MeCN. The mixture was refluxed 2 hours, and cooled overnight. The brown solution was evaporated under N_2, giving a brown solid containing traces of small colourless crystals. Chromatography on sephadex (MeCN eluent) gave a yellow solution which reduced to 84 mg of a brown solid when evaporated (16.5 % yield).

9.6. Experimental details for Chapter 7

9.6.1. Extraction of 6+4 imBT from bulk imBT

50 g of sephadex G50 (Sigma) was washed with acetone, ethanol, water, and then ethanol again, and air dried. The cleaned material was soaked in dichloromethane overnight, and a column packed the following morning.

A concentrated solution of approximately 1 g of imBT in 2 ml of dichloromethane was applied to the column, and eluted with dichloromethane, collecting 5-10 ml fractions. Thin layer chromatography (silica plates, immobile with hexane/ethyl acetate mixtures, streaks

with dichloromethane/MeOH mixtures, spots visualised by 254 nm UV) did not resolve 3+2 and 6+4 cryptands, but was useful in confirming the presence of an eluate.

9.6.2. 6+4 "barrel" preparation via trialdehyde

We attempted to form the trialdehyde in situ by adding 4.1 g (28 mmol) of tren to 200 ml of isopropanol, and adding it to a concentrated solution of 6.56 g (94 mmol) of glyoxal in 50 ml of 1:25 H_2O/isopropanol, and stirring at room temperature for 1 hour. A strong yellow colour developed during the addition, and the solution obtained was then divided into two portions.

a) One portion (containing 14 mmol of trialdehyde) was added dropwise (1 drop/2 sec) with stirring, at room temperature, to 2.05 g (14 mmol) of tren in 400 ml of isopropanol. The yellow solution was stirred for 4 hours, and rotovaped to dryness (see Note 1 below). The yellow solid obtained was stirred with 200 ml of chloroform, and then filtered, retaining the insoluble yellow orange solid (polymer) for subsequent soxhlet extraction (see Note 2 below, yield 8 mg of brown solid, 0.2%, labelled A1). The filtrate had 3 g of celite added, was rotovaped to dryness (Note 1), and the pale yellow powder transferred to a soxhlet thimble (Note 2, yield 40 mg of pale yellow solid, 0.8%, labelled A2).

b) The second portion was treated in a similar manner, only the concentration of the amine was increased to 2.05 g (14 mmol) in 50 ml of isopropanol, and the addition rate was increased to about 2 drops/sec. This resulted in a cloudy white mixture, which was subsequently handled as described for part a). The extract from the insoluble polymer (21 mg, 0.4% yield) was labelled B1, and from the filtrate B2 (63 mg, 1.2% yield).

Note 1: Rotary evaporation performed at 30-40°C

Note 2: Soxhlet extraction with 500 ml of 4:1 hexane/heptane for 48 hours, extract vacuum filtered and evaporated to dryness at 30-40°C.

9.7. References

1. Sheldrick, G.M., *SHELX97 [Includes SHELXS97, SHELXL97, CIFTAB (and SHELXA)] - Programs for Crystal Structure Analysis* 97-2. 1998: Institüt für Anorganische Chemie der Universität, Tammanstrasse 4, D-3400 Göttingen, Germany.

2. Coyle, J.L., M.G.B. Drew, C.J. Harding, J. Nelson, and R.M. Town, Journal of the Chemical Society, Dalton Transactions, 1997: p. 1123-1125.

3. Harding, C.J., Q. Lu, J.F. Malone, D.J. Marrs, N. Martin, Mck, and J. Nelson, Journal of the Chemical Society-Dalton Transactions, 1995(10): p. 1739-1747.

4. Smith, A., S.J. Rettig, and C. Orvig, Inorganic Chemistry, 1988. **27**: p. 3929-3934.

5. Smith, P.H., M.E. Barr, J.R. Brainard, D.K. Ford, H. Freiser, S. Muralidharan, S.D. Reilly, R.R. Ryan, L.A.I. Silks, and W.-h. Yu, Journal of Organic Chemistry, 1993. **58**: p. 7939-7941.

6. Fanshawe, R.L. and A.G. Blackman, Inorganic Chemistry, 1994. **34**(2): p. 421-423.

7. Streater, M., P. Taylor, R. Hider, and J. Porter, Journal of Medicinal Chemistry, 1990. **33**(6): p. 1749-1755.

8. Spek, A.L., Acta Crystallographica Section A, 1990. **46**: p. 194-201.

9. Spek, A.L., *PLATON, A Multipurpose Crystallographic Tool* 1998: Utrecht University Utrecht, The Netherlands.